A novel electrochemical/catalytic process to generate chlorine dioxide

DiMascio, Felice

Award date:
2003

Awarding institution:
University of Bath

A Novel Electrochemical / Catalytic Process To Generate Chlorine Dioxide

Submitted by Felice DiMascio

for the degree of PhD

of the University of Bath

2003

ProQuest LLC
789 East Eisenhower Parkway
P.O. Box 1346
Ann Arbor, MI 48106-1346

ACKNOWLEDGEMENTS

I would like to express my sincere appreciation to my advisor Frank Walsh for his untiring support and guidance throughout the course of this work. My thanks are also extended to all of the administrative staff members in the Chemical Engineering Department, particularly Sally Barker, for the assistance they provided me.

Additionally, I would like to thank Halox Technologies Incorporated, a division of IDEX Corporation in Northbrook, IL, U.S.A, for providing research support. I am grateful to all of my co-workers for their support and friendship.

Finally, my deepest appreciation to my wife Carrie for allowing me to live to complete this project and to Harvey dog, the biggest 'squish' of them all.

SUMMARY

The focus of this study was a novel process that generates chlorine dioxide by a three step process: passing a sodium chloride solution through an electrochemical acidification cell, blending the effluent from the electrochemical acidification cell with a solution of sodium chlorite, and passing the blend through a fixed-bed catalytic reactor.

The electrochemical acidification cell used a three-compartment electrolytic cell to convert a sodium chloride solution to a hydrochloric acid solution. A sodium chloride solution was passed through a bed of cation exchange resin, which was held between two cation-permeable membranes. Sodium ions were taken up from the solution by the cation exchange resin and exchanged with hydrogen ions. A direct electric current passed perpendicular to the direction of flow of liquid. Sodium ions were transported in the direction of the current, where they were removed from the resin bed through the membranes. Under these conditions, the functional groups of the cation exchange resin were converted to the hydrogen form by electrolytic regeneration.

The fixed-bed catalytic reactor used a bed of platinum-supported catalyst to efficiently react hydrochloric acid and sodium chlorite. According to the proposed concept, hydrogen ions combined with the platinum catalyst to form an intermediate compound, which then reacted with chlorite ions to provide the final chlorine dioxide product.

The electrochemical acidification cell and fixed-bed catalytic reactor were characterised through experimentation and mathematically modelled. For the electrochemical acidification cell, feed concentration, temperature, velocity, and applied current were found to be important operating variables. Particle size, temperature, velocity, and space-time were found to be important variables in the fixed-bed catalytic reactor.

Fitting experimental data to the predicted behaviour verified the models and their accuracy. Under all of the conditions studied, the model predicted results that were within 15.0 % of actual experimental data for the electrochemical acidification cell and within 6.5 % for the fixed-bed catalytic reactor.

TABLE OF CONTENTS

NOMENCLATURE

The symbols, abbreviations, and units that are used in this study are listed below.

a	Equilibrium Parameter
a_p	External surface area to volume ratio of a particle / s^{-1}
$\overline{a}$	Thermodynamic activity in the cation exchange resin
A_c	Cross-sectional area of reactor containing catalyst / cm^2
A_o	Frequency factor / cm s^{-1}
A_y	Cross-sectional area of the compartment in the y-axis / cm^2
b	Kinetic Parameter
C	Bulk liquid concentration / mol cm^{-3}
$\overline{C}$	Concentration in the cation exchange resin / mol cm^{-3}
C_i^*	Stagnant film liquid concentration / mol cm^{-3}
C_p	Heat Capacity / J g^{-1} $°C^{-1}$
d	Particle diameter / cm
D	Diffusion coefficient in the bulk liquid / cm^2 s^{-1}
$\overline{D}$	Diffusion coefficient in a particle / cm^2 s^{-1}
D_{eff}	Effective diffusion coefficient / cm^2 s^{-1}
$\overline{D}^{avg}$	Average diffusion coefficient in a particle / cm^2 s^{-1}
E_{act}	Activation energy / J mol^{-1}
E_A	Effect shown by a variable
E_d	Effect shown by a dummy variable
g_c	Acceleration due to gravity / cm s^{-2}
i	Current density / A cm^{-2}
I	Applied D.C. current / A
J	Molar flux rate / mol cm^{-2} s^{-1}
k_f	Stagnant film mass transfer coefficient / cm s^{-1}

k Global rate constant / s^{-1}

k_r Reaction rate constant / s^{-1}

K^{sel} Selectivity coefficient

K^{eq} Equilibrium coefficient

K_A Viscous parameter

K_B Inertial parameter

K_C Void fraction parameter

K_D Void fraction parameter

K_E Temperature dependent parameter for $NaClO_2$ density determination

K_F Temperature dependent parameter for $NaClO_2$ density determination

K_G Temperature dependent parameter for $NaClO_2$ viscosity determination

K_H Temperature dependent parameter for $NaClO_2$ viscosity determination

L Compartment length / cm

M Molar rate / mol h^{-1}

m Mass rate / g s^{-1}

n Number of dummy variables

P Pressure / kPa

q_{in} Heat generated by the applied current / J s^{-1}

q_{out} Heat removed by the flow of liquid / J s^{-1}

Q Flow rate / cm^3 s^{-1}

Q_i Anion concentration in cation resin; including the fixed ionic groups / eq cm^{-3}

r_o Radius of a particle / cm

r Ion exchange rate / mol cm^{-3} s^{-1}

r''' Rate of generation per volume of catalyst / mol cm^{-3} s^{-1}

R_r Response or result of a variable

S Specific surface area of a particle / cm^{-1}

SE_{eff} Standard error of an effect

t_t	T-Test parameter
t	Time / s
T	Absolute temperature / K
u	Liquid phase electrochemical mobility / $cm^2\ V^{-1}\ s^{-1}$
$\bar{u}$	Cation exchange resin phase electrochemical mobility / $cm^2\ V^{-1}\ s^{-1}$
$\bar{u}^o$	Mobility accounting for the interchange between fixed-charges / $cm^2\ V^{-1}\ s^{-1}$
$\bar{u}'$	Mobility in the pore liquid / $cm^2\ V^{-1}\ s^{-1}$
$\bar{u}_o$	Mobility in the pore liquid due to convection / $cm^2\ V^{-1}\ s^{-1}$
v	Superficial fluid velocity / $cm\ s^{-1}$
$\bar{v}$	Convection rate in a particle / $cm\ s^{-1}$
V_{eff}	Variance of an effect
W	Compartment width / cm
x	Coordinate in direction of current / cm
X	Concentration of the fixed charges on the ion-exchange resin / $mol\ cm^{-3}$
X•	Active catalytic site
y	Coordinate in direction of liquid flow / cm
Y	Compartment length / cm
z	Electrochemical valence

Greek Variables

α	Separation factor
δ	Thickness of the stagnant film / cm
ε	Liquid void fraction
ε_o	Theoretical void fraction for a given packing arrangement
Φ	Electrical potential / V
η_f	Effectiveness factor
η_c	Current efficiency / %
η_T	Dynamic viscosity / cP

φ Fractional pore volume of a particle

λ^o Equivalent ionic conductivity at infinite dilution / $cm^2\ V^{-1}\ s^{-1}$

υ Kinematic viscosity / $cm^2\ s^{-1}$

μ_i^o Chemical potential in a standard state

ρ_o Specific flow resistance in a particle / $g\ cm^{-3}\ s^{-1}$

ρ_T Density / $g\ cm^{-3}$

ϖ Sign of a fixed charge

τ Space time / s

Physical Constants

F Faraday's constant / 96,495 $C\ eq^{-1}$

R Gas constant / 8.314 $J\ mol^{-1}\ K^{-1}$

Dimensionless Numbers

J_D Mass Transport Factor

M_T Thiele Modulus $\left(\frac{d}{6}\sqrt{\frac{k_f}{D_{eff}}}\right) = \frac{\text{reaction velocity}}{\text{diffusion velocity}}$

Pe Peclet number $\left(\frac{d\,v}{D}\right) = \frac{\text{flow velocity}}{\text{diffusion velocity}}$

Re Reynolds number $\left(\frac{d\,v}{\mu}\right) = \frac{\text{flow velocity}}{\text{"momentum velocity"}}$

Sc Schmidt number $\left(\frac{\mu}{D}\right) = \frac{\text{diffusivity of momentum}}{\text{diffusivity of mass}}$

Sh Sherwood number $\left(\frac{k_f\,d}{D}\right) = \frac{\text{mass transfer velocity}}{\text{diffusion velocity}}$

LIST OF FIGURES

Appendices

LIST OF TABLES

Chapter 2

Chapter 3

CHAPTER 1

INTRODUCTION

This chapter gives an introduction to the uses and generation of chlorine dioxide and a brief background to this research project along with some elementary theory. It describes a unique chlorine dioxide generation process, comprising an electrochemical acidification cell and a fixed-bed catalytic reactor, and introduces some of the main principles behind their operation. The objectives of the project are described at the end of this chapter.

1.1 Water Disinfection

Water disinfection involves specialised treatment for the destruction of harmful organisms in a body of water. Most disinfection treatments are employed to destroy or inactivate disease-producing organisms by attacking cellular sites and inhibiting necessary cellular functions. Such disease-producing organisms include intestinal bacteria, intestinal protozoa, viruses, and some microorganisms. Water disinfection also encompasses destruction of other types of organisms; however, they are seldom carried out to the point of sterilisation or complete destruction of all living organisms. Many of the disease-producing organisms are partially or completely controlled by the treatment.

Water disinfection can be accomplished in many ways. Excluding processes that remove disease-producing organisms, such as filtration- and membrane-based systems, such as micro-filtration and reverse osmosis, the processes that are typically employed include one or a combination of the following:

- Physical Treatment; application of heat or other physical agents to kill organisms
- Irradiation; ultraviolet lamps which operate at a wavelength of 254 nm for the deactivation of particular target organisms
- Metal Ions; copper and silver ionisation where these ions are released into the water by an electrolytic process and act as a potent biocide
- Non-Oxidising Biocides; organic microbiocides which use a variety of biochemical mechanisms to destroy microbial pathogens, including cell membrane destruction, interference of vital mechanisms, or inactivation of critical processes

- Oxidising Biocides; halogens, ozone, and other inorganic and organic materials which tend to destroy the outer membrane cell of the bacterial cell and render it non-infectious

Except for some of the oxidising biocides, such as chlorine, bromine, and some of their compounds, and non-oxidising biocides, most of the other disinfection methods have one or more limitations that preclude their general acceptance and adaptability, by themselves, for many water disinfection applications.

Water disinfection using chlorine was established on a scientific basis in the early 1900s. By the 1950s, experimental development and refinement had firmly established certain practices and control procedures that ensured the effectiveness of chlorine for disinfection and other treatment applications. Disinfection using chlorine has become very popular compared to other disinfection methods and is widely accepted, particularly in the United States.

Although chlorine has been extensively and successfully used for many years, data uncovered over the past decade has shown that it is not as good as a disinfectant as previously thought. It also has many negative heath and environmental impacts. When chlorine is added to water, a mixture of hypochlorous (HOCl) and hydrochloric (HCl) acids is formed:

$$Cl_2 + H_2O \leftrightarrow HOCl + HCl \quad (1.1)$$

The hypochlorous acid dissociates into hydrogen (H^+) and hypochlorite (OCl^-) ions:

$$HOCl \leftrightarrow H^+ + OCl^- \quad (1.2)$$

The oxidising capacity of chlorine varies with pH because the variation of the resultant hypochlorous/hypochlorite ion ratio, decreasing at high pH levels whereby hypochlorite ions predominate.

More importantly, the demand that is seen when using chlorine makes it both expensive to use and environmentally unacceptable compared to today's standards. For effective disinfection control, chlorine must be applied to overcome the chlorine demand of the water. Species that react with chlorine include inorganic reducing substances, carbonaceous material, and various classes of organic materials; such as ammonia,

amino acids, phenols, and proteins. In addition many water treatment chemical are attached by chlorine. Among these are triazole corrosion inhibitors and the scale inhibitors EDTA, NTA, and AMP. These materials influence the chlorine demand and complicate the use of chlorine for disinfection in several ways.

Firstly, sufficient chlorine must be applied not only to destroy organisms, but also to compensate for the chlorine consumed by these secondary reactions. Increasing chlorine dosage in the presence of reactable materials is not advisable since this causes increased metal corrosion, wood delignification, and higher levels of total dissolved solids (TDS).

Secondly, chlorine consumed by some of these reactions may form by-products that are toxic to fish and potential carcinogens to humans [1]. For example, chlorine reacts with ammonia and most amines to form chloramines. When chlorine is used to treat surface water which contain decayed organic matter, such as humic and fulvic acids, it produces chloroform and other chloro- and bromo-organic derivatives, which are collectively known as trihalomethanes (THM's). THM's have been shown to be carcinogenic and in November 1979, an amendment to National Interim Primary Water Regulations established the 0.10 parts-per-million (ppm) maximum contamination level for total trihalomethanes [2,3].

Thirdly, chlorine combines with phenols (C_6H_5OH) and forms highly toxic chlorophenols. These chlorophenols impart an objectionable medicinal taste and odour in potable water supplies [4]. Ortho-chlorophenol is the most offensive of the phenol compounds. It is objectionable at concentrations as low as 102 parts-per-billion (ppb).

Fourthly, there have been some disease-producing organisms, including encysted parasites, identified that are chlorine resistant. These include *Giardia*, *Staphylococcus aureus*, *Cryptosporidium parvum* [5-7] and *Mycobacteria avium*, and most recently, *Legionella pneumophilia* [8], the bacteria identified in 1976 as responsible for Legionnaires Disease [9].

One of the oxidising biocides that has been used to overcome the deficiencies of chlorine is bromine. Bromine disinfection has been successfully employed in water disinfection applications since the 1940s [10], by the reaction between the organic compound, 1-bromo-3-chloro-5-dimethyhyantoin ($C_5H_6O_2N_2ClBr$) and water:

$$C_5H_6O_2N_2ClBr + 2H_2O \rightarrow HOBr + HOCl + C_5H_8O_2N_2 \quad (1.3)$$

1-bromo-3-chloro-5-dimethyhyantoin is known commercially as AquaBrom or Dihaol. Another form is by the reaction of sodium bromide (NaBr) with sodium hypochlorite (NaOCl):

$$NaBr + NaOCl + HCl \rightarrow HOBr + 2NaCl \quad (1.4)$$

Both reactions form hypobromus acid (HOBr) in water.

Like chlorine, the biocidal species is the oxyacid hypobromous acid. The pH curve for hypobromous acid is increased approximately one pH unit, *i.e.,* the fraction of hypobromous acid present at pH 8.5 is equal to the fraction of hypochlorous acid present at pH 7.5. While bromine also reacts with ammoniacal compounds to form bromamines, there is a significant difference between the biocidal activity of bromamines and chloramines. Bromamines are potent biocides, while chloramines are not. But like chlorine, bromine reacts with organic materials, whether treatment chemical or contaminants.

More recently, industrial cooling water treatment has shown the advantages of bromination over chlorination, though operating costs were reported to be significantly higher [11]. This is attributed to the cost differential between chlorine gas and AquaBrom. However, when chlorine is not an acceptable treatment method because of safety and high maintenance costs, AquaBrom has been shown to be a cost effective treatment method as compared to other available technologies.

Other combined forms of bromine, and the chemical oxidising chemicals necessary to produce available bromine residuals in water, have been evaluated as disinfection treatment alternatives. These include chlorine- or persulphate-activated bromine salts. But each of these activation methods has limitations that limit its use on a wide scale.

For these reasons, a great deal of research has been undertaken to find alternatives to the standard disinfection of water using chlorine and bromine. Various alternatives have been explored, including non-oxidising biocides and other oxidising biocides.

The chemical species used as non-oxidising biocides include; dibromo-nitrilo-propionamide ($SCN\text{-}CH_2\text{-}SCN$), glutaraldehyde ($O{=}CH(CH_2)_3CH{=}O$), quaternary

ammonium salts (alky-benzyl-dimethyl ammonium chloride ($RC_6H_5(CH_3)_3NCl$) and dioctyl-dimethyl ammonium chlorite ($((C_8H_{17})_2(CH_3)_2NCl)$), organo-sulfur compounds (sodium dimethyl-dithio-carbamate ($C_3H_6NS_2Na$), chloro-methyl-isothiazolinones (C_4H_4NOSCl and C_4H_5NOS), methylene-bis-thiocyanate ($SCN\text{-}CN_2\text{-}SCN$) tetrahydro 3,5-dimethyl-2H-1,3,5-thiadia-zone-2-thione ($C_5H_{10}N_2S_2$)) and formaldehyde (CH_2O).

This diverse collection of non-oxidising biocides is slow acting and slug-fed. They are typically added weekly to achieve a high concentration and then allowed to decrease until the next addition. This type of treatment overdoses the biocide with the intent that an effective residual remains until most of the microorganisms in the water are destroyed.

All non-oxidising biocides are metabolic toxins, meaning that they kill microorganisms only when they are active. As microorganisms spend a lot of their time dormant, non-oxidising biocides must be used at much higher concentrations and more frequently to affect a kill. In addition, microorganisms can build resistance to metabolic toxins.

Other oxidising biocides include hydrogen peroxide, ozone, and chlorine dioxide. These biocides are the only ones that are soluble as true gases. Hydrogen peroxide (10 % by volume solution) is used as a biocide because it rapidly degrades to water and oxygen. It is less effective and more expensive than chlorine. Ozone is approximately twice as powerful as chlorine at the same concentrations. It is extensively used in Europe for purifying water, but its usage is quickly decreasing. It is difficult to achieve high concentrations because of its limited solubility in water. Its reactivity is very quick, thereby not allowing a residual concentration to be maintained. If no residual concentration is present, microbes will continue to grow and cause the water quality to deteriorate in storage. Also, ozone is very expensive to buy, and to further increase efficiency, oxygen gas is required which brings on addition cost and complications. In summary, ozone is effective in clean systems, but lacks the selectivity to be effective in contaminated systems, even at high concentrations [12-14].

Chlorine dioxide's chemistry is best summarised not by its reactions, but by what it does not react with. It has a higher solubility than ozone and remains as a true gas in solution. Chlorine dioxide does not react with water nor does its chemical form or biocidal activity change with changes in pH. It can penetrate bacterial slime layers, making chlorine dioxide an excellent choice as a water disinfectant.

Chlorine dioxide is not a new chemical and has been used for almost 50 years in the United States, Europe, and Canada. Sir Humphrey Davy discovered it in 1814 when he added a strong solution of sulphuric acid to potassium chlorate. During the 1930s, chlorine dioxide was mostly used in small-scale oxidative applications. From the 1940s to the 1970s, chlorine dioxide was extensively researched for its biocidal properties and was found to be extremely effective in killing bacteria, spores, viruses, protozoa, mollusks, and algae. It was then used more commonly for its disinfectant properties rather than for its oxidising properties.

Chlorine dioxide offers some unique performance characteristics over chlorine that makes it ideal for many applications. It is much more effective as a bactericide, sporicide, and viricide than chlorine. As a bactericide, chlorine dioxide penetrates the bacteria cell walls and reacts with vital amino acids in the cycloplasm of the cells to kill the organism. Chlorine dioxide is a much stronger oxidising agent than chlorine; because of this, a smaller dosage of chlorine dioxide than chlorine should be possible for disinfection purposes [15-17]. A smaller dosage results in a lower residual. Unlike chlorine, the biocidal properties of chlorine dioxide are independent of pH, allowing it to be an effective bactericide over a wide pH range [18-20]. The use of chlorine dioxide reduces contact 3 to 10 times over chlorine while being effective over a wide pH range.

Because chlorine dioxide is a true gas and soluble in virtually anything, including most hydrocarbons and emulsions, it can efficiently penetrate bacterial slime layers (biofilm). Its ability to disperse a biomass is thought to be a result of its reaction with polysaccharide matrix (glycocalyx) that some organisms produce exocellularly and use to attach to surfaces [21-32]. Also, when reacted, chlorine dioxide reduces to the chlorite ion, which sits in any remaining biofilm. When the biofilm starts to grow, an acidic environment exists which converts the chlorite ion back to chlorine dioxide, resulting in delayed action kill of any remaining biofilm.

The reactions of chlorine dioxide with various classes of organic materials differ substantially from those of chlorine [33-38]. In particular, chlorine dioxide does not react with trihalomethane (THM) precursors, such as ammonia and humic, and fulvic acids, which are serious problems associated with chlorine, ozone and bromine compounds [39-41]. Chorine dioxide reacts with these substances primarily by oxidation, making them nonreactive or unavailable for THM formation.

By the mid 1980s, there were an estimated 200 to 300 chlorine dioxide applications for potable water treatment in the USA, and over a thousand applications in Europe [42]. Today, chlorine dioxide appears to be the most suitable treatment technology for disinfection and other treatment applications. Chlorine dioxide is being used increasingly to control microbiological growth in a number of industries, including the dairy industry [43-45], the beverage industry [46], the fruit and vegetable processing industries [47-50], various canning plants [51,52], the poultry industry [53-62], the beef processing industry [63], and miscellaneous food processing applications [64-68].

Chlorine dioxide is also used as a bleaching agent (approximately 2.5 times more powerful than chlorine) in the pulp and paper industry [69-73]. It is the chemical of choice because it produces a brighter, stronger fibre than when using chlorine, and does not form environmentally harmful chlorinated by-products, such as dioxins. Dioxins formed by use of chlorine in the pulp bleaching process can destroy the aquatic population in many rivers and streams. It is interesting to note that in the pulp and paper industry, which is by far the greatest user of chlorine dioxide, total replacement of chlorine by chlorine dioxide in the pulp bleaching process has been shown to produce an effluent which is essentially free of chlorinated dioxins and furans [74-78]. It was reported that dioxin emissions in the Great Lakes have declined by 96 % and attributed this decline to replacement of chlorine with chlorine dioxide in the bleaching process [79]. The EPA recommends elimination of the use of chlorine and replacement with chlorine dioxide.

Chlorine dioxide is seeing increased use in municipal potable water treatment facilities [80-84] and in industrial waste treatment facilities [85-90] because of its selectivity towards specific environmentally-objectionable waste materials, including phenols sulphides, cyanides, thiosulphates, and mercaptans [91]. It is being used in the oil and gas industry for downhole applications as well as stimulation enhancement additives [92]. Chlorine dioxide is also being applied to medical waste treatment. Despite the many advantages of chlorine dioxide, relatively few heavy industrial plants have made the switch to chorine dioxide for their cooling systems [93-101]. Today, municipal and industrial applications in the USA are estimated in the thousands. Details on some specific applications are described in Appendix E.

1.2 Chlorine Dioxide Generation

Chlorine dioxide has many different uses in water treatment. Among these are disinfection, bleaching, and chemical oxidation. The chlorine dioxide used in these

applications is always generated on-site. It is a gas whose physical properties make it unstable in nature (see Appendix B). Because of safety reasons, regulations prevent chlorine dioxide from being shipped and stored [102]. Chlorine dioxide must therefore be generated on-site in specially developed processes. Most small-scale generators use sodium chlorite as their precursor chemical.

There are three commercial methods of generating chlorine dioxide from sodium chlorite. The three feed chemical combinations include; 1) chlorine-sodium chlorite, 2) acid-sodium hypochlorite-sodium chlorite, and 3) acid-sodium chlorite.

The chlorine-chlorite method is the most flexible and efficient method of generating chlorine dioxide. Chlorine (Cl_2) reacts with water to form hypochlorous acid (HOCl) and hydrochloric acid (HCl). These acids then react with sodium chlorite ($NaClO_2$) to form chlorine dioxide (ClO_2) and sodium chloride (NaCl):

$$2\,NaClO_2 + Cl_2 \rightarrow 2\,ClO_2 + 2\,NaCl \qquad (1.5)$$

The acid-sodium hypochlorite-sodium chlorite method is an alternate method used when chlorine gas is not available. Sodium hypochlorite (NaOCl) is combined with HCl (or another mineral acid) to produce HOCl. $NaClO_2$ is the added to this reaction mixture to produce ClO_2. The net reaction is;

$$2\,NaClO_2 + NaOCl + 2\,HCl \rightarrow 2\,ClO_2 + 3\,NaCl + H_2O \qquad (1.6)$$

The chemistries in reactions (1.5) and (1.6) were due to the pioneering efforts of J.F. Synan, J.D. MacMahon, and J.P. Vincent [103] of Mathieson Chemical Company, now Olin Corporation (Norwalk, CT).

The acid-chlorite method is the simplest and easiest method to generate chlorine dioxide. Sodium chlorite reacts with a mineral acid, such as hydrochloric, sulphuric, and phosphoric acids, or with an organic acid, such as acetic, formic, and oxalic acids. Chlorine dioxide, sodium chloride, and sodium chlorate are produced in variable proportions. Several stoichiometries have been reported for acid-chlorite reaction [104], but the confusion that exists is to whether the chemistry is best described using chlorous acid ($HClO_2$) or chlorite ion (ClO_2^-). The most widely accepted stoichiometries are:

$$4\,NaClO_2 + H_2SO_4 \rightarrow 2\,ClO_2 + NaCl + NaClO_3 + Na_2SO_4 + H_2O \qquad (1.7)$$

$$5\,NaClO_2 + 4\,HCl \rightarrow 4\,ClO_2 + 5\,NaCl + 2\,H_2O \quad (1.8)$$

In the absence of chloride ions, chlorate and chloride species are formed as by-products. In the presence of chloride, only chloride species is formed as a by-product. At low chloride concentrations however, another reaction is possible:

$$3\,NaClO_2 \rightarrow 2\,NaClO_3 + NaCl \quad (1.9)$$

Reaction (1.9) does not yield chlorine dioxide and may be responsible for the observed inhibition effect of chloride at low acidities.

All of the acid reactions show that not all of the starting material produces chlorine dioxide. For example, the stoichiometry of reaction (1.8) shows that 20 % of the sodium chlorite does not produce chlorine dioxide, meaning that when all of the chlorite ions are consumed, only 80 % is converted to chlorine dioxide. In this case, high conversion efficiency does not result in a high yield.

The mixing of the reactants is typically done by two methods. One method uses positive displacement pumps to push the reactants together, while the other uses an eductor to pull the reactants together. These methods are reliable and can be efficient but for continuous high efficiency, low by-products, low residual chlorine and acid operation they require attention. In applications where the capacity changes frequently, they are difficult to monitor for yield, efficiency, and product purity.

All of the reactions require an excess of chlorine or mineral acid to maximise sodium chlorite conversion. The amount of excess is dependent upon the design and can be very high. The excess of Cl_2 in reaction (1.5) is a function of the generator efficiency and may range from 5 to 20 % above the stoichiometric amount. The excess of mineral acid in reaction (1.8) is on the order of 375 % above the stoichiometric amount.

In summary, the control and proportioning of two and three reactants in these systems is difficult. The final composition is dependent on several variables, including sodium chlorite concentration, purity of sodium chlorite used, acid concentration, pH of the reaction mixture, reaction time, and temperature of reaction. If not carefully monitored, it can cause unreacted chlorite or excessive amounts of chlorine leaving the system. This can lead to the formation of sodium chlorate via other side reactions or to the formation of chlorine related disinfection by-products in the finished water. Also, both chlorine and

mineral acids are highly corrosive and aggressive control measures must be implemented to prevent or minimise exposure to the worker. Everyone's primary goal when working with hazardous materials is to minimise the risk to people's heath, to facilities, and to the environment. The secondary goal is to understand how to monitor and safely handle the hazardous materials.

There are now some new approaches to generating chlorine dioxide, using an electrochemical method for the oxidative process. They employ the use of only one reactant, sodium chlorite, and eliminate the hazards of using chlorine and concentrated mineral acids. There are basically two types that are now in existence. One type replies on the electrolysis of chlorite ions on the surface of an anode, where the other relies on the generation of acid by the electrolysis of water.

A typical chlorite electrolysis process for producing chlorine dioxide from sodium chlorite operates as follows. In a two-compartment module, consisting of an anode and a cathode compartments and a cation exchange membrane located between the two compartments, sodium chlorite solution is passed through the anode compartment. A transverse DC electric field is imposed by an external power supply by the electrodes. Chlorite ions are converted to chlorine dioxide at the anode, and sodium ions pass through a cation membrane and into the adjacent cathode compartment, where they combined with hydroxyl ions, which are generated at the cathode with hydrogen gas by the reduction of water, to form sodium hydroxide. Sodium hydroxide and hydrogen gas are discharged from the cathode compartment, where the hydrogen gas is typically separated and vented.

As with all chlorite electrolysis processes, it is difficult to control the reactions on the anode. Some of the earlier improvements to control the chlorine dioxide reaction included:

- Specialised Coatings [105-107]: Specialised coatings on the anode surface allow for an enhanced generation of chlorine dioxide via a catalytic mechanism.
- Porous Anodes [108-112]: Porous or flow-through type anodes provide high surface area and a more uniform potential over the entire anode compartment.
- Modified Ion Exchange Materials [113-116]: Cation exchange resins are modified whereby counter ions are permanently attached to a portion of its ion exchange sites, creating semiconductor junctions. When subjected to an electrical potential, these

semiconductor junctions act as *'mini electrodes'* where the oxidation of chlorite ions to chlorine dioxide occurs. The remaining unmodified ion exchange sites serve as transfer sites for the sodium ions.

Although there are improvements seen with these approaches, they do not fully prevent the generation of undesirable side reactions. In particular, it is difficult to prevent further oxidation of ClO_2 to chlorate ions (ClO_3^-) and possibly perchlorate ions (ClO_4^-) as it decomposes in the anolyte:

$$ClO_2 + H_2O \leftrightarrow ClO_3^- + 2H^+ + e^- \quad (1.11)$$

$$ClO_3^- + H_2O \leftrightarrow ClO_4^- + 2H^+ + 2e^- \quad (1.12)$$

Typically, as the pH of the solution containing the chlorite ion increases, the chemistry favours the further oxidation of chlorine dioxide to chlorate ions. Therefore, it is therefore advantageous when oxidising chlorite ion to keep the pH low and to keep the ClO_2 away from the anode, where the oxidation is not easily controlled. Later improvements were developed which included:

- Specialised Flow Patterns [117]: The sodium chlorite feedstock enters the anode compartment through the flow gap region between the membrane and porous anode, flows through the anode where it is converted to chlorine dioxide, and exits the anode compartment on the backside of the anode. This specialised flow pattern minimises the contact between the generated chlorine dioxide and membrane so that the generation of undesirable by-products is reduced.
- Hydrophobic Gas Pore Membrane [118]: The hydrophobic gas pore membrane separates chorine dioxide and water vapour from the anolyte solution, which contains many of the oxychlorine species from the undesirable side reactions listed above. The depleted solution then returns to the electrochemical oxidation cell and is further fortified with sodium chlorite feed. The accumulated products from the undesirable side reactions are purged periodically from the circuit.

Extracting ClO_2 from the anode prevents further oxidation of ClO_2. Efficient ClO_2 extraction helps to increase the conversion efficiency by enabling unused chlorite ion to be recycled. Several methods for extracting ClO_2 from the reactor chamber have been

developed, including membrane distillation (perstraction), gas eductors/venturis, and low-pressure airflow over a packed bed.

Perstraction uses a gas-permeable hydrophobic membrane to separate a donor solution (anolyte) from an acceptor solution (water). The pressure gradient across the membrane is controlled such that ClO_2 can be extracted from the chemically complicated anolyte stream to a flowing water stream. Conventional stripping devices cannot match the high purity level achieved by perstraction.

Perstraction is mostly used with electrochemical processes, but may be used with all ClO_2 generation processes. However, when these methods are employed with electrochemical processes, acid and possibility chlorine can be formed, misted, and extracted with the ClO_2. Also, efficient long-term operation will require periodic cleaning to remove accumulation of impurities on the electrode surfaces.

All of the improvements and modifications made to chlorite electrolysis systems improved yield, efficiency, and product purity. However, many of them have limitations that preclude their general acceptance and adaptability in many applications.

The second method to electrochemically produce chorine dioxide from sodium chlorite involves the generation of acid by the electrolysis of water. A typical electrochemical acidification cell consists of three-compartments, an anode compartment, a cathode compartment, and a centre compartment located between the anode and cathode compartments. Two cation exchange membranes separate the compartments. Sodium chlorite solution is passed through the centre compartment. Under the force of a transverse DC electric field, water is oxidised at the anode to generate hydrogen ions. The hydrogen ions pass from the anode compartment, through a cation membrane and into the centre compartment to displace sodium ions and react with chlorite ions to produce chlorine dioxide. Sodium ions pass through the cation exchange membrane and into the cathode compartment, where they combined with hydroxyl ions, which are generated at the cathode with hydrogen gas by the reduction of water, to form sodium hydroxide. Sodium hydroxide and hydrogen gases are discharged from the cathode compartment, where the hydrogen gas is typically separated and vented.

The electrochemical acidification process has a major advantage, namely chloride ion is the only byproduct. Since there is no contact with the anode, there is no mechanism for generating chlorine or chlorate ions. However, it has some limitations in its operation.

Cation exchange resin is used in the centre compartment. They serve as a mediator, which can exchange and absorb sodium ions and release hydrogen ions. The hydrogen ions generated at the anode thus regenerate the resin to the hydrogen form, releasing sodium ions to pass into the cathode compartment. All ion exchange resins are susceptible to oxidation. Since chlorine dioxide is a strong oxidation chemical, the cation resin will degrade. The rate at which it degrades is a function of the oxidative strength of the sodium chlorite/chlorine dioxide solution and contact time, and its rate increases with increasing temperature. The level of decomposition products released by the cation resin is a concern since the decomposition products may potentially add organic and inorganic impurities into the chlorine dioxide solution. The physical properties of the cation resin, such as moisture content, are also affected by resin degradation. The loss of physical properties will result in an increase in pressure drop through the compartment, decrease in voltage, and breakage of resin. Also, sodium salts are often added to the sodium chlorite feed to increase the efficiency of the process. Salt additives bring in undesirable ions into the product stream, thereby decreasing the purity of the chlorine dioxide produced.

Figure 1.1 shows a process that addresses some of the limitations of the electrochemical acidification process. This process will be the focus of this study and utilises the chemistry in equation (1.8). In this scheme, an electrochemical acidification cell is integrated with a fixed-bed catalytic reactor for the generation of chlorine dioxide. The electrochemical acidification cell consists of three-compartment cell and two cation-permeable membranes separating the compartments. One end compartment contains an anode while the other a cathode. All three compartments are filled with cation exchange resin.

Sodium chloride solution is passed to the central compartment cell where sodium ions are exchanged for hydrogen ions on the cation exchange resin to form hydrochloric acid. Hydrogen ions formed in the anode compartment migrate through a cation-permeable membrane to the central compartment to displace the sodium ions. Sodium ions migrate through a further cation-permeable membrane to form sodium hydroxide with hydroxyl ions produced in the cathode compartment. The hydrochloric acid formed in the central compartment is blended with a solution of sodium chlorite and forwarded to a fixed-bed catalytic reactor.

The fixed-bed catalytic reactor contains a highly effective catalyst, whose function is to specifically catalyse the sodium chlorite and chlorine dioxide reaction, *e.g.* must catalyse

the sodium chlorite and chlorine dioxide reaction at a low over-potential and inhibit other thermodynamically preferred reactions. The preparation of the catalyst involves modifying a support particle in such a manner that an active metal oxide that exhibits good catalytic properties is attached to its surface. The active metal modifies the reaction pathway, or the nature of the activated complex, so that the reaction may proceed through an activated complex with lower activation energy.

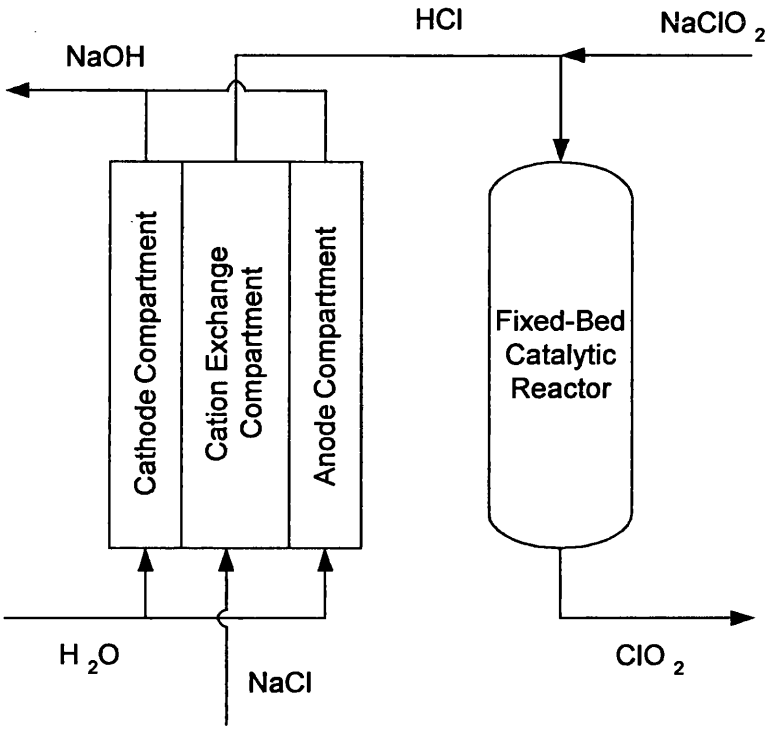

Figure 1.1 A Unique Method of Generating Chlorine Dioxide using an Electrochemical Acidification Cell and Fixed-Bed Catalytic Reactor

The cation resin used in the electrochemical acidification cell is not exposed to strong oxidising chemicals and the catalyst is optimised for producing chlorine dioxide. This will be the process characterised and modelled.

1.3 Electrochemical Acidification Cell Modelling

The ion exchange process in an electrochemical acidification cell is controlled by the kinetics of the system. The kinetic principles in conjunction with an equilibrium relationship, description of the movement of mobile ions in the liquid and resin phases, a

differential mass balance in the liquid and resin phases, and a set of initial and boundary conditions are used to model the system.

No matter how high the selectivity is in an ion exchange resin bead, it can be effective only if the ion to be removed can reach the exchange sites in the resin bead where the ion exchange occurs. An ion in the liquid must migrate across the liquid – resin interface, diffuse in the micropores of the resin phase, and reach exchange points where ion exchange reaction occurs. A stagnant film of liquid with a concentration gradient is thought to exist at the bulk liquid – resin interface, and this is known as the diffusion layer. This concentration gradient depends on the velocity pattern in the liquid near the surface of the resin bead and on the physical properties of the liquid and resin.

The rate of ion exchange is determined by the rate of diffusion of ions across the diffusion layer (film diffusion), and by the rate of diffusion of ions in the resin phase (particle diffusion). Which of these is the more important depends on conditions and the type of ion exchange resin. Film diffusion control prevails in systems with resins of high ion exchange capacity, low degree of cross-linkage, small particle size with dilute liquids and with inefficient agitation. Resins of lower cross-linkage have higher porosity and tend to have high diffusion coefficients in the resin bead, where inefficient agitation leads to large diffusion layer thicknesses. All factors with opposite tendencies favour particle diffusion control.

Ion exchange equilibrium expressions serve to represent the behaviour of an ion exchange resin in contact with a liquid. Factors that influence the selectivity of a resin of a given type include degree of cross-linkage, temperature, ionic activity in resin and liquid, ionic valance, and hydrated ionic radius. Modern theory permits semi-quantitative estimation of equilibrium constants in certain cases.

The expression for equilibrium relationships in ion exchange evolved from fitting empirical or semi-empirical equations to experimental results. The equations used were modifications of adsorption isotherms of the Langmuir or Freundlich type. The first attempt to give a quantitative expression of ion exchange equilibrium was developed from the mass-action law. The mass-action law is based on an ion exchange reaction that is a stoichiometric interchange of equivalent amounts of cations (or anions). An equilibrium constant is defined as the ratio of the activities of the cations (or anions) in the resin and liquid.

For the general expression for the exchange of two monovalent ions, the activity ratios of both ions in the resin and liquid phases are required. It is difficult to evaluate the activities, which cannot be physically measured, in both the liquid and resin phases. It is usually satisfactory to assume that the activity ratio of the two ions in the liquid is near unity, being especially valid in a dilute liquid. The activity ratio of the two ions in the resin is then combined with the equilibrium constant to yield a selectivity coefficient. Selectivity coefficients are not constant, but depend on the experimental conditions.

Mass transfer in the liquid phase requires a description of movement of mobile ions. The Nernst-Planck equation incorporating convection is one method that can be used to express ionic movement in dilute liquids. This modified Nernst-Planck equation relates the flux of an ion to gradients in electrochemical potential and momentum, resulting in diffusion, migration, and convection. Conditions of favourable equilibrium (when the counterion from the bulk liquid is preferred by the resin) and low liquid concentrations are prevalent in the electrochemical acidification process. The effects of the potential gradient on the ion fluxes are typically disregarded. Also, since the length in direction of flow is large with respect to the thickness of the compartment, the diffusion term can be neglected, having only convection responsible for the ion transport in the liquid phase.

Mass transfer in the resin phase requires a description of movement of mobile ions. Again, the Nernst-Planck equation incorporating convection can be used to express ionic movement in the resin. By virtue of electroneutrality, ion transport by convection can be disregarded, which is equivalent to saying that bulk motion of a fluid with no charge density cannot contribute to the current density. It can also be assumed that there are no concentration variations of the liquid. When these two assumptions, the transport of ions is strictly caused by the electrostatic potential whose gradient is the negative of the electric field; this is an expression of Ohm's law. Therefore, transport of charge carrying ions through the resin is expressed by using a transference number of those ions and the total current density. The product of these two terms represents the fraction of the current carried by that ion.

1.4 Fixed-Bed Catalytic Reactor Modelling

The conversion in a fixed-bed catalytic reactor is controlled by the kinetics of the system. The kinetic principles in conjunction with a molar flux rate, differential mass balance, and initial and boundary conditions are used to model the system.

In order for a conversion to take place, the reactants must transfer from the entrance of the reactor to the bed of catalyst particles. This transfer takes place by either convection and/or diffusion. The amount of reactants transported by diffusion in the axial direction is normally negligible compared with that transported by convection via the bulk liquid flow. The criteria for the 'pure convection' case can be justified if the diffusion Peclet (Pe) number is significantly greater than the ratio of reactor diameter and length. This is the case for almost all situations involving flow through fixed-bed catalytic reactors. Also, at high flow rates, radial concentration gradients are minimised, making radial diffusion negligible. Therefore, when axial and radial diffusion are negligible, the simplest description is created for the bulk liquid phase; one-dimensional plug flow.

The reactants diffuse from the bulk liquid to the surface of the catalyst particles. Mass transfer through a stagnant-film layer surrounding a catalyst particle describes this process. The concept of a stagnant-film layer is a fictitious quantity but represents a zone of defined thickness without any convection and with a sharp boundary separating it from the completely agitated solution very accurately. This mass transfer rate is calculated using the dimensionless Sherwood number, which is a function of the Reynolds (Re) and Schmidt (Sc) numbers. This quantity is dependent upon the properties of the bulk liquid and the flow conditions around the catalyst particles, as well as the size and shape of the catalyst particles.

For non-porous catalyst particles, the reactants are chemisorbed on their external surface. For porous catalyst particles, the main surface area is distributed inside the pores of the catalyst particles and the reactants diffuse through these pores in order to reach the internal surface of these particles. This diffusion is referred to as intra-particle (pore) diffusion of reactants. The reactants are then chemisorbed on the internal surface of the catalyst particle. Fickian diffusion models together with effective diffusion coefficients that account for porosity and tortuosity usually describe the diffusion through the pores. Tortuosity accounts for the complex porous structure of the catalyst particle. There are various models that are used to establish relationship between the effective diffusion coefficient and the diffusion coefficient in the absence of the matrix. Chemisorption is described through the net rate of absorption and desorption.

The chemisorbed reactants undergo surface reaction producing chemisorbed product. The surface reaction is the intrinsic kinetic rate of the chemical reaction. However, it is usual practice to group together the surface reaction step with the chemisorption steps. The global rate constant for a catalysed process combines the mass transfer across the

stagnant film surrounding each catalyst particle, the mass transfer through the porous solid, and the intrinsic kinetic rate of the chemical reaction. The global rate constant uses a dimensionless effectiveness factor to account for the pore diffusion rate in porous catalyst. The global rate constant is used because of the difficulties of separating the three steps experimentally and the ease by which they are combined mathematically in the formulation of a single kinetic rate constant.

The chemisorbed product desorbs from the surface into the liquid phase adjacent to the catalyst surface. For porous particles, it undergoes intraparticle back diffusion towards the surface of the catalyst particle. From there, the product diffuses through the stagnant-film layer and into the bulk liquid.

The non-uniformity of catalyst surfaces and lack of accurate knowledge of the structure of chemisorbed species and their concentration make if difficult to formulate an equation for the rate of reaction. The equations, or mathematical models, generally used to correlate reaction rate data fall into two broad classifications. One classification is based on a Langmuir-Hinshelwood single-site mechanism where several adsorption equilibrium constants for the catalytic site are used. These models are not generally preferred because of their large number of adjustable parameters when fitting experimental data. Also, kinetic data usually contains so much error that complicated mathematical forms like this cannot be justified. The second classification, wholly empirical, is the use of the power-law form of the rate equation, employed for homogeneous reactions. The values of the exponents on the concentrations, the apparent orders of the reactions, are determined by fitting the equation to experimental data. This approach ignores all the problems associated with adsorption, reaction, and desorption on catalytic surfaces and provides no information on how the reaction occurs. Frequently, but not always, such an equation can correlate experimental rates just as accurately, with fewer adjustable parameters, than more elaborate methods

1.5 Project Objectives

Full-scale chlorine dioxide generation systems are typically designed using data obtained from laboratory and pilot-plant operation. This design approach is system specific and evaluating the effect of system response to changes in variables can be very expensive on actual operating systems. An inexpensive approach is to derive mathematical models of the process. Validated models can be used to study the effect of different process

parameters on system response. The sensitivity of the system to perturbations on the different variables can also be tested. This is a cost-effective approach to system design.

System process models can be developed using two strategies; fundamental or 'black box' approaches. The fundamental approach is a precise and detailed model prepared from first principles using well-established and engineering expressions and approaches. Fundamental approach models are more rigorous and suitable for developing general models. The 'black box' approach is empirical relationships established from practical observations. Empirical correlations are system specific, and a model extension beyond the data studied is uncertain. To obtain a working process model, both approaches are often combined. The objectives of this thesis are:

1) To develop a working process model of the electrochemical acidification cell: The electrochemical acidification cell operating with cation exchange resin and a dilute liquid are assumed. In such case, film diffusion is the rate-limiting step. Since the system being studied here is a univalent exchange between hydrogen and sodium ions, the mass action law is used for describing the ion exchange equilibrium. A differential mass balance is performed for mobile ions in the liquid and resin phases. Due to the geometry of the compartments, only one component of current in the x-direction, transverse to the liquid flow, is assumed. It is also assumed that there is only one component of liquid flow in the y-direction. All of the derived expressions are combined with the appropriate mass balance to completely describe the electrochemical acidification cell.

2) To develop a working process model of the fixed-bed catalyst reactor: A power law model is used as the rate expression. Due to the various steps in a reaction occurring between a fluid and solid catalyst, it is difficult to determine the rate determine step since each of these steps respond in a different way to experimental variables, such as temperature, velocity, and physical structure of the catalyst. Therefore, a global rate constant is used, which incorporates film diffusion, particle diffusion and the intrinsic chemical reaction rate. A differential mass balance for the reactants to describe flow and reaction in the catalyst bed is performed. All of the derived expressions are combined with this equation to completely describe the operation of a fixed-bed catalyst reactor.

3) To study the kinetics of the electrochemical acidification cell for improving current efficiency: In the initial stage of testing, several types of cation exchange resins are

evaluated. The intent is to select the most suitable cation resin type for the experiments. A performance coefficient or figure of merit is used to make the selection. Once a cation resin is selected, an evaluation is conducted to understand the cells approach to steady state and determine the time to re-establish steady state when an operating variable is changed. The next stage of testing uses screening method to assure that the variable selected for study are the most important variables with respect to performance. The variables that are considered include feed concentration, feed temperature, linear velocity, and applied current. The last stage of testing is a detailed investigation of the operating variables that were selected to have a strong influence on current efficiency. The study consists of changing one variable at a time, while if possible, keeping the others constant. Also, model predictions are compared to the experimental data.

4) To study the kinetics of the fixed-bed catalytic reactor for improving reaction conversion: In the initial stage of testing, an evaluation is conducted to understand the steady state behaviour of the reactor. The next stage of testing uses a screening method to determine the most important variables. The variables that are considered include feed temperature, space-time, linear velocity, and particle size. The last stage of testing is a detailed investigation on the operating variables that were selected to have a strong influence on reaction yield. Several possibilities and diverse combinations are investigated. Temperature usually plays a large role in reaction kinetics, so the maximum number of experiments is performed on this single variable. The study is expanded to various combinations of temperature with other variables, such as particle size and velocity. Varying temperature, particle size and velocity so that the data covers conditions ranging from negligible to significant particle diffusion resistance is used to enable determination of the effect of particle diffusion on reaction rate and product selectivity. Also, model predictions are compared to the experimental data.

Once the objectives are achieved, a process model of a chlorine dioxide generation system is developed primarily on fundamental principles of reaction engineering and reactor hydrodynamics. This model will be useful for analysing, scaling up, designing, and optimising a chlorine dioxide reaction and reactor system. The model will also be useful in predicting performance for a wide variety of designs and operating conditions, as well as cover conditions beyond normal operation, with the intent to predict upset conditions.

References

1 Morris, J. C. (1978), *The Chemistry of Aqueous Chlorine in Relations to Water Chlorination, Water Chlorination: Environmental Impact and Health Effects, Vol. 1*, R.L. Jolley, Ed., Ann Arbor Science Publishers, Inc., 21-36, 1978

2 Report of the Carcinogenesis Bioassay of Chloroform (1976), *NTIS PB264018/AS,* National Cancer Institute.

3 Roe, F. J. C. (1976), Preliminary Report of Long-Term Tests of Chloroform in Rats, Mice and Dogs, unpublished Report. Cited in: Ozone, Chlorine Dioxide and Chloramines as alternatives to Chlorine for Disinfection of Drinking Water. Water Supply Research, Office of Research and Development, U.S. EPA, Cincinnati, OH, 1976.

4 Olin Chemical Report (1975), Treatment of Water Supplies with Chlorine Dioxide, Stamford, CT.

5 Korich, D. G., J. R. Mead, M. S. Madore, N. A. Sinclair, and C. R. Sterling (1990), 'Effects of Ozone, Chlorine Dioxide, Chlorine, and Monochloramine on Cryptospordium parum Oocyst Viability', *Appl. Environ. Microbiol.* **56** (5), 1423-1428.

6 Lorenzo-Lorenzo, M. J., M. E. Ares-Mazas, I. Villacorta-Martinez de Maturana, and D. Duran-Oreiuro (1993), 'Effects of Ultraviolet Disinfection of Drinking Water on the Viability of Cryptospordium parum Oocyst', *J. Parasitol.*, **79** (1), 67.

7 Ransome, M. E., T. N. Whitmore, and E. G. Carrington (1993), Effect of Disinfections on the Viability of Cryptospordium parum Oocyst, Water Supply, **11** 75.

8 Griffith, D. B., Mainz, E. L., and Etherington, R. E, Chlorine Dioxide as an Effective Antimicrobial Pesticide for Sanitation and Disinfection, Vulcan Chemical, Birmington, AL.

9 Geo. Clifford White (1999), H*andbook of Chlorination and Alternate Disinfection – 4th Edition*, John Wiley & Sons, New York, NY, 358.

10 Miriam Balaban, (editor) (1991), 'Desalination and Water Re-use: Proceedings of the twelfth International Symposium (Rugby, UK)', Institution of Chemical Engineers; NY, Hemisphere Publishing Corp.

11 Georges Belfort, (editor) (1984), 'Synthetic Membrane Processes: Fundamental and Water Applications', Orlando, Florida, Academic Press, New York, NY.

12 White, G. C. (1986) *Handbook of Chlorination*, Van Nostrand Reinhold Company, New York, NY.

13 Gomella, C. and P. Musquere (1980), 'Disinfection of Water by Chlorine, Ozone, and Chlorine Dioxide', *Int. Water Supply Assoc., Congr. [Proc.].*

14 Hoff, J.C. and Geldreich (1981), 'E.E., Comparison of the Biocidal Efficiency of Alternate Disinfectants', J. *Amer. Water Works Assoc.*, **73** (1), 40.

15 Tanner, R. S. (1989), 'Comparative Testing and Evaluation of Hard-Surface Biocides', *J. Ind. Microbiology*, **4**, 145.

16 Ingols, R. S., and G. M. Ridenour (1948), 'Chemical Properties of Chlorine Dioxide', *J. Amer. Water Works Assoc.*, **40**, 207.

17 Ridenour, G. M., and R. S. Ingols (1947), 'Bactericidal Properties of Chlorine Dioxide', J. *Amer. Water Works Assoc*, **39**, 561.

18 Rav-Acha, C. (1984), 'The Reactions of Chlorine Dioxide with Aquatic Organic Materials and Their Health Effects', *Water Res.*, **18** (11), 84.

19 Pacheco, A. M., H. E. Durham, R. Dhillon, and C. Edward (1989), 'The Use of Chlorine Dioxide to Control Microbiological Growth in an Ethylene Glycol Contaminated Cooling Tower. A Case History', *TP89-14, Cooling Tower Institute.*

20 Lykins, B. W., J. A. Goodrich, and J. C. Hoff (1990), 'Concerns with Using Chlorine Dioxide Disinfection in the USA', *Aqua (London),* **39** (6), 376.

21 Bernarde, M. A., B. M. Israel, V. P. Olivieri, and M. L. Granstrom (1965), 'Efficiency of Chlorine Dioxide as a Bactericide', *Appl. Microbiol*, **13**, 776.

22 Sussman, S., and W. J. Ward (1977), Microbiological Control with Chlorine Dioxide Helps Save Energy, Mater. Perform., **16** (7), 24.

23 Ward, W. J., J. W. Lee, and S. G. Freymark (1978), 'Advantages of Chlorine Dioxide as a Biocide', *Ammonia Plant Saf.*, **20**, 64.

24 McGuire, L., and T. Dishinger (1984), 'Chlorine Dioxide Solves Biofouling Problems in a Refinery Cooling Tower Used for Phenol Destruction', *TP 84-06, Cooling Tower Institute*, Houston, TX.

25 Rauh, J. S. (1976), 'Chlorine Dioxide. A Cooling Water Microbiocide', *Proc. Annu. Ind. Pollut. Conf. Water Wastewater Equip. Manuf. Assoc.* McLean, VA.

26 Mayack, L. A., R. J. Soracco, E. W. Wilde, and D. H. Pope (1984), 'Comparative Effectiveness of Chlorine and Chlorine Dioxide Regimes for Biofouling Control', *Water Res.*, **18** (5), 593.

27 Pacheco, A. M., H. E. Durham, R. Dhillon, and C. Edward (1989), 'The Use of Chlorine Dioxide to Control Microbiological Growth in an Ethylene Glycol Contaminated Cooling Tower. A Case History', *TP89-14, Cooling Tower Institute.*

28 Walker, G. S., F. P. Lee, and E. M. Aieta (1986), 'Chlorine Dioxide, Treatment for the Control of Taste and Odor', *J. Amer. Water Works Assoc*, **78** (3), 84.

29 Kemp, P. J. and N. Okimoto (1982), 'Subtoxic Chlorine Dioxide Treatment to Prevent Fouling in Once Through Sea Water Cooled Surface Condensers', *Proc. Int. Water Conf.*

30 Simpson, G. D. (1993), 'Use of Chlorine Dioxide to Clean Small Diameter High Efficiency PVC Film Fill', *Presented at the Cooling Tower Institute, New Orleans, LA.*

31 Simpson, G. D., G. D. Laxton, R. F. Miller, and W. R. Clements (1993), 'A Focus on Chlorine Dioxide: Biocide of Choice for 'Stressed' Cooling Water Systems', *Presented at WaterTech 93, Houston, TX.*

32 Kemp, P. J. and N. Okimoto (1982), 'Subtoxic Chlorine Dioxide Treatment to Prevent Fouling in Once Through Sea Water Cooled Surface Condensers', *Proc. Int. Water Conf.*

33 Sussman, S., and W. J. Ward (1977), 'Microbiological Control with Chlorine Dioxide Helps Save Energy', *Mater. Perform.*, **16** (7), 24.

34 Walker, G. S., F. P. Lee, and E. M. Aieta (1986), 'Chlorine Dioxide, Treatment for the Control of Taste and Odor', *J. Amer. Water Works Assoc*, **78** (3), 84.

35 Kemp, P. J. and N. Okimoto (1982), 'Subtoxic Chlorine Dioxide Treatment to Prevent Fouling in Once Through Sea Water Cooled Surface Condensers', *Proc. Int. Water Conf.*

36 Rauh, J. S. (1979), 'Disinfection and Oxidation of Wastes by Chlorine Dioxide', J. *Environ. Sci.*, **22** (2), 42.

37 Lykins, B. W., J. A. Goodrich, and J. C. Hoff (1990), 'Concerns with Using Chlorine Dioxide Disinfection in the USA', *Aqua (London),* **39** (6), 376.

38 Freymark, S. G., and J. S. Rauh (1978), 'Selective Oxidation of Industrial Wastewater Contaminants by Chlorine Dioxide', *Mid. Atl. Ind. Waste Conf., [Proc.]*, **10**, 120.

39 Ward, W. J., J. W. Lee, and S. G. Freymark (1978), 'Advantages of Chlorine Dioxide as a Biocide', *Ammonia Plant Saf.*, **20**, 64.

40 Ward, W., J. W. Lee, and S. G. Freymark (1977), 'Chlorine vs. Chlorine Dioxide for Ammonia Plant Bio Control', *Presented at Symposium on Safety in Ammonia Plants, AIChE.*

41 White, C. (1972), *Handbook of Chlorination*, Van Nostrand Reinhold Company, New York, NY, Chapt. 11.

42 Aieta, E. M., and J. D. Berg (1986), 'A Review of Chlorine Dioxide in Drinking Water Treatment', *J. Amer. Water Works Assoc.*, **78**, 62.

43 Drechsler, P. A., E. E. Wildman, and J. W. Pankey (1990), 'Evaluation of a Chlorous Acid-Chlorine Dioxide Teat Dip Under Experimental and Natural Exposure Conditions', *J. Dairy Sci.*, **73**, 2121.

44 Oliver, S. P., S. H. King, P. M. Torre, E. P. Shull, H. H. Dowlen, M. J. Lewis, and L. M. Sordillo (1989), 'Prevention of Bovine Mastitis by a Postmilking Teat Disinfectant Containing Chlorous Acid and Chlorine Dioxide in a Soluble Polymer Gel', *J. Dairy Sci.*, **72**, 3091.

45 Poutrel, R., F. Serieys, and M. Ducelliez (1990), 'Efficacy of a Germicidal Post Milking Barrier-Type Teat Dip in Preventing Intramamary Infections, Vet. Rec.', *J. Br. Vet. Assoc.*, **126**, 638.

46 Mir, Z. (1984), 'Chlorine Dioxide as a Sanitizer for Carbon Filters', *Beverage World*, **187**.

47 Anon, B. (1977), 'Chlorine Dioxide Gains Favour as Effective Sanitizer', *Food Eng.*, **143**.

48 Costilow, R. N., M. A. Uebersax, and P. J. Ward (1984), 'Use of Chlorine Dioxide for Controlling Microorganisms During the Handling and Storage of Fresh Cucumbers', *J. Food Sci.*, **49**, 296.

49 Roberts, R. G., and S. T. Reymond (1989), Evaluation of Post-Harvest Treatments for Eradication of Erwinia Amylovora From Apple Fruit, *Crop Prot.*, **8**, 283.

50 Synan, J. F. (1979), 'Chlorine Dioxide - An Effective Biocide for Recycled or Reused Water Systems', *Trans. Citrus Eng. Conf.*, **25**, 66.

51 Ito, K. A., and M. L. Seeger (1980), 'Effects of Germicides on Microorganisms in Can Cooling Waters', *J. Food Prod.*, **43**, 484.

52 Welch, J. L., and J. F. Folinazzon (1958), 'Use of Chlorine Dioxide for Cannery Sanitation and Water Conservation', *Food Tech.*, **179**.

53 Baran, W. L., L. E. Dawson, and R. V. Lechowich (1973), 'Influence of Chlorine Dioxide Water Treatment on Numbers of Bacteria Associated with Processed Turkey', *Poultry Sci.*, **52**, 1053.

54 Blankenship, R. (1986), 'Reduction of Spoilage, Pathogenic Bacteria', *Broiler Industry*, **24**.

55 Dougherty, T. J. (1974), 'Salmonella Contamination in a Commercial Poulty (Broiler) Processing Operation', *Poultry Science*, **53**, 814.

56 Lillard, H. S. (1979), 'Levels of Chlorine and Chlorine Dioxide of Equivalent Bactericidal Effect in Poultry Processing Water', *J. Food Sci.*, **44**, 1594.

57 Lillard, H. S. (1980), 'Control of pH in Generating Chlorine Dioxide for Bactericidal Use in Poultry Processing Water', *J. Food Sci.*, **45**, 154.

58 Lillard, H. S. (1980), 'Effect on Broiler Carcasses and Water of Treating Chiller Water with Chlorine or Chlorine Dioxide', *Poultry Sci.*, **59**, 1761.

59 Patterson, P. H., S. C. Ricke, M. L. Sunde, and D. M. Shaeffer (1990), Hatching Eggs Sanitized with Chlorine Dioxide Foam... Egg Hatchability and Bactericidal Properties', *Avian Diseases*, **34**, 1.

60 Robinson, D., G. C. Mead, and K. A. (1981), 'Barnes, Detection of Chloroform in the Tissues of Freshly Eviscerated Poultry Carcasses Exposed to Water Containing Added Chlorine or Chlorine Dioxide, Bull', *Environm. Contam. Toxicol.*, **27**, 145.

61 Thiessen, G. P., W. R. Usbome, and H. L. Orr (1984), 'The Efficacy of Chlorine Dioxide in Controlling Salmondla Contamination and Its Effect on Product Quality of Chicken Broiler Carcasses', *Poultry Sci.*, **63**, 647.

62 Villarreal, M. E., R. C. Baker, and J. M. Regenstein (1990), 'The Incidence of Salmonella on Poultry Carcasses Following the Use of Slow Release Chlorine Dioxide (Alcide)', *J. Food Prot.*, **53**, 465.

63 Emswiler, B. S., A. W. Kotula, and D. K. Rough (1976), 'Bacterial Effectiveness of Three Chlorine Sources Used in Beef Carcass Washing', *J. Anim. Sci.*, **42**, 1445.

64 Frazer, A. C., I. R. Hickman, H. G. Sammons, and M. J. Sharratt (1956), 'Studies on the Effects of Treatment with Chlorine Dioxide on the Properties of Wheat Flour. III. Lipid Changes and Vitamin Content of Treated Flours', *J. Sci., Food Agric.*, **375**.

65 Fukayama, M. Y., H. Tan, W. B. Wheeler, and C. I. Wei (1986), 'Reactions of Aqueous Chlorine And Chlorine Dioxide with Model Food Compounds', *Environmental Health Perspectives*, **69**, 267.

66 Krysinski, E. P., L. J. Brown, and T. J. Marchisello (1992), 'Effect of Cleaners and Sanitizers on Listeria Monocytogenes Attached to Product Contact Surfaces', *J. Food Prot.*, **55**.

67 Meredith, P., H. G. Sammons, and A. C. Frazer (1956), 'Studies on the Effects of Treatment with Chlorine Dioxide on the Properties of Wheat Flour. I. The Chemical Composition of Protein of Treated Flours', *J. Sci. Food Agric.*, **7**, 361.

68 Wei, C. I., D. L. Cook, and J. R. Kirk (1985), 'Use of Chlorine Compounds in the Food Industry', *Food Technology*, **39**, 107.

69 Gray, J., and P. Axegard (1984), 'Chlorine Dioxide Systems Can Be a Key to Reducing Bleaching Costs', *Pulp & Paper*, **64**.

70 Nelson, T. R. (1982), 'Appleton Papers Finds Chlorine Dioxide to be an Alternative to Conventional Biocides in Alkaline Systems', *TAPPI J.*, **65** (6), 69.

71 Nelson, T. R. (1982), 'Chlorine Dioxide: An Alternative to Conventional Biocides in Alkaline Systems', Paper presented at the Annul. Meet. - Tech. Assoc. Pulp Pap. Ind., **261**.

72 Balcer, E. R. (1981), 'Using Chlorine Dioxide for Slime Control in Alkcaline Paper Machine Systems', *TAPPI J.*, **648**, 91.

73 Baker, E. R. (1980), 'Chlorine Dioxide Proves an Effective Biocide in Alkaline Whitewater Systems', *Pulp and Paper*, **54** (8), 140.

74 Johnson, D., J. Concle, S. Hashimoto, and M. Minday (1993), 'Simpson Tacoma Kraft Operates Dioxin-Free with High Percentage ClO_2 Substitution', *J. of Technical Association for the Worldwide Pulp, Paper and Converting Industry (TAPPI)*, **76** (3), 89.

75 Rapson, H. (1989), 'Dioxin: Perceived Problem Yields Real Improvements', *Paper Industry Management Association (PIMA)*, **35**.

76 Pryke, D. (1989), 'Substituting Chlorine Dioxide for Chlorine', *J. of Technical Association for the Worldwide Pulp, Paper and Converting Industry (TAPPI)*, **147**.

77 Hise, R. (1992), 'Process Changes to Lower the Formation of Dioxins and Chlorinated Organics During Chemical Pulp Bleaching', *J. of Technical Association for the Worldwide Pulp, Paper and Converting Industry (TAPPI)*, 1992 Bleach Plant Operations Short Course, **201**.

78 Pryke, D. (1994), 'ClO_2 - Strong Performer, Bright Future', *Paper Age*, 18.

79 Hess, G. (1995), 'Dioxin Releases are Down', *Chem. Mark. Rep.*, **248** (15), 20.

80 Lykins, B. W., and M. H. Griese (1986), 'Using Chlorine Dioxide for Trihalomethane Control', *J. Amer. Water Works Assoc.*, **78** (6), 88.

81 Monscvitz, J. T., and D. J. Rexing (1981), 'A Pilot Study of Chlorine Dioxide Use to Reduce Total Trihalomethanes', *J. Amer. Water Works Assoc.*, **94.**

82 Myers, G. L., and A. L. Thompson (1986), 'Controlling Taste and Odor with Chlorine Dioxide', *SW & Texas WWJ*, 4.

83 Myers, G. L., A. Thompson, D. M. Owen, and J. M. Baker (1986), *Control of Trihalomethanes and Taste and Odor at Galveston County Water Authority*, Paper presented at American Water Works Assn, 1986 Annual Conference, Denver, Co.

84 Ringer, W. C., and S. J. Campbell (1955), 'Use of Chlorine Dioxide for Algae Control at Philadelphia', *J. Amer. Water Works Assoc.*, **47**, 740.

85 Berg, J. D., E. M. Aieta, P. V. Roberts, and R. C. Cooper (1979), *Effectiveness of Chlorine Dioxide as a Wastewater Disinfectant, in Progress in Wastewater Disinfection Technology*, A. Venosa, Ed., EPA-600/9-79-018. EPA, Cincinnati, OH.

86 Lauer, W. C., S. R. Lohman, and S. E. Rogers (1986), 'Experience With Chlorine Dioxide at Denver's Reuse Plant', *J. Amer. Water Works Assoc.*, **78** (6), 79.

87 Rauh, J. S. (1979), 'Disinfection and Oxidation of Wastes by Chlorine Dioxide', *J. Environ. Sci.*, **22** (2), 42.

88 Roberts, P. V., E. M. Aieta, J. D. Berg, and B. M. Chow (1981), *Chlorine Dioxide for Wastewater Disinfection: A Feasibility Evaluation*, EPA-600/2-81.

89 Tifft, E. C., P. E. Moffa, S. L. Richardson, and R. I. Field (1977), 'Enhancement of High-Rate Disinfection by Sequential Addition of Chlorine and Chlorine Dioxide', *J. Water Pollut. Control Fed*, **49** (7), 1652.

90 Wajon, J. E., D. J. Rosenblatt, and E. P. Burrows (1982), 'Oxidation of Phenol and Hydroquinone by Chlorine Dioxide', *Environ. Sci. Technol.*, **16** (7), 396.

91 Freymark, S. G., and J. S. Rauh (1978), 'Selective Oxidation of Industrial Wastewater Contaminants by Chlorine Dioxide', *Mid. Atl. Ind. Waste Conf., [Proc.]*, **10**, 120.

92 McCafferty, J. F., E. W. Tate, and D. A. Williams (1990), *Field Performance in the Practical Application of Chlorine Dioxide as a Stimulation Enhancement Fluid*, paper No. SPE 20626, presented at the 65th Annual Technical Conference and Exhibition of the Society of Petroleum Engineers, New Orleans, LA.

93 Sussman, S., and W. J. Ward (1979), 'Chlorine Dioxide is an Attractive Treatment Alterative', *W & SW*, 120.

94 Sussman, S., and W. J. Ward (1979), 'Microbiological Control with Chlorine Dioxide Helps Save Energy', *MP*, **16** (7), 24.

95 Vaska, M., and W. Go (1992), *Evaluation of Alternatives to Gaseous Chlorine for Cooling Water Microbiological Control, Cooling Tower Institute*, Ann. Mtg, Technical Paper No TP92-14.

96 Ward, W. J., J. W. Lee, and S. G. Freymark (1978), 'Advantages of Chlorine Dioxide as a Biocide', *Ammonia Plant Saf.*, **20**, 64.

97 McGuire L. and T. Dishinger (1984), 'Chlorine Dioxide Solves Biofouling Problems in a Refinery Cooling Tower Used for Phenol Destruction', CTI, Houston.

98 Rauh, J. S. (1976), 'Chlorine Dioxide. A Cooling Water Microbiocide,' *Proc. Annul Ind. Pollut. Conf.*, Water Wastewater Equipment Manufac. Assoc.

99 Freund, J. L., J. M. Booker Jr., and W. J. Ward (1984), *Biocontrol - Key to Heat Exchanger Efficiency in Grain Alcohol Plant*, Proc., Int. Water Conf.

100 Mayack, L. A., R. J. Soracco, E. W. Wilde, and D. H. Pope (1984), 'Comparative Effectiveness of Chlorine and Chlorine Dioxide Regimes for Biofouling Control', *Water Res.*, **18** (5), 593.

101 Pacheco, A. M., H. E. Durham, R. Dhillon, and C. Edward (1989), *The Use of Chlorine Dioxide to Control Microbiological Growth in an Ethylene Glycol Contaminated Cooling Tower. A Case History*, TP89-14, Cooling Tower Institute.

102 US CFR (Code of Federal Regulations), (49 CFR), 172.101, 1984.

103 Synan, J. F., J. D. MacMahon, and G. P. Vincent (1975), 'Chlorine Dioxide, A Development in the Treatment of Potable Water', *Water Wks. and Sew.*, **91**, 566.

104 Gordon, G., R. G. Kieffer, and D. H. Rosenblatt (1972), 'The Chemistry of Chlorine Dioxide', *Prog. Inorganic Chemistry*, S.J. Lippard, Ed., John Wiley & Sons, New York, NY, **15**.

105 Hinden, J. M., L. M. Ernes, and P. E. Visel, *Electrocatalytic Electrode*, U.S. Patents 4,517,068, May 14, 1985.

106 Beer, H. B. and D. Arnouts, *Electrode with a Platinum Metal Catalyst in Surface Film and its Use*, U.S. Patent 4,797,182, January 10, 1989.

107 Klotz, H., R. Weber, and N. Lonhoff, *Dimensionally Stable Anodes and their Use in the Preparation of Alkali Metal Dichromates and Chromic Acid*, U.S. Patent 5,128,000, July 7, 1992.

108 Cawlfield, D. W. and J. J. Kaczur, *Electrochemical Method for Producing Chlorine Dioxide Solutions*, U.S. Patent 5,041,196, August 20, 1991.

109 Kaczur, J. J. and D. W. Cawlfield, *Electrolytic Process for Producing Chlorine Dioxide*, U.S. Patent 5,084,149, January 28, 1992.

110 Cawlfield, D. W. and J. J. Kaczur, *Electrochemical Chlorine Dioxide Generator*, U.S. Patent 5,158,658, October 27, 1992.

111 Kaczur, J. J. and D. W. Cawlfield, *High Surface Area Electrode Structures for Electrochemical Processes*, U.S. Patent 5,294,319, March 15, 1994.

112 Kaczur, J. J., D. W. Cawlfield and J. F. Watson, *Process for Producing an Electrode by Electroless Deposition*, U.S. Patent 5,298,280, March 29, 1994.

113 Sampson, R. L. and A. H, Sampson, *Electrolytic Process and Apparatus for the Controlled Oxidation and Reduction of Inorganic and Organic Species in Aqueous Solutions*, U.S. Patent 5,419,816, May 30, 1995.

114 Sampson, R. L. and A. H, Sampson, *Electrolytic Process and Apparatus for the Controlled Oxidation and Reduction of Inorganic and Organic Species in Aqueous Solutions*, U.S. Patent 5,609,742, March 11, 1997.

115 Sampson, R. L. and A. H, Sampson, *Electrolytic Process and Apparatus for the Controlled Oxidation and Reduction of Inorganic and Organic Species in Aqueous Solutions*, U.S. Patent 5,705,050, January 6, 1998.

116 Sampson, R. L. and A. H, Sampson, *Modified Ion Exchange Materials*, U.S. Patent 6,024,850, February 15, 2000.

117 Lipsztajn, M., G. Cowley, and J. J. Kaczur, *Electrolytic Process for Producing Chlorine Dioxide*, U.S. Patent 6,203,688, March 20, 2001.

118 PCT Published International Patent Application WO 94/26670.

CHAPTER 2

ELECTROCHEMICAL ACIDIFICATION CELL

This chapter provides a detailed background to the electrochemical acidification cell. It describes ion exchange and electrolytic regeneration processes and some of the main principles behind their operation. A mathematical model to describe the electrochemical acidification cell is developed. The experimental arrangement is discussed, as well as the experimental methods and the methodology used to process the data for parameter estimation. Model verification and the accuracy of the models are checked by the application of experimental data.

2.1 Introduction

Adjusting the pH of an aqueous solution is one of the major impediments in any water treatment process. The addition of mineral acid is the method most commonly used to decrease solution pH. The major negative aspect to chemical addition methods is the requirement to handle acidic solutions. The use of these hazardous chemicals, such as hydrochloric, sulphuric, and nitric acids, can present many safety problems. Also, the capital requirement of bulk chemical storage can be a major impact in plants where these facilities do not currently exist.

The electrochemical acidification process is a method that can lower solution pH without the need for mineral acids. The principle of the process is the utilisation of hydrogen ions, which are generated electrochemically by the oxidation of water and a source of anions from a sodium salt solution to decrease solution pH. Cation exchange resin is used between two cation-permeable membranes to exchange sodium ions for hydrogen ions and a DC electric current to displace and remove sodium ions and replace them with hydrogen ions. The system can be considered as an ion exchange process with continuous electrolytic regeneration.

2.2 Ion Exchange

2.2.1 Principles of Ion Exchange

The most prevalent method of removing ions from water is by an ion exchange process. Water containing cations, such as sodium ions, passes through a bed of hydrogen form cation exchange resin. Sodium ions, which are in solution as a chloride and/or sulphate

salt, are attracted to and remain adsorbed on the resin. They are replaced in solution by hydrogen ions from the resin.

$$Na^+ + R_c \cdot H^+ \leftrightarrow H^+ + R_c \cdot Na^+ \qquad (2.1)$$

where R_c represents the insoluble polymeric cation exchange resin. Most of the polymer bases used for ion exchange resins are copolymers of styrene and divinylbenzene, the industrial product generally consisting of spherical particles of 14 to 50 mesh (0.03 to 0.12 cm).

When the resin has given up all or most of its available hydrogen ions, the resin is 'exhausted'. Passing a concentrated acid solution through the resin reverses the sodium removal process and 'regenerates' the resin. This inter-diffusion of ions is what is referred to as ion exchange.

The transport of ions within the ion exchange resin is through the channels in the latticework of the resin matrix. The surface of the resin particle is the interface with the surrounding solution. The ions migrate through this interface when the concentrations in the two phases are not in equilibrium. Given enough time, ionic diffusion between the resin particle and surround solution will tend to bring the two phases into balance, with no further exchange occurring.

It is the concentration differences that drive the entire ion exchange process. The concentration equilibrium can be plotted for any given system, and is greatly dependent upon the total ion concentration. An equilibrium plot for the sodium/hydrogen exchange is shown in Figure 2.1.

The solid equilibrium curves represent the affinity of the resin for sodium ions. The dotted diagonal line is the isotherm of a fictitious ion exchange resin that has no preference for either counter ion. Curve A represents the affinity of the resin for sodium ions at low total ion concentration, such as what would be present during the service cycle. The ion exchange resin easily exchanges sodium for hydrogen ions, and the sodium ion concentration in the water decreases accordingly, and the solution become more and more acidic. The accumulation of hydrogen ions in the solution impedes the ion exchange process. In Curve B, the total ion concentration has been raised, such as what would be present during the regeneration cycle. The curve appears to be nearly

flat, and the resin is seen to have a much lower affinity for sodium ions. The solution phase readily accepts sodium ions, and the sodium ion concentration in the resin decreases. The difference of equilibrium states makes it possible the repeated exhaustion and regeneration cycles of the ion exchange system.

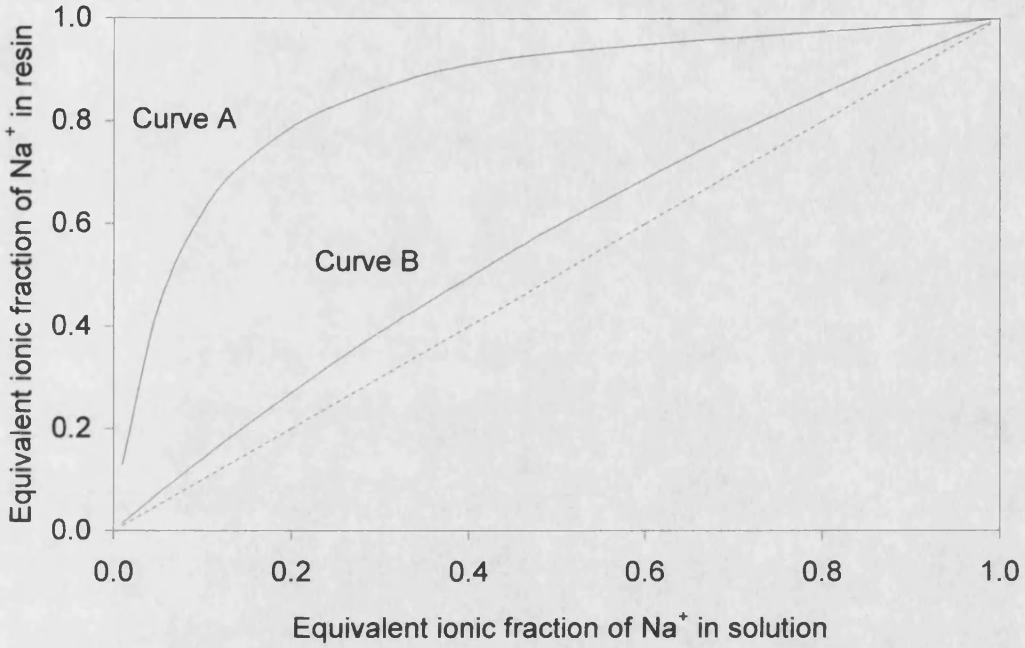

Figure 2.1 Selectivity of a Cation Exchange Resin: The diagram shows an isotherm for the Na^+/H^+ exchange on cation exchange resin. The dotted diagonal line is the isotherm of a fictitious ion exchange resin that has no preference for either counter ion

At every cross section of the resin bed, these equilibrium relationships apply. The bed can be considered as having a large number of layers, each of which is participating in the ion exchange process to a greater or lesser degree, according to the concentration equilibrium of the layer.

When untreated water flows through a regenerated resin layer, the concentration difference brings about ion exchange until the differences are balanced out and the concentrations are in equilibrium. Throughout the bed, a longitudinal concentration profile is development both in the ion exchange phase and in the water. The height or sharpness of the concentration profile varies with the flow rate. Figure 2.2 is a schematic representation of a partially charged resin bed, and the corresponding concentration profile of the ion exchange phase at one moment during the service cycle.

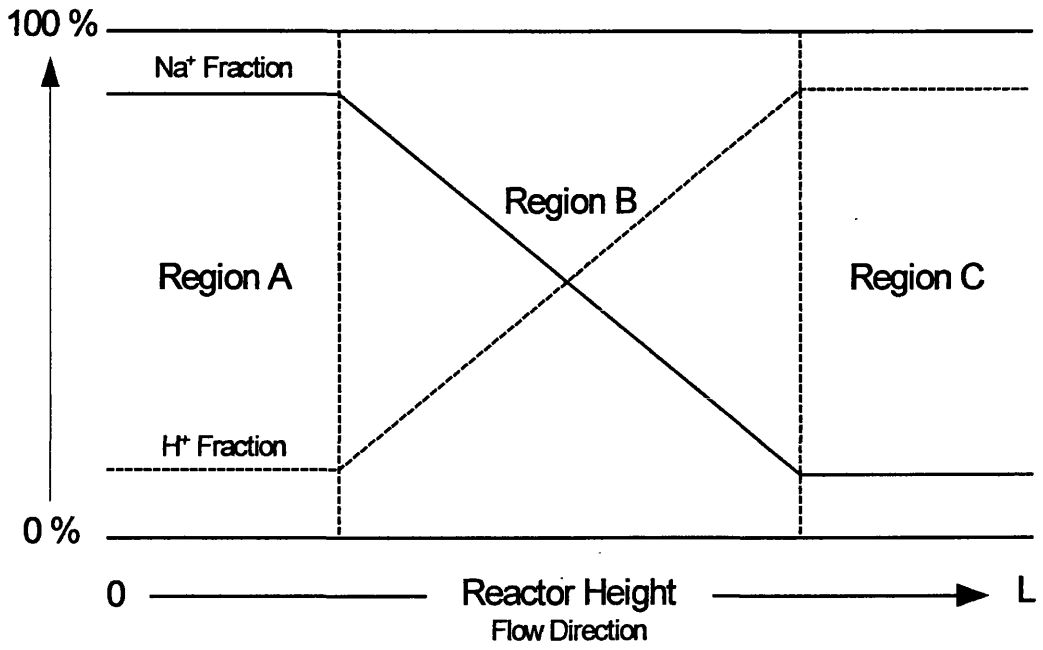

Figure 2.2 Schematic Illustration of Concentration of Na^+ and H^+ in an Ion Exchange Resin Bed During the Service Cycle

As shown in the diagram, ion exchange occurs only in region B, not in regions A or C. In region A, the resin is already fully exhausted with sodium and is therefore in equilibrium. No exchange is possible. Region C sees only acidic water; the sodium ions have been exchange with hydrogen ions as the water passed through region B. Again no exchange is possible.

At any given time, only a relatively narrow segment of the resin bed actively participates in the ion exchange process. This segment may only a few centimetres in depth, depending on the kinetics of the system, which in turn is dependent upon the flow rate, temperature, particle diameter, and overall bed depth.

The residual sodium ion concentration in the treated water is dependent entirely on the equilibrium position of the last ion exchange layer through which water flows. The better this segment is regenerated, the lower the sodium ion concentration in the product water.

The limits of an ion exchange process as described by chemical equilibrium are not always obtainable within the physical limitations of an ion exchange unit. Understanding the capability of an ion exchange process to achieve the highest performance under

specific process conditions also requires knowledge of the limits imposed by the kinetics of the process. Diffusion resistances control the kinetic of an ion exchange process.

2.2.2 Properties of Ion Exchange Resins

Ion exchange resins are materials that allow specific ionic species in an electrolytic solution to be exchanged with different ionic species of similar charge that are fixed to functional groups on the surface of the resins. The resin selectivity characteristics and the ability for ions to diffuse to the functional groups allow for the ion exchange.

Ion-exchange resins consist of small spherical particles made out of crosslinked polymer chains that are covered with chemical functional groups. The two main kinds of functional groups are anionic (positively charged) and cationic (negatively charged). Most anionic groups are amine-based, such as ammonium (Type 1) and ethanolamine (Type II). Most cationic groups are sulphonate-based, typically sulphonic acid. The charge on these functional groups is neutralised by appropriately charged free ions in the electrolyte solution, which flow through the pore structure of the resin particles and attach themselves to the oppositely charged groups.

The selectivity of the ion-exchange resin determines what fraction of functional groups is covered by the various ions. Selectivity is dependent upon the surrounding chemical environment. For low ion concentrations, the resins are more selective for ions of high valance (e.g. $Ca^{2+} < Al^{3+} < Th^{4+}$). For ions of the same valance, the resins are more selective for higher atomic number ($Li^{+} < Na^{+} < Cs^{+}$; $Mg^{2+} < Ca^{2+} < Ba^{2+}$), but the difference is much less pronounced than the case of ionic valance. As ion concentration increases, differences in selectivity become less marked, and the order is occasionally reversed [1].

The bulk of an ion-exchange particle is made of hydrocarbon polymer chains that are insoluble in water. The chemical functional groups attached to the polymer chains are what make the resin more soluble in water and allow water (electrolyte solution) to be drawn into the pore structure of the resin bead. This is crucial because the functional groups are dispersed throughout the volume of the resin particle, and the ions need to diffuse through the electrolyte solution in the pores of the particle to reach the functional groups. Divinylbenzene (DVB) crosslinks are added to the resin to hold the long polymer chains together in a bead structure. Commercial DVB contains approximately 55 % DVB, 35 % ethylvinylbenzene, and 10 % saturates, principally diethylbenzene and

naphthalene. The porosity of the resin is inversely related to the DVB crosslinking. DVB crosslinkage of 8 % is generally chosen as a standard for cation and anion exchange resins. Without crosslinks, the resin will dissolve in the electrolyte solution. Too many crosslinks will cause a particle to be too tightly bound and have a constricted pore structure, inhibiting the diffusion of ions to the functional groups.

The total resin exchange capacity is fixed and is determined by the number of chemical functional groups within the particle, however the particle size and the contents of the pores can change with different chemical environments. A resin bead behaves in a manner similar to a sponge, swelling as the internal pore structure expands and fills with fluid. Chemical species in the surrounding electrolyte solution add to the complexity of the resin swelling. Not all of the ions absorbed into the resin beads bind to functional groups. The concentration of ionic species inside the pores is proportional to the bulk ion concentration and is determined by Donnan equilibrium operating at the interface between the resin phase and the electrolyte solution phase. Osmotic forces determine the distribution of water between the two phases. The lower the electrolyte concentration, the more the resin particle will swell and vice-versa [2]. Helfferich [1] and Kunin [3] give an excellent comprehensive review of ion-exchange resins.

2.2.3 Ion Flux Expression in Bulk Liquid

The ion flux in the bulk liquid is driven by gradients in electrochemical potential and by convection. The electrochemical potential of a species *i* is defined as:

$$\mu_i = \mu_i^\circ + RT \ln a_i + z_i F \Phi \tag{2.2}$$

where μ_i° is the electrochemical potential of species *i* at an arbitrarily chosen reference state, R the universal gas constant, T the absolute temperature, a_i the liquid phase activity of species *i* relative to the reference state, z_i the valence, F Faraday's constant, and Φ the electrical potential relative to the reference state.

Electrochemical potential gradients must arise because of differences in activity and/or electrical potential. The resulting flux of species *i* in the bulk liquid, relative to bulk flow, is expressed as:

$$J_i = -\left(\frac{C_i D_i}{RT}\right) \nabla \mu_i \tag{2.3}$$

where D_i is the diffusion coefficient of species i, C_i the concentration of species i, R the universal gas constant, and T the absolute temperature. The above flux is superimposed upon the bulk liquid flow, incorporating a convection term. Therefore, the net flux of transporting ion i in the bulk liquid is:

$$J_i = -\left(\frac{C_i D_i}{RT}\right) \nabla \mu_i + C_i v \tag{2.4}$$

where v is the liquid velocity. Substituting the electrochemical potential expression into equation (2.4) yields:

$$J_i = -\frac{D_i C_i}{a_i} \nabla a_i - \left(\frac{z_i F}{RT}\right) D_i C_i \nabla \Phi + C_i v \tag{2.5}$$

The above equation is a more rigorous form of the Nernst-Planck equation [4], since it includes activity and convection. Activity is referred to as the effective or thermodynamic concentration.

2.2.4 Selectivity Coefficient

Ion exchange reactions are reversible; by contacting a resin with an excess of electrolyte, it can be entirely converted to the desired salt form:

$$B^+ + R_c \cdot A^+ \leftrightarrow A^+ + R_c \cdot B^+ \tag{2.6}$$

where A^+ and B^+ represent cations in solution and R_c the insoluble polymeric cation exchange resin. However, with a limited quantity of solution B^+ in batch contact, a reproducible equilibrium is established. This equilibrium is dependent on the proportions of A^+ and B^+ and also on the selectivity of the resin.

The equilibrium constant $K_{i/j}^{eq}$ for an ion exchange reaction is given by:

$$K_{A/B}^{eq} = \left(\frac{a_B^*}{a_A^*}\right)\left(\frac{\bar{a}_A}{\bar{a}_B}\right) \tag{2.7}$$

where a and $\bar{a}$ refer to activities at equilibrium in the thin film surrounding the resin and in the resin, respectively.

It is often satisfactory to assume that the liquid activity coefficient ratio is near unity, which is especially valid in dilute liquids. The resin-phase activity coefficient ratio is combined in the equilibrium constant to yield the following relationship:

$$K_{A/B}^{sel} = K_{A/B}^{eq}\left(\frac{\bar{\gamma}_B}{\bar{\gamma}_A}\right) = \left(\frac{C_B^*}{C_A^*}\right)\left(\frac{\bar{C}_A}{\bar{C}_B}\right) \tag{2.8}$$

where K^{sel} is the selectivity coefficient, C^* the concentration at the surface of the resin, and $\bar{C}$ the concentration in the resin.

The existing theories of ion exchange are a combination of two older and distinct theories. Bauman and Eichhorn [5] conceived a type of Donnan membrane equilibrium between each ion-exchange resin particle and the surrounding solution. The ion-exchange resin is regarded as a soluble electrolyte solution, restrained only by the network crosslinkages. At low solution concentrations in the case of cation resins, anions are completely excluded from the resin phase and *vice-versa* for anion resins. The ionic activity product of any particular electrolyte is the same within the resin as without. This theory has been extensively studied and applied to several ion exchange systems.

A second, and quite distinct, theory of equilibrium introduced by Gregor [6] bases resin selectivities on the swelling of the polymer network accompanying the incorporation of different ions. In as much as work is required to swell the resin, as in the stretching of a spring, the resin will be selective for that ion (hydrated ion) occupying the least volume. The equation is essentially that of Hooke's law. Neither of these two basic concepts has been discarded; both are realised to be contributing factors to the equilibria. A more refined treatment, the approximate validity of which has been demonstrated by Glueckauf [7] and Boyd and Soldano [8], includes both an activity coefficient term for chemical interaction and a swelling term.

All ions that leave the resin particle are replaced by an equivalent amount of the other ions, preserving electroneutrality. When an ion diffuses out of the resin into the thin film, the resin is left with a surplus charge, and another ion is taken up to compensate this surplus charge. This causes the total ion concentration to remain constant in the resin particle, irrespective of ionic composition.

Since the resin does not take up or release co-ions, the co-ion concentration (and thus the total concentration) in the thin film is constant. Therefore, an equilibrium condition exists. The total concentration of both exchanging ions in the thin film is related to the total concentration in the bulk liquid as:

$$z_i C_i = z_i C_i^* + z_j C_j^* \tag{2.9}$$

where C_i^* and C_j^* are the concentration of two exchanging ions, species *i* and *j*, in the thin film and C_i is the total concentration of species *i* in the bulk liquid.

2.2.5 Ion Exchange Kinetics

There are several processes that determine the rate at which ions are exchanged. Considering a single particle model [9], the definition of the key interfaces and resistances controlling the transport of ions is shown in Figure 2.3.

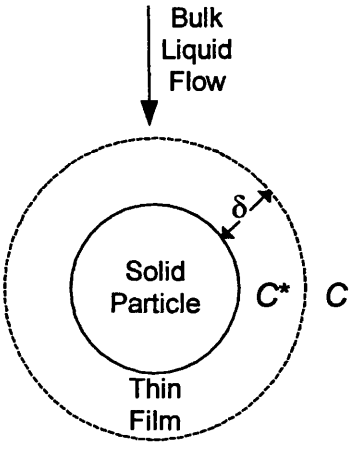

Figure 2.3 Single Particle Kinetic Model, showing the key interfaces and resistances controlling the transport of ions; δ is the thickness of the thin film layer, C is the concentration of ions in the bulk liquid, and *C**, the lower concentration limit determined by the ion exchange equilibrium.

The major steps in the ion transport process are; 1) diffusion from the bulk liquid to the thin film adhering to the surface of the resin, 2) diffusion through the thin film, and 3) diffusion within the solid particle.

The thickness of the thin film layer δ is the distance along which the concentration of ions in the bulk liquid C is constantly decreasing until at the bead surface C approaches C^*, the lower concentration limit determined by the ion exchange equilibrium.

If the resistance to mass transport is the diffusion of ions through the thin film, the overall rate of exchange will be film diffusion controlled. This mechanism suggests that a thin film adheres to the surface of the resin, and that there is no convection within this film. The thickness of the thin film controls the resistance in this step.

Since the liquid is flowing through the ion exchange bed, the bulk liquid is well agitated and local concentration gradients are minimised. The agitation assists the distribution and transport of ions within the bulk liquid. For this reason, the diffusion from the bulk liquid to the thin film surrounding the resin particle is negligible.

Once ions reach the exchange sites on the resin, the ion exchange reaction occurs very rapidly such that the concentration of ions in the thin film is much lower than that in the bulk liquid. The concentration of ions at the very surface of the resin approaches the concentration predicted from equilibrium theory.

After the ion exchange reaction has occurred, the only remaining resistance is the transport of ions within the resin particle. Agitation does not penetrate the interior of the resin, although it reduces the thickness of the thin film that adheres to the surface of a resin particle. Within the resin, ion transfer is by diffusion only, which is related to physical and chemical properties of the resin polymer and to the resin size.

Therefore, the rate-determining step in an ion exchange process is typically associated with the diffusion of ions through the thin film (film diffusion) and/or within the solid particle (particle diffusion). The rate of ion exchange is primarily determined by the slower of these two diffusion processes. Helfferich's criteria [10] can be used to determine whether film diffusion or particle diffusion controls an exchange process:

$$\frac{\overline{CD}_i \delta}{CD_i r_o}(5+2\alpha_{ij}) \;<<\; 1 \quad \text{(Particle diffusion control)}$$
$$\frac{\overline{CD}_i \delta}{CD_i r_o}(5+2\alpha_{ij}) \;>>\; 1 \quad \text{(Film diffusion control)} \tag{2.10}$$

where $\overline{C}$ is the concentration in the resin, $\overline{D}$ the resin phase diffusion coefficient, δ the thickness of the thin film adhering to the surface of the resin, C the bulk liquid concentration, D_i the liquid phase diffusion coefficient, r_o the radius of the resin particle, and α_{ij} the separation factor of the exchanging ions.

Equation (2.10) is a simple method for predicting the rate-determining step. It is valid for counter ions of equal mobility and infinite solution volume. The 'hypothetical' half times of film and particle diffusion controlled exchange are equal when $(\overline{CD}_i \delta / CD_i r_o)(5 + 2a_{ij})$ equals one. This dimensionless modulus becomes smaller than unity when particle diffusion has a longer half time, and larger than unity when film diffusion has a longer half time. The slower step determines the overall rate, thus the value of the modulus indicates whether film or particle diffusion is rate controlling.

2.2.6 Particle Diffusion Control

Concentrated liquids, large diameter resins, and high degrees of resin crosslinking all with efficient liquid agitation favour particle control. The rate of ion exchange, r_{ij}, for two ions can be approximated by the equation that describes diffusion in the interior of the ion exchange resin:

$$r_{i/j} \;=\; \overline{D}_{i/j}^{avg}\, S \frac{\partial \overline{C}_i}{\partial r_o} \tag{2.11}$$

where $\overline{D}^{avg}$ is the average diffusion coefficient in the resin, S the specific surface area of the resin particle, $\overline{C}$ the concentration in the resin, and r_o the radius. The average diffusion coefficient in the resin, $\overline{D}^{avg}$, is approximated using the individual diffusion coefficients as:

$$\overline{D}_{i/j}^{avg} \;\cong\; \frac{\overline{D}_i \overline{D}_j (z_i + z_j)}{z_i \overline{D}_i + z_j \overline{D}_j} \tag{2.12}$$

where $\overline{D}$ is the resin phase diffusion coefficient and z is the valance. The diffusion coefficient in the resin is related to the diffusion coefficient in liquid as follows [11]:

$$\overline{D}_i \cong D_i\left(\frac{\vartheta}{2-\vartheta}\right)^2 \tag{2.13}$$

where ϑ is the fractional pore volume of the ion exchange resin. The specific surface area, S, is the total resin surface area per resin volume of a spherical particle:

$$S = \left(\frac{3}{r_o}\right) \tag{2.14}$$

2.2.7 Film Diffusion Control

The concept of film diffusion control involves a thin film on the resin surface. The film represents a zone of defined thickness without any convection and with a sharp boundary separating it from the completely agitated bulk solution. As flow rate increases through the compartment, the resins cause static mixing of the bulk liquid, which increases agitation and effectively decreases the thickness of the thin film. The mass transport increases as a result of the film thickness decreasing. The rate increase will reach a limiting value, whereas an additional increase in flow rate beyond a critical flow rate will have no effect on the rate.

The diffusion coefficient and the film thickness on the resin's surface govern the rate at which ions diffuse through the thin film. Since the resin particles are close together, the diffusion through the thin film of one resin is strongly affected by the position of adjacent resins. As a result, film diffusion is difficult to predict. The classical relation involving the driving potential between the bulk liquid and the resin particle's surface can estimate the rate of ion exchange, $r_{i/j}$, for ions i and j as:

$$r_{i/j} = k_f S(C_i - C_i^*) \tag{2.15}$$

where k_f is the thin film mass transport, S the specific surface area of the resin particle, and $(C_i - C_i^*)$ the concentration difference of ion i between the two boundaries of the thin film.

Average transport coefficients between the bulk liquid and resin surface can be correlated in terms of dimensionless groups that characterise the flow condition. For film mass transport, the film mass transport coefficient, k_f, for a packed bed of particles can be determined from the Sherwood (Sh) number and mass transport factor (J_D). The Sherwood (Sh) number is an empirical function of the Reynolds (Re) and Schmidt (Sc) numbers:

$$\mathrm{Sh} = J_D \, \mathrm{Re}^{1/2} \, \mathrm{Sc}^{1/3} \tag{2.16}$$

where

$$\mathrm{Sh} = \left(\frac{k_f \, d}{D_{ij}^{avg}} \right) \tag{2.17}$$

$$\mathrm{Re} = \left(\frac{d \, v}{\upsilon} \right) \tag{2.18}$$

$$\mathrm{Sc} = \frac{\upsilon}{D_{ij}^{avg}} \tag{2.19}$$

d is the diameter of the resin particle, ε the liquid void fraction, v the bulk liquid velocity and υ the kinematic viscosity.

In mass transport systems, the mass transport factor (J_D) is known to be a function of Re in long smooth pipes. Colburn [12] proposed this empirical relationship. J_D represents a friction factor or drag coefficient. In systems in which liquid flows through a packed bed, the frictional loss is often due more to form drag than to frictional drag, therefore the Colburn's analogy may or may not be valid.

2.2.8 Hydraulic Resistance

The normal particle size distribution of ion-exchange resins is fairly broad, generally 14 to 50 mesh (0.03 to 0.12 cm). However, uniform size distributions are also available in any mesh sizes between 14 to 50. When resins are packed within a compartment, the

packing density and size of voids between the resin particles will vary depending on the compartment to be filled, as well as the size and uniformity of the particles. When non-uniform particles are used, the particles are typically packed more tightly in some areas, resulting in a variety of void sizes or volumes, with the void volumes varying within the compartment. Consequently, the liquid will travel through the loose packed areas and its flow path continuously distorted, resulting in a non-uniform flow distribution.

Cations are removed from the bulk liquid by diffusion into the resin through the thin film surrounding the resin surface (film diffusion) and in the resin surface itself (particle diffusion). The rate at which they are removed is dependent on the accessible area on the resin surface. It is advantageous to use the smallest possible resin size in order to maximise the available surface area for the ion exchange process. The smaller the resins size the greater the hydraulic resistance or pressure-drop through the compartment. Therefore, the maximum acceptable pressure drop across the compartment limits the size of the particles, which may vary depending on the compartment design.

Darcy's law predicts that for any given bed and fluid, the flow rate is proportional to the pressure drop. Ergun [13] has derived a relationship to describe the flow rate based on the concept that pressure drop across packing material is a result of both viscous and inertial forces. A consideration of flow at intermediate Reynolds numbers lead Ergun to relate a friction factor, f_p, to the flow conditions by the equation:

$$f_p = \frac{(1-\varepsilon)}{Re} K_A + K_B \qquad (2.20)$$

where ε is the liquid void fraction and K_A and K_B are the viscous and inertial parameters. The friction factor accounts for all of the frictional resistances in the packed bed, including the shear stress on the wall.

Ergun set K_A and K_B to 150 and 1.75, respectively, after consideration of the least squares of 640 experiments. However, Gupte *et al.* [14] investigated flow through a bed consisting of smooth particles. Better accuracy was found when K_A was equal to 109.5 and K_B equal to 1.2775.

With the use of the mechanical energy balance, the pressure drop $-\Delta P$ across the packed bed of resin of length L is calculated by:

$$\frac{-\Delta P}{L} = \frac{f_p v^2 \rho}{2 r_o g_c} \frac{(1-\varepsilon)}{\varepsilon^3} \tag{2.21}$$

where L is the resin bed height, v is the bulk liquid velocity, and g_c the acceleration due to gravity.

2.2.9 Liquid Void Fraction

The liquid void fraction, ε, in a rectangular compartment filled with resin particles of uniform size is dependent on the packing arrangement of the resins. If a tetragonal sphenoididal orientation is assumed as the packing arrangement of the particles, then the theoretical maximum void fraction will be 0.32. This void fraction will be valid and remain constant only if the walls of the compartment conform to this arrangement. Since they do not, a wall effect occurs whereas the void fraction at the walls of the compartment is higher than the theoretical value. The void fraction is highest at the wall of the compartment and then oscillates with decreasing amplitude towards a uniform value as the centre of the compartment is approached. This behaviour, minus the oscillations, can be described using an empirical equation of the form [15]:

$$\varepsilon = \varepsilon_o \left[1 + K_C \exp\left(\frac{-K_D W}{r_o} \right) \right] \tag{2.22}$$

where W is the compartment thickness and r_o is the radius of the resin particle.

2.2.10 Calculation of Liquid Void Fraction

Constants K_C and K_D in equation (2.22) were determined experimentally. Square compartments were machined from an acrylonitrile butadiene styrene (ABS) block. The compartments were 5.40 cm wide by 5.40 cm long and of varying thicknesses, ranging from 0.45 to 4.50 cm. Precision 316L stainless steel spheres at diameter of 0.45 cm were carefully packed into the compartments. The spheres were then removed from the compartments and loaded into a graduated cylinder filled with a precise volume of water - the graduated cylinder had volume increments of 0.20 cm^3. The spheres were allowed to

settle in the graduated cylinder. The water level in the graduated cylinder was measured. By subtracting the initial volume of water from the volume of water/spheres, the volume of the spheres in each compartment was determined. The solid fraction of the spheres in each compartment was then determined by the calculated volumes of the spheres divided by the volume of each compartment. To confirm the calculation, the spheres were also counted and the volume of spheres was determined by multiplying the number of spheres by the volume of a single sphere. The solid fraction was again determined by the calculated volumes of the spheres divided by the volume of each compartment. Results are shown in Table 2.1.

Table 2.1 Void Fraction Analysis Results, showing the relationship between compartment thickness and liquid void fraction

Compartment Thickness / cm	Thickness / Ball Diameter	Compartment Volume / cm^3	# of Balls	Solid Volume Measured / cm^3	Solid Volume Calculated / cm^3	Void Fraction
0.45	1	13.11	150	7.2	7.16	0.451
0.90	2	26.22	315	15.0	15.03	0.428
1.35	3	39.33	495	23.6	23.62	0.400
1.80	4	52.44	682	32.6	32.54	0.378
2.25	5	65.55	875	41.6	41.75	0.365
2.70	6	78.66	1,064	50.8	50.77	0.354
3.15	7	91.77	1,251	59.8	59.69	0.348
3.60	8	104.88	1,450	68.8	68.66	0.344
4.05	9	117.99	1,625	77.6	77.53	0.342
4.50	10	131.10	1,820	86.2	86.22	0.342

Table 2.1 shows that the liquid volume fraction decreases as the compartment thickness increases, resulting in an increasing packing density with increasing compartment thickness. As previously discussed, the liquid void fraction can be described using equation (2.22). The data in Table 2.1 is plotted in Figure 2.4. Equation (2.22) is fitted quite well to the experimental data with $\varepsilon_o = 0.342$, $K_C = 0.498$, and $K_D = 0.196$:

$$\varepsilon = 0.342\left[1 + 0.498\exp\left(\frac{-0.196\,W}{d}\right)\right] \qquad (2.23)$$

Great care was taken in packing the compartment to generate reproducible packing and to minimise large voids. However, non-tamped, randomly dumped spheres would expect

to give larger porosity values. This would also be true for beds of non-uniform size spheres.

Equation (2.23) described the liquid void fraction in a square compartment as a function of compartment thickness and particle diameter. The equation was derived using precision metallic spheres that were not compressible. Due to their polymeric nature, ion exchange resins are compressible. Resin expansion beyond the true volume of the compartment (discussed in section 2.3.3) may have a lower liquid void fraction than what is calculated in equation (2.23).

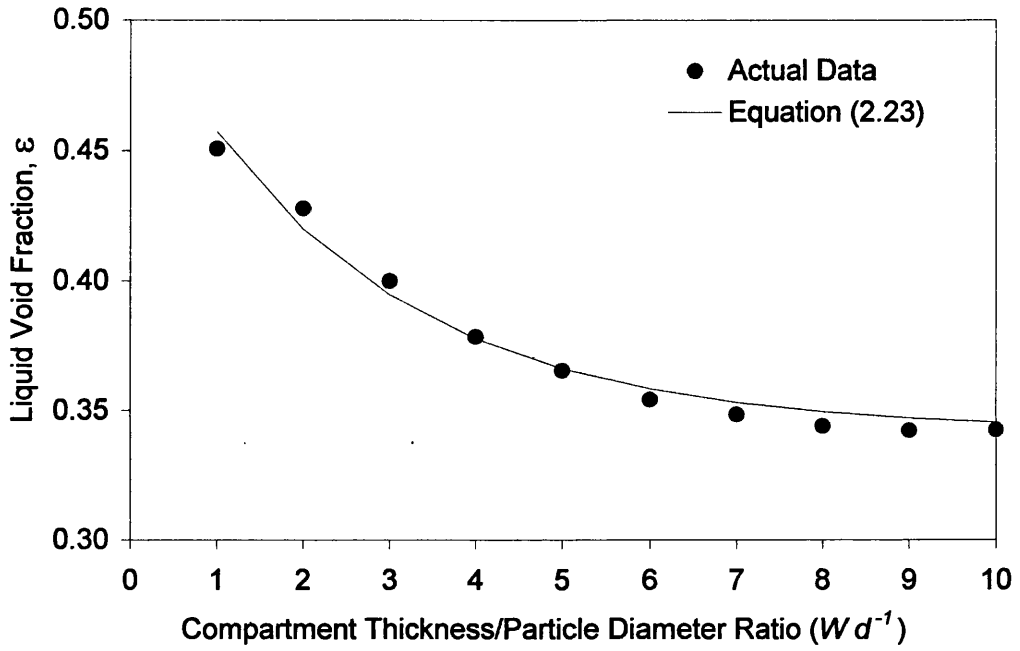

Figure 2.4 Void Fraction as a Function of Compartment Thickness in a Random Packing of Uniformly Sized Spheres.

2.3 Electrolytic Regeneration

2.3.1 Conductivity of Ion Exchange Resins

The functional groups in an ion exchange resin create regions of fixed charge that are associated with mobile ions, which allow the resin particles to be conductive. Ion exchange resin consists of two phases because of their porosity. One phase is the polymer matrix in which fixed-charge sites, referred to as functional groups, are attached. The other phase is the interstitial pore liquid. Because of the two-phase nature of ion exchange resins, ion movement can occur along two different paths. The first path allows

ions to proceed along the relatively widely separated function groups, while the second path allows ions to proceed through the interstitial pore liquid [16]. Figure 2.5 is a schematic illustration of a pore within a cation exchange resin. In both cases, ion movement is partially obstructed due to the geometry of the particles and pores, and thus movement is tortuous rather than straight.

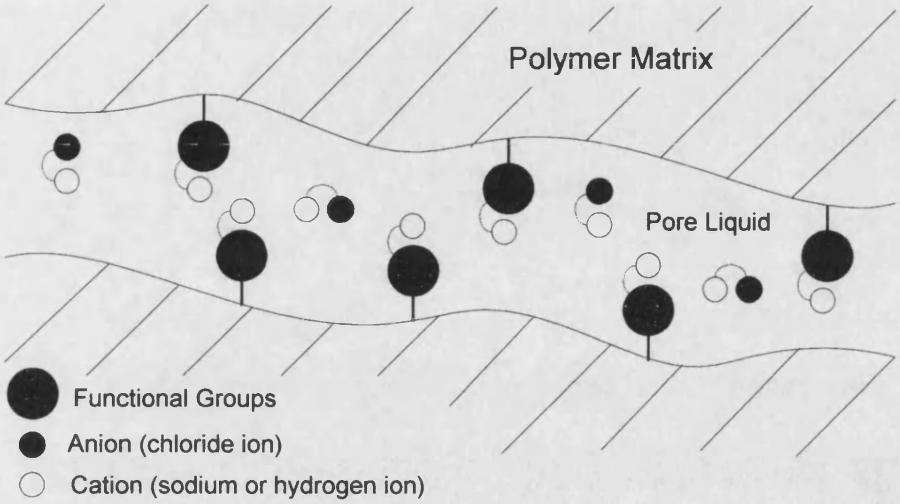

Figure 2.5 Schematic illustration of a pore within a cation exchange resin; the functional groups, cations, and anions are hydrated species: The diameter of hydrated inorganic ions rarely exceeds 8 Å. The average pore width in the polymer matrix is large, 10 X greater than the dimensions of the free ions in the pore liquid.

When the interstitial pore liquid is dilute, in which the concentration of cations and anions absorbed is negligible, the transfer takes place exclusively through the first path. In the case of a cation exchange resin, its conductivity is therefore dependent solely on the nature of the cations. As the concentration of the interstitial pore liquid increases, an easier path becomes available through the presence of anion carriers, and the transfer takes place by both paths. Therefore, absorbed cations and anions contribute to the conductivity.

2.3.2 Principles of Electrolytic Regeneration

The concentration and mobility of the charge carriers contained in ion exchange resin essentially determine its conductivity. Similar to an electrolyte solution, ion exchange resins contain mobile ions and are ionic conductors. The concentration of these mobile ions is typically on the order of one molar. The mobility of an ion can be expressed in terms of its diffusion coefficient. The diffusion coefficient in ion exchange resins depends

on various physical factors. Ion exchange resins consist of two phases; solid framework and interstitial pore phase. Mobility in the resin is lower than in aqueous solution of comparable concentrations due to:

- Only a fraction of the total cross-section which is not occupied by the solid framework available for diffusion
- The diffusion path is tortuous rather than straight due to obstructions created by the framework
- The actual mobility of the diffusing ion in the pores is reduced by mechanical 'friction' or other interactions with the pore walls

Due to the high concentration of the mobile ions, the conductivity of ion exchange resins is high, even though the mobility in the resins is lower than in aqueous solution of comparable concentrations. A high conductivity is favoured by:

- High ion exchange capacity
- Strong acid functional groups; weak acid functional groups do not dissociate at neutral and acid pH
- Low degree of crosslinking; resins of low crosslinkage have large micropores, so diffusion of ions within the resin is facile
- Small size and low valence of the counter-ions
- High concentration of the solution that is in equilibrium with the ion exchange resin
- Elevated temperature

The ion exchange capacity and concentration of the contacting solution determine the concentration of mobile ions in the resin. The degree of crosslinkage, nature of the counter-ions, and the temperature determine its mobility.

When an electric field is applied to a cation exchange resin bed, the current is carried through the resin by cations whose movement is facilitated if the phase, or phases, that it travels through are highly conductive. Since a resin bed is a mixture consisting of two phases, resin and bulk liquid, the electric current can take three different paths [17]. The first paths leads through alternating layers of resin particles and bulk liquid, the second exclusively through the resin particles which are in contact with one another, and the third exclusively through the bulk liquid. Figure 2.6 is a schematic representation of the three paths which the current takes place.

The proportion of the cation transport passing through each path is dependent on the conductivity of the bulk liquid and cation exchange resin. The conductivity of an ion exchange resin is not constant but depends on the nature of the counter ion and to a lesser degree, on the concentration of the solution with which the resin is in equilibrium. As long as the solution is rather dilute, the concentration of the resin, which has a higher ionic concentration, is greater than that of the solution.

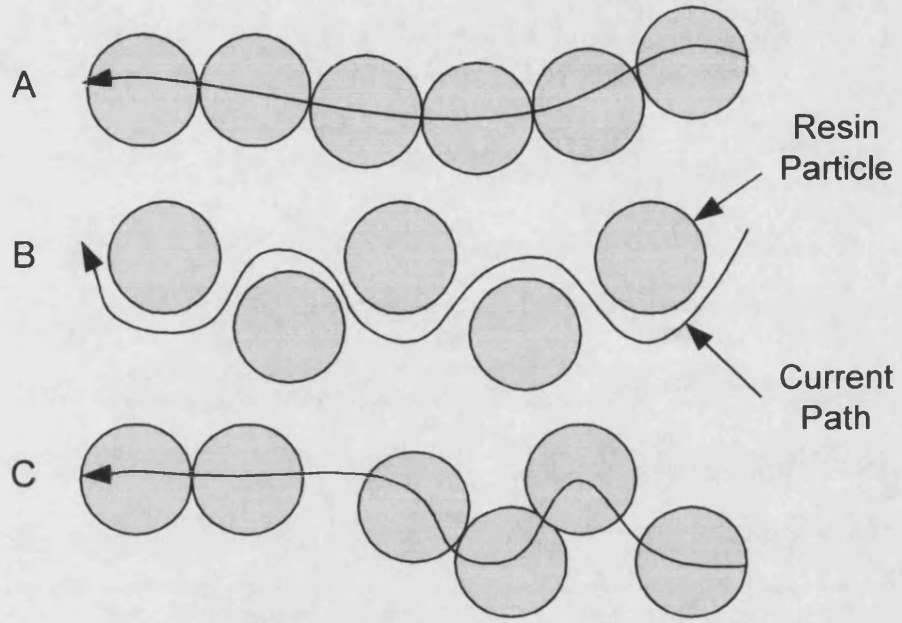

Figure 2.6 A schematic representation of the three current paths; (A) exclusively through the resin, (B) exclusively through the liquid, and (C) alternating through the resin and liquid.

When the solution concentration is increased, the concentration in the resin is also increased, but to a lesser degree. Hence the conductivity of the solution increases faster than that of the resin and eventually becomes the larger one. The effect of higher ionic concentration in the resin is now offset by the higher mobility in the solution. The point at which the conductivities of the ion exchange resin and solution are equal is called the *equiconductance* point.

Figure 2.7 shows the conductivity of a cation exchange resin in the sodium (Na^+) form in equilibrium with sodium chloride (NaCl) solution. If a direct electric current is passed through a cation exchange resin bed, mainly the cations, sodium and hydrogen ions, will accomplish the charge transfer (see Figure 2.8). As shown in Figure 2.7, the ion exchange resins are much more conductive that the solution surrounding them, therefore

whenever possible, the cations migrate from resin bead to resin bead in the direction of the cathode. When sodium ions are removed from the exchange sites of the resin, they are replaced by the most readily available cations, which may be sodium or hydrogen ions from nearby exchange sites or from the surrounding solution.

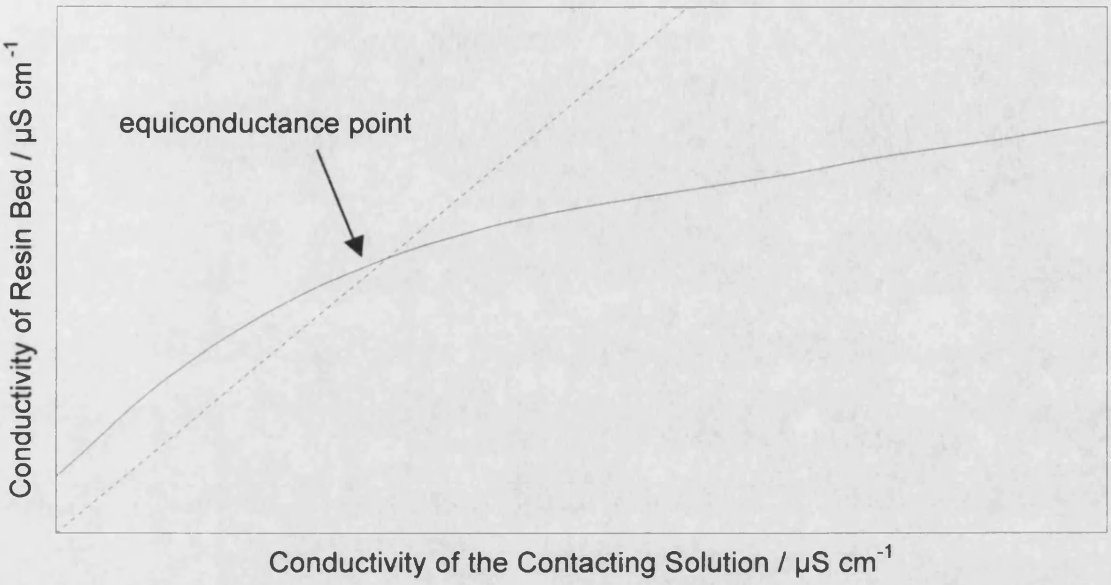

Figure 2.7 Typical plot of the conductivity of a resin bed (solid line) as a function of the conductivity of the contacting solution (dotted line).

In Figure 2.8, hydrogen ions are generated from the oxidation of water at the anode at a rate proportional to the applied current, following Faraday's law. The hydrogen ions will contact the cation resin closest to the anode and efficiently displace sodium ions for hydrogen ions in a comparatively narrow cross section of the resin bed adjacent the anode. The solution, now containing hydrogen and sodium ions, passes through the next layer of the bed. The sodium ions are again replaced by the most readily available cations.

As the direct electric current is continued, the layers closest to the anode are constantly exposed to hydrogen ions. At some distance beyond the anode, the resin will be regenerated, converted to the hydrogen form, across the cross-section of the resin bed, forming a 'front'. Once established, the front moves through the resin bed towards the cathode. If the sodium hydroxide generated at the cathode is removed, the front will continue until the entire resin bed as been regenerated.

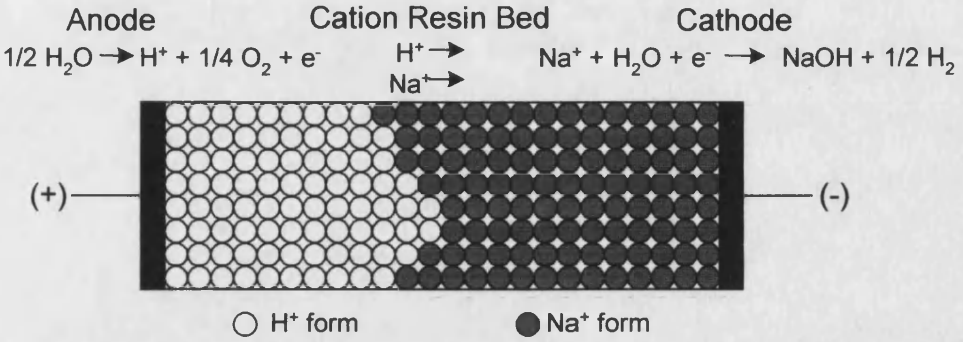

Figure 2.8 Electrolytic Regeneration of Cation Exchange Resin.

The current utilisation is always significantly lower than theoretically calculated. It decreases with the degree of regeneration and reaches extremely low values when complete regeneration of the resin is achieved. This is due to the difference in mobility of the hydrogen and sodium ions in the strongly acidic cation exchange resin. Since the mobility of the hydrogen ions is much higher than that of the sodium ions, a 'breakthrough' of hydrogen ions can occur. Figure 2.9 shows the movement of the regeneration 'front' through the resin.

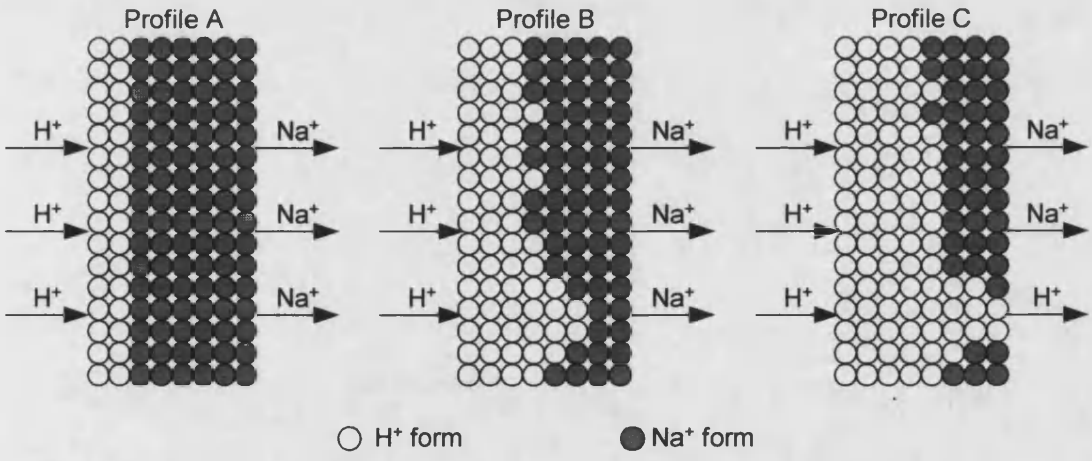

Figure 2.9 Movement of the Regeneration 'front' through a Resin Bed, showing the breakthrough' of hydrogen ions

In profile A the regeneration is just beginning and the current from the anode to the resin is carried by hydrogen ions and from the resin to the cathode by the sodium ions. The current density through the resin is identical over the entire cross-section of the resin. In

profile B, a the regeneration 'front' becomes distorted and because of the higher mobility of the hydrogen ions, more current will pass through the lower part of the resin bed. The distortion effect will increase until a 'breakthrough' of hydrogen ions occurs as indicated in profile C. The current will be nearly completely carried by hydrogen ions and the current utilisation is drastically affected.

To obtain a high degree of regeneration at a reasonable current utilisation, a distortion of the regeneration front must be prevented. One method is to select a cation resin with a low degree of hydrogen ion dissociation. Weakly acidic cation exchange resins do not dissociate in acid or neutral salt solutions. Therefore, the mobility of the hydrogen ions in weakly acidic cation exchange resins is significantly lower than that in strongly acidic cation exchange resins, lowering the conductivity of the resin and increase in energy consumption.

2.3.3 Packing Density of Resin

The cation exchange resin in a compartment acts as a path for the applied DC current to travel and also serve to increase the conductive bridge between the membranes for the movement of cations. Since the majority of the DC current travels through the resin, a packing density must be established such that the contact between cation exchange resins, as well as between the cation exchange resin and cation-permeable membranes, is at a state where the electrical and hydraulic resistances are balanced. If the packing density is too low, the contact between the resins tends to be 'loose', whereas the electrical resistance is likely to increase. Also, channels through the resin bed are created allowing the water to be treated to have a shorter path through the depleting compartment (channelling), which will result in a lower performance. On the other hand, if the packing density is too high, the contact between the resins tends to be 'tight'. The pressure drop is likely to increase thereby decreasing the flow of water to be treated. Also, a high expansion of volume in the compartment can increase the hydraulic resistance as to prevent passage of fluid. It can also cause damage to the ion-selective membranes; shedding, surface abrasion, or tearing of the membrane can result. Special care must be taken when selecting and/or treating of resins prior to filling a compartment. The packing density is typically determined by a trial-and-error method. However, it can be related to a pressure, *i.e.,* pressure formed between the resins. This pressure is typically in a range from 35 to 210 kPa.

In order to establish a packing density within a compartment, the ion exchange resins are typically treated such that they are at some compressed state prior to use. There are several methods for reducing the volume of ion exchange resins to a level smaller than the volume of its regenerated form. Such methods involve differences of moisture content as a result of environmental changes or changes of ionic form. They include changing the ionic form of the resin, the use of lower crosslinked resins, resin dehydration, and electrolyte sorption.

When the ionic form of the resin changes, a volume change occurs. Typically, a compartment is filled to the true volume of the compartment with resin in a form other than its regenerated form. It is preferred to convert the resin to a monovalent ionic form, *i.e.,* sodium form for cation exchange resin, since such that they can be easily exchanged. During the operation, a portion of the resin changes to their regenerated forms, causing the resin volume to increase in a fixed compartment volume, thus increasing the resin density in the compartment. For a standard 8 % DVB crosslinked resin, the swelling is approximately 7 % from the sodium to hydrogen form. This volume change is greater for resins of lower crosslinkage.

When dry resin is soaked in water, it absorbs a certain portion of water and swells up. If the swollen resin is allowed to come in contact with a solution of a strong electrolyte, its volume contacts, but when returned to water it swells up again and recovers its volume. Therefore, a greater volume change can be accomplished if the resin is immersed in a solution of an electrolyte or partially dried prior to filling the compartment.

Electrolyte sorption involves soaking the resin in a strong electrolyte solution, typically sodium chloride. The packing density through electrolyte sorption can be increased by as much as 20 %. Depending on the resin type, the true equilibrium volume of resin in contact with an electrolyte solution may take a long time, 12 to 36 hours, due to slow relaxation effects that follow the initial rapid contraction. Typically, resin contraction is not quite complete after several hours or even days, but the majority of the volume change occurs immediately and the remaining some time afterwards.

Resin dehydration involves lowering the moisture content of the resin using a drying oven or a stream of dry hot air. Resin dehydration can increase the packing density by as much as 35 %. However, large volume changes may cause problems, therefore it is preferred to reduce the water content (weight) to a level between 5 and 15 %. It is not practical to decrease the water content below 5 % because of the time requirement to

reach such a level. It is also not practical to decrease the water contact above 15 % because the volume increase tends to be too small.

Chemically bonded exchange groups are randomly dispersed on the surface and within the matrix of the resin bead. In the condition that resins are received, there is a large electrostatic repulsion between the fixed charges on the surfaces of neighbouring resin beads. This repulsion does not allow for good compaction, making the consistent measurement of a precise volume difficult. Differences in resin volume will cause large variations in electrical resistance and pressure drop between compartments and cells. This electrostatic repulsion can be significantly reduced if the resin is soaked in a moderate concentration of the corresponding electrolyte solution and air-dried prior to use. The remaining electrolyte solution sorbed in the resin will shield the electrostatic repulsion between fixed charges, allowing a good and uniform compaction. This will reduce the difficulties in consistently making a precise measurement. If the air-drying procedure is designed to allow for consistent moisture content, a weight measurement may be used for improved accuracy.

2.3.4 Ion Flux Expression in Resin

The movement of cations in cation exchange resin accomplishes the majority of the charge transfer if a direct current is passed through the cation exchange resin bed. The *driving forces* for such movement in the resin are the gradient of the chemical potential and convection of the pore liquid:

$$\overline{J}_i = -\left(\frac{\overline{C}_i \overline{D}_i}{RT}\right)\nabla\overline{\mu}_i + \overline{C}_i\overline{v} \qquad (2.24)$$

where $\overline{C}_i$ is the concentration in the resin, $\overline{D}_i$ the diffusion coefficient in the resin, and $\overline{v}$ the convection rate. There are two driving forces that make up the convection rate; the pressure gradient and electric potential gradient. The convection rate is:

$$\overline{v} = \varpi\,\overline{u}_o\nabla\Phi - \frac{\nabla P}{\rho_o} \qquad (2.25)$$

where ϖ is the sign of the fixed charges on the resin (-1 for cation exchange resin and +1 for anion exchange resin). $\bar{u}_0$ has dimensions of electrochemical mobility and may be referred to as the 'electroosmosic mobility' of the pore liquid. It is defined as:

$$\bar{u}_0 = -\frac{F X}{\rho_0 \vartheta} \tag{2.26}$$

where X is the concentration of the fixed charges on the ion-exchange resin, φ the fractional pore volume, and ρ_0 the specific flow resistance of the ion-exchange resin. The specific flow resistance of common ion exchange resins is usually of the order of 10^{15} to 10^{19} g m^{-3} s^{-1}.

The chemical potential μ_i of an ion is given by:

$$\bar{\mu}_i = \bar{\mu}_i^{\circ} + RT \ln \bar{a}_i + z_i F \Phi \tag{2.27}$$

where μ_i° is the chemical potential in a standard state, R the gas constant, T the temperature, $\bar{a}_i$ the thermodynamic activity, z_i the valency, F Faraday's constant, and Φ the electric potential.

Inserting the proper proportionality factor $\left(\frac{\bar{C}_i \bar{D}_i}{RT}\right)$ and differentiating yields:

$$\bar{J}_i = -\bar{D}_i \nabla \bar{a}_i - \left(\frac{z_i F}{RT}\right) \bar{D}_i \bar{C}_i \nabla \Phi + \bar{C}_i \bar{v} \tag{2.28}$$

The factor $\left(\frac{F}{RT}\right) \bar{D}_i$ can be substituted by the ionic mobility $\bar{u}_i$:

$$\bar{J}_i = -\frac{\bar{D}_i \bar{C}_i}{\bar{a}_i} \nabla \bar{a}_i - z_i \bar{u}_i \bar{C}_i \nabla \Phi + \bar{C}_i \bar{v} \tag{2.29}$$

This relationship is referred to as the Nernst-Einstein relationship. In ion-exchange resins, this relationship is found to hold rather well, and is often used to determine ionic mobility from self-diffusion measurements.

The ionic mobility in the resin $\overline{u}_i$ can be described as:

$$\overline{u}_i = \overline{u}_i^{\circ}\left(\frac{X}{Q_i}\right) + \overline{u}_i^{'}\left(1 - \frac{X}{Q_i}\right) \tag{2.30}$$

where $\overline{u}_i^{\circ}$ is the ionic mobility accounting for the interchange between fixed-charge sites, $\overline{u}_i^{'}$ the ionic mobility in the pore liquid, X the concentration of fixed ionic groups in the resin, Q_i the total concentration of anions, including the fixed ionic groups. The first term on the right side of the equation (2.31) can be considered as the contribution of the fixed ionic groups to the total cation mobility in the resin.

The mobility in the pore liquid $\overline{u}_i^{'}$ can be related to the mobility in the absence of the matrix following Mackie [18]:

$$\overline{u}_i^{'} = u_i\left(\frac{\vartheta}{2-\vartheta}\right)^2 \tag{2.31}$$

where ϑ is the fractional pore volume of the ion exchange resin. This relationship accounts for the obstruction by the resin's matrix, or the tortuous nature of the structure, and does not include the retardation by interactions with the pore walls.

This overall flux $\overline{J}_i$ is related to the current density i by:

$$i = F\sum_i z_i \overline{J}_i \tag{2.32}$$

Conservation of electroneutrality requires that the electric charge of all species balance one another every where is the system:

$$\sum_i z_i \overline{C} + \omega X = 0 \tag{2.33}$$

where X is the concentration of the fixed charges on the resin and ω is the sign of the fixed charge. Combining the following relationships for the current density i in a cross section to the direction of the current yields:

$$i = -F\left[\sum z_i \overline{D}_i \nabla \overline{a}_i + \sum z_i^2 \overline{u}_i \overline{C}_i \nabla \Phi - \sum z_i \overline{C}_i \overline{v}_i\right] \quad (2.34)$$

2.4 Electrochemical Acidification Process

2.4.1 Electrochemical Acidification Background

The concept of using electrically generated hydrogen ions in an electrochemical acidification process has been practiced for a variety of purposes since the 1960's. Bodamer [19] describes a process for the electrolytic conversion of weak acid salts to the corresponding weak acid in an arrangement where a single intermediate compartment is located between end electrode compartments with the individual intermediate compartment bounded on both sides by cation-permeable membranes. Guiffrida [20] describes a process where an aqueous solution of a metal salt solution is converted to the corresponding acid by hydrogen ion substitution in a four-compartment electrolytic cell, containing three cation-permeable membranes defining the cell compartments. Sloan [21] describes a carbonate reduction process using an electrolytic cell equipped with cation-permeable membranes, by selective addition of hydrogen ions whereby carbonate ions are converted to carbonic acid. Lacey [22] discusses an ion-replacement reaction where the continuous cation replacement may be achieved in an electrodialysis cell will all cation-permeable membranes.

Stratman and Kock [23] outline the principle of electrolytic regeneration as follows: a cation-exchange resin is placed between two cation-permeable membranes and two electrodes. By applying a direct current, hydrogen ions generated at the anode migrate through cation-permeable membranes into the resin and replace metal-ions, which migrate through the opposite membrane toward the cathode.

Bachot and Grosbois [24] describe a crystalline methionine preparation process in an intermediate compartment of an electrolytic cell comprising an anode compartment, an intermediate compartment separated from the anode compartment by a cation-permeable membrane, and a cathode compartment separated from the intermediate compartment by a cation-permeable membrane.

Twardowski [25] describes a hydrochloric acid-based chlorine dioxide generating process that is integrated with an electrolytic process for sodium hydroxide production. Generator liquor in the form of a sodium chloride-enriched solution from the chlorine dioxide generator is passed to the central compartment of a three-compartment cell. Hydrogen ions formed in the anode compartment of the three-compartment cell migrate through a cation-permeable membrane to the central compartment to form hydrochloric acid with the sodium chloride solution. Sodium ions migrate through a further cation-permeable membrane to form sodium hydroxide with hydroxyl ions produced in the cathode compartment of the three-compartment cell. The acidified generator liquor containing the hydrochloric acid formed in the central compartment is forwarded to the chlorine dioxide generator to provide half the acid requirement therefor.

Wood and Bradbury [26] describe a process for removing radioactive burden from spent nuclear reactor decontamination solutions using electrochemical ion exchange. The application of electric current to the electrochemical cell causes hydrogen ions to replace captured cations held on the ion exchange resin, thereby regenerating the resin for subsequent processing. The displaced cations migrate into the cathode compartment. The radioactive burden and metallic impurities are removed from the cathode compartment of the electrochemical cell.

Kaczur and Cawlfield [27] describe a process for electrolytically producing an aqueous solution of chlorine dioxide in an electrolytic cell having an anode compartment, a cathode compartment, and at least one ion exchange compartment between the anode compartment and the cathode compartment. The process comprises of feeding an aqueous solution of an alkali metal chlorite to the ion exchange compartment, electrolysing an anolyte in the anode compartment to generate hydrogen ions, passing the hydrogen ions from the anode compartment through a cation-permeable membrane into the ion exchange compartment to displace alkali metal ions and produce an aqueous solution of chlorine dioxide, and passing alkali metal ions from the ion exchange compartment into the cathode compartment.

2.4.2 Electrochemical Acidification Process

The principle involved is the use of an electrolytic cell to generate hydrogen ions that displace sodium ions in a sodium salt feed solution. A solution containing a sodium salt is passed through a bed of strong acid cation exchange resin, which is held between two cation- permeable membranes. Sodium ions are taken up from the solution by the cation

exchange resin and are exchanged with hydrogen ions. A direct electric current passes at perpendicular to the direction of flow of liquid. The sodium ions taken up are transported in the direction of the current, passing through the resin bed towards the membranes, where they are removed from the resin bed through the membranes. Under these conditions, the functional groups of the cation exchange resin are partially converted to the hydrogen form by electrolytic regeneration.

Figure 2.10 shows a description of an electrochemical acidification cell. The cell contains three compartments; (1) anode compartment, (2) cation exchange compartment, and (3), cathode compartment. All of the compartments are filled with strong acid cation exchange resins and are separated by cation-permeable membranes.

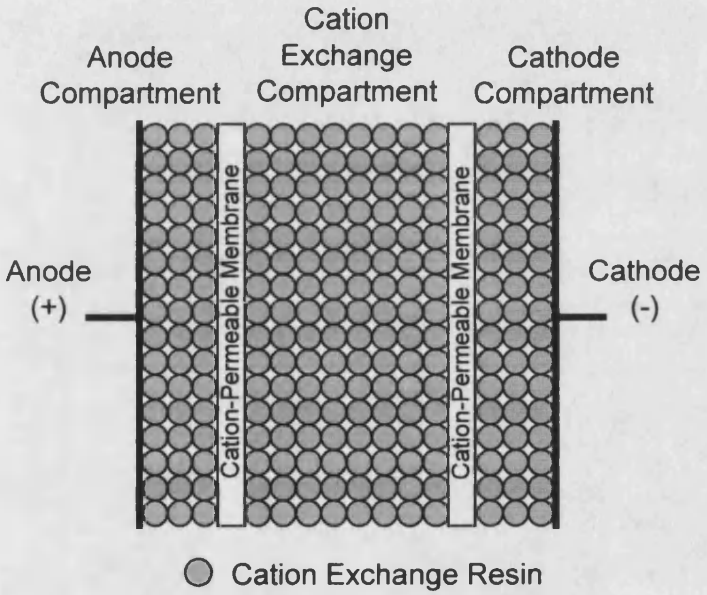

Figure 2.10 Description of an Electrochemical Acidification Cell, showing the three resin-filled compartments

As seen in Figure 2.11, a sodium salt solution, such as sodium chloride, flows through the cation exchange compartment where sodium ions from the solution are absorbed on the cation exchange resin and exchange for hydrogen ions. The hydrogen ions released are combined with the available anions to form the corresponding acid; sodium chloride will be converted to hydrochloric acid. Simultaneously, a DC current is applied to the cell. The charge is carried through the cell, from anode to cathode, by the migration of cations in solution and on the cation exchange resin. The overall reaction in the anode compartment is;

$$2\,H_2O \rightarrow O_2 + 4H^+ + 4e^- \qquad (2.35)$$

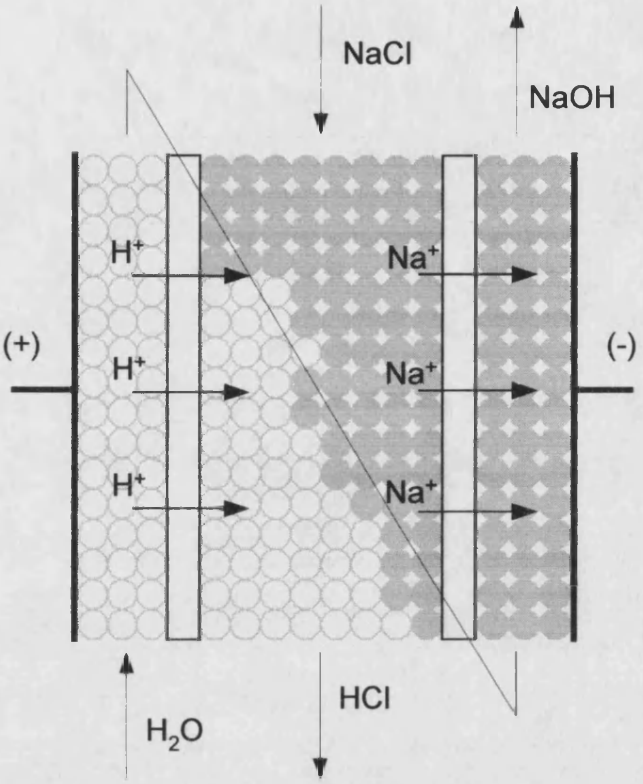

Figure 2.11 Operation of an Electrochemical Acidification Cell, showing ion and fluid movement.

The hydrogen ions migrate out of the anode compartment and into the cation exchange compartment. The reaction in the cation exchange compartment leads to the conversion of the cation exchange resin from the sodium to the hydrogen form:

$$H^+ + R_c \cdot Na^+ \leftrightarrow Na^+ + R_c \cdot H^+ \qquad (2.36)$$

where R_c is the polymeric cation exchange resin. Finally, in the cathode compartment, the migrating sodium ions react with the hydroxyl ions, which are generated at the cathode with hydrogen gas by the reduction of water:

$$2\,H_2O + 2e^- \rightarrow 2OH + H_2 \qquad (2.37)$$

and discharged as sodium hydroxide and hydrogen gas. The hydrogen gas can be separated and vented.

Most electrolytic cells use liquid acid and caustic electrolytes in the anode and cathode compartment, respectively. Most electrolytic cells require weekly or monthly additions of electrolytes to replace what is lost or consumed during operation. Figure 2.10 shows both electrode compartment filled with cation exchange resin. Ion exchange resins have been previously used in place of liquid electrolytes in the electrode compartments of an electrochemical cell [28]. They serve as an immobile electrolyte, providing a media for ion migration. In the anode compartment, cation exchange resin acts as the counter-ion for the hydrogen ions produced at the surface of the anode by the oxidation of water - equation (2.36). The use of resin-filled electrode compartments also has two other advantages; improved support for the membranes and higher electrical conductivity when operating with a dilute electrolyte.

2.5 Development of a Model

2.5.1 Governing Mechanisms

The electrochemical acidification process is understood as having a number of ionic mechanisms occurring simultaneously. These mechanisms are driven by gradients in electrochemical potential, which include gradients in concentration, electrical potential, and pressure, and by convection. Due to the standard operating conditions of an electrochemical acidification cell, the effect of temperature and pressure gradients on the flux of individual ions can be disregarded. The ionic and fluid movements are illustrated in Figure 2.12.

The operating principles involved are as follows. A solution of a sodium salt passes through a bed of cation exchange resin, which is held between two cation-permeable membranes. Sodium ions from the liquid are taken up by the cation exchange resin and are exchanged with hydrogen ions by an *Ion Exchange Process*. The hydrogen ions are substantially removed from the equilibrium by combining with the anions previously associated with the exchanged sodium ions. An electric field is passed perpendicular to the liquid flow in such a way that the sodium ions taken up are migrated across the surface of the cation resin particles from the resin bed through cation-permeable membrane into the adjacent cathode compartment by an *Electromigration Process*. In the cathode compartment, hydroxyl ions generated by the reduction of water on the

cathode combine with the sodium ions, forming a sodium hydroxide solution. Simultaneously, hydrogen ions generated by the oxidation of water on the anode migrate from the anode compartment, through a cation membrane, and into the cation exchange compartment. The hydrogen ions partly convert the cation resin into its regenerated form, as well as take part in electrolytic current conduction. Accompanying the cation migration is the transport of water in the pores of the resin and membranes by an *Electroosmosis Process.*

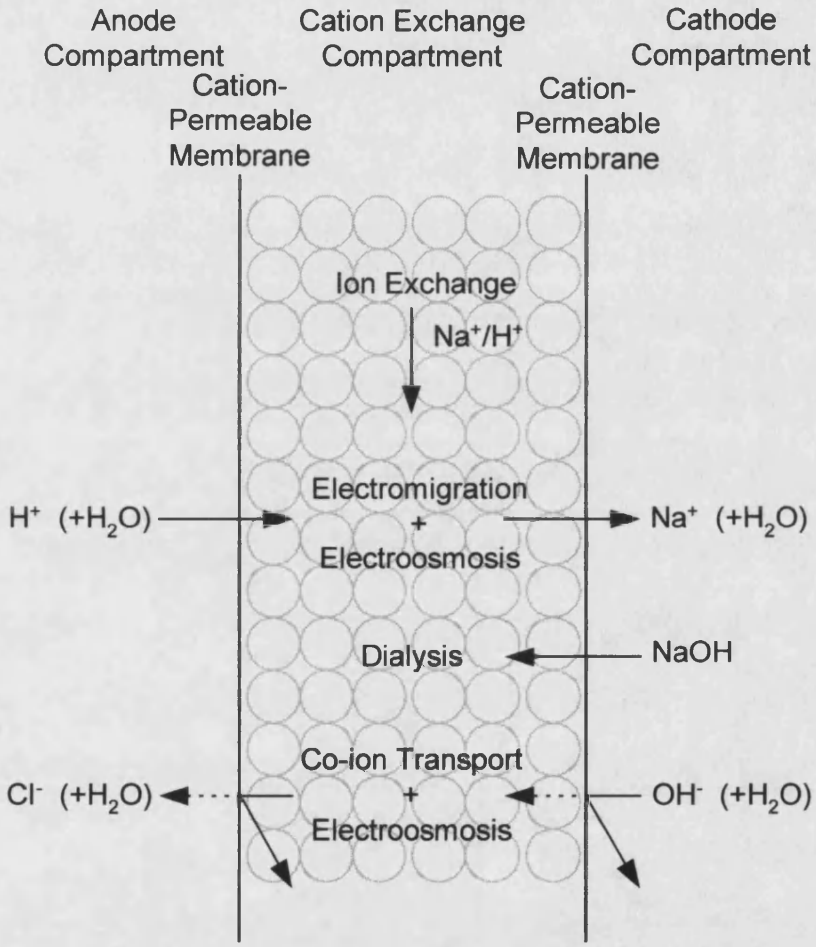

Figure 2.12 Processes Occurring in an Electrochemical Acidification Cell, showing the number of ionic mechanisms that occur simultaneously.

Back diffusion can occur when the sodium hydroxide concentration in the cathode compartment becomes too high, resulting in some of the sodium hydroxide solution from the cathode compartment diffusing back through the membrane into cation exchange compartment, against the force of the electrical potential by a *Dialysis Process.* Back diffusion is controlled by the concentration difference across the membrane; back diffusion increases as the concentration difference increases.

Because cation-permeable membranes are not truly selective, the transfer of anions can occur from the cation exchange to anode compartments and from the cathode to the cation exchange compartments by a *Co-Ion Transport Process.* The transfer of anions is comparatively small and is dependent on the characteristics of the cation-permeable membrane, such as water content, exchange capacity, transport number, and on the ion concentration in the concentrating compartment. Water is also transported electroosmotically with the anion transfer.

The *Electromigration Process* constitutes the major electrical movement. The counter effects of the *Dialysis* and *Co-Ion Transport Processes* have the largest negative effect on overall performance. The *Electroosmosis Process* only results in a water loss. The effect of these unwanted transfer processes could be reduced by the correct selection of cation-permeable membranes and by the selection of optimum operational procedure for a particular application.

Besides having such qualities as chemical stability, mechanical strength, and dimensional stability under conditions of use, the cation-permeable membranes have a high transport number or a negligible permeability towards anions. The higher the transport number, the smaller the relative increase in the back diffusion for a given increase in concentration difference and the smaller the water loss from osmotic permeability. However, relatively small water loss is not a significant factor and does not actually detract much from performance.

It is obvious that the main governing mechanisms in the electrochemical acidification process are the ion exchange and transfer processes. For the present analysis, the *Electromigration Process* will be the only transfer process considered.

2.5.2 Model Description and Assumptions

The electrochemical acidification process has not been subject to numerous theoretical studies because of its low interest in using it as a viable method of generating acid. From an electrochemical-engineering standpoint, models or calculations to predict the performance or to design an electrochemical acidification cell have not been proposed in great detail. The reason is that it is difficult to analytically solve a full set of equations describing all of the mechanisms including fluid hydrodynamics, charge and mass

transport, and electrochemical kinetics. This causes the theoretical approach to generally rely upon one or several restrictive assumptions.

The model presented here uses dilute solution theory to describe the electrochemical acidification process. The basic physical, geometrical, and operational assumptions defining the model are outlined, as well as the governing equations that result. It will be confined to the two-dimensional geometry with plane parallel membranes. Only sodium and hydrogen ions are considered during the cation transport and exchange process.

The treatment that follows is based upon several assumptions as to the nature of the bulk liquid and cation exchange resin. Any one or all of the assumptions made could be relaxed resulting in additionally complicated analysis, however, it is felt that the assumptions made still provide a realistic model for an actual electrochemical acidification cell.

The following assumptions are applied to the bulk liquid and cation exchange resin:

1) Steady-state operation
2) Isothermal operation
3) Bulk liquid is a dilute solution
4) Cation transport in the bulk liquid is by convection only
5) Cation exchange is controlled by film diffusion
6) Current transport is through the cation exchange resin and is described by migration only
7) Cation-permeable membrane has negligible osmotic permeability and is perfectly selective
8) Flow distribution is uniform within the cation resin bed

The third assumption is based on the bulk liquid consists of sodium chloride solution at a concentration of less than 300 eq m^{-3}. Although liquid density and viscosity will change with distance down the length of the compartment, they will be treated as constant. It will be assumed that the densities and viscosity of the sodium chloride is approximately equal to that of pure water. Activity coefficient of each dissociated ion is assumed to equal unity.

Assumption four is consistent with the fact that the flow velocity is through a thin and long compartment and the bulk solution is considered dilute. For systems dilute in the

transported ion *i*, the Nernst-Plank equation with flow velocity can be used to describe ion transport in the bulk liquid:

$$J_i = -D_i \nabla C_i - z_i u_i C_i \nabla \Phi + C_i v \tag{2.38}$$

where D is the diffusion coefficient, C the molar concentration, z the electrochemical valance, u the mobility coefficient, Φ the electric potential, and v the bulk liquid velocity.

In equation (2.39), the flux of an ion J_i is related to gradients in concentration, potential, and pressure, resulting in diffusion, migration, and convection, respectively. Transverse gradients (x-coordinate) are negligible compared to longitudinal gradients (y-coordinate).

Due to conditions of favourable equilibrium (when cations from the bulk liquid is preferred by the cation exchange resin) and low sodium chloride concentration, the effects of the potential gradient on the ion fluxes can be disregarded [29] and the Nernst-Plank equation reduces to:

$$J_i = -D_i \frac{\partial C_i}{\partial y} + C_i v \tag{2.39}$$

where y is the direction of bulk liquid flow.

Since the length in direction of flow is large, Y, with respect to the thickness of the compartment, W, the following criteria [30] can be used to determine the governing mechanism for ion transport:

$$\mathrm{Pe} \equiv \mathrm{Re\,Sc} >> \frac{W}{L} \tag{2.40}$$

Typically, in plate-and frame designs, the Pecklet number is much greater than the ratio of compartment thickness and length. In this case, the diffusion term can be neglected, having only convection responsible for the ion transport.

$$J_i = C_i v \tag{2.41}$$

Also, the motion of the bulk liquid down the compartments is assumed to be uniform, *i.e.*, that all volume elements proceed at the same rate and that the bulk liquid concentration is only a function of the y-direction and is uniform in any horizontal plane in the compartment.

The fifth assumption assumes that the kinetic limitation of the rate at which cations are exchanged at concentrations below 300 eq m^{-3} in the cation exchange compartment occurs in the thin film between the bulk liquid and cation exchange resin surface.

This assumption is based on equation (2.10). The cation exchange between hydrogen and sodium ions on a 10 % DVB crosslinked strong acid cation exchange resin at 25 °C will be considered. In this case, at a concentration of 300 eq m^{-3} (NaCl conductivity of approximately 20,000 µS cm^{-1}), the value of $(\overline{CD}_i \delta / CD_i r_o)(5 + 2a_{ij})$ is 2.0, and at a concentration of 30 eq m^{-3} (NaCl conductivity of approximately 3,000 µS cm^{-1}), it is 13.6. If it is assumed that the ratio of film diffusion to particle diffusion coefficients remains constant under the influence of a potential gradient, then the assumption of film diffusion control is reasonable.

The sixth assumption is a consequence of the third assumption. In a dilute solution, the cation transfer proceeds exclusively along the resin's functional groups. The conductivity of the resin is therefore dependent solely on the nature of the cations:

$$\overline{u}_i \approx \overline{u}_i' \tag{2.42}$$

and the mobility ratio of two cations in bulk liquid is equal to that in the cation exchange resin:

$$\frac{u_i}{u_j} \approx \frac{\overline{u}_i}{\overline{u}_j} \tag{2.43}$$

The electric current produces no concentration changes in the resin. Thus there are no gradients of activity and pressure, and the transport is due solely to migration. The Nernst-Plank equation in the resin reduces to:

$$\overline{J}_i = -z_i \overline{u}_i \overline{C}_i \nabla \Phi \tag{2.44}$$

Longitudinal gradients (y-coordinate) of potential are negligible compared to transverse gradients (x-coordination). Substituting the above expression into the flux equation yields;

$$\overline{J_i} = -z_i\overline{u_i}\overline{C_i}\frac{\partial\Phi}{\partial x} \tag{2.45}$$

Defining a current efficiency as:

$$\overline{\eta_i} = \frac{z_i\overline{u_i}\overline{C_i}}{z_i\overline{u_i}\overline{C_i} + z_j\overline{u_j}\overline{C_j}} \tag{2.46}$$

The current efficiency is used to quantify the portion of the total current that is being provided by species *i*. The flux equation can be expressed in terms of the current density:

$$\overline{J_i} = \frac{i}{z_i F}\overline{\eta_i} \tag{2.47}$$

Although ion-permeable membranes exhibit anomalous osmotic behaviour in electrolyte systems, the most common effect being the abnormally high osmotic flow which takes place in electrolyte systems as compared to non-electrolyte system, it is assumed that the amount of water passage by the flow of current is negligible compared to the volume of solution flowing through the compartments. Also, it is known that ion-permeable membranes are not truly selective; some of the current is carried through the cation-permeable membranes by anions. The selectivity of commercial membranes is typically above 95 % for liquids with a total-dissolved-solids (TDS) of 500 eq m^{-3} but decrease rapidly at higher TDS. However, liquids with much lower TDS, the selectivity is likely to be much greater, making assumption seven closely satisfied.

It is felt that the eight assumptions made retain the essential features of the system while avoiding unnecessary mathematical complexity. The validity of the assumptions will be checked through an analysis of the experimental results.

2.5.3 Development of an Electrochemical Acidification Cell Model

A mass balance will be performed over the volume element ΔV, neglecting any transverse variations in concentrations and assuming steady state. Derivatives of potential in the y-direction along the compartment are neglected in comparison with the corresponding derivatives in the x-direction across the compartment. This results in there being only a component of current in the x-direction, transverse to the flow. With the ratio of compartment length to width being large, this approximation is closely satisfied.

The following symbols will be used in developing the model:

A_y = cross-sectional area in the flow direction (y-axis) / cm^2
J_i = molar flux rate / mol m^{-2} s^{-1}
ε = liquid void fraction
r = rate of ion exchange / mol m^{-3} s^{-1}
D = diffusion coefficient / m^2 s^{-1}
C = bulk liquid concentration / mol m^{-3}
C^* = thin film liquid concentration / mol m^{-3}
z = electrochemical valence of an ion
u = electrochemical mobility factor / m^2 V^{-1} s^{-1}
Φ = electrical potential / V
v = linear flow velocity / m s^{-1}
x = coordinate in direction of current / m
W = compartment width / m
y = coordinate in direction of liquid flow / m
Y = compartment length / m
k = thin film mass transport coefficient / m s^{-1}
K = molar selectivity coefficient
S = specific surface area of the resin particle / m^{-1}
i = current density / A m^{-2}
F = Faraday's constant / 96,4954 C eq^{-1}
η_c = current efficiency

Quantities and symbols with overbars are used for the solid phase.

A mass balance of component A over the volume element (A_y Δy) in the liquid phase yields:

$$\underbrace{A_y J_A\big|_y}_{\text{Rate In}} - \underbrace{A_y J_A\big|_{y+\Delta y}}_{\text{Rate Out}} - \underbrace{(1-\varepsilon) r_{AB}(A_y\ \Delta y)}_{\text{Rate of Exchange of A}} = 0 \qquad (2.48)$$

Dividing equation (2.49) by (A_y Δy) and taking the limit $\Delta y \rightarrow 0$:

$$-\frac{\partial J_A}{\partial y} - (1-\varepsilon) r_{AB} = 0 \qquad (2.49)$$

Applying the first-order rate (equation 2.15) and molar flux rate (equation 2.41) expressions, the overall mass balance equation in the liquid phase reduces to:

$$\frac{\partial C_A}{\partial y} = -\left(\frac{(1-\varepsilon) k_f\ S}{v}\right)(C_A - C_A^*) \qquad (2.50)$$

A mass balance of A over the volume element ΔV in the resin phase yields:

$$\underbrace{A_x \bar{J}_A\big|_x}_{\text{Rate In}} - \underbrace{A_x \bar{J}_A\big|_{x+\Delta x}}_{\text{Rate Out}} + \underbrace{(1-\varepsilon) r_{AB} \Delta V}_{\text{Rate of Exchange of A}} = 0 \qquad (2.51)$$

Dividing equation (2.57) by Δx and taking the limit $\Delta x \rightarrow 0$,

$$-\frac{\partial \bar{J}_A}{\partial x} + (1-\varepsilon) r_{AB} = 0 \qquad (2.52)$$

Applying the first-order rate expression, equation (2.15), to the resin particle:

$$\frac{\partial \bar{J}_A}{\partial x} = (1-\varepsilon) k_f\ S (C_A - C_A^*) \qquad (2.53)$$

Relating the ionic flux to the total current density for a single species:

$$\bar{J}_A = \frac{i}{z_A F} \bar{\eta}_A \qquad (2.54)$$

Figure 2.13 shows a schematic of the electrochemical acidification cell.

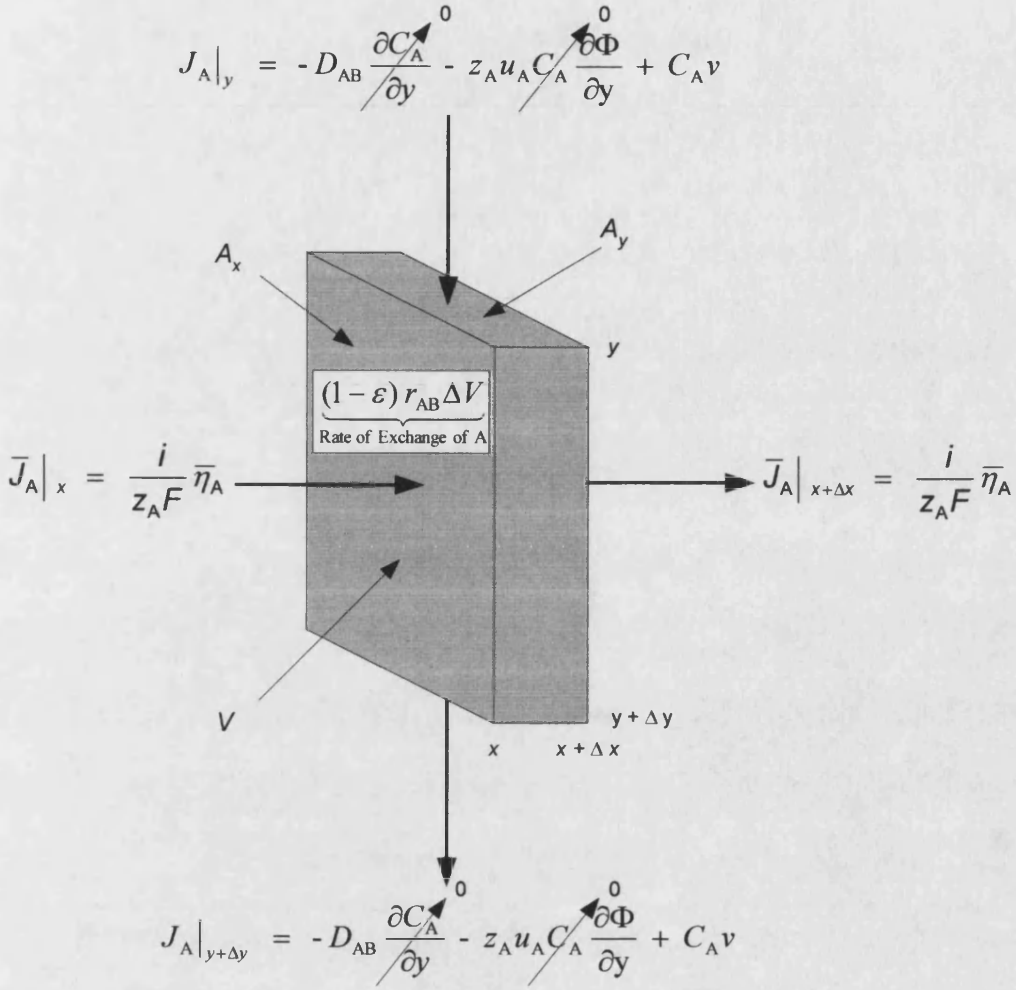

Figure 2.13 Schematic of the electrochemical acidification cell neglecting any radial variations in concentrations and assuming steady state

Expanding the current efficiency:

$$\bar{\eta}_A = \frac{z_A \bar{u}_A \bar{C}_A}{z_A \bar{u}_A \bar{C}_A + z_B \bar{u}_B \bar{C}_B} \tag{2.55}$$

Making the appropriate substitution, the mass balance equation becomes:

$$\frac{i}{z_A F}\frac{\partial\left(\frac{z_A \bar{u}_A \bar{C}_A}{z_A \bar{u}_A \bar{C}_A + z_B \bar{u}_B \bar{C}_B}\right)}{\partial x} = (1-\varepsilon)\, k_f\, S\, (C_A - C_A^*) \tag{2.56}$$

or

$$\frac{i}{z_A F}\frac{\partial\left(\dfrac{1}{1+\dfrac{z_B \bar{u}_B \bar{C}_B}{z_A \bar{u}_A \bar{C}_A}}\right)}{\partial x} = (1-\varepsilon)\, k_f\, S\,(C_A - C_A^*) \qquad (2.57)$$

Applying the equilibrium relations, equations (2.8) and (2.9), the overall mass balance equation in the resin phase reduces to:

$$\frac{1}{(C_A - C_A^*)}\partial\left(\frac{1}{1+\dfrac{a(C_A - C_A^*)}{C_A^*}}\right) = \frac{z_A F}{i} b\, \partial x \qquad (2.58)$$

where

$$a = \frac{\bar{u}_B}{\bar{u}_A K_{AB}} \qquad (2.59)$$

$$b = (1-\varepsilon)\, k_f\, S \qquad (2.60)$$

Constant *a* is a function of the electrolyte and ion exchange resin properties, while *b* is a function of particle size and to some extent, temperature. Constant *b* can be adjusted to improve the operating conditions.

If the membrane closest to the anode compartment, at x = 0, is only permeable to hydrogen ions from the water oxidation reaction on the anode, the following boundary condition holds for equation (2.58):

$$x = 0 \quad C_A^* = 0$$

Equation (2.58) integrates to (see Appendix F):

$$a \ln\frac{a C_A - (a-1) C_A^*}{a (C_A - C_A^*)} - \frac{(a-1) C_A^*}{a C_A - (a-1) C_A^*} = \frac{z_A F}{i} b\, C_A\, W \qquad (2.61)$$

where x was replaced by W, the width of the compartment. Substituting equilibrium relations, equations (2.8) and (2.9), and the current efficiency (equation 2.55) into equation (2.61) yields:

$$-a\ln(1-\overline{\eta}_A)-(a-1)\overline{\eta}_A = \frac{z_A F}{i} b C_A W \tag{2.62}$$

Differentiating equation (2.62) yields:

$$\partial C_A = -\frac{i}{z_A F b W}\left[\frac{a}{(1-\overline{\eta}_A)}-(a-1)\right]\partial\overline{\eta}_A \tag{2.63}$$

With $\overline{\eta}_A$ known, the mass balance equation can be written:

$$v\frac{\partial C_A}{\partial y} = \frac{i}{z_A F W}\overline{\eta}_A \tag{2.64}$$

Making the appropriate substitution, equation (2.63) into equation (2.64):

$$-\frac{b}{v}\partial y = -a\,\partial\ln(1-\overline{\eta}_A)+\partial\ln(\overline{\eta}_A) \tag{2.65}$$

Integrating with the following boundary conditions,

$$y = 0 \qquad \overline{\eta}_A = \overline{\eta}_{in}$$
$$y = Y \qquad \overline{\eta}_A = \overline{\eta}_{out}$$

Equation (2.65) integrates to:

$$\frac{b}{v}Y = \ln\left(\frac{\overline{\eta}_{in}}{\overline{\eta}_{out}}\right)-a\ln\left(\frac{1-\overline{\eta}_{in}}{1-\overline{\eta}_{out}}\right) \tag{2.66}$$

Equation (2.62) is used to calculate $\overline{\eta}_{in}$. With $\overline{\eta}_{in}$ known, equation (2.66) is used to calculate $\overline{\eta}_{out}$. The overall current efficiency is determined by:

$$\eta_c = \frac{(\overline{\eta}_{in} + \overline{\eta}_{out})}{2} \quad (2.67)$$

2.6 *Experimental Details*

The experiments described in this chapter were designed to show the conditions necessary for the operation of an electrochemical acidification cell; the operating characteristics and the optimum operation with respect to current efficiency.

2.6.1 Electrochemical Acidification Cell

An electrolytic cell from Halox Technology (Bridgeport, CT) was used in the study. The cell was selected because of its design. The cell has extremely good flow and current distribution and its specifications allow for easy operation on a laboratory scale. The specifications of the cell are presented in Table 2.2.

Table 2.2 Specifications of the Electrochemical Acidification Cell

Dimensions	
Overall Cell Dimension	14.0 cm x 36.5 cm x 6.0 cm
Frame Width	5.1 cm
Frame Height	30.1 cm
Frame Thickness	1.2 cm
Membranes Active Area	153.5 cm^2
Electrical Data	
Electrode Active Area	153.5 cm^2
Max. Current Density	100 A m^{-2}
Flow Data	
Max. Flow Rate	20 cm^3 s^{-1}
Max. Electrolyte Flow Rate	10 cm^3 s^{-1}
Cell Volume	185 cm^3
Max. Operating Temperature	60 °C
Max. Operating Pressure	350 kPa
Materials	
Anode	Dimensionally Stable Anode (DSA-600)
Cathode	316L Stainless Steel
Membrane	Cation-Permeable Membrane
Moulded Frame and End Block	Acrylonitrile Butadiene Styrene (ABS) plastic

The dimensions of the cation exchange resin bed; thickness of 1.2 cm and a depth of 30.1 cm, best characterise the three-compartment cell used. The solution and the

electric current flowed parallel to the length and depth of the resin bed, respectively. Two cation-permeable membranes acted as separators between the compartments. The active area of the cation-permeable membranes was 153.5 cm^2. All compartments were filled with cation exchange resin. The arrangement of resin on both sides of the membranes assured that the membranes remained flat.

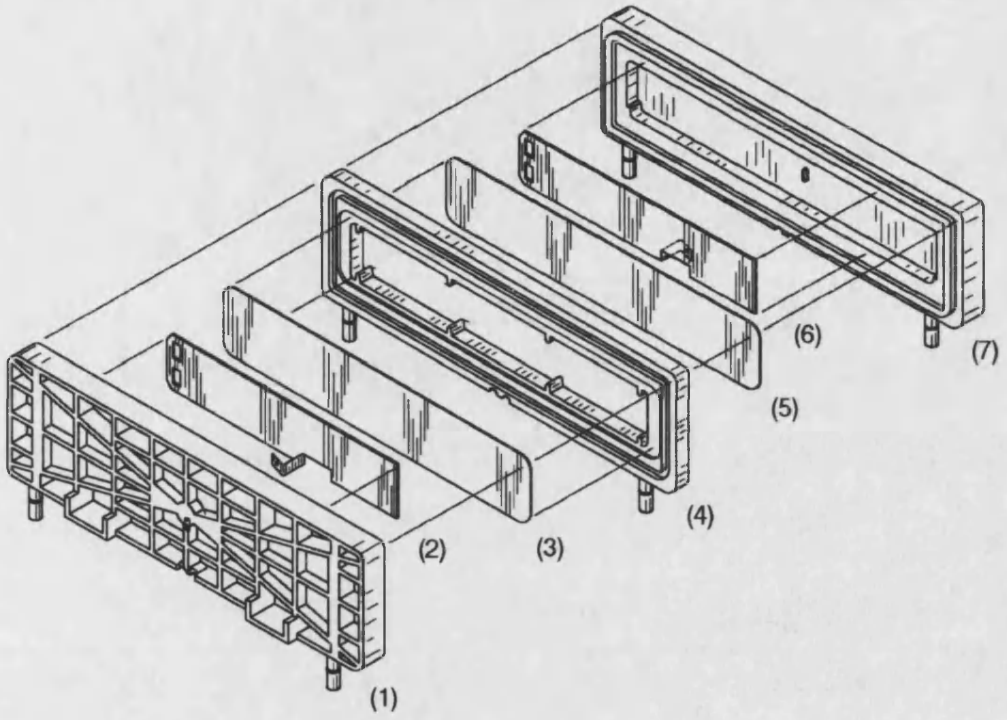

Figure 2.14 Exploded View of the Electrochemical Acidification Cell: (1)/(7) ABS End Compartments, (2) 316L Stainless Steel Cathode, (3)/(5) Cation-Permeable Membrane, (4) ABS Cation Exchange Compartment, and (6) DSA® Anode. The overall dimensions of the cell (width x height x depth) were 14.0 cm x 36.5 cm x 6.0 cm. (Courtesy: Halox Technologies, Inc., Bridgeport, CT).

The metallic electrodes in the end compartments were separated from the membranes by the cation exchange resin. The cathode comprised of 316L stainless steel and a dimensionally stable anode (DSA®) [31] was used as an anode. DSAs® are now a family of coatings which are applied to titanium and their name arise because they are inert and very stable to corrosion and their service life can be many years. The coating is a mixed precious metal oxide coating, but may also contain valve metal, precious metal, or transition metal oxides to improve performance for a particular application. DSA® EC-600 was selected for this project primarily for its excellent catalytic properties for oxygen

evolution. EC-600 is an iridium dioxide based precious metal coating, containing a small amount of tantalum.

All of the compartments were structural foam moulded using acrylonitrile butadiene styrene (ABS) plastic. An acrylic adhesive compound was used to adhere and seal the end compartments to the centre compartment. Figure 2.14 shows an exploded view of the electrochemical acidification cell used.

The solutions flowed upwardly from bottom to top in every compartment and were in parallel, *i.e.,* the liquid in the cation exchange compartment flowed in the same direction as the liquid in the two electrode compartments. Sodium chloride solution was passed through the cation exchange compartment. Softened water was passed in series through the electrode compartments; first through the anode compartment and then through the cathode compartment. The flow configuration is outlined in Figure 2.15.

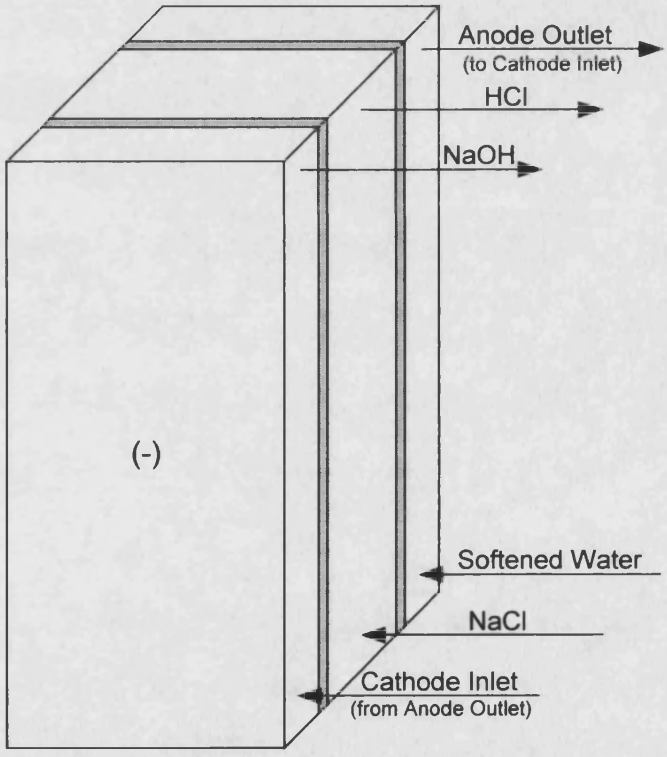

Figure 2.15 Flow Configuration in the Electrochemical Acidification Cell, showing the fluid inlets and outlets.

2.6.2 Cation Exchange Resins and Cation-Permeable Membranes

Various types of cation exchange resins from Mitsubishi Chemical (Tarrytown, NJ) were evaluated in the study. The specifications of the strongly acidic cation exchange resins – gel and porous types and weakly acidic cation exchange resins are listed in Tables 2.3 and 2.4.

Table 2.3 Specifications of Strongly Acidic Cation Exchange Resins – Gel Type

Grade	SK104	SK106	SK1B	SK110	SK112	SK116
Crosslinkage / %	4	6	8	10	12	16
Moisture Content / %	57-67	47-57	43-50	35-45	32-42	37-37
Total Capacity / eq m^{-3}	1,200	1,600	2,000	2,000	2,100	2,100
Effective Size / mm	0.4-0.6	0.4-0.6	0.4-0.6	0.4-0.6	0.4-0.6	0.4-0.6
Max. Operating Temp. / °C	120	120	120	120	120	120

Table 2.4 Specifications of Strongly Acidic Cation Exchange Resins – Porous Type and Weakly Acidic Cation Exchange Resins

Type	Strongly Acidic – Porous Type			Weakly Acidic	
Grade	PK228	HPK25	EXCO4	WK10	WK40
Crosslinkage / %	14	25	> 50	-	-
Moisture Content / %	37-43	37-47	50-60	53-59	43-50
Total Capacity / eq m^{-3}	2,050	1,700	1,200	2,500	4,400
Effective Size / mm	0.40	0.40	0.45	0.40	0.40
Max. Operating Temp. / °C	120	120	-	150	120

Unless otherwise stated, the cation exchange compartment contained a 10 % DVB crosslinked strong acid cation exchange resin (SK110, Mitsubishi Chemical, Tarrytown, NJ) and the two electrode compartments contained a 6.0 % DVB strong acid crosslinked cation exchange resin (SK106, Mitsubishi Chemical, Tarrytown, NJ).

Cation-permeable membranes (CMI-7000, Membrane International, Glen Rock, NJ) were used between compartments. The properties of the cation-permeable membranes are listed in Table 2.5.

The cells were assembled with cation exchange resin in the sodium form. For the cation exchange resin types being studied, the swelling property of each type was determined prior to cell assembly. Based on this information, cells were filled with a particular

volume that corresponded to the cation exchange resin type. This allowed all of the cells to have a constant packing density.

Table 2.5 Properties of Cation-Permeable Membrane

Grade	CMI-7000
Electrical Resistance @ 25 °C / Ω cm 1.0 N NaCl 0.1 N NaCl	 18 0.46
Permselectivity / % 0.2 N KCl / 0.1 N KCl	97
Transport Number 0.5 N KCl / 0.1 N KCl	0.98
Total Capacity / eq kg^{-1}	1.3
Mullen Burst Strength / kPa	1,375
Temperature Stability / °C	125
Water Permeability @ 5-psi, cm^{-3} s^{-1} m^{-2}	< 0.03

The cation-permeable membranes used were conditioned and activated by soaking in 10 % sodium chloride solution at 55 °C for three hours and cut accurately to size. The cation resin and membranes were kept damp during the assembly of the cell.

2.6.3 Solutions

The cation exchange compartment of the electrochemical acidification cell was fed with a sodium chloride solution. The sodium chloride feed solution was prepared by dissolving reagent grade sodium chloride salt in deionised water in a 113 dm^3 polypropylene tank. The anode compartment was fed with softened water.

Figure 2.16 shows the water treatment system was used to produce the softened and deionised water. A twin alternating water softener (LCTA 150 Series, Alamo Water Refiners, San Antonio, TX) was used to soften the feed water; to exchange sodium ions for iron, magnesium, manganese and calcium ions. The water softener system utilised two 0.20 m^3 fibreglass columns arranged in a service/standby configuration. A carbon filter was used to absorb free available chlorine, organics, and some suspended solids from the softened water. The carbon filtration system contained one 14 dm^3 fibreglass column filled with granulated activated carbon. A single 10 micron filter cartridge was then used to remove suspended solids. This also removed silt and carbon fines from the

carbon filter. The 25.4 cm cartridge filter housing contained one 24.8 cm polyester filter media at a 5 nominal micron rating. Two mixed-bed ion exchange columns in series were used to completely deionise the water to a resistivity of 18.3 MΩ cm.

Prior to the mixed-bed columns, a portion of the softened water was drawn off to feed the electrode compartments. The softened water had at a conductivity of approximately 150 μS cm^{-1} at 20 °C.

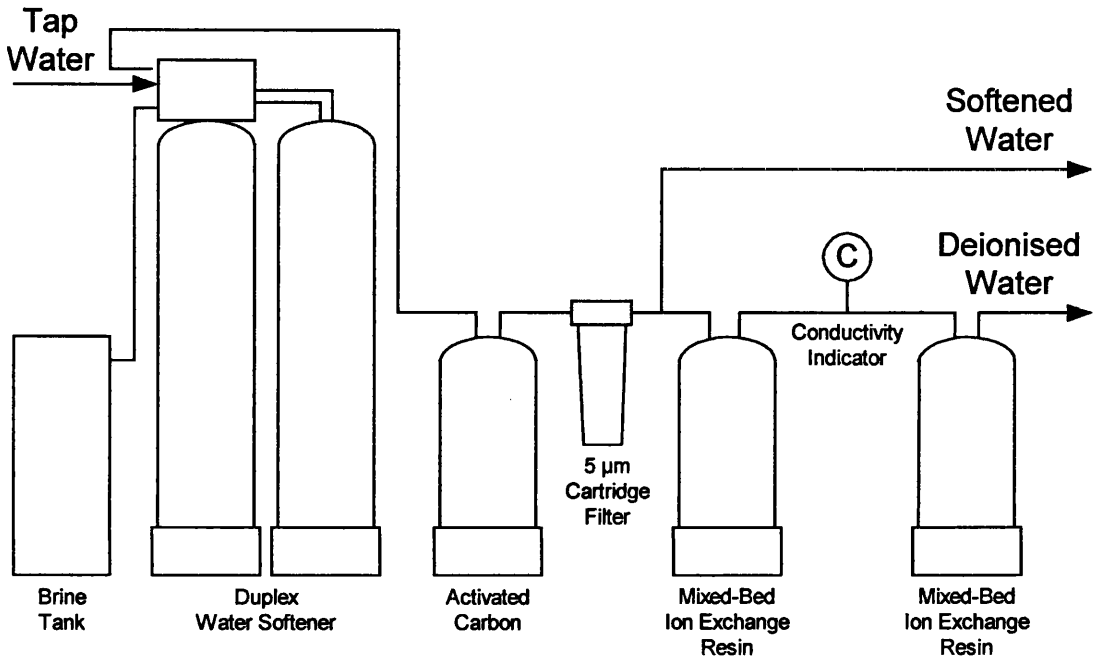

Figure 2.16 Water Treatment System Used in this Study

2.6.4 Experimental Arrangement

The experimental arrangement for the electrochemical acidification cell is schematically represented in Figure 2.17. Flow rates were controlled by needle valves (F20BK, Deltrol, Bellwood, IL) and kept constant by adjusting the flow of liquid to constant flow meter readings (CR-440 Blue White, Westminster, CA). Absolute flow rates were determined by timing a measured volume each time a sample was taken from the effluents. Pressure to circulate liquid through the cation exchange compartment was supplied by a centrifugal pump (25 cm^3 s^{-1} at 200 kPa, WMD 305SZ, Iwaki WalChem, Holliston, MA). Tap water pressure was used to force liquid through the electrode compartments. It was found that these methods kept the flow rates constant within a few percent.

Circulating cooled or heated water through a heat exchanger controlled feed water temperature. Water temperature was monitored between 17 to 34 °C. Temperature fluctuations over the course of an experimental run were less than 1 °C.

Water pH was measured by a pH/ORP analyser (SCL-P-014-M2, Rosemount, Irvine, CA). Conductivity measurements were determined with a hand held conductivity meter (EP, Myron L, Carlsbad, CA). The water temperature was measured using an in-line thermometer (GT-300, Tel-Tru Manufacturing Co., Rochester, NY). The inlet and outlet pressures (PI) were determined using 0 to 200 kPa pressure gauges (47738, Ametek, Sheboygan, WI).

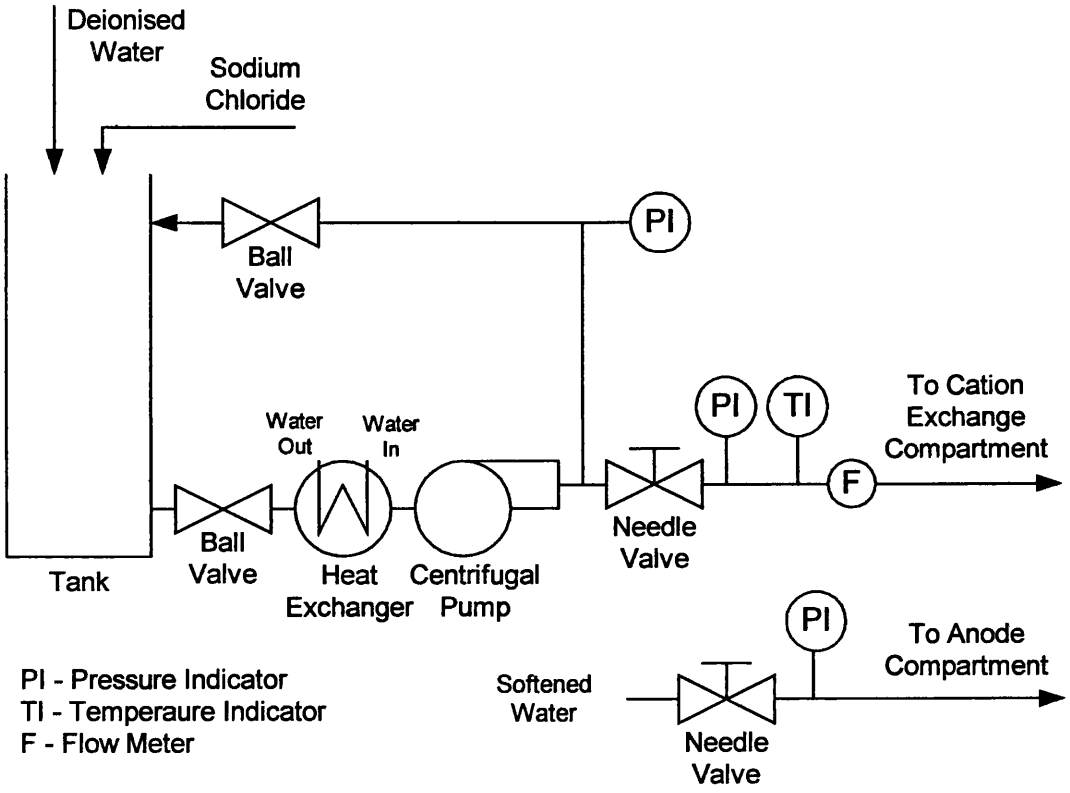

Figure 2.17 Arrangement for the Electrochemical Acidification Cell Experiments

The hydrogen ion concentration of the feed and acidified product was determined by volumetric titration. A desired volume of the product (50 cm^3) was measured into a flask. Sodium hydroxide of a known concentration (0.1 N) was added from a burette; the volume used was carefully measured. A few drops of an indicator (phenolphthalein) were used to signal when to stop adding sodium hydroxide; the indicator changed colour (clear to pink) when the reaction was completed. From this data, the molarity of acid was calculated.

While passing the solutions through the compartments of the cell, a controlled current was applied to the anode and cathode. The current was supplied to the cell by a constant voltage/amperage power supply (Electrolab, San Antonio, TX). The output of the power supply was 60 VDC at 10.0 A, with an AC ripple of 3 %. The applied DC current was set to the desired value in each of the experiments and measured using a digital multi-meter (21 III, Fluke Corp., Everett, WA). The total voltage across the cell was also measured using a digital multi-meter. There were small periodic variations, less than 1 %, in the voltage during operation, attributable to the formation and release of bubbles on the electrode surfaces.

2.6.5 Sampling and Analysis

Samples were taken of the inlet and outlet solutions to the acidification cell. The following data was recorded at one-hour intervals; cell voltages (V), applied current (A), flow rate ($cm^3\ s^{-1}$), temperature (°C), pH, and hydrogen ion concentration (mol m^{-3}). Each run was continued until a steady-state condition had been established; when three consecutive one-hour samples gave constant readings.

Measurement of current efficiency permits the determination of the intensity of acidification and characterisation of this process regardless of equipment size, design, and output. Current efficiency is defined by the flow rate, change in the sodium ion concentration from the liquid entering and exiting the cation exchange compartment, and applied current. It can be determined by:

$$\eta_c = \frac{Q\ (C_{Na}^{in} - C_{Na}^{out})\ z\ F}{I} \tag{2.68}$$

where η_c is the current efficiency, Q the flow rate through the cation exchange compartment, C the concentration of sodium ions, z the valency, F Faraday's constant, and I the applied current. Since sodium ions were being exchanged with hydrogen ions, the decrease in sodium ions was equal to the increase of hydrogen ions:

$$(C_{Na}^{in} - C_{Na}^{out}) = -(C_H^{in} - C_H^{out}) \tag{2.69}$$

Therefore, the current efficiency was calculated by:

$$\eta_c = -\frac{Q\,(C_H^{in} - C_H^{out})\,z\,F}{I} \qquad (2.70)$$

The total experiment of the electrochemical acidification cell was conducted in four phases;

1. Approach to Steady State
2. Cation Exchange Resin Selection
3. Variable Screening
4. Performance Characterisation / Model Prediction

The first phase investigated the cells approach to steady state. The intent was to observe the performance of the cell when a change was made with one of the operating variables.

The second phase evaluated several types of cation resins for the cation exchange compartment with the intent to select the most suitable cation resin type for the third phase experiments. The types of resins evaluated included:

- Strong acid cation exchange resins based on crosslinked polystyrene matrix having sulfonic acid groups - all were gel-types with crosslinkages of 4, 6, 8, 10, 12, and 16 % divinylbenzene
- Strong acid cation exchange resins based on a porous styrene divinylbenzene polymer matrix - all were porous with crosslinkage between 14, 25, and 55 %
- Weak acid cation exchange resins having carboxylic acid functionality
- Weak acid cation exchange with carboxylic acid functionality based on a porous acrylic polymer matrix

A performance comparison for the cation exchange resins evaluated was made possible by introducing a coefficient of performance or figure of merit. Among the normal characteristics of a cation exchange resin such as effective particle size, total capacity, moisture content, degree of crosslinkage, swelling, etc., perhaps the most important single parameter is that of the 'effectiveness' of operation in an electromechanical acidification cell. This can be related in terms of amount of power required to produce a

given quantity of acid per unit time from a given sodium chloride feed concentration. The figure of merit (FM) used to compare the performance of the various cation exchange resins in an electrochemical acidification cell is defined as:

$$FM = \frac{-Q(C_{H^+}^{in} - C_{H^+}^{out})}{\Phi I} \qquad (2.71)$$

where Q is the flow rate, C the concentration of hydrogen ions, Φ the applied cell potential, and I the applied current.

The third phase used a practical method to preliminary screen variables that affect the performance of the electrochemical acidification cell. There are a large number of possible variables but the ones chosen were variables that tend to influence the rate of diffusion within the cation resin particle or through the thin film around the cation resin particle. The parameters investigated included sodium chloride concentration, temperature, flow rate, and applied DC current.

The fourth phase investigated the more important variables determined by a screening experiment. The evaluation was designed to show the conditions necessary for the operation of an electrochemical acidification cell; the operating characteristics and the optimum operation with respect to current efficiency. Only one variable was changed at a time, while when possible, keeping all others constant. Predictions from the model were also superimposed on the actual data.

2.6.6 Accuracy of Results

Values of flow rate and current quoted are accurate to within 5.0 %. The hydrogen ion analysis would at best be accurate to within 2.0 %. From a consideration of the accuracy of these measurements and the overall variability of the system, conclusions should not be drawn in results that depend on differences between values of current efficiency with a separation of less than 5.0 %. The accuracy of any one result is on the order of ± 2.5%.

2.7 Results and Discussion

Unless otherwise stated, all of the experiments were operated as follows: A stream of sodium chloride feed solution at a conductivity of 3,000 μS cm^{-1} was passed through the cation exchange compartment packed with the cation exchange resin being evaluated.

The two electrode compartments contained Daion SK106 cation exchange resin. The sodium chloride solution at a conductivity of 3,000 μS cm^{-1} at approximately 20 °C was passed through the cell from bottom to top through the cation exchange compartment at a flow rate of approximately 2.5 cm^3 s^{-1}. Softened water was passed upwardly through the anode compartment and then upwardly through the cathode compartment in series at a flow rate of approximately 1.7 cm^3 s^{-1}. While passing the solutions through the compartments of the cell, a controlled DC current of approximately 8.0 A (521 A m^{-2}) was applied to the anode and cathode.

2.7.1 Establishment of Steady State

Steady state is achieved in an electrochemical acidification cell when the total number of sodium ions entering the cell equals the total number of sodium ions exiting the cell, signifying that there is no change in the number or accumulation of sodium ions in the cell. The flow rate and sodium ion concentration in the sodium chloride feed and outlet solutions from the cation exchange and cathode compartments can be measured to determine steady state.

Due to the electrochemical nature of the system, steady state can also be determined by the pH of the combined outlet streams. The moles of hydrogen and hydroxyl ions are generated at an equal rate at the anode and cathode, respectively. Since the pH of the sodium chloride feed solution is neutral, steady state is achieved when the pH of the combined outlet streams is neutral; when the total number of hydrogen ions in the cation exchange compartment effluent equals the total number of hydroxyl ions in the cathode compartment effluent. This will hold true at any current efficiency, since the hydrogen ions that are not used to exchange sodium ions on the cation exchange resin will migrate into the cathode compartment and combine with hydroxyl ions to form water.

The approach of an electrochemical acidification cell to steady state is illustrated in Figure 2.18, with respect to the hydrogen ion concentration in the effluent from the cation exchange compartment with a cell whose cation exchange resin began totally in the sodium form. The sodium chloride solution was passed through the cation exchange compartment from bottom to top such that the flow rate was approximately 2.5 cm^3 s^{-1}. Softened water was passed upwardly through the anode compartment and then upwardly through the cathode compartment in series such that the flow rate was approximately 1.7 cm^3 s^{-1}. While passing the solutions through the compartments of the cell, a controlled current of 8.0 A (521 A m^{-2}) was applied to the anode and cathode.

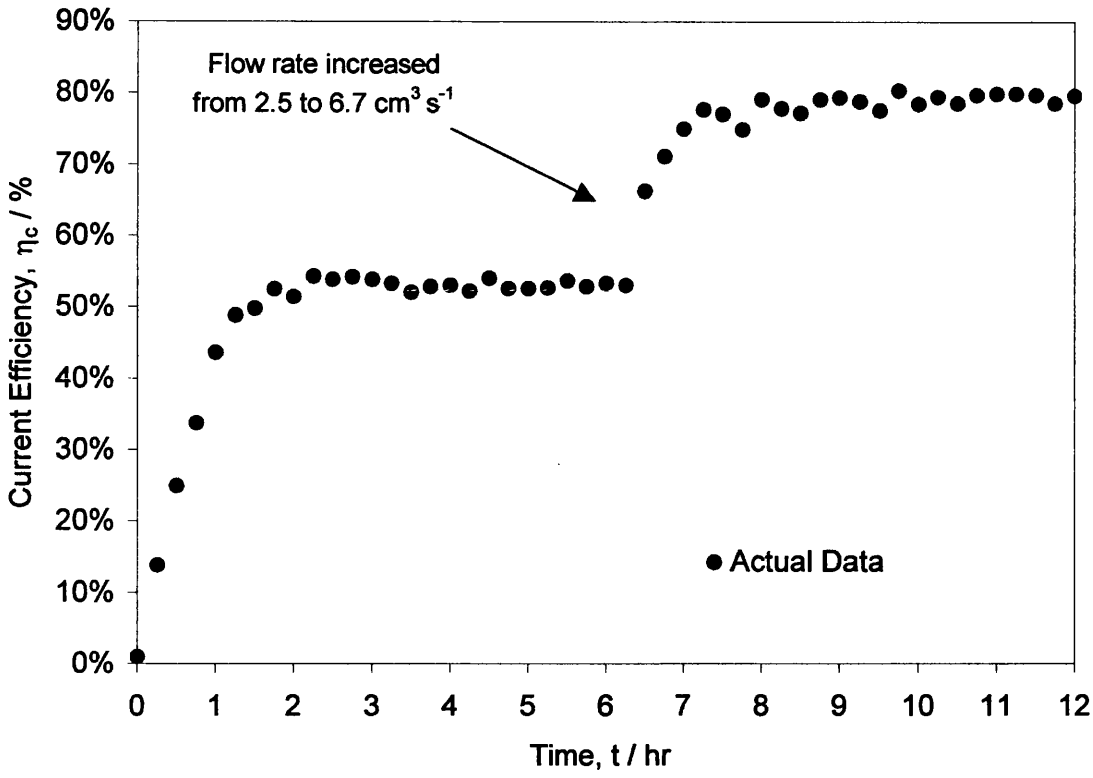

Figure 2.18 Behaviour of an Electrochemical Acidification Cell as it Approaches Steady State: Conductivity of sodium chloride was 3,000 µS cm^{-1} (~1,800 ppm) at a temperature of approximately 22 °C. The applied current was 8.0 A (521 A m^{-2}). The active area of the cell measured 153.5 cm^2. Diaion SK110 cation exchange resin was used in the cation exchange compartment.

The rise in the curve from 0 to 2 hours arises from the hydrogen/sodium equilibrium being established in the cation exchange resin bed in the cation exchange compartment. Hydrogen ions from the anode compartment pass through the cation-permeable membrane and into the cation exchange compartment to replace captured sodium ions held on the cation exchange resin, thereby regenerating the cation resin for subsequent processing. These sodium ions pass through the cation-permeable membrane and into the cathode compartment, combining with the hydroxyl ions in the cathode compartment to form sodium hydroxide. Sodium ions from the sodium chloride feed solution are taken up onto the regenerated resin. Steady state was achieved within three hours of operation.

Steady state had to be re-established each time after a change in flow rate, feed concentration or applied current. Between 6 to 7 hours in Figure 2.18 shows the

variation of current efficiency after increasing the flow rate from 2.5 to 6.7 $cm^3 s^{-1}$. The cell adjusted itself very rapidly, within one hour of operation. Continuation of experiment for period of up to eight hours showed no further change in conditions.

It could be assumed for practical purposes that steady state can be reached after three hours of operation when an adjustment is made to the operating conditions. Therefore, experimental runs will continue until three consecutive one-hour samples give steady readings in voltage, flow rate, and pH.

2.7.2 Cation Exchange Resin Selection

Selection of cation exchange resins for use in the electrochemical acidification cell is very important because some resins possess significant chemical and mechanical advantages over others, which will allow some cation exchange resins to be used more efficiently than others.

Cation exchange resins are classified as either strongly or weakly acidic depending on the degree of acidity. Strong acid cation exchange resins have sulphonic acid groups as exchange groups. They are considered strongly acidic due to their high hydrogen ion dissociation over the entire pH range. These cation exchange resins are much more conductive in the regenerated form than in the exhausted form. Therefore, when a portion of the bed is electrically regenerated, most of the current will pass through the regenerated portion and will not be effective in regenerating the remaining portion of the bed. On the other hand, weak acid cation exchange resins having carboxylic acid functionality have low hydrogen ion dissociation, especially in the low pH range. These types have a very low conductivity in the regenerated form and are more conductive in the exhausted form. Therefore, weak acid cation resin may be used more efficiently than the strongly acidic types.

Swelling and shrinking are normal functions for all ion exchange resins. The resin will swell and shrink when hydrated, immersed in an electrolyte solution, or when converted to a different ionic form. The extent at which the resin swells is determined by the ratio of styrene to divinylbenzene on the resin matrix. The percentage of divinylbenzene on the resin matrix is defined as crosslinking.

Ion exchange resins with lower percentages of crosslinking are capable of absorbing greater amounts of water into the resin matrix. The absorbed water in the resin matrix

will cause the resin to have a high degree of porosity, which is independent of any physical porosity resulting from the presence of discrete pores in the resin matrix. The high degree of porosity will result in channels through the resin matrix where ions can rapidly diffuse [32]. The characteristic of a low crosslinked ion exchange resin may be beneficial if the ions absorbed are the current carrying ions.

Ion exchange resins with higher percentages of crosslinking are capable of absorbing less amounts of water into the resin matrix. These resins exhibit slower gel phase kinetics than resins with lower percentages of crosslinking, thereby, creating a resistance to ions carrying current.

There are normal porous cation resins with moderate degrees of crosslinkage and highly porous cation resins with high degrees of crosslinkage. In general, normal porous cation resins have higher porosity and specific surface area than the gel-types. The size of the micropores in the resin matrix is large, and has excellent swelling and contracting characteristics. There are also macroporous cation resins with a high degree of crosslinkage. They have high specific surface area and pore volume, and are, therefore, useful in applications where the surface of the resin is mainly used. Due to the high degree of crosslinkage, the micropores are small, making diffusion of ions in the resin very slow.

Several types of cation exchange resins for the cation exchange compartment were selected with the intent to select the most suitable cation resin type for the second phase of experiments. The cation resins selected were all Daion cation exchange resins (Mitsubishi Chemical - Tarrytown, NJ) and are listed in Table 2.6.

Samples were taken of the inlet and outlet solutions. Each run was continued until steady state. Equation (2.71) was used to compare the performance of the various cation exchange resins evaluated. The results are displayed in Table 2.7.

The weakly acidic cation exchange resins had a high electrical resistance. It confirms that the low hydrogen ion dissociation creates a very low conductivity in the regenerated form as opposed to the strongly acidic cation exchange resins who are much more conductive in the regenerated form due to their high hydrogen ion dissociation over the entire pH range. Due to the high electrical resistance, the energy input per volume of feed solution was enough to cause a considerable rise in temperature of the solution.

Table 2.6 Cation Exchange Resins Evaluated

Grade	Type
Daion PK228L	14 % DVB, Strong Acid, Porous
Daion HPK25	25 % DVB, Strong Acid, Porous
Daion EXCO4	> 50 % DVB, Strong Acid, Porous
Daion SK104	4 % DVB, Strong Acid, Gel
Daion SK106	6 % DVB, Strong Acid, Gel
Daion SK1B	8 % DVB, Strong Acid, Gel
Daion SK110	10 % DVB, Strong Acid, Gel
Daion SK112	12 % DVB, Strong Acid, Gel
Daion SK116	16 % DVB, Strong Acid, Gel
Daion WK10	Weak Acid
Daion WK40	Weal Acid, Acrylic

Table 2.7 Performance of the Various Daion Cation Exchange Resins Evaluated

Resin Type	Outlet H^+ Concentration / eq m^{-3}	Outlet Temperature / °C	Volt / V	FM
SK110	18.60	26.7	14.6	1.37
SK106	17.33	26.0	13.7	1.37
SK1B	18.00	27.0	14.8	1.37
PK228L	17.33	28.5	16.6	1.25
SK104	16.53	27.8	15.3	1.22
SK112	18.53	30.2	17.3	1.16
SK116	18.47	27.0	18.8	1.11
HPK25	17.07	31.0	21.9	0.82
EXCO4	17.13	30.2	26.7	0.68
WK10	17.00	45.3	62.3	0.30
WK40	16.53	43.3	68.2	0.28

The following parameters were held constant throughout the experiment; inlet H^+ concentration of 0.08 eq m^{-3}, inlet temperature of 20 °C, flow rate of 2.5 cm^3 s^{-1}, and applied current of 8.0 A (521 A m^{-2}).

Strongly acidic cation exchange resins with a higher percentage of crosslinking brought about a definite increase in electrical resistance. It confirms that the high degree of porosity provided channels in the resin matrix, which allowed the DC current carrying ions to rapidly diffuse. No differences were seen between the porous and gel types. The energy input per volume of feed solution was enough to cause a moderate rise in temperature of the solution. Cation exchange resins containing sulphonic acid groups are thermally stable. However, their stability depends on pH. In the hydrogen form, cation resin is stable up to 140 °C, where in the sodium form, up to 200 °C.

The figure of merit (FM) in Table 2.7 favours Daion SK106, SK1B, and SK110. Since the stability at elevated temperatures and chemical resistance increases with increasing crosslinkage, SK110 was selected as the cation exchange resin to be used for the second phase of experiments solely on the fact that it has a higher level of crosslinkage than the other two cation exchange resins.

2.7.3 Screening Operating Variables

There are typically a large number of variables that can affect the performance of any chemical process. Prior to conducting the experiments to characterise or optimise the process, it is necessary to screen said variables such that the more important variables are known and can be further studied in greater detail. Experimental designs offer a method of getting the maximum information from a minimum numbers of tests. There are many experimental designs methods available who all have the same objectives of determining the most important variables. Some commonly used experimental design methods include; one-shot, static group, random group, factorial, Latin square, incomplete block, randomised block, time-series, covariance, split-plot designs [33-42].

The classical method of studying one variable at a time while holding all others constant is extremely inefficient in many cases if the important variables are unknown. If the less important variables are chosen, the evaluation may result in great effort and expense while not providing much useful information. The Plackett-Burman design [43] is a practical method of screening large numbers of variables. The design is based on balanced incomplete blocks. If efficient preliminary screening of variables can be accomplished, a relatively small number of important variables could be selected for further, more detailed study. This will allow the majority of the effort and expense to be concentrated on the most important variables.

Table 2.8 shows the matrix of the design used to screen variables for both the electrochemical acidification cell and the fixed-bed catalytic reactor, with each variable tried at two levels, (+) denoting high level, and (-) low level. Eight variables were selected for study, leaving three dummy variables from which error was estimated. Tables 2.9 shows the list of variables and the levels at which they were studied for the electrochemical acidification cell.

Table 2.8 shows that each variable appears at its high level four times and at its low level four times. The effect of a variable on the response is simply the difference between the average value of the response for the four runs at the high level and the average value of the response for the four runs at the low level:

$$E_A = \frac{\sum R_r \text{ at } (+)}{4} - \frac{\sum R_r \text{ at } (-)}{4} \tag{2.72}$$

where E_A is the effect of variable A and R_r the response or result.

Table 2.8 Design Matrix for Eight Variables with Each Variable Tried at Two Levels

Run #	Variables						
	A	B	C	D	E	F	G
1	+	+	+	-	+	-	-
2	-	+	+	+	-	+	-
3	-	-	+	+	+	-	+
4	+	-	-	+	+	+	-
5	-	+	-	-	+	+	+
6	+	-	+	-	-	+	+
7	+	+	-	+	-	-	+
8	-	-	-	-	-	-	-

Table 2.9 Variables and Levels for the Electrochemical Acidification Cell

Variables	Process Variable	(-)	(+)
A	Flow Rate / $cm^3\ s^{-1}$	2.5	6.7
B	Concentration / $\mu S\ cm^{-1}$	3,000	7,500
C	Current / A	8.0	10.0
D	Dummy	-	-
E	Temperature / °C	23.0	37.0
F	Dummy	-	-
G	Dummy	-	-

Variables A, B, C, and E are process variables. The test matrix shows that when A is at its high level, B is at its high level two times and at its low level two times. Likewise, when A is at its low level, B is high in two runs and low two times. Thus, the net effect of changing variable B cancels out in calculating the effect of A. The remaining variables balance in this same way so that the net difference is only the effect of A.

Variables D, F, and G in the test matrix are dummy variables – no changes are made corresponding to the (+) and (-) in these columns. The effects of the dummy variables are calculated in the same way as the effects of the real variables. If there are no interactions and all of the levels are reproduced perfectly with no error in measuring the response, the effect shown by a dummy variable will be zero. If the effect is not equal to zero, it is assumed to be a measure of the lack of experimental precision plus any analytical error in measuring the response. Typically, three such estimates of experimental error, or three dummy variables, will provide adequate confidence. The variance of an effect is estimated by combining the dummy effects as follows:

$$V_{eff} = \frac{\Sigma(E_d)^2}{n} = \frac{(E_E)^2 + (E_F)^2 + (E_G)^2}{3} \tag{2.73}$$

where V_{eff} is the variance of an effect, E_d the effect shown by a dummy, and n the number of dummy variables. This equation shows that the variance is equal to the average of the squares of the dummy effects. The relationship between the variance of an effect and the standard error of an effect is:

$$SE_{eff} = \sqrt{V_{eff}} \tag{2.74}$$

Therefore, from the responses of the eight runs, it is possible to calculate the effect of each of the four real variables and to find the standard error of each of the effects from the effects of the dummies. The significance of each effect can then be determined by using the familiar *t*-test:

$$t_t = \frac{effect}{SE_{eff}} \tag{2.75}$$

The three dummy variables provide three degrees of freedom for entering the tabulated values of t_t. The *t*-test for any individual effect allows an evaluation of the probability of determining if the effect is significant. The confidence level was determined from the *t*-test value. A confidence level greater than 90 % is often used to indicate variables that have an affect on performance.

The eight experiments were performed in the order defined by the matrix in Table 2.8. The cells were operated until steady state and their performance was expressed as

current efficiency. These experimental results are the eight responses that are used to calculate the effects. Table 2.10 shows the effects found for each of the variables and the corresponding confidence levels. Flow rate, concentration, and current all have a significant effect on performance. Varying all three of these variables can allow for negligible to significant film diffusion resistance. Temperature had a confidence level of 85.2 %, indicating that it has a minimal effect on performance. Surprisingly, it appears that the temperature dependent variables, resin selectivity coefficient, ionic diffusion coefficients, and viscosity and density of the bulk solution have opposing overall effects in the ion exchange process.

Table 2.10 Screening Results for the Electrochemical Acidification Cell

Process Variable	Levels		Effect	Relative Significance, *t*-test	Confidence Level* (> 90 %)
	(-)	(+)			
Flow Rate / $cm^3\ s^{-1}$	2.5	6.7	0.115	2.496	91.2 %
Concentration / mS cm^{-1}	3.0	7.5	0.105	2.271	89.2 %
Current / A	8.0	10.0	-0.113	2.433	90.7 %
Dummy	-	-	-0.056	1.212	-
Temperature / °C	23.0	37.0	-0.090	1.937	85.2 %
Dummy	-	-	-0.009	0.204	-
Dummy	-	-	-0.056	1.221	-

Dummy variables D and G are large compared with dummy variable F. The values may be due to one of the possible two-factor interactions with which variables D and G are confounded. Alternatively, this may be due to experimental error. In any case, these are included in the calculation of the variance as a measure of the uncertainty of the results.

2.7.4 Process Characterisation

The experiments described in this section were designed to show the conditions necessary for the operation of an electrochemical acidification cell; the operating characteristics and the optimum operation with respect to current efficiency. The data will also be used to derive a mass transport factor for the mathematical model of the electrochemical acidification cell. Mathematical model calculations were performed using Solver in Microsoft® Excel 2000 (see Appendix D).

The values of current efficiency were calculated using equation (2.70). These values were only calculated when three consecutive one-hour samples gave steady readings

and when a mass balance for the complete system was obtained. Hydrogen and hydroxyl ion concentrations were determined by volumetric titration in the product and electrode streams, respectively. When the concentrations were within experimental error from one another, a difference of less than 5.0 %, then it was assumed that a mass balance was achieved. An example of the mass balance is given in Table 2.11.

Table 2.11 Example of a Mass Balance in an Electrochemical Acidification Cell

Experiment	From Cation Exchange Compartment H^+ Conc. / eq L^{-1}	From Cathode Compartment OH^- Conc. / eq L^{-1}	Deviation	Percent Deviation
1a	0.0210	0.0200	+0.0010	+4.8 %
1b	0.0200	0.0191	+0.0009	+4.5 %
1c	0.0204	0.0210	+0.0005	+2.3 %
7a	0.0140	0.0142	-0.0002	-1.4 %
7b	0.0137	0.0130	+0.0007	+5.1 %
7c	0.0144	0.0150	-0.0006	-4.2 %
14a	0.0071	0.0068	+0.0003	+4.2 %
14b	0.0071	0.0069	+0.0002	+2.8 %
14c	0.0072	0.0071	+0.0001	+1.4 %

Table 2.12 displays the results from the experiments that evaluated the effect of feed temperature on current efficiency. Feed temperatures from 20 to 36 °C were investigated in these experiments.

Table 2.12 Effect of Feed Temperature on Current Efficiency

Experiment	Temperature T / °C	Outlet Na^+ Conc. C_{out} / eq m^{-3}	Current Efficiency η_c / %
19a	21.0	0.013	53.7
19b	21.0	0.013	52.9
19c	22.0	0.013	50.8
20a	27.0	0.012	54.9
20b	27.5	0.012	54.3
20c	28.0	0.012	53.7
21a	35.0	0.012	59.1
21b	37.0	0.011	61.4
21c	36.0	0.010	62.1

The following parameters were held constant throughout the experiment; inlet Na^+ concentration of 0.03 eq m^{-3}, flow rate of flow rate of 2.5 cm^3 s^{-1}, and applied current of 8.0 A (521 A m^{-2}).

Table 2.13 displays the results from the experiments that evaluated the effect of sodium chloride concentration on current efficiency. Sodium chloride solution conductivities from 2,000 to 18,000 μS cm^{-1} (~1,185 to 11,000 ppm) were investigated in these experiments.

Table 2.13 Effect of Sodium Chloride Concentration on Current Efficiency

Experiment	Inlet Na^+ Conc. C_{in} / eq m^{-3}	Outlet Na^+ Conc. C_{out} / eq m^{-3}	Current Efficiency η_c / %
7a	0.020	0.006	39.3
7b	0.021	0.006	42.5
7c	0.020	0.006	43.1
8a	0.030	0.012	59.7
8b	0.031	0.012	47.6
8c	0.030	0.012	53.0
9a	0.063	0.037	68.0
9b	0.063	0.036	70.8
9c	0.063	0.039	79.1
10a	0.078	0.052	74.8
10b	0.079	0.053	79.5
10c	0.077	0.051	84.6
11a	0.125	0.093	86.1
11b	0.124	0.097	91.5
11c	0.124	0.096	85.8
12a	0.163	0.134	90.0
12b	0.168	0.136	91.9
12c	0.167	0.136	93.9
13a	0.203	0.172	91.5
13b	0.203	0.170	91.4
13c	0.204	0.173	93.5

The following parameters were held constant throughout the experiment; flow rate of 2.5 cm^3 s^{-1}, inlet temperature of 25 °C, and applied current of 8.0 A (521 A m^{-2}).

Tables 2.14 displays the results from the experiments that evaluated the effect of flow rate on current efficiency. Flow rates from 1.57 to 15.5 cm^3 s^{-1} were investigated in these experiments.

Table 2.15 displays the results from the experiments that evaluated the effect of applied current on current efficiency. Applied currents from 2.0 to 10.0 A (130 to 651 A m^{-2}) were investigated in these experiments.

Table 2.14 Effect of Flow Rate on Current Efficiency

Experiment	Outlet Na^+ Conc. C_{out} / eq m^{-3}	Flow Rate Q / cm^3 s^{-1}	Current Efficiency η_c / %
1a	0.009	1.57	38.6
1b	0.010	1.68	40.7
1c	0.010	1.67	39.4
2a	0.013	2.17	46.9
2b	0.013	2.13	45.9
2c	0.013	2.37	50.8
3a	0.015	3.43	62.9
3b	0.015	3.33	61.1
3c	0.015	3.18	60.1
4a	0.018	4.50	69.9
4b	0.018	4.50	66.5
4c	0.019	5.28	76.7
5a	0.021	7.70	84.4
5b	0.021	6.60	78.5
5c	0.021	7.47	85.2
6a	0.026	15.4	90.0
6b	0.026	14.7	90.1
6c	0.025	15.5	90.4

The following parameters were held constant throughout the experiment; inlet Na^+ concentration of 0.03 eq m^{-3}, inlet temperature of 25 °C, and applied current of 8.0 A (521 A m^{-2}).

2.7.5 Mass Transport Factor

A mass transport factor (J_D) is commonly used to correlate experimental data. For mass transfer in packed beds, many experimental studies found it to be a function of the Re [44]. In the electrochemical acidification process, liquid flow is through a packed bed that is under an applied electric field. Because of this, the customary form of J_D was tested and found to be unsuitable.

Table 2.15 Effect of Current on Current Efficiency

Experiment	Outlet Na^+ Conc., C_{out} / eq m^{-3}	Current, I / A	Current Efficiency, η_c / %
14a	0.024	2.01	84.2
14b	0.024	2.01	83.5
14c	0.024	2.02	84.3
15a	0.018	4.02	79.9
15b	0.019	4.02	74.4
15c	0.019	4.07	70.2
16a	0.016	6.14	67.4
16b	0.014	6.17	62.0
16c	0.014	6.13	59.1
17a	0.012	8.10	59.7
17b	0.012	8.08	47.6
17c	0.012	8.15	53.0
18a	0.011	10.0	54.0
18b	0.012	10.0	45.8
18c	0.011	10.1	45.9

The following parameters were held constant throughout the experiment; inlet Na^+ concentration of 0.03 eq m^{-3}, inlet temperature of 25 °C, and flow rate of flow rate of 2.5 cm^3 s^{-1}.

An analysis was then performed which correlated all of the experimental mass transport data using the iterative least squares method [45]. The aim was to deduce a mass transport factor correlation for the electrochemical acidification process. J_D was found to be a function of the following parameter:

$$J_D = f\left(\frac{C\,v\,F}{i}\right) \tag{2.80}$$

where C is the sodium chloride concentration, v the velocity, F Faraday's constant, and i the current density.

The experimental data used for determining J_D contained a wide range of operating conditions. A range of flow rates from 1.6 to 15.5 cm^3 s^{-1}, applied currents of 2.0 to 10.0 A (130 to 651 A m^{-2}), and sodium chloride concentrations of 2,000 to 18,000 µS cm^{-1} (~1,185 to 11,000 ppm) were used in these experiments. The effluent from the cation

exchange compartment was monitored for hydrogen ion concentration. The current efficiency was calculated and presented from this data. A preliminary regression analysis was done to fit the experimental data to the following form:

$$J_D = A\left(\frac{C v F}{i}\right)^n \tag{2.81}$$

All of the data was considered during the regression analysis. There was some data that had a large deviation from the bulk of the data. Although it was not investigated, these deviations may be the result of the following: the predominate of natural convection at low flow rates, presence of protuberances on the resin surface, differences in the temperature from the top and bottom ends of the compartment, and the presence of back diffusion from the electrode compartments.

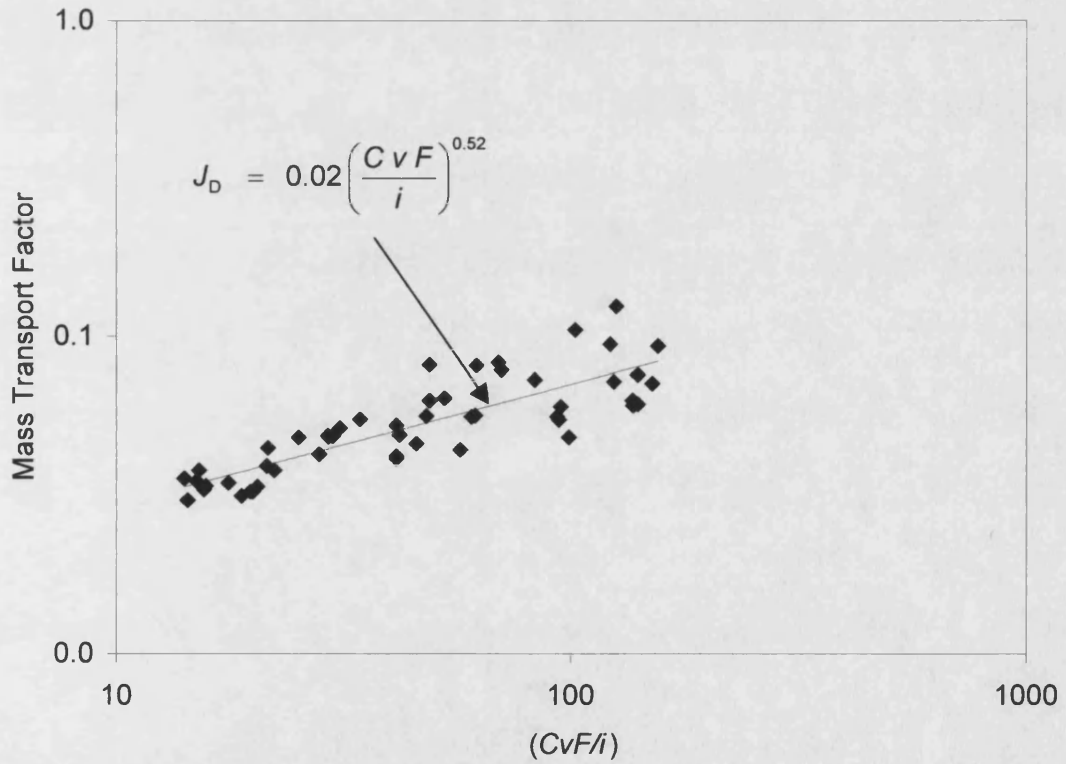

Figure 2.19 Liquid-Phase Mass Transport in Electrochemical Acidification Cell: Sodium/Hydrogen Ion Exchange: Conductivity of sodium chloride range was from 2,000 to 18,000 μS cm^{-1} (~1,185 to 11,000 ppm) at a temperature range between 18 to 26 °C. Total volumetric flow rate range entering the cell was between 1.5 to 15.8 cm^3 s^{-1} and the applied current between 2.0 to 10.0 A (130 to 651 A m^{-2}). The active area of the cell measured 153.5 cm^2. Diaion SK110 cation exchange resin was used in the cation exchange compartment.

Typically, back diffusion from the electrode compartments will have the most influence. If the sodium hydroxide concentration in the cathode compartment becomes too high, back diffusion of hydroxyl ions from the cathode to cation exchange compartment can occur. The reason is that cation-permeable membranes are not truly perfect in passing cations. Limited quantities of anions, such as hydroxyl ions, can penetrate through the membrane and into the cation exchange compartment as the concentration of sodium hydroxide increases.

Hydroxyl ions originating from the catholyte and entering the cation exchange compartment through the cation-permeable membrane as a result of the back diffusion creates a strongly alkaline boundary layer on the surface of the membrane inside the cation exchange compartment. This will neutralise the acid in the center compartment, thus lowering current efficiency.

Although the experimental data of the various experiments scattered widely, a single relation of the form of equation (2.81) can correlate the data by (see Figure 2.19):

$$J_D = 0.02\left(\frac{C\,v\,F}{i}\right)^{0.52} \tag{2.78}$$

The mass transport coefficient, k_f, in the thin film is related to Sh as:

$$k_f = \left(\frac{D_{i/j}^{avg}}{d}\right)\mathrm{Sh} \tag{2.79}$$

or

$$k_f = 0.02\left(\frac{D_{i/j}^{avg}}{d}\right)\left(\frac{C\,v\,F}{i}\right)^{0.52}\mathrm{Re}^{1/2}\,\mathrm{Sc}^{1/3} \tag{2.80}$$

The mass transport coefficient determined is in reality an overall mass transport coefficient and may include both film and particle effects. Expanding the terms yields:

$$k_f = \left(0.02\,F^{0.52}\right)\left(\frac{D^{0.67}}{\upsilon^{0.17}}\right)\left(\frac{C}{i}\right)^{0.52}\left(\frac{v^{1.52}}{d^{0.50}}\right) \qquad (2.81)$$

The first term on the right is a constant, while the second term is dependent on physical properties, such as temperature and pressure. The third and fourth terms are dependent on system properties, such as flow rate, concentration, current density, and particle size. One observes from this equation that the mass transport coefficient increases as the particle size and current density decreases and/or when the velocity or concentration increases. Manipulating these variables offers a technique to escape from the mass transport limited regime into the reaction rate limited regime. Equation (2.81) shows that increasing the velocity has the greatest impact on increasing the mass transport coefficient, whereas a moderate increase is seen when increasing the concentration or when decreasing particle size or current density.

2.7.6 Effect of Flow Rate on Current Efficiency

Table 2.14 shows that current efficiency increased as the flow rate of the feed water increased from 1.6 to 15.5 $cm^3\ s^{-1}$. At a given applied current, the concentration change between the inlet and outlet of the cation exchange compartment is dependent upon the flow rate through the compartment. The majority of the electrolyte ions exit the cation exchange compartment through the cation exchange resins. Cations must first be transferred to the cation exchange resins before being removed. As previously described, the major resistance to mass transport has been identified as the diffusion across the resin/liquid interface. The overall rate of exchange is then said to be liquid film diffusion controlled. The thickness of the thin film controls the resistance of this step. Factors such as liquid velocity in the region of the resin bead control the thickness of the thin film. As velocity increases, the thickness of the film decreases, thus increasing the rate of mass transport, and hence current efficiency.

Figure 2.20 superimposes the model prediction over the actual data. The calculated values of current efficiency show a good agreement with actual data, especially at flow rates less than approximately 8.3 $cm^3\ s^{-1}$.

The prediction overestimated the current efficiency at high flow rates. There is not much of an effect from 8.3 to 16.7 $cm^3\ s^{-1}$. Hence the external mass transport is less important. The levelling off may indicate that internal-diffusion gradients are limiting the process.

This occurs when the movement of cations within the resin particle is slow and is referred to as particle diffusion control. Concentrated liquids, large resin particle diameters, and high degrees of crosslinking favour particle control, as well as efficient liquid agitation. The model does not account for internal-diffusion gradients, and this maybe the cause of the overestimation of current efficiency at the high flow rates.

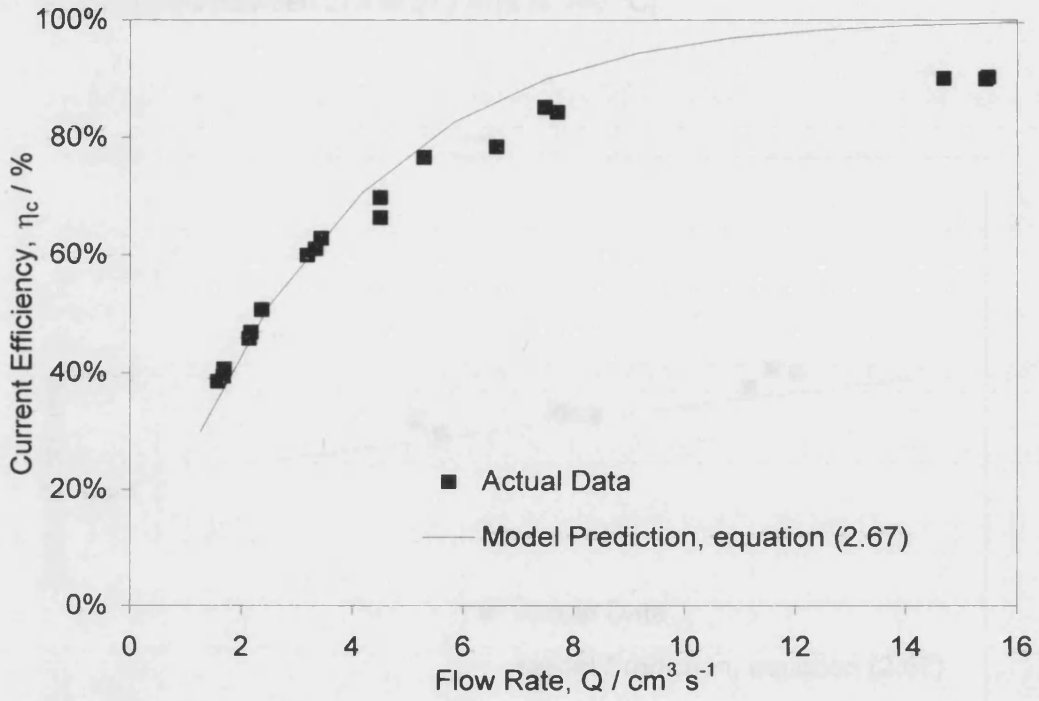

Figure 2.20 Effect of Flow Rate on Current Efficiency: Conductivity of sodium chloride was 3,000 µS cm^{-1} (~1,800 ppm) at a temperature of approximately 25 °C. Total volumetric flow rate entering the cell was varied from 1.6 to 15.5 cm^3 s^{-1} and the applied current was 8.0 A (521 A m^{-2}). The active area of the cell measured 153.5 cm^2. Diaion SK110 cation exchange resin was used in the cation exchange compartment

2.7.7 Effects of Temperature on Current Efficiency

Table 2.12 shows that current efficiency slightly increased as the temperature of the feed water increased from 17 to 31 °C. There are three temperature-dependent parameters that affect the ion exchange process; selectivity coefficient, diffusion coefficient, and kinematic viscosity of the bulk solution. The selectivity coefficient and kinematic viscosity decrease as temperature is increased, while the diffusion coefficient increases with increasing temperature. The relative contributions of these opposing effects are dependent on the properties of the cation exchange resin. For the case of strongly acidic cation exchange resin, the current efficiency is only slightly affected by temperature. Model simulations have been examined to observe the combined effects.

The effect of temperature on kinematic viscosity was determined by an empirical relationship suggested by Bird *et al.* [46] as:

$$\upsilon = \exp(0.0001T^2 - 0.0832T + 11.2197) \qquad (2.82)$$

for temperatures between 273 to 373 K (0 to 100 °C).

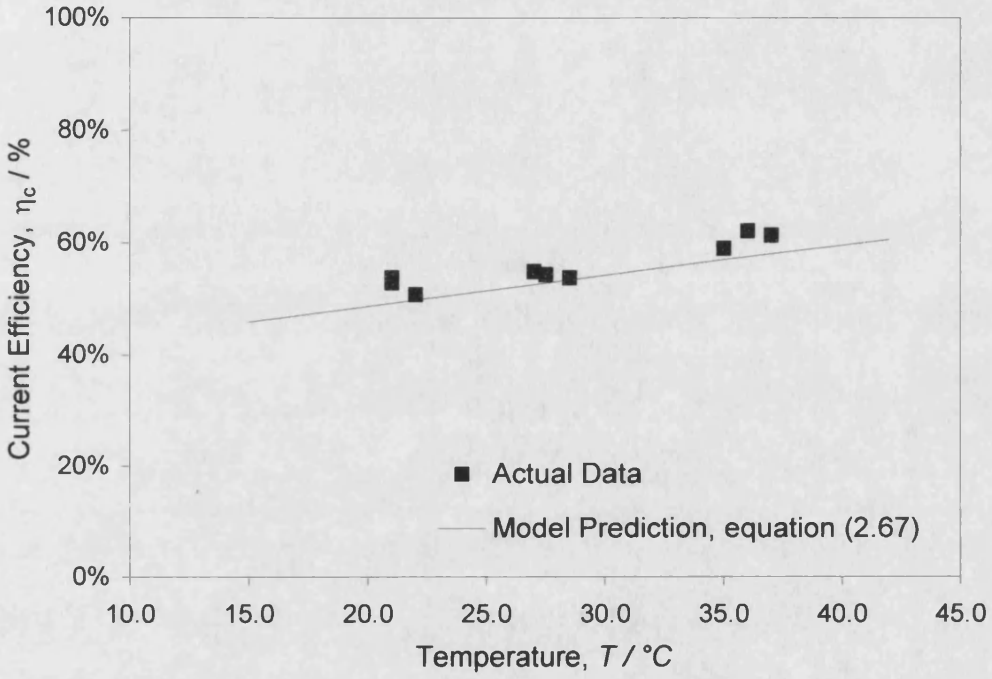

Figure 2.21 Effect of Feed Temperature on Current Efficiency: Conductivity of sodium chloride was 3,000 μS cm^{-1} (~1,800 ppm) at a temperature between 20 to 36 °C. Total volumetric flow rate entering the cell was approximately 150 cm^3 s^{-1} and the applied current was 8.0 A (521 A m^{-2}). The active area of the cell measured 153.5 cm^2. Diaion SK110 cation exchange resin was used in the cation exchange compartment.

Divekar *et al.* [47] have determined the effect of temperature on the selectivity coefficient for a 16 % DVB cation exchange resin. Based on this information, the model used a selectivity coefficient of 1.48 for the cation exchange resin at 298 K (25 °C), which is typical for 10 % DVB cation exchange resins. The following equation was generated by a symmetrical fit to the equation developed by Divekar *et al.* through a value of 1.48 at 298 K (25 °C).

$$K_{Na/H}^{sel} = 201.95 - \frac{1.323}{T} + \frac{0.002}{T^2} \quad (2.83)$$

The effect of temperature on the mobility factor can be estimated based on work done by Harned and Owen [48]:

$$\lambda_H = -2331.4 + 13.174T - 0.014T^2 \quad (2.84)$$

$$\lambda_{Na} = -43.88 - 0.574T + 0.003T^2 \quad (2.85)$$

where T is absolute temperature (K). As a consequence of assumption six, the mobility of species i in the resin can be estimated by:

$$\overline{u}_i = \frac{\lambda_i}{F} \quad (2.86)$$

The diffusion coefficient can be calculated by using the Nernst-Einstein relation:

$$D_i = \left(\frac{RT}{F^2}\right)\lambda_i \quad (2.87)$$

Figure 2.21 superimposes the model prediction over the actual data. The calculated values of current efficiency show a good agreement with actual data over the entire range of data. The slight increase is current efficiency with increasing temperature gives the indication that the exchange is slightly better at higher temperatures. The decrease in resin selectivity coefficient and kinematic viscosity with increase in temperature is slightly overridden by the increase in diffusion coefficient. The effect of the decrease in kinematic viscosity with increased temperature will also influence the pressure drop through the resin bed.

Process temperature is typically limited by the thermal stability of the internal components of the cell. Generally, plastic components used in the cell determine the operating temperature and not necessarily the cation exchange resins and membranes. Most plastics used tend to lose their rigidity at temperatures above 45 °C. However, the use of higher quality or engineered plastics can raise the maximum operational temperature to 60 °C. On the other hand, cation exchange resins and membranes containing sulphonic acid groups are thermally stable. Their stability depends on pH; in

the H^+ form, cation resin is stable up to 140 °C and up to 200°C in the exhausted form. The carbon-sulphur bond in the resin's matrix determines the stability. This is due to the hydrolysis of the carbon-sulphur bond, which increases as pH decreases.

2.7.8 Effect of Current on Current Efficiency

Table 2.15 shows that as the current was increased from 2 to 10 A (130 to 651 A m^{-2}), the current efficiency decreased accordingly. Since the current efficiency determines to a large extent the economics of the process, a high current efficiency is essential.

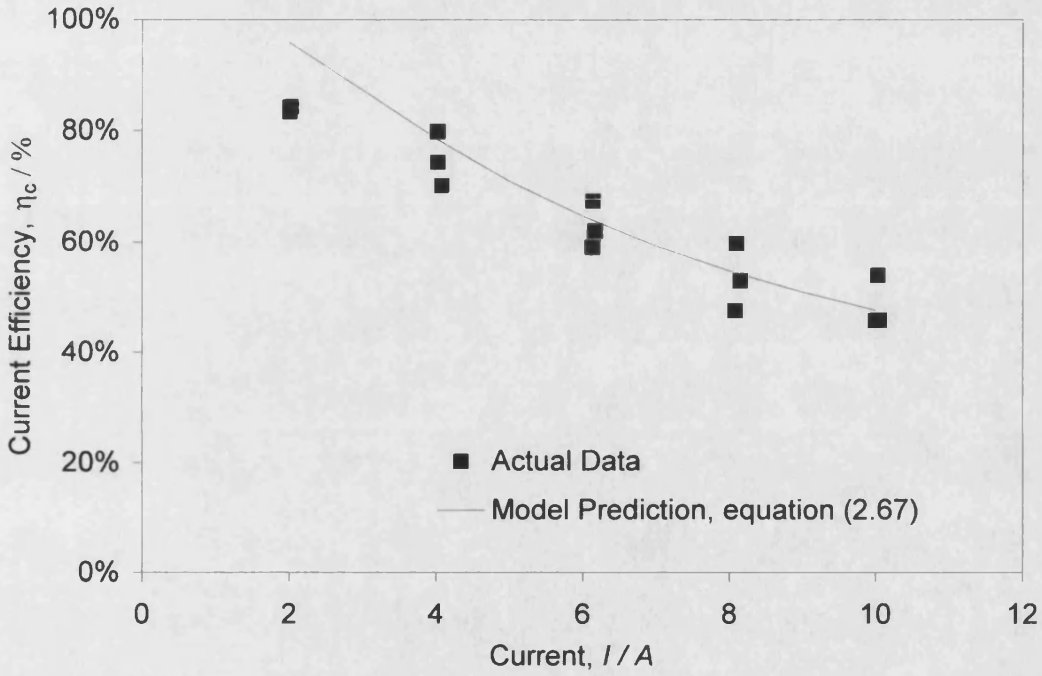

Figure 2.22 Effect of Applied Current on Current Efficiency: Conductivity of sodium chloride was 3,000 µS cm^{-1} (~1,800 ppm) at a temperature 25 °C. Total volumetric flow rate entering the cell was approximately 2.5 cm^3 s^{-1} and the applied current was varied from 2.0 to 10.0 A (130 to 651 A m^{-2}). The active area of the cell measured 153.5 cm^2. Diaion SK110 cation exchange resin was used in the cation exchange compartment.

It is apparent that low current efficiencies are due to the difference of mobility and concentration between hydrogen and sodium ions. The probability that a particular ion in a mixture of other ions to be a charge carrier is proportional to its mobility and concentration as compared to that of the other ions of similar charge. In the cation exchange compartment, current is carried exclusively by the cations in the cation exchange resin. In this case, the mobility of hydrogen ions is much higher than sodium ions. As the current is increased, a greater amount of hydrogen ions are produced from

the oxidation of water at the anode and are transferred through the cation ion exchange membrane and into the cation exchange compartment. As the ratio of current density to feed concentration increases hydrogen ions begin to compete with sodium ions for being transported across the compartment. With its higher mobility and higher concentration, a 'breakthrough' of hydrogen ions occurs through the cation exchange resin bed. The current efficiency drops because of hydrogen ion transfer. As the current increases, the 'breakthrough' increases and the current efficiency decreases accordingly.

Figure 2.22 superimposes the model prediction over the actual data. The calculated values of current efficiency show a good agreement with actual data at currents greater than 4.0 A (261 A m^{-2}).

The model overestimates the current efficiency at lower currents. This may be a result of a non-uniform distribution of hydrogen ions entering from the anode compartment through the cation-permeable membrane. This will lower the effective area of the cation resin bed and therefore lower performance.

Also, the life of the electrodes should always be one of the factors that require constant evaluation, especially in the case of the anode. Anodes typically used in electrochemical cells are DSA® type anodes, where a mixed precious metal oxide is coated on a titanium substrate.

The lifetime of the anode is lowered when the coating begins to dissolve and the exposed titanium substrate oxidises into a non-conducting titanium oxide. Such deterioration will affect performance by increasing the local current densities, disrupting the current distribution profiles, and increasing the energy consumption by the anode. Generally, the coating life on an anode is mainly a function of current density. Therefore the current density should be chosen such that the anode coating exhibits stability towards dissolution and will not form insulating layers. With most DSA® anodes employed in electrochemical cells, the current density is usually below 100 A m^{-2}, since above this value the life of the anode will diminish rapidly. In this study, the current densities were between 130 to 651 A m^{-2}, well above the 100 A m^{-2} design limit for DSA® anodes.

Operating experience with the electrochemical cells using ion exchange resins and ion-permeable membranes indicate that an estimated life of seven years for the resins, membrane, and plastic materials in the cell is probably conservative if the required maintenance program, supplied by the manufacturer, is followed. However, the life can

vary depending on the nature of the liquid being processed and the temperature of operation. Therefore, the anode loading, current density, and temperature should be selected to coincide with the operating life of the components in the cell.

2.7.9 Effect of Feed Concentration on Current Efficiency

Table 2.13 shows that current efficiency decreased as the sodium chloride concentration in the feed water decreased from 2,000 to 18,000 μS cm^{-1} (~1,185 to 11,000 ppm). As the concentration or availability of sodium ions to be transported across the cation exchange cell becomes lower, the current efficiency for transporting sodium ions will diminish. The decrease in current efficiency is due to the fact that competition of hydrogen ions becomes greater since their availability as charge carriers in the resin become proportionally greater than the less populated sodium ions as the concentration is decreased.

Figure 2.23 superimposes the model prediction over the actual data. The calculated values of current efficiency show a good agreement with actual data at sodium chloride conductivity of less than approximately 10,000 μS cm^{-1} (~6,000 ppm). The prediction slightly overestimates the current efficiency at high conductivities. In more concentrated solutions, diffusion within the resin particle begins to control the overall rate. Heating the system or using a cation resin having a lower degree of cross linkage can improve the exchange kinetics. The exchange rate in less concentrated solutions can be improved by decreasing the diameter of the resin by less than 0.05 cm. Generally, the rate is inversely proportional to the square of the radius when the rate-controlling step is particle diffusion. The model does not account for internal-diffusion gradients, and the overestimation of current efficiency at high conductivities may be the result of this.

As the feed water concentration increases, the energy input per volume of solution increases, which can cause a considerable rise in temperature of the solutions. Heat generation is directly related to the applied current. Not all of the applied energy is converted to heat, since work is required to facilitate the reaction. At a first approximation, the heat generated from the applied current, q_{in}, can be written as:

$$q_{in} = \Phi I \tag{2.88}$$

where Φ the cell potential and is I the applied current. This heat is referred to as Joule heating.

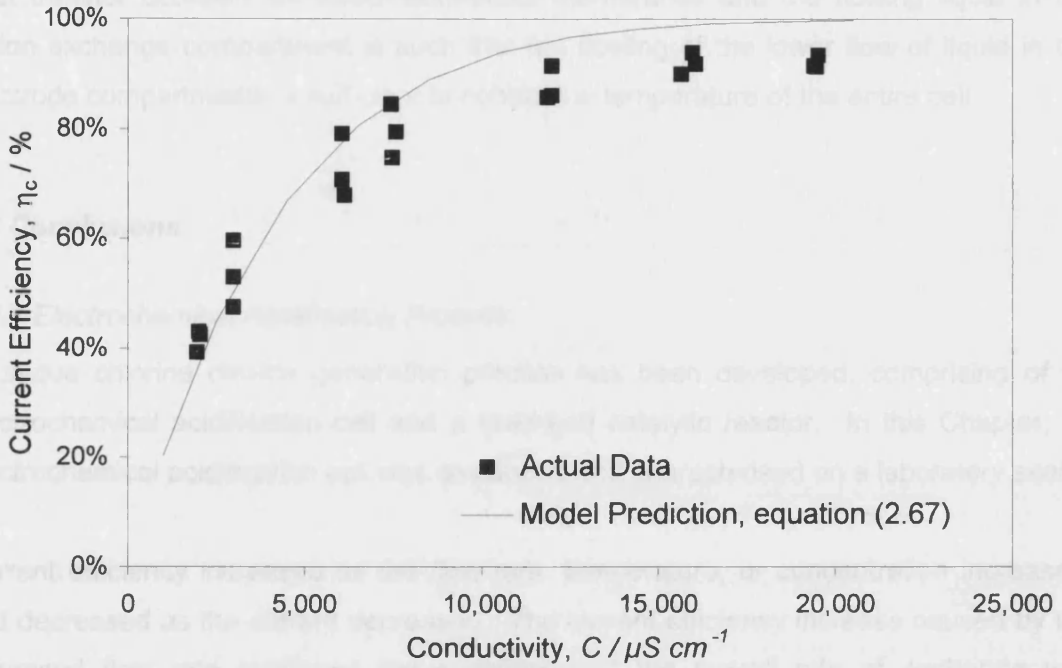

Figure 2.23 Effect of Sodium Chloride Conductivity on Current Efficiency: Conductivity of sodium chloride was varied from 2,000 to 18,000 µS cm^{-1} (~1,185 to 11,000 ppm) at a temperature 25 °C. Total volumetric flow rate entering the cell was approximately 2.5 $cm^3\ s^{-1}$ and the applied current was at 8.0 A (521 A m^{-2}). The active area of the cell measured 153.5 cm^2. Diaion SK110 cation exchange resin was used in the cation exchange compartment.

In flow-through cells, the solution acts as a heat-exchanger fluid. The heat removed by the solution, q_{out}, is directly related to flow rate and can be written as:

$$q_{out} = C_p\, m\, \Delta T = C_p\, Q\, \rho_T\, \Delta T \qquad (2.89)$$

where C_p is the heat capacity, m the mass rate, ΔT the rise in temperature, Q the flow rate, and ρ_T the liquid density.

Heat generation occurs when q_{in} is greater than q_{out}. If properly controlled, there are many practical implications of heat generation in electrochemical cells. As previously discussed, mass transport will be enhanced if the temperature is allowed to rise, possibly

leading to higher reaction rates. Also, the mobility factors increase with an increase in temperature, thus increasing the electrical conductivity of the system and decreasing the input power, or energy consumption. Keeping in mind the thermal stability of the material in the cell, the temperature of operation must be carefully controlled. The coefficient of heat transfer between the cation-permeable membranes and the flowing liquid in the cation exchange compartment is such that the cooling of the lower flow of liquid in the electrode compartments is sufficient to control the temperature of the entire cell.

2.8 Conclusions

2.8.1 Electrochemical Acidification Process

A unique chlorine dioxide generation process has been developed, comprising of an electrochemical acidification cell and a fixed-bed catalytic reactor. In this Chapter, an electrochemical acidification cell was developed and characterised on a laboratory scale.

Current efficiency increased as the flow rate, temperature, or concentration increased, and decreased as the current decreased. The current efficiency increase caused by the increased flow rate confirmed the suspicion that the overall rate of exchange was controlled by film diffusion. The combined effects of the temperature-dependent parameters that affected the ion exchange process resulted in a minimal overall effect. The current efficiency was always less than 100 %. This is most likely to be caused by the difference of mobility and concentration between hydrogen and sodium ions.

2.8.2 Electrochemical Acidification Model

A mathematical model was developed to evaluate the operation of an electrochemical acidification cell. The model provided a method to systematically study the effects of applied current, concentration, flow rate, and temperature on the operation of the cell. The model predicted cell performance by using the Nernst-Planck equation incorporating convection to describe the ionic movement occurring within the cell and film diffusion as the governing kinetic mechanism. Dilute electrolyte theory was used and the model considered isothermal and steady state operation. The mass transport rate constant developed used a mass transport factor to correlate the experimental data.

Test simulations were made and compared to the experimental data. Under the temperature range studied (17 to 31 °C), the calculated values of current efficiency were

in good agreement with actual data over the entire range of data. There was a slight increase in current efficiency with increasing temperature giving the indication that the exchange was slightly better at higher temperatures.

The calculated values of current efficiency matched well with actual data at flow rates less than 8.3 cm^3 s^{-1}. The model overestimated the current efficiency at higher flow rates. Since the model used film diffusion as the governing kinetic mechanism, the overestimation may be attributed to the model's inability to predict the effect of particle diffusion.

The calculated values of current efficiency were in good agreement with actual data at currents greater than 4.0 A (261 A m^{-2}). The model slightly overestimates the current efficiency at lower currents, which may be the result of a non-uniform distribution of hydrogen ions entering from the anode compartment through the cation-permeable membrane.

The calculated values of current efficiency matched well with actual data at sodium chloride conductivity of less than approximately 10,000 µS cm^{-1} (~6,000 ppm). The prediction slightly overestimates the current efficiency at high conductivities, which again may be attributed to the model's inability to predict the effect of particle diffusion.

Under all of the conditions studied, the model predicted results that were within 15 % of actual experimental data. It is best to consider that the model development is a satisfactory interpretation of the performance data of an electrochemical acidification cell and for use in scale-up.

2.9 Recommendations

2.9.1 Electrochemical Acidification Process

For the electrolytic conversion of sodium chloride to hydrochloric acid, an arrangement was described and studied in which a single intermediate compartment was located between the end electrode compartments, with the individual intermediate compartment bounded on both sides by cation-permeable membranes. All three compartments were filled with cation exchange resin.

The use of a three-compartment cell did not allow for the preparation of a reasonably pure solution of the acid at high yields. This may be due to the state of equilibrium established which was partly determined by the high dissociation constant of the hydrochloric acid and the high ratio of the transport number of the hydrogen to that of the sodium ion.

Sodium ions may be replaced more completely with hydrogen ions by use of two intermediate compartments between the end electrode compartments to form a total of four compartments. This configuration is illustrated in Figure 2.24.

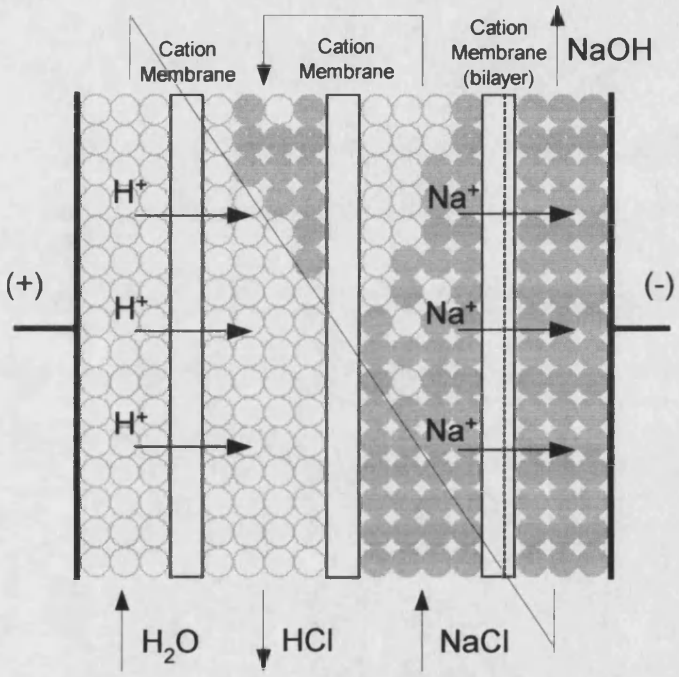

Figure 2.24 Operation of a Four Compartment Electrochemical Acidification Cell, showing ion and fluid movement.

If the sodium chloride solution is initially treated in the intermediate compartment located adjacent to the cathode compartment and further treated by passing into the intermediate compartment located adjacent the anode compartment, the loss of hydrogen ions into the cathode compartment can be reduced. This will result in an increased acid yield with increased current efficiency.

Also, the use of a bilayer membrane may also improve performance (see Figure 2.24). Developed for the chlor-alkali industry, one side of a strong acid membrane is coated with a thin layer of weak acid membrane. Replacing the membrane closed to the cathode, such that the weak acid side is facing the cathode, a barrier to sodium

hydroxide transport from the cathode compartment to the adjacent compartment will be created.

Bilayer membranes are produced by several methods, including lamination, grafting, and chemical conversion of some of the sulphonic acid groups to carboxylate groups. Several American and Japanese companies are marketing such bilayer membranes.

2.9.2 Electrochemical Acidification Model

The mathematical model developed in this Chapter describes a simple but general model of an electrochemical acidification cell based upon an original chemical engineering approach. Dilute electrolyte theory was used and the model considered isothermal and steady state operations. The validity of the model was successfully tested in the few cases studied.

Development of the system to a commercial product up to a scale in cubic meter per hours ($m^3\ h^{-1}$) may require a more comprehensive model. There is no experimental data available in the literature on a commercial product. Therefore, there may be a need to re-consider some of the assumptions made in the development of the model for future work.

The dilute electrolyte theory used may be sufficient, but can be modified by a more complete theory for concentrated solutions. The Nernst-Planck equation rests on the fact that the primary driving force for both migration and diffusion is the gradient of electrochemical potential, and that the electrochemical potential is broken down into concentration and electrical potential terms without basic physical significance. It is not sufficient to allow the diffusion and mobility coefficients to become concentration dependent.

Isothermal operation was considered. Because of the applied current to the cell, the energy input per unit volume of solution can be enough to cause a considerable increase in temperature of the solutions if there are flow rate fluctuations. This increase in temperature may create thermal effects, such a thermal diffusion, that may be significant to the operation of the system. The first law of thermodynamics can be used to deduce a differential energy balance, which can include the kinetic energy of the flowing liquid.

Finally, steady-state operation was considered. Knowing the response to variations in feed composition, temperature, or flow rate may be important. The dynamic response of the process to these involuntary disturbances will determine the control instrumentation needed in a commercial product.

References

1 Helfferich, F. (1994), Ion Exchange, Reprint – Dover Publications, Inc., NY.

2 Mackie, J. S. and P. Meares (1955),'The Diffusion of Electrolytes in a Cation-Exchange Resin Membrane', *Proc. Roy. Soc. (London),* **A232**, 498.

3 Kunin, R. (1960), *Elements of Ion Exchange*, Van Nostrand Reinhold Company, New York, NY.

4 Newman, J. (1973), *Electrochemical Systems*, Prentice-Hall, Englewood Cliffs, NJ

5 Bauman, W. C. and J. Eichhorn (1947),'Fundamental Properties of a Synthetic Cation Exchange Resin', *J. Am. Chem. Soc.*, **69**, 2830.

6 Gregor, H. P. and M. H. Gottlieb (1953),'Studies on Ion Exchange Resins. VIII. Activity Coefficients of Diffusible Ions in Various Cation-exchange Resins', *J. Am. Chem. Soc.*, **75**, 3539.

7 Glueckauf, E. (1952),'A Theoretical Treatment of Cation Exchangers: I. The Prediction of Equilibrium Constants from Osmotic Data', *Proc. Roy. Soc. (London),* **A214**, 207.

8 Boyd, G. E. and B. A. Soldano (1953), 'Self-diffusion of Cations in Hetero-ionic Cation Exchangers', *Z. Elektrochem.*, **57**, 162.

9 Tittle, K. (1981), Proceedings of American Power Conference, **43**, 1126.

10 Helfferich, F. (1994), *Ion Exchange* (Reprint), Dover Publications, Inc., NY.

11 Mackie, J. S. and P. Meares (1955),'The Diffusion of Electrolytes in a Cation-Exchange Resin Membrane', *Proc. Roy. Soc. (London),* **A232**, 498.

12 Colburn, A. P. (1933), *Trans. Am. Inst. Chem. Eng.*, **29**, 174.

13 Ergun, S. (1952), 'Fluid Flow through Packed Columns', *Chem. Engr. Prog.*, **48**, 89.

14 Stueve, E. and M. McCoy (1999), 'Prediction of IX Resin Bed Differential Pressure at High Flow Rate using Ergun Equation Modifications', *Ultrapure Water,* **16** (8), 17.

15 Chandrasekhara, B.C. and D. Vortmeyer (1979), 'Flow Model for velocity Distribution in Fixed Porous Beds under Isothermal Conditions', *Wärme-und Stoffübertragung*, **12**, 105.

16 Schlögl R. (1952), 'Zur Theorie des Potentials von Austauscher Membranen', *Ber. Bunsen-Ges. Phys. Chem. Z. Elektrochem.*, **56,** 644.

17 Spiegler, K. S, R. L. Yoest, and M. R. J. Wyllie (1956), Electrical Potential Across Porous Plugs and Membranes, *Discussions Faraday Soc.*, **21**, 174.

18 Mackie, J. S. and P. Meares (1955),'The Diffusion of Electrolytes in a Cation-Exchange Resin Membrane', *Proc. Roy. Soc. (London),* **A232**, 498.

19 Bodamer, G. W., *Electrolytic Conversions with Permselective Membranes*, U.S. Patent 2,921,005, January 12, 1960.

20 Giuffrida, A. J., *Electrodialysis Apparatus and Process for Ion Modification*, U.S. Patent 3,964,985, June 22, 1976.

21 Sloan, W. J., *Carbonate Reduction*, U.S. Patent 4,049,519, September 20, 1977.

22 Lacey, R. E. (1979), *Industrial Processing with Membranes*, Roberts E. Kreiger Publishing Company, Huntington, NY.

23 Stratman, H. and K. Kock (1982), 'Effluent Free Electrolytic Regeneration of Ion-Exchange Resins', *Polym. Sci. Tech.*, **16**, 145.

24 Bachot, J. and J. Grosbois, *Process for the Preparation of Methionine*, U.S. Patent 4,454,012, June 12, 1984.

25 Twardowski, Z., *Combined Process for Production of Chlorine Dioxide and Sodium Hydroxide*, U.S. Patent 4,806,215, February 21, 1989.

26 Wood, C. J. and D. Bradbury, *Process of Removing Radioactive Burden from Spent Nuclear Reactor Decontamination Solutions using Electrochemical Ion Exchange*, U.S. Patent 5,078,842, January 7, 1992.

27 Kaczur, J. J. and D. W. Cawlfield, *Electrochemical Process for Producing Chlorine Dioxide Solutions from Chlorites*, U.S. Patent 5,092,970, March 3, 1992.

28 DiMascio, F., A. Jha, J. Fenton, and D. Hobro, *Electrodiaresis Polishing (An Electrochemical Deionisation Process)*, Proceedings of the Symposium on Water Purification by Photocatalytic, Photoelectrochemical, and Electrochemical Processes, Volume 94-19, 164, 1994.

29 Helfferich, F. G. (1962), *Ion Exchange*; McGraw-Hill, New York, NY.

30 Probstein, R. F., Physicochemical Hydrodynamics, John Wiley & Sons, New York, NY, 1994.

31 Beer, H. B., *Electrode Coating Therefor.*, U.S. Patent No. 3,632,498, February 2, 1968. DSA® is a registered trademark of ELECTRODE Corporation, but has become used by the scientific community as a term which includes a wide range of very corrosive-resistant coatings.

32 Klei, H. E. and D. W. Sundstrom (1979), *Wastewater Treatment*, Prentice-Hall, Inc. Englewood Cliffs, NJ, 356.

33 Normand, C. (1987), *Analysing Multivariate Data*, Harcourt Brace Jovanovich, Troy, MO.

34 Cochran, W. and G. Cox (1957), *Experimental Design (2nd ed.)*, John Wiley & Sons, New York, NY.

35 Edwards, A. L. (1977), *Experimental Design in Psychological Research (4th ed.)*. Holt, Rinehart and Winston, New York, NY.

36 Harris, R. (1985), A Primer of Multivariate Statistics (2nd ed.), Academic Press, New York, NY.

37 Kempthorne, O. (1952), *The Design and Analysis of Experiments*, John Wiley & Sons, New York, NY.

38 Kirk, R. (1982), *Experimental Design (2nd ed.)*, Wadsworth Publishing, Belmont, CA.

39 Kuehl, R. O. (1994), *Statistical Principles of Research Design and Analysis*, Wadsworth Publishing, Belmont, CA.

40 Pedhazur, E. J. (1982), *Multiple Regression in Behavioural Research (2nd ed)*, Holt, Rinehart and Winston, New York, NY

41 Barbara, T. and L. Fidel (1996), *Using Multivariate Statistics*, HarperCollins, New York, NY.

42 Winer, B. J. (1962), *Statistical Principles in Experimental Design*, McGraw-Hill, New York, NY.

43 Plackett, R. L. and J. P. Burman (1946), "The Design of Optimum Multifactorial Experiments", Biometrika **33**, 305.

44 Dwivedi, P. N. and S. N. Upadhay (1977), 'Particle-Fluid Mass Transfer in Fixed and Fluidized Beds', *Ind. Eng. Chem. Proc. Des. Dev.*, **16**, 157.

45 de Beer, R. and D. van Ormondt (1992), Analysis of NMR Data using Time Domain Fitting Procedures, Chapter in *NMR Basic Principles and Progress 26*, Springer-Verlag, Berlin, 202

46 Bird, R. B., W. E. Stewart and E. N. Lightfoot (1960), *Transport Phenomena*, John Wiley & Sons, New York, NY.

47 Divekar, K (1987). *Ind. Eng. Chem. Res.*, **26** (9). 1906.

48 Harned, F. and A. Owen (1950), *Physical Chemistry of Electrolytes*, Van Nostrand Reinhold Company, New York, NY, 589.

CHAPTER 3

FIXED-BED CATALYTIC REACTOR

This chapter provides a detailed background to the fixed-bed catalytic reactor. It describes the function of the reactor and some of the main principles behind its operation. A mathematical model to describe the fixed-bed catalytic reactor is developed. The experimental arrangement is discussed, as well as the experimental methods and the methodology used to process the data for parameter estimation. Model verification and the accuracy of the models are checked by comparison with experimental data.

3.1 Introduction

Fixed-bed reactors are commonly used in the chemical industry. They remain by far the most dominant reactor in the chemical industry despite some of their disadvantages and justified criticisms when compared to more sophisticated reactors, such as bubbling fluidised beds and circulating fluidised beds.

Despite the relatively simple and passive external appearance of fixed-bed catalytic reactors, the processes taking place within the boundaries of the system and their interactions are quite complex and can give rise to rather complicated problems in design safe operation, and optimisation. Therefore, mathematical models for these fixed-bed catalytic reactors can be a very strong tool in their design, optimisation, and operation.

3.2 Principles of Fixed-Bed Catalytic Reactors

Tubular-flow type reactors are commonly used in the chemical process industry. A common heterogeneous reactor of the tubular-flow type is the liquid-solid catalytic form. Here the reacting fluid flows through a bed of relatively small catalyst particles, on the order of millimetres, held in a stationary position. This form is referred as a fixed-bed catalytic reactor. The reactants are transferred to the active surface of a catalyst, reaction takes place, and the products are transferred back to the main body of the bulk liquid.

These reactors are reasonably inexpensive and easily fabricated. Because a solid phase supports the catalyst and the reactants and products remains in a fluid phase, separating

the product fluid from the catalyst is simple, as long as the catalyst remains where it should in the reactor. Replacing spent catalyst with new catalyst is straightforward, providing the opportunity to use a regenerable catalyst, thus reducing operating costs.

A typical reactor design is shown in Figure 3.1. A set of baffles is positioned below the opening to provide more uniform flow of liquid onto the bed. A layer of dense, nonporous, inert material in a size larger than the catalyst is usually placed on top of the catalyst to catch scale and impurities and to assist in flow distribution. The catalyst fills the internal volume of the reactor and is typically supported on a grid, such as a screen and/or a layer of inert material between the grid and catalyst.

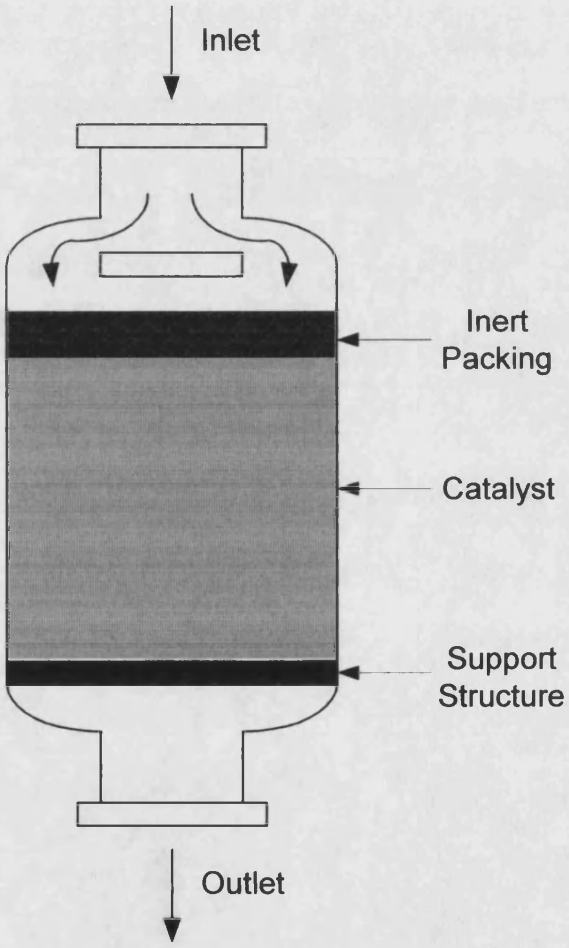

Figure 3.1 Typical Fixed-Bed Catalyst Reactor Design

In heterogeneous catalytic reactions, the catalyst often loses activity with operating time. If this decrease is rapid and severe, it is desirable to regenerate the catalyst. In fixed-bed

reactors, regenerating the catalyst continuously without shutting down the reactor is not possible. Therefore, it is removed for subsequent treatment. Spent catalyst is usually removed by vacuuming.

In contrast to batch reactors, concentration in steady state fixed-bed catalytic reactors is not a function of time but of position. The time of reaction cannot be measured directly and is therefore, not a convenient variable for correlation of rate data. The basic relationship for a fixed-bed catalytic reactor is between the reactor volume, kinetics, feed rate, and yield efficiency, but is generally designed using space-time as the scaling parameter [1]. Space-time is the time required to process one reactor volume at a specified feed condition. The space-time is thus the ratio of reactor volume to volumetric feed rate and is independent of reactor size, shape, and value of feed rate as long as longitudinal diffusion is negligible. This makes scale-up simple even when the kinetic theory may not be well understood. The pilot plant data, in effect does the necessary integration to predict yield efficiency as a function of space-time.

Process temperature and fluid dynamics determine the kinetics of fixed-bed catalytic reactors. Yield efficiency in a fixed-bed catalytic reactor can be improved by knowing the rate-limiting step. If the mass transfer across the thin film surrounding the catalyst particle is the rate-limiting step, all reactants react as soon as they reach the surface of the catalyst particle and not in the pores. This can only arise if the rate of chemical reaction is considerable faster that the rate of diffusion. This is the case at low linear flow velocities and high process temperatures. Inefficient agitation will result in a large film thickness. In most cases, the activation energy of the chemical reaction is considerable higher than that of diffusion; a rise in process temperature increases the rate of chemical reaction greater than the rate of diffusion. Therefore, at low linear flow velocities and/or high process temperatures, diffusion across the thin film surrounding the catalyst particle limits the overall rate. Increasing the linear flow velocity or decreasing the particle size will improve performance when the rate-limiting step is the mass transfer across the thin film surrounding the catalyst particle.

However, the rate of diffusion across the thin film depends upon the linear flow velocity through the fixed-bed of catalyst. As the velocity increases, the thickness of the thin film surrounding the catalyst particle decreases; therefore the reactants move faster from the bulk liquid to the catalyst surface and from the surface to the bulk liquid. The reactants will react before they have time to penetrate into the interior of the catalyst particle. Eventually, the thin film diffusion rate will balance the chemical reaction rate. When this

occurs, the rate-limiting step becomes the mass transfer through the catalyst particle. Changing the physical properties of the catalyst, such as shape, size, pore-size distribution, mean pore size, and surface area will affect performance when the rate-limiting step is the mass transfer through the catalyst particle.

If the chemical reaction at the catalytic site is the rate-limiting step, sorption equilibrium of the reactants is established and maintained throughout the catalyst particle, since the mass transfer across the thin film is fast enough to make up for the disappearance of reactants by the chemical reaction. This is due to the activation energy for the reaction being much larger than that for diffusion. Under these conditions, the effectiveness factor, which accounts for intra-particle diffusion, is very close to unity. This suggests that that the pores of the catalyst are saturated with reactant. This is the case at low process temperatures. Also, the rate of the chemical reaction throughout the catalyst particle is independent of particle size and on agitation, whereas the rates of both film and particle diffusion are proportional to the catalyst surface area. Therefore, with low process temperatures and/or small particle sizes, the rate of chemical reaction throughout the catalyst governs the overall rate. Altering the chemical composition of the catalyst will enhance performance if the process is chemical-reaction rate limited.

Flow maldistribution can also affect reactor performance. The magnitude of this effect can be determined independently by measurements of the residence time spread. To make allowances for flow maldistribution, fixed-bed reactors are normally over designed by at least 20 %.

3.3 Principles of Catalytic Reactions

Catalysts are widely used to enhance reactions in chemical manufacturing, abate pollutants in exhaust gases and effluent streams, and promote combustion at reduced temperatures in fired equipment. Present theory of catalyst activity postulates a material that enters into a reaction, which is neither a reactant nor product. The presence of a catalyst can either accelerate or hinder the reaction process without being modified itself. The mechanism involved is that the catalyst either lowers the activation energy of a reaction or completely changes the reaction path or mechanism. This causes an increase in the rate of reaction because it makes possible alternate mechanisms, each step of which has a lower activation energy than that for the uncatalysed process. Using catalysts will reduce the size of the equipment needed to achieve a certain throughput,

thereby cutting the capital and operating costs for a process. Further, catalysts often exhibit a high selectivity, leading to improved product quality.

Heterogeneous catalysts involve a fluid and a solid catalyst. The reactants are adsorbed onto the surface, forming an intermediate, which either reacts with other species or is desorbed as a final product. The transport of species to and from these sites depends on the system's fluid dynamics. Consider the reaction between hydrogen and chlorite ions in the presence of a platinum-supported catalyst. According to the proposed concept, hydrogen ions combine with the catalyst to form an intermediate compound, which then reacts with chlorite ions to produce chlorine dioxide and the catalyst in its original form. It is postulated that the steps involving the surface of the catalyst occurs at a faster rate than the homogeneous reactions between hydrogen and chlorite ions. For example, suppose the following reaction mechanism for the generation chlorine dioxide:

$$5\,ClO_2^- + 4\,H^+ \rightarrow 4\,ClO_2 + Cl^- + 2\,H_2O \qquad (3.1)$$

This reaction has a very high activation energy and the equilibrium can only be established with the aid of a catalyst. One possible reaction mechanism for the generation chlorine dioxide using a platinum-supported catalyst may be:

$$H^+ + X\bullet \rightarrow X\cdot H^+ \qquad (3.2)$$

$$5\,ClO_2^-\ 4\,X\cdot H^+ \rightarrow 4\,ClO_2 + Cl^- + 2\,H_2O + X\bullet \qquad (3.3)$$

The hydrogen ion is catalysed via one active centre, or catalytic site X•, which forms a very reactive platinum hydrogen complex. The platinum hydrogen complex modifies the reaction pathway or the nature of the activated complex so that the reaction may proceed through an activated complex with lower activation energy. This phenomenon is very similar to the mechanism in a hydrogen electrode. Typical requirements for a metal catalyst include:

- The metal must be noble and must not itself react or dissolve in solution
- The metal must be a good catalyst for the hydrogen reaction, *i.e.,* the metal can absorb hydrogen atoms on the surface but will not react them to form a stable hydride

- The metal must not absorb hydrogen atoms into its crystal lattice

The catalyst surface should be finely divided. Because the catalytic activity of the surface is associated with crystal imperfections, the surface made by finely divided deposits increases not only the real surface area but also the number of active catalytic sites.

The reaction is truly catalytic if the sequence of steps is such that the centre X• is regenerated after it has enabled the formation of chlorine dioxide. Although X• is occupied and regenerated a number of times, it does not necessarily follow that its catalysing ability and/or number remains constant for a long period of time.

Understanding the functionality of solid catalysts is a very challenging problem. Some theories point towards geometric properties [2-4] while others point towards electronic properties [5-7]. According to the geometric property concept, the catalytic activity of a solid surface depends on the spacing of atoms so as to facilitate adsorption of reactant molecules. Electronic property theories are directed towards the electronic mobility properties of the material, where the materials are classified as conductors, semiconductors, and insulators.

The conductor catalysts are active metals, such as platinum, palladium, iridium, ruthenium, etc., and have the properties of chemisorption by electron transfer. The semiconductor catalysts are the oxides of the active metals and have the capability of interchanging electrons from the filled valance bands in a compound when sufficient energy is provided. Upon this electron transfer, the semiconductor becomes a conductor. The insulator catalysts include materials such as silica gel, alumina, and their combinations. Electrons are not able to move freely through these solids so their activity is based on the formation of carbonium ions at the acid sites on the surface.

The experimental method and technique for catalyst manufacture is very important because the activity is based on both chemical composition and physical properties, such as surface area, pore size, particle size, and particle structure.

There are two types of solid catalysts; one in which the entire material constitutes the catalyst, while the other, an active ingredient is dispersed on a support or carrier having a large surface area. For the first type, precipitation provides a method of obtaining a solid

material in a porous form. It consists of adding a precipitation agent to solutions of the desired components. Washing, drying and usually calcination/activation are subsequent steps in the process. The second type involves an impregnation method on a porous carrier. The steps in the impregnation procedure consist of evacuating the carrier, contacting the carrier with the impregnating solution, removing the excess solution, drying, and calcination/activation. There is a lot of information available on solid catalysts. Some helpful sources of summary information are available [8-11].

The nature of the carrier can affect catalyst activity and selectivity. The effect presumably arises because the carrier can influence the surface structure of the atoms of dispersed catalytic agent. When only a small fraction of a monomolecular layer is added to the surface of a carrier, increases in the amount of catalyst will increase the rate. A relatively small amount of catalyst can cause a significant increase in yield efficiency, indicating that the amount of catalyst is important. When the reaction does not entail a 'chain' mechanism, the rate of reaction is usually proportional to the amount of the catalyst [12].

This can be understood by considering the case of surface catalytic reactions. In the reaction between hydrogen and chlorite ions on the surface of a platinum-supported catalyst, the rate is proportional to the catalyst surface area. Here a simple proportionality exists between the surface area and the number of active sites X• that catalyse the reaction. While such a simple relationship may not often exist in solid-catalysed reactions, in homogeneous catalysis there is frequently a direct proportionality between rate and catalyst concentration.

However, adding a large amount of active ingredient to the carrier may not necessarily increase the rate. The dispersion of active ingredient on the carrier is also an important factor. Depositing a concentrated active ingredient solution to the carrier may lead to larger clusters as well as atoms depositing on top of each other, leading to a non-uniform dispersion. Multi-dispersion methods are typically used to improve the dispersion, whereby several dispersions of a dilute concentration are applied to the carrier individually.

Promoters are substances that are added during the preparation of the catalyst that improve activity and selectivity or stabilise the catalyst agent so as to prolong its operating life [13]. A promoter is generally added in a small amount and by itself has

very little activity. Inhibitors lessen activity, stability, or selectivity and are typically used to reduce the activity of a catalyst for an undesirable side reaction.

Most catalyst will deactivate with time. Curves of yield efficiency versus time for long-term (typically, hundred of hours) experiments will show some degree of decay. The deactivation of catalyst can occur by two mechanisms; one mechanism is spatially dependent while the other is temporally dependent [14]. Moving front poisoning is the major spatially dependent mechanism. It involves the reaction of a poison in the feed solution with a catalytically active site at a specific spatial location, deactivating the active site. Catalyst deactivation begins where the feed enters the catalyst bed and proceeds across through the bed. At some distance beyond the feed inlet, the catalyst bed will be uniformly deactivated across the cross-section of the bed, forming a 'front'. Once established, this front moves through the bed until the entire catalyst bed has been deactivated.

Temporally dependent catalyst deactivation occurs by one of three mechanisms; mechanical, chemical, or thermal. Mechanical deactivation is caused by the formation of small particles in the bed, either by attrition or crushing. The remainder of the bed acts as a filter and portions of it plug, thus decreasing the effectiveness of the catalyst. This type of deactivation is easily diagnosed. Reactor pressure drop will increase and filters downstream of the reactor will plug.

Chemical deactivation is caused by the product further reacting with the catalyst to produce a catalyst poison. Similar to the spatially dependent mechanism, the catalyst deactivation begins where the product is first produced and proceeds through the bed until the entire catalyst bed is deactivated.

Thermal deactivation can occur by two methods; sintering and phase transition. Sintering takes place when a catalytic site becomes mobile, migrates, and then reacts with another site to form an inactive moiety. Sintering generally occurs during catalyst regeneration, *i.e.,* a process of heating the catalyst to thermally degrade the poison, but can ensue at low operating temperatures for porous solids impregnated with metal-containing solutions.

The crystalline phase of the catalytically active site may be thermally unstable; temperature excursions therefore could induce a phase transition to an inactive

crystallinity. Phase transition can occur not only during regeneration, but also because of hot spots that can occur by poor heat transfer.

In summary, poisons can interfere to slowly remove X• from the system, deactivating the catalytic site. However, when compared to noncatalytic system, the complexing-regenerating sequence occurs a significant number of times before the active sites become inactive. While a catalyst can deteriorate, its active lifetime is far greater than the time required for reaction.

3.4 Model Development

In this section, a steady state model for an actual reaction occurring within and on the surface of a porous catalyst is formulated. Although the reaction is known to be heterogeneous, it is analysed as if it was homogeneous. This serves as a simple illustration for the use of the foregoing information for the analysis of an actual catalytic system for generating chlorine dioxide.

3.4.1 Governing Mechanisms

The chemical reaction is carried out in a continuous operation in which a solution is passed through a bed of catalyst particles contained in a reactor. The process is understood as having a number of steps that occur in series and/or in parallel. These steps can be considered as the elements of the function of the catalyst bed and controls the rate of reaction at the catalytic site. These processes are illustrated in Figure 3.2.

The fixed-bed catalytic reactor can be viewed as having three subsystems; 1) reactor, 2) catalyst bed contained within the reactor, and 3) flowing liquid (reactants) through the catalyst bed. The operating principles involved are as follows: A solution containing sodium chlorite and hydrochloric acid is transferred (*Radial and Axial Diffusion and Convection*) from the entrance of the reactor to the bed of catalyst particles, which is stationary and distributed along the length of the reactor. Hydrogen ions from the bulk liquid diffuse from the bulk liquid to the surface of the catalyst particles by mass transfer (*Film Diffusion*). The hydrogen ions continue to diffuse through the pores of the catalyst (*Particle Diffusion*) until they reach the internal surface where they are chemisorbed on the internal surface of the catalyst particle. The chemisorbed hydrogen ions undergo a surface reaction producing a very reactive platinum hydrogen complex.

Simultaneously, chlorite ions from the bulk liquid diffuse from the bulk liquid to the surface of the catalyst particles by a *Film Diffusion* process. They continue to diffuse through the pores of the catalyst (*Particle Diffusion*) until they reach the internal surface of the catalyst particle. They then undergo a chemical reaction with the platinum hydrogen complex, producing chlorine dioxide. The chlorine dioxide transfers from the surface into the liquid phase adjacent to the catalyst surface. It diffuses back towards the surface of the catalyst particle (*Particle Diffusion*), and continues to diffuse through the thin film and into the bulk liquid (*Film Diffusion*).

The main governing mechanisms in the fixed-bed catalytic reactor are transfer of reactants to the catalyst bed and the diffusion processes of the reactants and product occurring within the catalyst. For the present analysis, a global rate constant will be used to describe the mass transfer across the thin film surrounding each catalyst particle, the mass transfer through the porous solid, and the intrinsic kinetic rate of the chemical reaction.

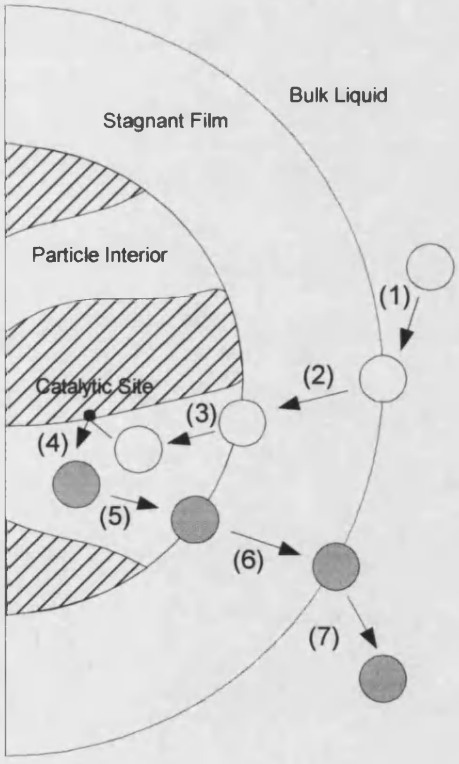

Step 1: Transport of reactants from the bulk liquid to the thin film surrounding the catalyst particle

Step 2: Transport of reactants from the thin film to the liquid-solid interface - external surface of the catalyst particle

Step 3: Intraparticle transport of reactants into the porous catalyst particle

Step 4:a) Absorption of reactants at a catalytic site, b) Chemical reaction of absorbed reactants to adsorbed products; surface reaction - the intrinsic chemical step, and c) Desorption of adsorbed products

Step 5: Transport of products from the interior sites to the outer surface of the catalyst particle

Step 6: Transport of products from the liquid-solid interface to the thin layer

Step 7: Transport of products from the thin film into the bulk liquid

Figure 3.2 Sequence of Steps for Converting Reactants to Products using a Porous Catalyst: Although the reaction is actually heterogeneous, it is analysed as if it was homogeneous.

3.4.2 Model Description and Assumptions

Fixed-bed catalytic reactors have been subject to numerous theoretical studies because of its popularity in industry. Many mathematical models to predict the performance or to design fixed-bed catalytic reactors have been proposed in the literature. The most fundamental of these are based on thermodynamic principles and on this basis, they are broken down into three classes; 1) isolated, closed, and open systems [15], 2) lumped and distributed systems [16], and 3) homogeneous and heterogeneous systems [17].

The model developed here uses a pseudo-homogeneous approach to describe the fixed-bed catalytic reactor. The fluid is assumed to move as a plug through the reactor and the reaction rate, which depends on local species concentration, is described as a rate of species generated or consumed per unit reactor volume. The basic physical, geometrical, and operational assumptions defining the model are outlined, as well as the governing equations that result. It will be confined to the one-dimensional geometry and isothermal operation.

A one-dimensional model assumes that the concentration varies only in the axial direction. The only transport mechanism operating in this direction is the overall convective flow. The conservation equation is obtained from a mass balance on a reference component over an elementary cross section of the tubular reactor.

A first-order kinetic expression is used to describe the rate of generation. A global rate constant is used to account for film diffusion, particle diffusion, and the intrinsic chemical reaction rate. The Sherwood number and Arrhenius Law expression are used to describe film diffusion and the intrinsic chemical reaction rate, respectively. An effectiveness factor is used to represent particle diffusion.

The effectiveness factor is defined as the ratio of the actual reaction rate to that which would occur if all of the surface through out the inside of the catalyst particle were exposed to reactants and products of the same concentration and temperature as that existing in the bulk liquid. The effectiveness factor depends on the conditions inside the porous catalyst and in the bulk liquid. It is multiplied by the chemical reaction rate at the bulk conditions to describe the rate that is actually taking place when the conditions inside the catalyst are different from the bulk conditions.

The following assumptions are used in the derivation of the model equations:

1) Steady state operation
2) Isothermal operation
3) Axial dispersion is negligible
4) Interphase and intraparticle concentration gradients in the catalyst are negligible
5) Flow distribution is uniform within the reactor catalyst bed
6) Catalyst decay is negligible
7) Different parts of the same catalyst are exposed to the same external conditions

3.4.3 Model Development

Chlorine dioxide can also be generated by acidification of sodium chlorite solution. The following stoichiometry taking place in a fixed bed catalytic reactor will be studied:

$$5\,NaClO_2 + 4\,HCl = 4\,ClO_2 + 5\,NaCl + 2\,H_2O \qquad (3.4)$$

A mass balance will be performed over the volume element ($A_c \Delta y$), neglecting any radial variations in concentrations and assuming steady state. The following symbols will be used in developing the model:

J = molar flow rate (mol m^{-2} s^{-1})
r''' = rate of generation of A per volume of catalyst (mol m^{-3} s^{-1})
A_c = cross-sectional area of reactor containing catalyst (m^2)
y = coordinate in direction of liquid flow (m)
D_{AB} = liquid-phase diffusion coefficient (m^2 s^{-1})
v = superficial fluid velocity through the catalyst bed (m s^{-1})
τ = space-time (s)
k = global rate constant (s^{-1})
k_f = film mass transfer coefficient (m s^{-1})
k_r = reaction rate constant (s^{-1})
a_p = external surface area to volume ratio of the catalyst particle (m^{-1})
η_f = effectiveness factor
d = particle diameter (m)
υ = kinematic viscosity (m^2 s^{-1})
ε = void fraction
A_o = frequency factor (m s^{-1})
E_{act} = activation energy (J mol^{-1})
R = gas constant (8.314 J mol^{-1} K^{-1})
T = absolute temperature (K)
M_T = Thiele Modulus
D_{eff} = effective diffusion coefficient (m^2 s^{-1})

φ = fractional pore volume of the catalyst

A mass balance of sodium chlorite, designated as A, over the volume element ($A_c\ \Delta y$) yields:

$$\underbrace{A_c\ J_{Ay}\big|_y}_{\text{Rate In}} - \underbrace{A_c\ J_{Ay}\big|_{y+\Delta y}}_{\text{Rate Out}} + \underbrace{(1-\varepsilon)\, r_A'''\ (A_c\ \Delta y)}_{\text{Rate of Generation}} = \underbrace{0}_{\text{Rate of Accumulation}} \qquad (3.5)$$

Dividing equation (3.5) by ($A_c\ \Delta y$) and taking the limit $\Delta y \rightarrow 0$:

$$-\frac{\partial J_{Az}}{\partial y} + (1-\varepsilon)\, r_A''' = 0 \qquad (3.6)$$

The molar flow rate of A in the axial direction is expressed by diffusion (and/or dispersion) and convection:

$$J_{Ay} = D_{AB}\frac{\partial^2 C_{Ao}}{\partial y^2} + v\frac{\partial C_{Ao}}{\partial y} \qquad (3.7)$$

In almost all situations involving flow in packed-bed reactors, the amount of material transported by diffusion/dispersion in the axial direction is negligible compared with that transported by convection:

$$v\frac{\partial C_{Ao}}{\partial y} >>> D_{AB}\frac{\partial^2 C_{Ao}}{\partial y^2} \qquad (3.8)$$

Therefore, the resultant differential equation is:

$$-v\frac{\partial C_{Ao}}{\partial y} + (1-\varepsilon)\, r_A''' = 0 \qquad (3.9)$$

Figure 3.3 shows a schematic of the fixed-bed catalytic reactor.

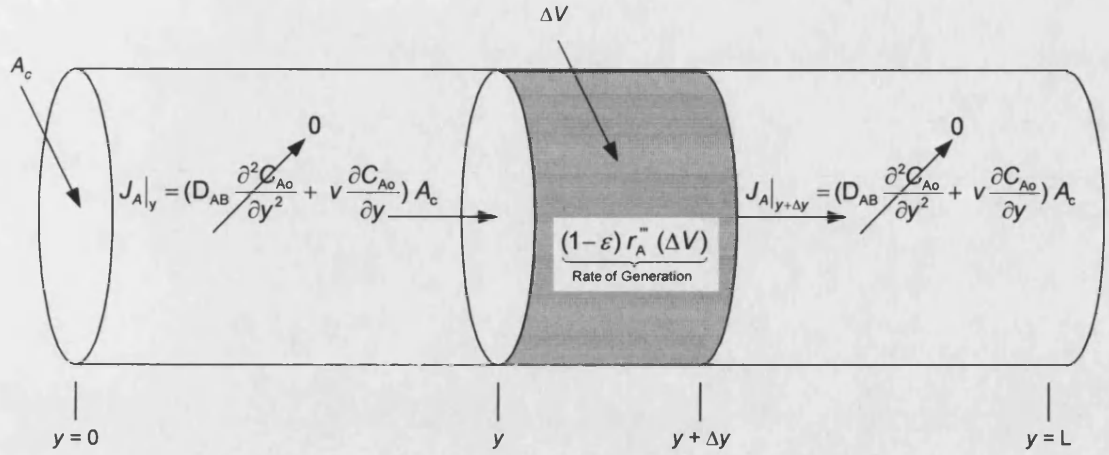

Figure 3.3 Schematic of the fixed-bed catalytic reactor neglecting any radial variations in concentrations and assuming steady state

The above equation accounts for the component in the differential element of the reactor of length ∂y. For the reactor as a whole, the expression must be integrated. Note that the velocity is constant, but the rate of generation is a function of the reaction concentration within the catalyst. Separating the variables:

$$-\frac{\partial y}{v} = -\frac{1}{(1-\varepsilon)}\frac{\partial C_A}{r_A'''} \tag{3.10}$$

The right side of equation (3.10) can be integrated with the limit at y = 0 to L to give a performance equation for the fixed-bed catalytic reactor:

$$\frac{L}{v} = \tau = \frac{1}{(1-\varepsilon)}\int_{C_{Ao}}^{C_A}\frac{\partial C_A}{r_A'''} \tag{3.11}$$

where space-time τ is the time required to process one reactor volume of feed, measured at specified conditions.

With the irreversible pseudo-homogeneous reaction on a solid catalyst following a first-order mechanism:

$$-r_A''' = k\,C_{Ao} \tag{3.12}$$

Substituting equation (3.12) into the equation (3.11) yields:

$$\tau = -\frac{1}{(1-\varepsilon)\,k}\int_{C_{Ao}}^{C_A}\frac{\partial C_A}{C_A} \tag{3.13}$$

The right side of equation (3.13) can be integrated with the limit at $C_A = C_{Ao}$ to C_A to yield:

$$(1-\varepsilon)\,k\,\tau = \ln\left(\frac{C_{Ao}}{C_A}\right) \tag{3.14}$$

The global rate constant, k, for a solid catalysed reaction is best expressed as a sum of resistances:

$$\frac{1}{k} = \frac{1}{k_f\,a_p} + \frac{1}{\eta_f\,k_r} \tag{3.15}$$

The Sherwood number (Sh) is commonly used to describe the film mass transfer coefficient for spherical particles:

$$\mathrm{Sh} = \frac{k_f\,d}{D} \tag{3.16}$$

The Sherwood number is an empirical function of the Reynolds (Re) number:

$$\mathrm{Re} = \frac{d\,v}{\upsilon} \tag{3.17}$$

and the Schmidt (Sc) number:

$$\mathrm{Sc} = \frac{\upsilon}{D} \tag{3.18}$$

and is calculated from a relationship which describes forced convection around a solid sphere, known as the Frössling correlation [18]:

$$\begin{aligned} \mathrm{Sh} &\approx 2 + 0.6\,\mathrm{Re}^{1/2}\,\mathrm{Sc}^{1/3} \quad \text{for } 25 < \mathrm{Re} \\ \mathrm{Sh} &\approx 0.6\,\mathrm{Re}^{1/2}\,\mathrm{Sc}^{1/3} \quad \text{for } 25 < \mathrm{Re} < 150{,}000 \end{aligned} \tag{3.19}$$

For reactors packed with spherical catalyst, the external surface area to volume ratio of the catalyst particle is:

$$a_p = \frac{6}{d} \tag{3.20}$$

The intrinsic chemical reaction rate constant, k_r, is only constant at a given temperature and varies with temperature following the Arrhenius equation:

$$k_r = A_o \exp(\frac{-E_{act}}{R\,T}) \tag{3.21}$$

The effectiveness factor is dependent on the reaction order and can be determine by the Thiele Modulus for first order irreversible reactions on spherical particles:

$$\eta_f = \frac{1}{M_T} (\frac{1}{\tanh(3\,M_T)} - \frac{1}{3\,M_T}) \tag{3.22}$$

where the Thiele Modulus can be defined as:

$$M_T = \frac{d}{6} \sqrt{\frac{k_f}{D_{eff}}} \tag{3.23}$$

The Thiele modulus was originally derived for reactant penetration into the pores of uniform cross section (one dimensional geometry).

The effective diffusion coefficient combines the effects of longer pores and small area within the catalyst and is commonly defined as:

$$D_{eff} = \varphi \frac{D}{2} \tag{3.24}$$

3.5 Experimental Details

The experiments described in this chapter were designed to show the conditions necessary for the operation of a fixed-bed catalytic reactor; the operating characteristics and the optimum operation with respect to chlorine dioxide yield effciency.

3.5.1 Fixed-Bed Catalytic Reactor

The reactor consisted of a polyvinyl chloride (PVC) pipe with PVC couplings glued at each opening. At one end of the reactor, designated as the bottom, a fluoropolymer woven screen to support the catalyst was placed and secured between the pipe and coupling prior to gluing. Figure 3.4 shows a dissected view of the fixed-bed catalytic reactor used.

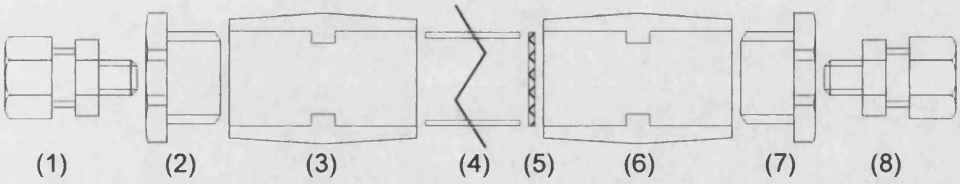

(1) / (8)	Tube Fitting: Male connector, 0.95 cm Tube OD, 0.64 cm NPT thread
(2) / (7)	PVC Fitting: Reducing Bushing, 2.54 cm x 0.64 cm
(3) / (6)	Coupling Adapter, Socket x Thread, 2.54 cm
(4)	Clear PVC pipe, two bed lengths studied; 30.48 cm and 60.96 cm
(5)	Fluoropolymer woven screen

Figure 3.4 Dissected View of the Fixed-Bed Catalytic Reactor: Two catalyst bed lengths were studied; 30.48 cm and 60.96 cm. The inside diameter of the reactor was 2.62 cm.

The dimensions of the catalyst bed best characterise the two reactors studied. The catalyst bed lengths in reactor 1 and 2 were 30.48 cm and 60.96 cm, respectively. Both reactors had a 2.62 cm inside diameter and 3.34 cm outside diameter.

The overall length of reactors 1 and 2 were 48.48 cm and 78.96 cm, respectively. The reactor contained a bed of platinum-supported catalyst; 0.5 wt % Pt on ceramic. A solution containing the sodium chlorite and hydrochloric acid reactants flowed from top to bottom. The flow configuration is outlined in Figure 3.5.

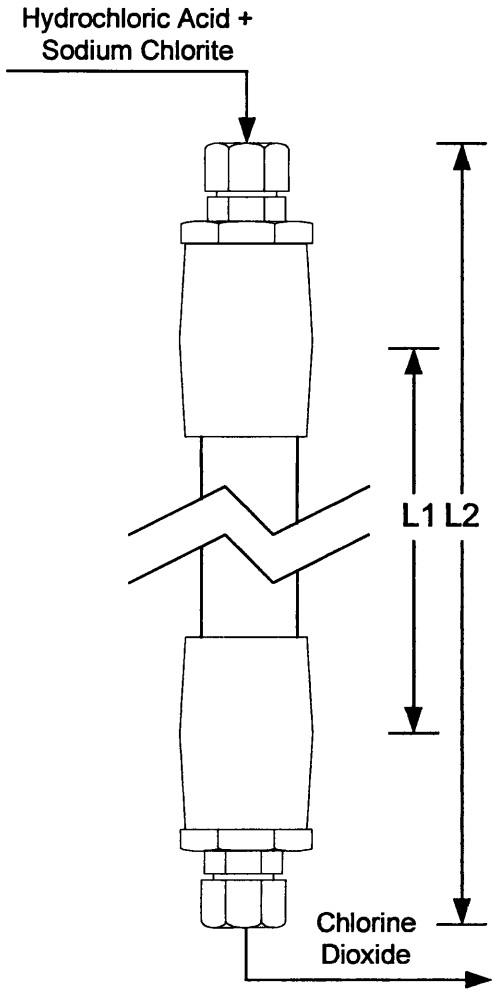

	Reactor 1	Reactor 2
L1	30.48 cm	60.96 cm
L2	48.48 cm	78.48 cm

Figure 3.5 Flow Configuration in the Fixed-Bed Catalytic Reactor: L1 and L2 are the catalyst bed and overall lengths, respectively.

3.5.2 Platinum-Supported Catalyst

The platinum-supported catalyst was prepared by impregnating a platinum precursor solution to a ceramic support with subsequent oxidation of the platinum precursor to its oxide form. Ceramic spheres (Macrolite, Kinetico, Newbury, OH) were used as a support. Two particle sizes, 0.55 and 1.20 mm, and were selected for study and were labelled as Catalyst A and Catalyst B.

The average particle size of each catalyst was determined by screen analysis. Sieves of mesh sizes of 20, 30, 40, and 50 were arranged in descending order over a pan, and approximately 100 cm^3 of sample was poured onto the 20-mesh sieve. The quantity that remained on each sieve was measured and plotted as a logarithmic probability distribution against the sieve mesh size (mm) on the opposite axis. Three points were taken in increasing order of sieve retention fraction, and the best fitted line was drawn

through them. From this line, the sieve mesh size (mm) that retained 50 % of the catalyst was found and taken to be the effective size. Table 3.1 and Figure 3.6 show screen analysis for the two types of catalyst used.

Table 3.1 Screen Analysis for Catalysts A and B

Catalyst A Mesh Size	Catalyst Volume / cm^{-3}	Catalyst Retained on Each Sieve	Total Catalyst Retained
on 14 mesh (1.40 mm)	20.8	21%	21%
on 16 mesh (1.18 mm)	44.5	45%	65%
on 20 mesh (0.85 mm)	20.6	21%	86%
on 30 mesh (0.60 mm)	13.0	13%	99%
over 30 mesh	1.1	1%	100%
TOTAL	100	100%	

Catalyst B Mesh Size	Catalyst Volume / cm^{-3}	Catalyst Retained on Each Sieve	Total catalyst Retained
on 20 mesh (0.85 mm)	1.0	1%	1%
on 30 mesh (0.60 mm)	8.2	8%	9%
on 40 mesh (0.43 mm)	74.5	75%	84%
on 50 mesh (0.30 mm)	13.4	13%	97%
over 50 mesh	2.9	3%	100%
TOTAL	100	100%	

The catalyst particles used in the fixed-bed reactors were spherical and had a fairly broad size distribution. A bed of porous catalyst gives a system containing two void regions. There are small void spaces within the individual particles and larger spaces between particles. The shape and nature of these two void regions may vary from thin cracks to a continuous region surrounding a group of particles. The void spaces within the particles are referred to as micropores where the void regions between the particles are called macropores.

The micropore void fraction was determined by boiling a weighed sample immersed in water. After the air in the pores was displaced, the catalyst sample was superficially dried and weighed. The pore volume was calculated by the increase in weight divided by the density of the water. From this and the dry weight of the sample and its density, the

micropore void fraction was obtained. Table 3.2 shows the pore volume analysis for the two types of catalyst used.

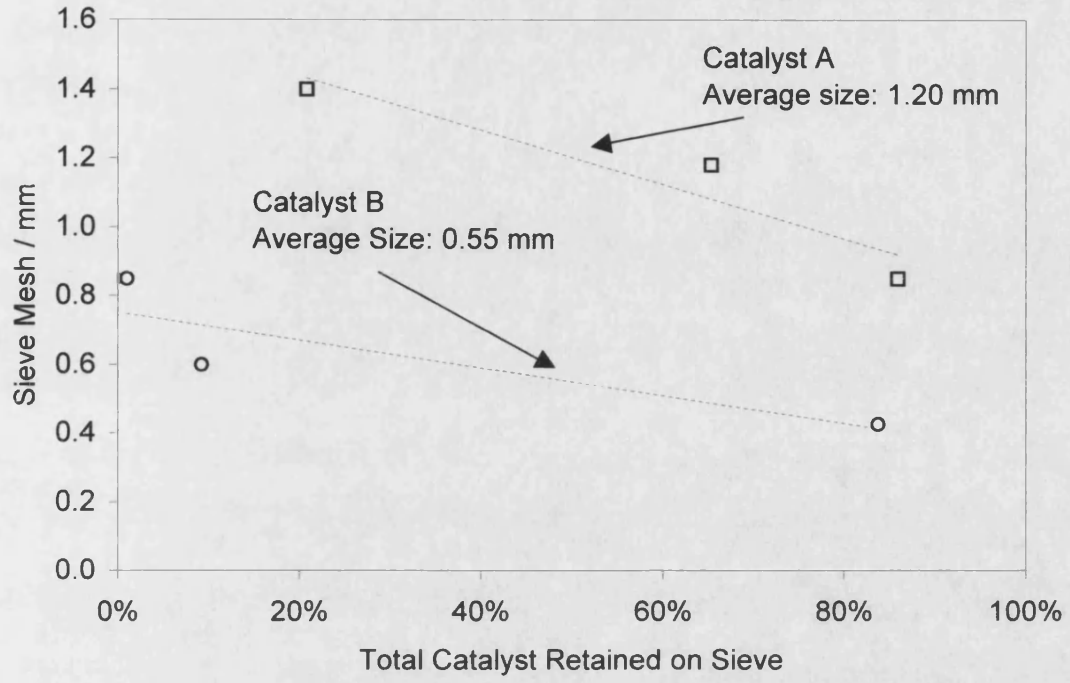

Figure 3.6 Computation of Average Size for Catalysts A and B

Table 3.2 Micropore Void Fraction Analysis for Catalysts A and B

	Dry Weight / g	Wet Weight / g	Water Volume / cm^3	Catalyst Volume / cm^3	Micropore Void Fraction
Catalyst A	390.5	515.2	124.7	816.6	0.132
	389.8	508.4	118.6	815.1	0.127
	391.1	514.5	123.4	817.8	0.131
					0.130_{avg}
Catalyst B	716.5	799.5	83.0	759.5	0.099
	720.4	802.8	82.4	763.6	0.097
	719.1	799.3	80.2	762.3	0.095
					0.097_{avg}

The low fractional pore volume is an indication that only the surface of the catalyst is porous. If so, only the surface near the outer periphery of the catalyst particle is effective and the central portion of the particle is not utilised. In this case, the effectiveness factor

will be much less than unity, suggesting that the pores of the catalyst will not be saturated with reactant.

The macropore void fraction was estimated by loading a weighed sample of superficially dried catalyst into a graduated cylinder. After being mixed with water, the catalyst was allowed to settle in the graduated cylinder. Excess water was removed with a syringe until the water level and catalyst were identical in the graduated cylinder. Following this, the catalyst/water mixture was removed graduated cylinder and the water was centrifuged off at 1,200 revolutions per minute (rpm) for 15 seconds. The water was collected and its volume determined by a weight measurement divided by density. The macropore void fraction in the reactor was calculated by dividing the calculated volume of the water by the volume of the catalyst/water mixture. Results are shown in Table 3.3.

Table 3.3 Macropore Void Fraction Analysis for Catalysts A and B

	Catalyst Weight / g	Water Volume / mL	Catalyst/Water Volume / mL	Macropore Void Fraction
Catalyst A	20.16	13.23	30.0	0.441
	20.27	13.08	30.0	0.436
	20.19	13.11	30.0	0.437
				0.438_{avg}
Catalyst B	40.75	7.77	30.0	0.259
	40.68	7.44	30.0	0.248
	40.71	7.92	30.0	0.264
				0.257_{avg}

The catalysts used in this study were prepared by Halox Technologies Incorporated (Bridgeport, CT) using a proprietary method. In general, the platinum-supported catalyst was prepared by soaking the ceramic spheres in a precursor solution; the precursor was prepared by dissolving a platinum salt, tetraammineplatinum (II) chloride crystal, in 60 % isopropyl alcohol at 35 °C. The excess solution was drained and the impregnated ceramic spheres were dried. A thermal process accomplished subsequent oxidation to the oxide form; the impregnating ceramic was heated in an oxygen-containing atmosphere at a temperature in excess of 500 °C. The amount of platinum was approximately 0.5 % by weight of ceramic support. The catalyst dispersion of atoms exposed, determined from hydrogen chemisorption, was found to be 48.2 %.

3.5.3 Solutions

The fixed-bed catalytic reactor was fed with a solution containing sodium chlorite and hydrochloric acid. Hydrochloric acid solution was prepared by dissolving reagent-grade hydrochloric acid in deionised water in a 30-gallon polypropylene tank. The hydrochloric acid solution was passed downwardly through the reactor at the desired flow rate. Prior to the reactor, a sodium chlorite solution was added to the hydrochloric acid solution such that the final concentration of sodium chlorite was approximately 1,000 ppm.

Sodium chlorite is available in dry form or as a 25 or 38 % active solution. Commonly, solutions of 25 % active sodium chlorite or less are used to charge chlorine dioxide generators. In these experiments, a 25 % active sodium chlorite solution was used. Chemical properties of sodium chlorite and chlorine dioxide are given in Appendix B.

3.5.4 Experimental Arrangement

The experimental arrangement for the fixed-bed catalytic reactor is schematically shown in Figure 3.7.

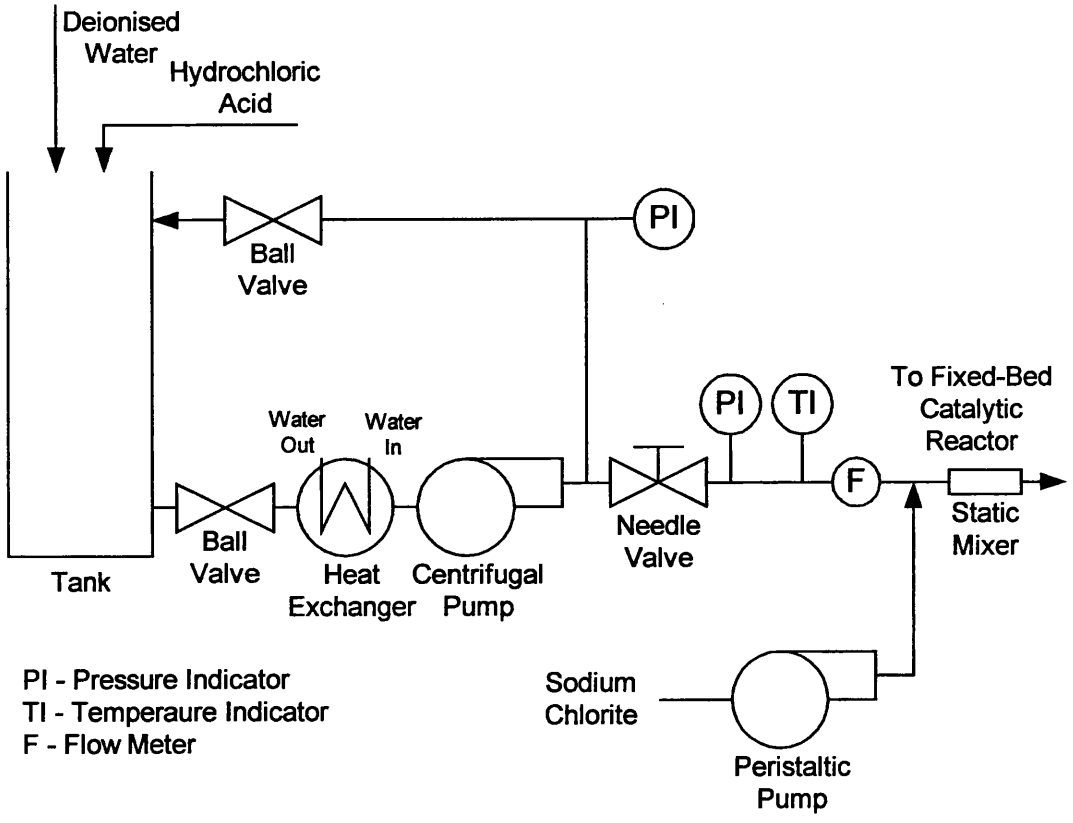

Figure 3.7 Experimental Set-Up for the Fixed-Bed Catalytic Reactor Experiments

The flow rates were controlled by a needle valve (F20BK, Deltrol, Bellwood, IL) and kept constant by adjusting the flow of liquid to constant flow meter readings (CR-440 Blue White, Westminster, CA). Absolute flow rate was determined by timing a measured volume each time a sample was taken from the effluent. Pressure to circulate liquid through the reactor was supplied by a centrifugal pump (25 cm^3 s^{-1} at 200 kPa, WMD 305SZ, Iwaki WalChem, Holliston, MA). Sodium chlorite solution was added to the hydrochloric acid solution using a peristaltic pump (L/S 14, Cole-Parmer, Vernon, Hills, IL) using precision 1.6 mm ID Norprene® tubing. The mixture was passed through a static mixer prior to the inlet of the reactor. The chlorine dioxide solution exiting the reactor was passed through a flow cell in a HACH Spectrophotometer Model 2010 (HACH Company, Loveland, CO) for the on-line measurement of chlorine dioxide from 0 to 770 ppm. The absorbance was monitored at a wavelength of 445 nm.

For the calibration of the spectrophotometer, a pure chlorine dioxide solution was prepared according to the method described in Standards Method [19], Section 411A. The concentrations of sulphuric acid and sodium chlorite were increase by 50 %, compared to the recommendations in Standard Methods, to obtain higher chlorine dioxide concentrations in the stock solution. The concentration obtained was 750 to 1,000 ppm as ClO_2. The chlorine dioxide solution was standardised immediately prior to calibration by the iodometric method described in Standards Methods [19], Section 411A.

Before the spectrophotometer was calibrated for chlorine dioxide readings, the U.V. lamp was replaced and the wavelength calibrated according to manufacturer's instruction for calibrating wavelength on Model 2010 series meters. A calibration curve was prepared by appropriate dilutions of the pure chlorine dioxide solution to produce concentrations in the range of 50 to 750 ppm range. With the measured spectrophotometer value, the concentration of chlorine dioxide was calculated using the calibration equation.

The hydrogen ion concentration of the feed was determined by volumetric titration: A desired volume of the product (50 cm^3) was measured into a flask. Sodium hydroxide of a known concentration (0.1 N) was added from a burette; the volume used was carefully measured. A few drop of an indicator (phenolphthalein) was used to signal when to stop adding sodium hydroxide; it changed colour (clear to pink) when the reaction was completed. From this data, the molarity of acid was calculated.

3.5.5 Sampling and Analysis

Samples were taken of the inlet and outlet solutions to the fixed-bed catalytic reactor. The following data was recorded at 15-minute intervals; sodium chlorite flow rate ($cm^3\ s^{-1}$), hydrochloric acid flow rate ($cm^3\ s^{-1}$), temperature (°C), pH, chlorine dioxide concentration ($g\ m^{-3}$), and hydrogen ion concentration ($mol\ m^{-3}$). Each run was continued until a steady state condition had been established; when three consecutive 15-minute samples gave constant readings.

Measurement of yield efficiency gives a standard for evaluating actual performance of the fixed-bed catalytic reactor. Yield is defined as the actual amount of reactant transformed or converted. Actual yield in a reaction is ordinary less than the theoretical yield. The yield efficiency is expressed as a percentage and is defined as:

$$\%\ \text{Yield} = \frac{\text{actual yield}}{\text{theoretical yield}} \times 100 \qquad (3.25)$$

The actual yield is determined from amount of chlorine dioxide that is actually generated. The theoretical yield is calculated by the amount of the chlorine dioxide that could possibly be obtained from the concentration of sodium chlorite in the feed solution. Since the chorine dioxide reaction takes five moles of chlorite ions to make four moles of chlorine dioxide, it can be calculated by:

$$\%\ \text{Yield} = \frac{[ClO_2]_{product}}{(4/5) * [NaClO_2]_{feed} * (90.5/67.5)} \times 100 \qquad (3.26)$$

where (90.5/67.5) is the molecular weight ratio of sodium chlorite to chlorine dioxide. The chlorine dioxide concentration in the product can be calculated by the amount of sodium chlorite consumed:

$$[ClO_2]_{product} = ([NaClO_2]_{feed} - [NaClO_2]_{product}) * (4/5) * (90.5/67.5) \qquad (3.27)$$

Substituting equation (3.27) into equation (3.26) yields:

$$\%\ \text{Yield} = \frac{[NaClO_2]_{feed} - [NaClO_2]_{product}}{[NaClO_2]_{feed}} \times 100 \qquad (3.28a)$$

or

$$\% \text{ Yield} = \frac{C_{Ao} - C_A}{C_{Ao}} \times 100 = 1 - \frac{C_A}{C_{Ao}} \quad (3.28b)$$

Substituting equation (3.14) into equation (3.28b) yields:

$$\% \text{ Yield} = 1 - \frac{1}{\exp((1-\varepsilon)\, k\, \tau} \quad (3.29)$$

The total experiment of the fixed-bed catalytic reactor was conducted in four phases;

1. Approach to Steady state
2. Effect of Excess Acid / Reaction Order
3. Variable Screening
4. Performance Characterisation / Model Prediction

The first phase investigated the reactors approach to steady state. The intent was to observe the performance of the reactor when a change was made to one of the operating variables.

The second phase investigated the effect of excess acid on yield efficiency. The kinetic data also revealed the order of the reaction.

The third phase used a practical method to preliminary screen variables that affect the performance of a fixed-bed catalytic reactor. There are a large number of possible variables but the ones chosen were variables that tend to influence the rate of reaction. The parameters investigated included particle size, space-time, temperature, and velocity.

The fourth phase investigated the more important variables determined by a screening experiment. The evaluation was designed to show the conditions necessary for the operation of a fixed-bed catalytic reactor; the operating characteristics and the optimum operation with respect to yield efficiency. Only one variable was changed at a time, while when possible, keeping all others constant. Predictions from the model were also superimposed on the actual data.

3.5.6 Accuracy of Results

Values of flow rate and currents quoted are accurate to within 5.0 %. The chlorine dioxide measurement and hydrogen ion analysis would both at best be accurate to within 2.0 %. From a consideration of the accuracy of the accuracy of these measurements and the overall variability of the system, conclusions should not be drawn in results that depend on differences between values of yield efficiency with a separation of less than 5.0 %. The accuracy of any one result is of the order of ± 2.5%.

3.6 Results and Discussion

3.6.1 Establishment of Steady State

Steady state is attained in a fixed-bed catalytic reactor when the temperature, flow rate and composition of the reactants are kept constant. The concentration of the solution in any layer normal to the reactor axis remains constant, and so does the reaction rate in the layer. With a single reaction, the change in free energy is zero at steady state.

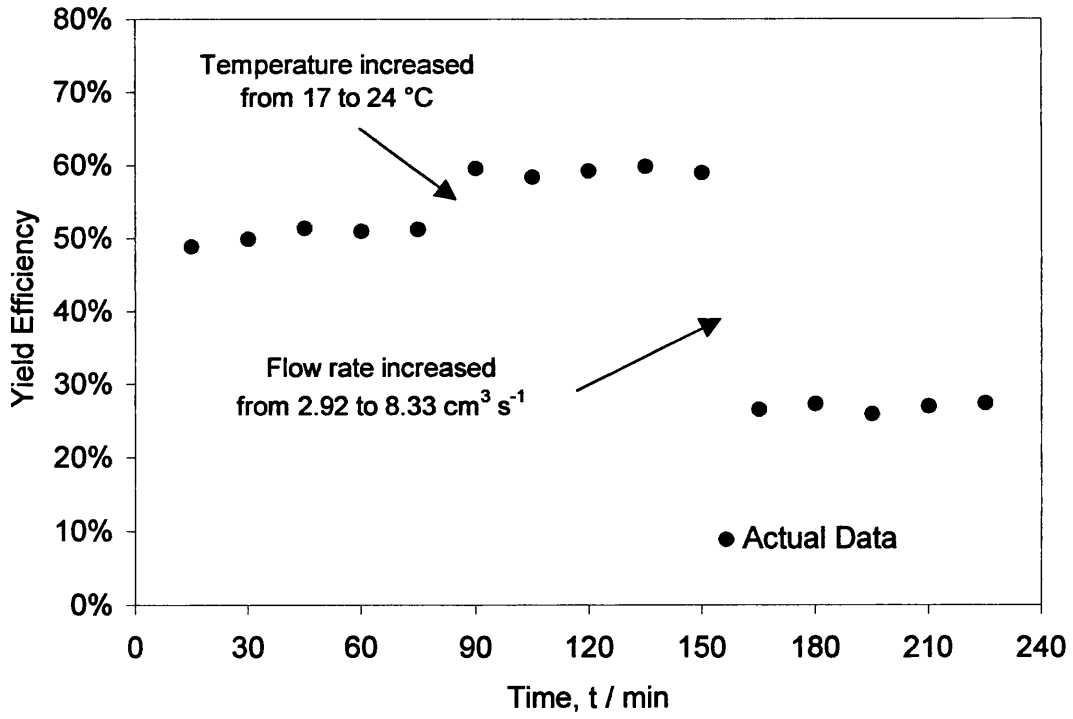

Figure 3.8 Behaviour of a Fixed-Bed Catalytic Reactor as it Approaches Steady State: Concentration of $NaClO_2$ was 0.011 M and initial molar ratio of $NaClO_2$ and HCl was 1:1. Diameter of the reactor was 2.62 cm and length of 30.46 cm. Total mass of catalyst was 77 g and average particle size of 0.12 cm.

The approach of a fixed-bed catalytic reactor to steady state is illustrated in Figure 3.8, with respect to the chorine dioxide concentration in the effluent. The platinum-supported catalyst particles used in the fixed-bed catalytic reactor were spherical at an average diameter of 0.12 cm. The sodium chlorite and hydrochloric acid solutions were passed through the reactor from top to bottom such that the flow rate was approximately 2.9 cm^3 s^{-1} at 17 °C.

The rise to steady state occurred quickly, within 15 minutes of operation. It appears that the sorption equilibrium of the chlorite and hydrogen ions between the catalyst and solution was rapidly established and maintained through the process. This gives an indication that the rate may be internal reaction controlled at the conditions that which the reactor was operated. If so, the reaction occurred only within the catalyst, and the concentration of the reactants in the catalyst was uniform.

Steady state has to be re-established each time after a change in temperature, flow rate or composition of the reactants. At 60 minutes, Figure 3.8 shows an increase in yield efficiency of approximately 9 % after increasing the temperature from 17 to 24 °C. At 150 minutes, the yield efficiency rapidly decreased by approximately 30 % after an increase in the flow rate from 2.92 to 8.33 cm^3 s^{-1}. In both cases, the reactor adjusted itself within 15 minutes of operation. Continuation of the experiment for a period of up to one hour after a change in condition showed no further change in yield efficiency.

It was therefore assumed that steady state could be reached after 15 minutes of operation when an adjustment is made to the operating conditions. Therefore, experimental runs will continue until three consecutive 15-minute samples give steady readings in temperature, flow rate, and chlorine dioxide concentration.

3.6.2 Screening Operating Variables

Tables 3.4 shows the list of variables and the levels at which they were studied for the fixed-bed catalytic reactor. The design matrix used for the electrochemical acidification cell was used for the fixed-bed catalytic reactor (see Table 2.8).

Table 3.5 shows the effects found for each of the variables and the corresponding confidence levels for the fixed-bed catalytic reactor. The reactors were operated until steady state and their performance was expressed as yield efficiency of sodium chlorite to chorine dioxide:

$$5\,NaClO_2 + 4\,HCl \rightarrow 4\,ClO_2 + 5\,NaCl + 2\,H_2O \qquad (3.30)$$

Table 3.4 Variables and Levels for the Fixed-Bed Catalytic Reactor

Variables	Process Variable	(-)	(+)
A	Linear Flow Velocity / cm s^{-1}	0.54	1.53
B	Particle Size / mm	0.6	1.2
C	Space Time / s	19.1	39.0
D	Temperature / °C	18.0	39.0
E	Dummy	-	-
F	Dummy	-	-
G	Dummy	-	-

Table 3.5 Screening Results for the Fixed-Bed Catalytic Reactor

Process Variable	Levels		Effect	Relative Significance, *t*-test	Confidence Level (> 90 %)
	(-)	(+)			
Linear Flow Velocity / cm s^{-1}	0.54	1.53	0.075	1.861	84.0 %
Particle Size / mm	0.6	1.2	-0.096	2.377	90.2 %
Space-time / s	19.1	39.0	0.165	4.080	97.3 %
Temperature / °C	18.0	39.0	0.241	5.933	99.0 %
Dummy	-	-	-0.066	1.632	-
Dummy	-	-	0.023	0.577	-
Dummy	-	-	0.003	0.069	-

Temperature, space-time, and particle size all have a significant effect on performance. As expected, temperature plays a key role in the reaction kinetics of most chemical systems. For reactions involving solid catalysts, particle size and temperature together are important since both of these variables can be varied to allow for negligible to significant particle diffusion resistance. Space-time depends on fluid dynamics and can also be varied to allow for negligible to significant particle diffusion resistance. Linear flow velocity had a confidence level of 84.0 %, indicating that it had a minimal effect on performance. If so, film diffusion is not the rate limiting step, and increasing the flow velocity through the catalyst bed will not increase yield efficiency. Dummy variables E and F are large compared with dummy variable G. The values may be due to two-factor interactions or due to the experimental or analytical error in measuring the response.

3.6.3 Reaction Rate Form

The pseudo-homogeneous reaction between sodium chlorite and hydrochloric acid in equation (3.30) was studied in a fixed-bed catalytic reactor with a diameter of 2.62 cm and a volume of 80.0 cm^3. The reactor contained a bed of platinum-supported catalyst impregnated on 1.2 mm diameter ceramic spheres.

A complete set of kinetic data was obtained, which consisted of measurements of the yield efficiency for different flow rates through the reactor, with each experiment made at nearly a constant ratio of reactants and a fixed temperature. An additional set of yield efficiency versus flow trails were made at different reactants ratio but at the same temperature.

In all of the runs, the sodium chlorite concentration was approximately 1,000 ppm at approximately 17 to 18 °C. Hydrochloric acid to sodium chlorite molar ratios of 1:1, 2:1, and 3:1 were evaluated, which corresponded to 0, 100, and 200 % excess HCl above the stoichiometric requirements according to equation (3.30). Tables 3.6 to 3.8 display the kinetic data that was used to determine the reaction order.

Table 3.6 Reaction Rate Data; [HCl]:[$NaClO_2$] Molar Ratio of 1:1

Run #	1a	2a	3a	4a	5a
Temperature / °C	17.0	18.0	17.5	17.0	17.0
Flow Rate / $cm^3\ s^{-1}$	608	505	317	229	175
$NaClO_2$ Concentration / ppm	1,044	989	1,011	1,012	1,022
Initial Molar Ratio $NaClO_2$:HCl	0.93	0.90	0.92	0.99	1.01
ClO_2 Concentration / ppm	125	135	203	247	312
ClO_2 pH	2.37	2.46	2.47	2.40	2.37
Yield Efficiency / %	20.1	22.8	33.7	41.0	51.2

Table 3.7 Reaction Rate Data; [HCl]:[$NaClO_2$] Molar Ratio of 2:1

Run #	1b	2b	3b	4b	5b
Temperature / °C	18.0	18.0	17.5	17.5	17.5
Flow Rate / $cm^3\ s^{-1}$	622	508	315	232	179
$NaClO_2$ Concentration / ppm	1,020	983	1,018	998	999
Initial Molar Ratio $NaClO_2$:HCl	2.06	2.12	2.07	2.10	2.09
ClO_2 Concentration / ppm	123	140	208	272	324
ClO_2 pH	2.03	2.01	2.06	2.04	1.95
Yield Efficiency / %	20.1	23.8	34.3	45.6	52.6

Table 3.8 Reaction Rate Data; [HCl]:[$NaClO_2$] Molar Ratio of 3:1

Run #	1c	2c	3c	4c	5c
Temperature / °C	18.0	17.5	18.0	18.0	18.0
Flow Rate / $cm^3\ s^{-1}$	178	235	314	517	635
$NaClO_2$ Concentration / ppm	1,005	986	1,021	966	999
Initial Molar Ratio $NaClO_2$:HCl	3.07	3.11	3.03	3.16	3.08
ClO_2 Concentration / ppm	321	267	203	127	108
ClO_2 pH	1.78	1.80	1.78	1.78	1.79
Yield Efficiency / %	53.5	45.4	33.4	22.1	18.1

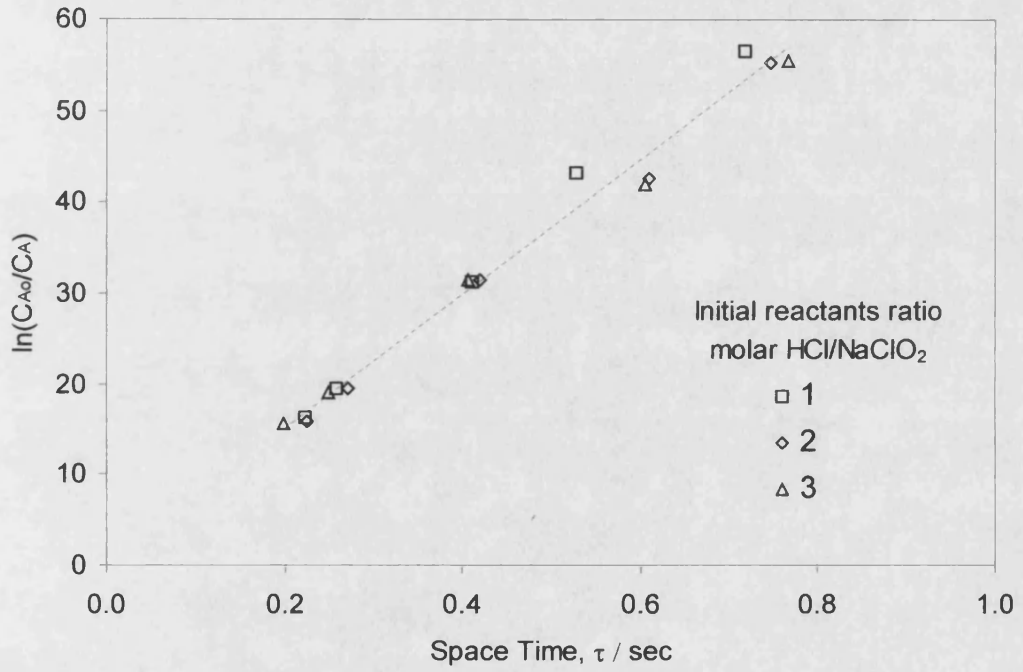

Figure 3.9 Test of First-Order Mechanism with Respect to $NaClO_2$: Concentration of $NaClO_2$ was 0.011 M. Diameter of the reactor was 2.62 cm and length of 30.49 cm. Total volumetric flow rate entering the reactor was varied from approximately 2.8 to 10.8 $cm^3\ s^{-1}$. Total mass of catalyst was 77 g and average particle size of 0.12 cm.

Figure 3.9 is a plot of $\ln(C_{Ao}/C_A)$ as a function of space-time at initial [HCl][:$NaClO_2$] ratios of 1, 2, and 3. At a [HCl]:[$NaClO_2$] ratio of 1, the points fell on a straight line. The points for the other two reactants ratio are all in good agreement. Therefore, Figure B gives a satisfactory interpretation of the kinetic data for a first-order mechanism with respect to $NaClO_2$ (equation 3.12).

The largest discrepancy between the points occurred at a space-time of greater than 0.6 sec. In strong acidic solutions, chlorine dioxide decomposes to chloric acid ($HClO_3$) and hydrochloric acid (HCl):

$$6\,ClO_2 + 3\,H_2O \rightarrow 5\,HClO_3 + HCl \qquad (3.31)$$

This degradation reaction occurs at pH of less than 2.0 [20]. This may explain the discrepancy since the pH of the chlorine dioxide solution at the 2:1 and 3:1 molar ratios were 2.0 and 1.8, respectively.

Therefore, unless otherwise stated, a hydrochloric acid to sodium chlorite molar ratio of 1:1 was used in all of the experiments and the reaction rate is considered to follow a first-order mechanism with respect to $NaClO_2$.

3.6.4 Fixed-Bed Catalytic Reactor Performance

Four series of experiments were conducted in an effort to characterise the performance of the fixed-bed catalytic reactor and to show the effect of intra-particle diffusion on reaction rate and yield efficiency. Temperature, particle size, reactor length, and flow rate were varied so that the data covered conditions ranging from negligible to significant intra-particle diffusion resistance. Tables 3.9 to 3.12 show the characteristics of the fixed-bed catalytic reactor and catalyst.

In all of the runs, the sodium chlorite concentration was constant at approximately 1,000 ppm and a sodium chlorite to hydrochloric acid molar ratio of 1:1. The total volumetric flow rate entering the reactor was varied from 2.8 to 10.8 $cm^3\ s^{-1}$. At each flow rate, the temperature was varied from 17 to 31 °C. Each run was continued until three consecutive 15-minute samples gave steady readings in chlorine dioxide concentration and pH. The results are shown in Tables 3.13 to 3.16.

Plots of the kinetic data displayed in Tables 3.13 to 3.16 are shown in Figures 3.10 to 3.12. Linear flow velocity was represented by the weight of catalyst divided by the molar flow rate, ($W\ M^{-1}$). This factor permits the determination of the effectiveness of the process regardless of reactor size, design, and output.

Table 3.9 Characteristics of Reactor A: Short reactor length and large catalyst size to investigate the significance of mass transport effects.

Diameter of reactor / cm	2.62
Length of reactor / cm	30.5
Particle diameter / cm	0.120
Density of catalyst bed / g cm^{-3}	0.478
Pore volume fraction of catalyst	0.130
Void fraction in catalyst bed	0.438

Table 3.10 Characteristics of Reactor B: Long reactor length and large catalyst size to investigate the significance of mass transport effects.

Diameter of reactor / cm	2.62
Length of reactor / cm	61.0
Particle diameter / cm	0.120
Density of catalyst bed / g cm^{-3}	0.478
Pore volume fraction of catalyst	0.130
Void fraction in catalyst bed	0.438

Table 3.11 Characteristics of Reactor C: Short reactor length and small catalyst size to investigate the significance of mass transport effects.

Diameter of reactor / cm	2.62
Length of reactor / cm	30.5
Particle diameter / cm	0.055
Density of catalyst bed / g cm^{-3}	0.973
Pore volume fraction of catalyst	0.097
Void fraction in catalyst bed	0.257

Table 3.12 Characteristics of Reactor D: Long reactor length and small catalyst size to investigate the significance of mass transport effects.

Diameter of reactor / cm	2.62
Length of reactor / cm	61.0
Particle diameter / cm	0.055
Density of catalyst bed / g cm^{-3}	0.973
Pore volume fraction of catalyst	0.097
Void fraction in catalyst bed	0.257

Table 3.13 Performance of Reactor A: Short reactor length and large catalyst size to investigate the significance of mass transport effects at total volumetric flow rates from 2.8 to 10.8 $cm^3 s^{-1}$ and temperatures of 17, 24, and 31 °C.

Run #	6a	7a	8a	9a	10a
Temperature / °C	17.0	18.0	17.5	17.0	17.0
Flow Rate / $cm^3 s^{-1}$	10.13	8.42	5.28	3.82	2.92
$NaClO_2$ Concentration / ppm	1,044	989	1,011	1,012	1,022
$NaClO_2$:HCl Molar Ratio	0.93	0.90	0.92	0.99	1.01
ClO_2 Concentration / ppm	125	135	203	247	312
ClO_2 pH	2.37	2.46	2.47	2.40	2.37
Yield Efficiency / %	20.1	22.8	33.7	41.0	51.2

Throughout the experiment, the following parameters were held approximately at: $NaClO_2$ concentration of 1,000 ppm, $NaClO_2$ to HCl molar ratio of 1:1, and temperature of 17 °C. The volumetric flow rate varied from 2.9 to 10.1 $cm^3 s^{-1}$.

Run #	6b	7b	8b	9b	10b
Temperature / °C	24.0	24.5	24.0	24.0	24.0
Flow Rate / $cm^3 s^{-1}$	10.32	8.42	5.13	3.80	2.98
$NaClO_2$ Concentration / ppm	1,025	989	1,041	1,016	999
$NaClO_2$:HCl Molar Ratio	0.91	0.93	0.90	0.91	0.92
ClO_2 Concentration / ppm	140	157	223	293	357
ClO_2 pH	2.3	2.34	2.38	2.48	2.42
Yield Efficiency / %	22.8	26.6	35.9	48.3	60.0

Throughout the experiment, the following parameters were held approximately at: $NaClO_2$ concentration of 1,000 ppm, $NaClO_2$ to HCl molar ratio of 1:1, and temperature of 24 °C. The volumetric flow rate varied from 3.0 to 10.3 $cm^3 s^{-1}$.

Run #	6c	7c	8c	9c	10c
Temperature / °C	31.0	31.0	30.5	31.0	31.0
Flow Rate / $cm^3 s^{-1}$	10.40	8.28	5.28	3.92	2.88
$NaClO_2$ Concentration / ppm	1,017	1,005	1,011	986	1,034
$NaClO_2$:HCl Molar Ratio	0.95	0.96	0.95	0.97	0.87
ClO_2 Concentration / ppm	171	198	274	327	397
ClO_2 pH	2.31	2.38	2.45	2.43	2.83
Yield Efficiency / %	28.3	33.1	45.5	55.6	64.3

Throughout the experiment, the following parameters were held approximately at: $NaClO_2$ concentration of 1,000 ppm, $NaClO_2$ to HCl molar ratio of 1:1, and temperature of 31 °C. The volumetric flow rate varied from 2.9 to 10.4 $cm^3 s^{-1}$.

Table 3.14 Performance of Reactor B: Long reactor length and large catalyst size to investigate the significance of mass transport effects at total volumetric flow rates from 2.8 to 10.8 $cm^3 s^{-1}$ and temperatures of 17, 24, and 31 °C.

Run #	11a	12a	13a	14a	15a
Temperature / °C	17.0	18.0	17.0	17.0	17.0
Flow Rate / $cm^3 s^{-1}$	10.53	8.28	5.35	3.87	2.87
$NaClO_2$ Concentration / ppm	1,004	1,005	998	998	1,040
$NaClO_2$:HCl Molar Ratio	0.99	0.96	0.96	0.96	0.93
ClO_2 Concentration / ppm	252	279	333	400	463
ClO_2 pH	2.52	2.54	2.64	2.63	2.87
Yield Efficiency / %	42.1	46.5	55.9	67.2	74.6

Throughout the experiment, the following parameters were held approximately at: $NaClO_2$ concentration of 1,000 ppm, $NaClO_2$ to HCl molar ratio of 1:1, and temperature of 17 °C. The volumetric flow rate varied from 2.9 to 10.5 $cm^3 s^{-1}$.

Run #	11b	12b	13b	14b	15b
Temperature / °C	23.0	24.0	24.0	24.0	24.0
Flow Rate / $cm^3 s^{-1}$	9.72	8.38	5.23	3.67	2.87
$NaClO_2$ Concentration / ppm	1,088	993	1,021	1,053	1,040
$NaClO_2$:HCl Molar Ratio	0.90	1.00	0.98	0.96	0.97
ClO_2 Concentration / ppm	284	305	395	465	520
ClO_2 pH	2.51	2.45	2.72	2.82	3.71
Yield Efficiency / %	43.7	51.4	64.9	74.0	83.9

Throughout the experiment, the following parameters were held approximately at: $NaClO_2$ concentration of 1,000 ppm, $NaClO_2$ to HCl molar ratio of 1:1, and temperature of 24 °C. The volumetric flow rate varied from 2.9 to 9.7 $cm^3 s^{-1}$.

Run #	11c	12c	13c	14c	15c
Temperature / °C	31.0	31.0	31.0	31.0	31.0
Flow Rate / $cm^3 s^{-1}$	10.45	8.33	5.38	3.90	2.95
$NaClO_2$ Concentration / ppm	1,012	999	992	990	1,010
$NaClO_2$:HCl Molar Ratio	0.99	1.00	1.00	1.00	0.99
ClO_2 Concentration / ppm	301	355	436	487	559
ClO_2 pH	2.53	2.69	2.79	3.57	3.13
Yield Efficiency / %	49.9	59.5	73.6	82.5	92.8

Throughout the experiment, the following parameters were held approximately at: $NaClO_2$ concentration of 1,000 ppm, $NaClO_2$ to HCl molar ratio of 1:1, and temperature of 31 °C. The volumetric flow rate varied from 3.0 to 10.5 $cm^3 s^{-1}$.

Table 3.15 Performance of Reactor C: Short reactor length and small catalyst size to investigate the significance of mass transport effects at total volumetric flow rates from 2.8 to 10.3 $cm^3 s^{-1}$ and temperatures of 17, 24, and 31 °C.

Run #	16a	17a	18a	19a	20a
Temperature / °C	17.0	17.0	17.0	17.0	17.0
Flow Rate / $cm^3 s^{-1}$	10.33	8.28	5.12	3.97	2.90
$NaClO_2$ Concentration / ppm	1,023	1,005	1,044	973	1,028
$NaClO_2$:HCl Molar Ratio	0.98	0.99	0.96	1.02	0.97
ClO_2 Concentration / ppm	244	280	392	435	501
ClO_2 pH	2.44	2.43	2.58	2.60	2.85
Yield Efficiency / %	39.9	46.7	62.9	74.8	81.6

Throughout the experiment, the following parameters were held approximately at: $NaClO_2$ concentration of 1,000 ppm, $NaClO_2$ to HCl molar ratio of 1:1, and temperature of 17 °C. The volumetric flow rate varied from 2.9 to 10.3 $cm^3 s^{-1}$.

Run #	16b	17b	18b	19b	20b
Temperature / °C	24.0	24.0	24.0	24.0	24.0
Flow Rate / $cm^3 s^{-1}$	10.47	8.22	5.23	3.68	2.90
$NaClO_2$ Concentration / ppm	1,010	1,013	1,021	1,048	1,028
$NaClO_2$:HCl Molar Ratio	0.99	0.99	0.98	0.96	0.97
ClO_2 Concentration / ppm	298	335	421	509	564
ClO_2 pH	2.54	2.57	2.78	3.02	2.99
Yield Efficiency / %	49.4	55.5	69.1	81.4	92.0

Throughout the experiment, the following parameters were held approximately at: $NaClO_2$ concentration of 1,000 ppm, $NaClO_2$ to HCl molar ratio of 1:1, and temperature of 24 °C. The volumetric flow rate varied from 2.9 to 10.5 $cm^3 s^{-1}$.

Run #	16c	17c	18c	19c	20c
Temperature / °C	31.0	31.0	31.0	31.0	31.0
Flow Rate / $cm^3 s^{-1}$	10.32	8.32	5.12	3.85	2.90
$NaClO_2$ Concentration / ppm	1,025	1,001	1,044	1,003	1,028
$NaClO_2$:HCl Molar Ratio	0.98	1.00	0.96	0.99	0.97
ClO_2 Concentration / ppm	361	392	490	523	581
ClO_2 pH	2.79	2.73	3.24	3.49	5.06
Yield Efficiency / %	59.1	65.6	78.6	87.4	94.8

Throughout the experiment, the following parameters were held approximately at: $NaClO_2$ concentration of 1,000 ppm, $NaClO_2$ to HCl molar ratio of 1:1, and temperature of 31 °C. The volumetric flow rate varied from 2.9 to 10.3 $cm^3 s^{-1}$.

Table 3.16 Performance of Reactor D: Long reactor length and small catalyst size to investigate the significance of mass transport effects at total volumetric flow rates from 2.8 to 10.8 $cm^3 s^{-1}$ and temperatures of 17, 24, and 31 °C.

Run #	21a	22a	23a	24a	25a
Temperature / °C	17.0	17.0	17.0	17.0	17.0
Flow Rate / $cm^3 s^{-1}$	10.63	8.33	5.32	3.87	3.00
$NaClO_2$ Concentration / ppm	994	999	1,005	998	993
$NaClO_2$:HCl Molar Ratio	1.00	1.14	1.17	1.14	1.15
ClO_2 Concentration / ppm	379	439	519	563	585
ClO_2 pH	2.88	2.57	2.7	2.72	3.01
Yield Efficiency / %	64.0	73.7	86.6	94.5	98.7

Throughout the experiment, the following parameters were held approximately at: $NaClO_2$ concentration of 1,000 ppm, $NaClO_2$ to HCl molar ratio of 1:1, and temperature of 17 °C. The volumetric flow rate varied from 3.0 to 10.6 $cm^3 s^{-1}$.

Run #	21b	22b	23b	24b	25b
Temperature / °C	24.0	24.0	24.0	24.0	24.0
Flow Rate / $cm^3 s^{-1}$	10.48	8.30	5.27	3.85	2.93
$NaClO_2$ Concentration / ppm	1,009	1,003	1,014	1,003	1,016
$NaClO_2$:HCl Molar Ratio	1.13	1.14	1.13	1.14	1.13
ClO_2 Concentration / ppm	441	476	563	581	606
ClO_2 pH	2.53	2.54	2.62	2.63	3.08
Yield Efficiency / %	73.2	79.5	93.0	97.2	99.9

Throughout the experiment, the following parameters were held approximately at: $NaClO_2$ concentration of 1,000 ppm, $NaClO_2$ to HCl molar ratio of 1:1, and temperature of 24 °C. The volumetric flow rate varied from 2.9 to 10.5 $cm^3 s^{-1}$.

Run #	21c	22c	23c	24c	25c
Temperature / °C	31.0	31.0	31.0	31.0	31.0
Flow Rate / $cm^3 s^{-1}$	10.65	8.32	5.35	3.93	3.03
$NaClO_2$ Concentration / ppm	993	1,001	998	982	983
$NaClO_2$:HCl Molar Ratio	1.15	1.14	1.14	1.16	1.16
ClO_2 Concentration / ppm	491	519	570	579	585
ClO_2 pH	2.55	2.62	2.61	2.58	2.59
Yield Efficiency / %	82.9	86.9	95.7	98.9	99.8

Throughout the experiment, the following parameters were held approximately at: $NaClO_2$ concentration of 1,000 ppm, $NaClO_2$ to HCl molar ratio of 1:1, and temperature of 31 °C. The volumetric flow rate varied from 3.0 to 10.7 $cm^3 s^{-1}$.

Figures 3.10 to 3.12 show effects of particle size, velocity, and temperature on product yield efficiency. The changing of velocity alone in a fixed-bed catalytic reactor is not a significant test for determining the effect of velocity since space-time is also changed. It was necessary to change velocity and bed depth in proportion in order to keep the space-time constant. Reactor lengths of 30.6 and 61.0 cm were used in the experiment.

Chlorine dioxide yield efficiency was not affected by the change in velocity; an increase in velocity had a negligible increase in the generation of chlorine dioxide. Approximately the same yield efficiency was obtained with the same value of the ratio of bed depth to flow rate at two different bed depths at all temperatures. Hence, film diffusion was not encountered.

Figures 3.10 to 3.12 also showed a difference in performance between the small and large particles. At 17 °C, a slight difference existed, but the difference was more noticeable at 31 °C. This is an indication that particle diffusion limitations exist, particularly in the large particles.

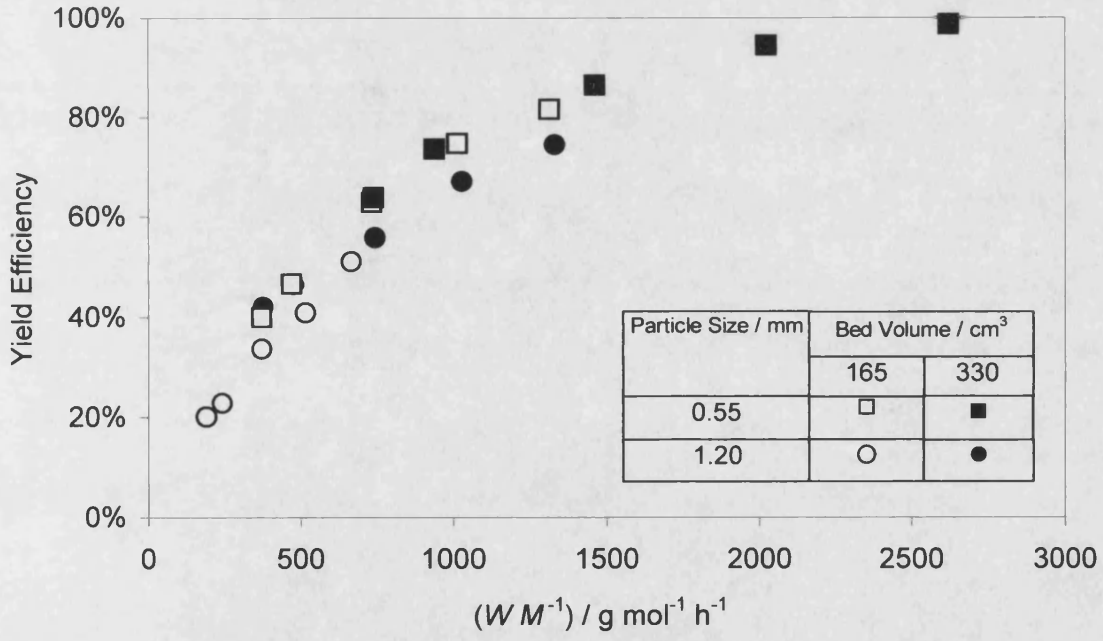

Figure 3.10. Effect of Particle Size and Velocity on Yield Efficiency at 17 °C: Concentration of $NaClO_2$ was 0.011 M and initial molar ratio of $NaClO_2$ and HCl was 1:1. Diameter of the reactor was 2.62 cm. Total volumetric flow rate entering the reactor ranged from 2.8 to 10.8 $cm^3\ s^{-1}$.

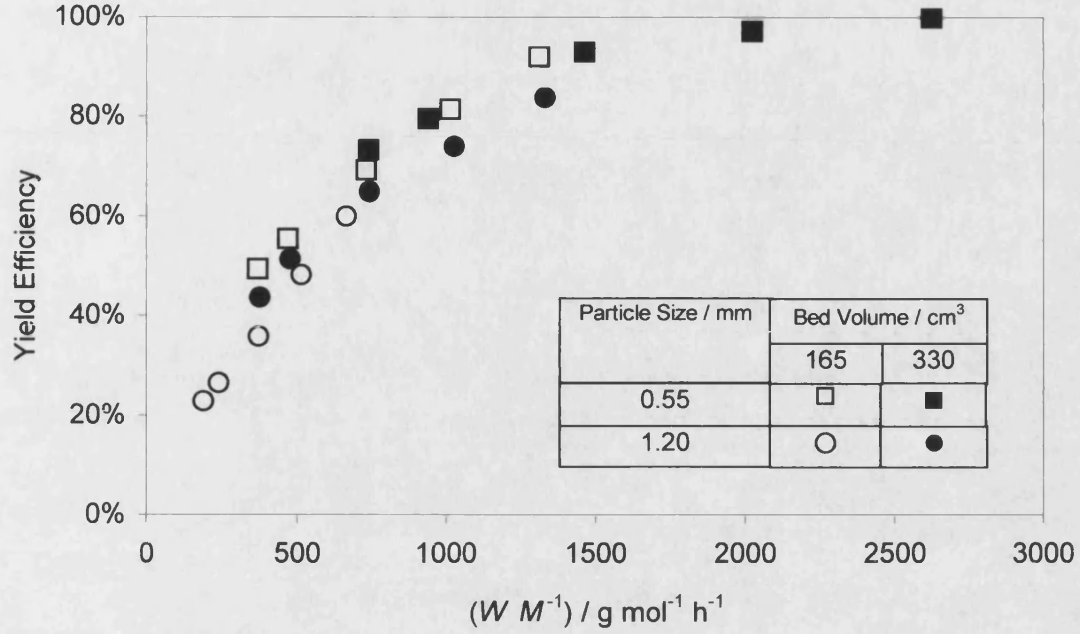

Figure 3.11 Effect of Particle Size and Velocity on Yield Efficiency at 24 °C: Concentration of $NaClO_2$ was 0.011 M and initial molar ratio of $NaClO_2$ and HCl was 1:1. Diameter of the reactor was 2.62 cm. Total volumetric flow rate entering the reactor ranged from 2.8 to 10.8 $cm^3\ s^{-1}$.

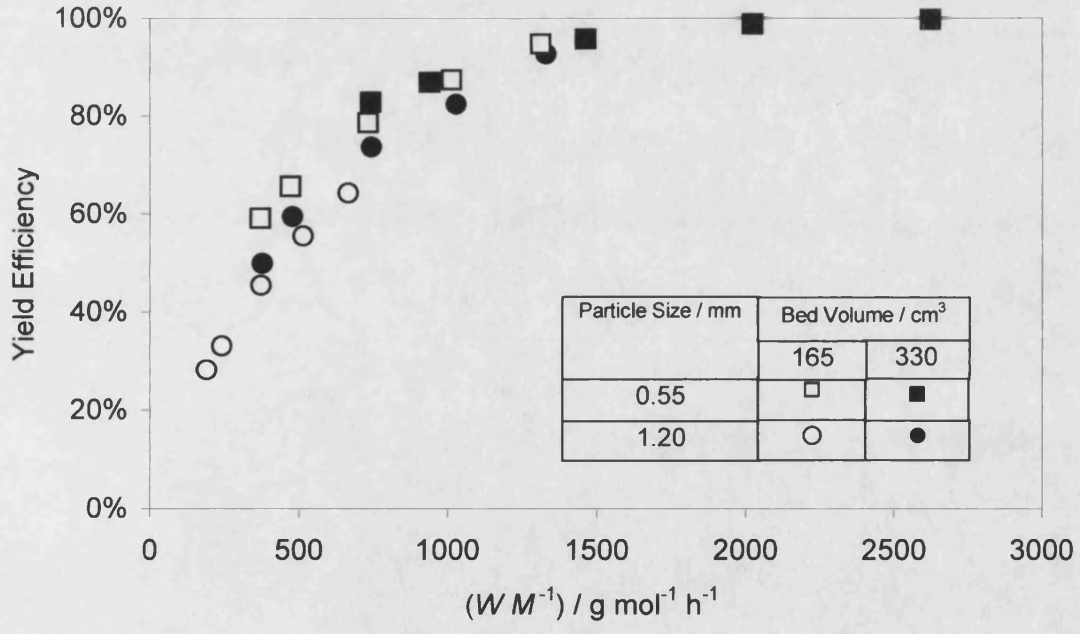

Figure 3.12 Effect of Particle Size and Velocity on Yield Efficiency at 31 °C: Concentration of $NaClO_2$ was 0.011 M and initial molar ratio of $NaClO_2$ and HCl was 1:1. Diameter of the reactor was 2.62 cm. Total volumetric flow rate entering the reactor ranged from 2.8 to 10.8 $cm^3\ s^{-1}$.

Chlorine dioxide yield efficiency was affected by the change in temperature; an increase in temperature had an increase in the generation of chlorine dioxide. At the conditions of this study, the yield efficiency increase was approximately 2.5 % per °C. The levelling off of yield efficiency at high space times at 31 °C utilising both the smaller and larger particle reflects the approach to equilibrium.

3.6.5 Model Parameters

The data was interpreted with a first-order kinetic expression (equation 3.12), using a global rate constant for solid catalysed reaction (3.15). In liquid systems, the intrinsic chemical reaction rate k_r is usually a function of only temperature. k_r can be a function of other parameters such as ionic strength, solvent, or total pressure. For the purpose of this study, it is assumed that k_r depends only on temperature. The dependency of k_r on temperature for an elementary reaction can usually be correlated by the Arrhenius Law expression:

$$k_r = A_o \exp\left(\frac{-E_{act}}{RT}\right) \tag{3.32}$$

where E_{act} is the activation energy and A_o is the frequency (or pre-exponential) factor. Low values for the E_{act} may indicate that the reaction is mass transfer controlled; a change in the slope of the Arrhenius plot could suggest the onset of mass-transfer control. The frequency factor is related to the number of active sites available for reaction; this is the parameter that will decrease with time if the catalyst deactivates.

Equation (3.32) shows that numerical values of A_o and E_{act} can be obtained by plotting experimental data for rate constants at different temperatures. The logarithmic form of equation (3.32) is:

$$\ln k_r = -\frac{E_{act}}{R}\left(\frac{1}{T}\right) + \ln A_o \tag{3.33}$$

A plot of $\ln(k_r)$ vs. $1/T$ called an Arrhenius plot yields a slope equal to $-E_{act}/R$ and a intercept equal to $\ln A_o$. The Arrhenius Law expression can be used to calculate reaction rate constant at a third temperature when it is given for two different temperatures:

$$\ln\left(\frac{k_2}{k_1}\right) = \frac{E_{act}}{R}\left(\frac{1}{T_1} - \frac{1}{T_2}\right) \tag{3.34}$$

Using the information in Tables 3.13 to 3.16 for the first-order kinetic reaction, A_o and E_{act} were determined as follows. The global rate constant was calculated using:

$$k = \frac{1}{(1-\varepsilon)\tau}\ln\left(\frac{C_{Ao}}{C_A}\right) \tag{3.35}$$

The Sherwood number was then used to determine the mass transfer coefficient:

$$k_f a_p = \left(\frac{6}{d}\right)\left(\frac{D_A}{d}\mathrm{Sh}\right) \tag{3.36}$$

The diffusion coefficient for a single ion can be estimated by:

$$D_A^\circ = \frac{RT}{F^2}\lambda_A^\circ \tag{3.37}$$

where λ_A° is the equivalent ionic conductivity at infinite dilution. The conductance of the electrolyte increases with temperature. The variation of equivalent conductance with temperature at infinite dilution can be expressed by a second-order polynomial equation:

$$\lambda_T^\circ = A_3 T^2 + B_3 T + C_3 \tag{3.38}$$

where T is in absolute temperature (K). The variation of equivalent conductance with temperature for the chloride ion is:

$$\lambda_{Cl^-}^\circ = 3.32\times10^{-3}\,T^2 - 4.23\times10^{-1}\,T - 9.24\times10^{+1} \tag{3.39}$$

The equivalent conductance of chlorite ion at infinite dilution at 298 K (25 °C) is 52.0 $cm^2\ \Omega^{-1}\ eq^{-1}$. Assuming that the chlorite ion behaves similar to the chloride ion with respect to temperature, the following relationship was generated by a symmetrical fit to equation (3.39) through the value of 52.0 $cm^2\ \Omega^{-1}\ eq^{-1}$:

$$\lambda_{ClO_2^-}^\circ = 3.32\times10^{-3}\,T^2 - 4.23\times10^{-1}\,T - 1.22\times10^{+2} \tag{3.40}$$

Combining equations (3.37) and (3.40) provides an expression to relate the effect of temperature on diffusion coefficient for chlorite ions in the form:

$$D^{o}_{ClO_2^-} = \frac{RT}{F^2}(3.32\times10^{-3}\,T^2 - 4.23\times10^{-1}\,T - 1.22\times10^{+2}) \qquad (3.41)$$

Experimental viscosity-concentration-temperature and density-concentration-temperature data for sodium chlorite solutions is available from Sterling Pulp Chemical [21]. From this data, empirical relationships between viscosity-concentration-temperature and density-concentration-temperature have been developed. Both viscosity and density decrease with temperature and increase with sodium chlorite concentration.

For sodium chlorite solutions between 278 to 313 K (5 to 40 °C), the empirical relationships for density is:

$$\rho_T = K_E C_A + K_F \qquad (3.42)$$

where ρ_T is density (g cm^{-3}) and C is the concentration (g L^{-1}). Constants K_E and K_F are both a function of absolute temperature (K):

$$K_E = 9.44\times10^{-9}\,T^2 - 6.81\times10^{-6}\,T + 1.87\times10^{-3} \qquad (3.43)$$

$$K_F = -6.41\times10^{-6}\,T^2 + 3.58\times10^{-3}\,T + 5.03\times10^{-1} \qquad (3.44)$$

The empirical relationships for viscosity is:

$$\eta_T = K_G \exp(K_H C_A) \qquad (3.45)$$

where η_T is the viscosity (cP) and C is the sodium chlorite concentration (g L^{-1}). Constants K_G and K_H are both a function of absolute temperature (K):

$$K_G = 5.05\times10^{-4}\,T^2 - 3.21\times10^{-1}\,T + 5.17\times10^{1} \qquad (3.46a)$$

$$K_H = -1.21\times10^{-7}\,T^2 + 8.37\times10^{-5}\,T - 1.12\times10^{-2} \qquad (3.46b)$$

The reaction rate constant at each temperature was calculated by:

$$\eta_f k_r = \frac{1}{\frac{1}{k} - \frac{1}{k_f a_p}} \quad (3.47)$$

Assuming that the effectiveness factor was the same value at the two different temperatures, the activation energy was estimated by:

$$E_{act} = \frac{R \ln\left(\frac{k_2}{k_1}\right)}{\left(\frac{1}{T_1} - \frac{1}{T_2}\right)} \quad (3.48)$$

Table 3.17 shows the range of activation energy obtained from the kinetic data:

The average value of the activation energy was found to be:

$$E_{act} = 28{,}358 \text{ J mol}^{-1} \quad (3.49)$$

The average value of the activation energy is relatively low; signifying that the reaction is temperature insensitive in the temperature range studied and can easily occur at room temperature. In this case, the catalyst has caused a significant reduction in overall activation energy, presumably by replacing a difficult homogeneous step by a more easily executed surface reaction involving adsorbed chlorite and/or hydrogen ions.

Using the average value of the activation energy, the frequency factor was found by the procedure outlined in this section. The best value that correlated the kinetic data was:

$$A_o = 51{,}758 \text{ s}^{-1} \quad (3.50)$$

The effectiveness factors were determined by equation (3.22). The value for each particle size evaluated was found to be 0.078 for the 0.120 cm particle and 0.126 for the 0.055 cm particle. The effectiveness factor is a function of temperature but is not a function of flow rate. However, the change in effectiveness factor for both particle sizes in the temperature ranged selected for study was negligible. In both cases, particle

diffusion had a significant negative effect on the rate of chemical reaction at the catalytic site.

Table 3.17 Activation Energy Obtained from the Kinetic Data

Run #	5a	5c	6a	6c	7a	7c	8a	8c
T / °C	17.0	31.0	18.0	31.0	17.5	30.5	17.0	31.0
k / s^{-1}	0.025	0.037	0.024	0.036	0.023	0.035	0.022	0.034
$k_f a_p$ / s^{-1}	0.115	0.179	0.116	0.160	0.092	0.139	0.078	0.123
$\eta_f k_r$ / s^{-1}	0.031	0.047	0.030	0.046	0.031	0.046	0.030	0.048
E_{act} / J mol^{-1}	21,633		25,496		21,552		23,985	

Run #	9a	9c	10a	10c	11a	11c	12a	12c
T / °C	17.0	31.0	17.0	31.0	18.0	31.0	17.0	31.0
k / s^{-1}	0.023	0.032	0.031	0.039	0.028	0.041	0.024	0.039
$k_f a_p$ / s^{-1}	0.069	0.107	0.117	0.180	0.115	0.160	0.091	0.142
$\eta_f k_r$ / s^{-1}	0.034	0.046	0.042	0.050	0.037	0.055	0.032	0.053
E_{act} / J mol^{-1}	16,230		8,477		22,034		26,756	

Run #	13a	13c	14a	14c	15a	15c	16a	16c
T / °C	17.0	31.0	17.0	31.0	17.0	31.0	17.0	31.0
k / s^{-1}	0.023	0.037	0.021	0.042	0.042	0.091	0.036	0.084
$k_f a_p$ / s^{-1}	0.078	0.123	0.069	0.108	0.409	0.636	0.370	0.578
$\eta_f k_r$ / s^{-1}	0.033	0.052	0.031	0.068	0.046	0.107	0.040	0.098
E_{act} / J mol^{-1}	24,028		41,917		43,914		46,370	

Run #	17a	17c	18a	18c	19a	19c	20a	20c
T / °C	17.0	31.0	17.0	31.0	17.0	31.0	17.0	31.0
k / s^{-1}	0.036	0.071	0.041	0.067	0.039	0.072	0.043	0.091
$k_f a_p$ / s^{-1}	0.299	0.466	0.267	0.413	0.234	0.366	0.415	0.646
$\eta_f k_r$ / s^{-1}	0.041	0.083	0.048	0.080	0.047	0.090	0.048	0.107
E_{act} / J mol^{-1}	36,564		26,469		34,476		41,535	

Run #	21a	21c	22a	22c	23a	23c	24a	24c
T / °C	17.0	31.0	17.0	31.0	17.0	31.0	17.0	31.0
k / s^{-1}	0.044	0.077	0.045	0.071	0.047	0.074	0.055	0.079
$k_f a_p$ / s^{-1}	0.371	0.578	0.304	0.475	0.264	0.416	0.237	0.373
$\eta_f k_r$ / s^{-1}	0.050	0.089	0.053	0.084	0.058	0.090	0.071	0.101
E_{act} / J mol^{-1}	29,933		24,127		23,455		18,041	

An effectiveness factor of 0.126 indicates that the effect of particle diffusion reduced the intrinsic rate or catalyst activity by approximately 87 %. This shows that the rate constant will drop as the size of the catalyst particle increases, even when the total catalyst area increases. The decrease in reaction rate is the result of slow diffusion within the pores of the catalyst particle.

3.6.6 Model Predictions

Equation (3.29) was used to plot yield efficiency versus space-time In Figures 3.13 to 3.16. A spreadsheet in Microsoft® Excel 2000 was used for the calculations. The reaction rate constant was determined from the experimental data. From the reaction rate constant, the activation energy and frequency factor were calculated and used in the model.

The predicted performance for a variety of operating conditions matched well with the actual experimental data. Under the conditions studied, the model predicted results that were within 6.5 % of the actual data.

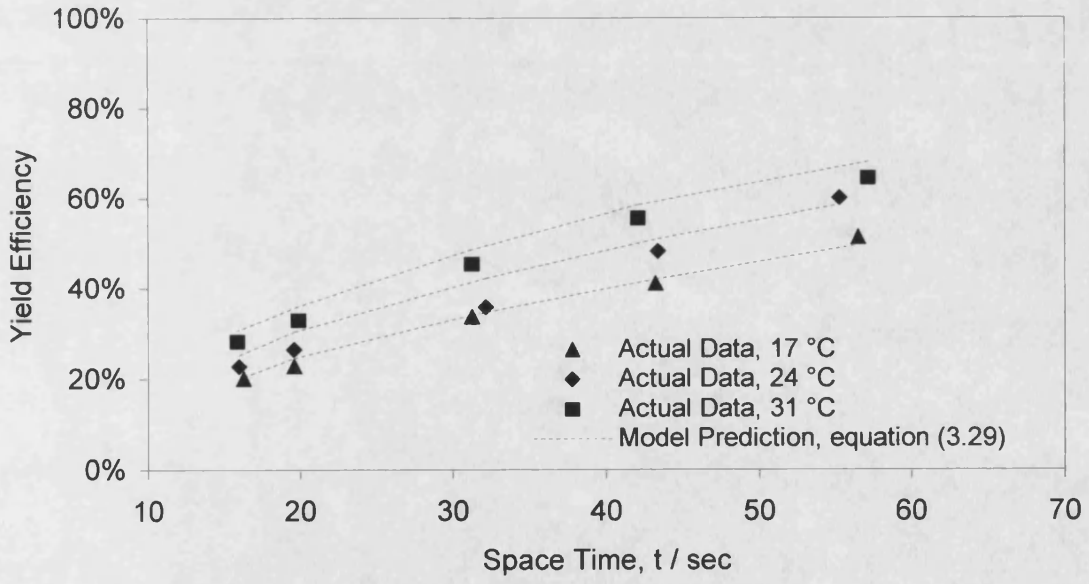

Figure 3.13 Chlorine Dioxide Yield Efficiency versus Space-Time at Various Temperatures – Reactor A: Concentration of $NaClO_2$ was 0.011 M and initial molar ratio of $NaClO_2$ and HCl was 1:1. Diameter of the reactor was 2.62 cm and length of 30.48 cm. Total volumetric flow rate entering the reactor was varied from 2.8 to 10.8 $cm^3\ s^{-1}$. Total mass of catalyst was 78.8 g, average particle size 0.12 cm.

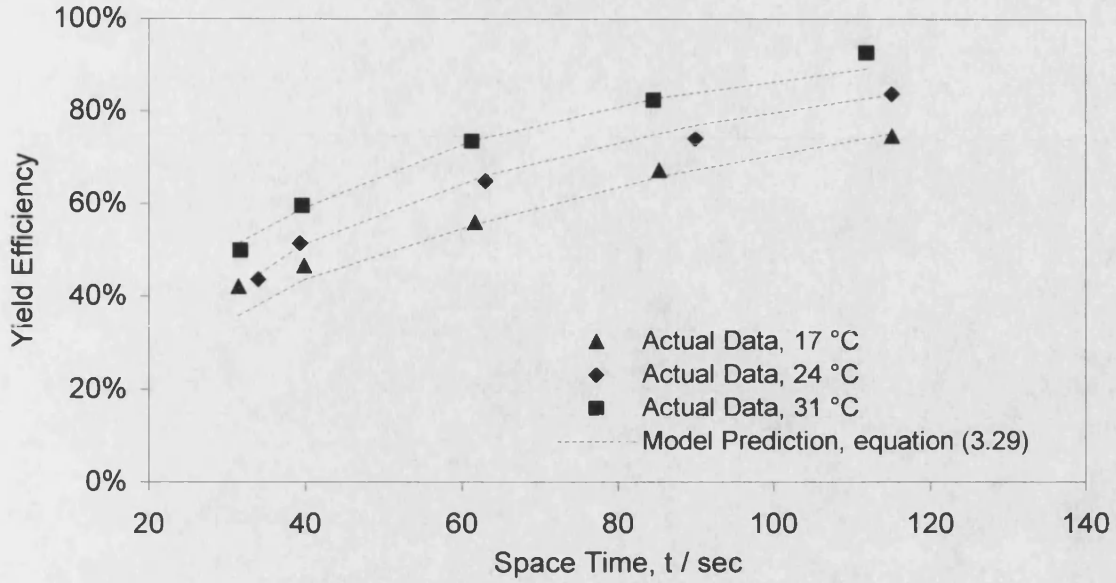

Figure 3.14 Chlorine Dioxide Yield Efficiency versus Space-Time at Various Temperatures – Reactor B: Concentration of $NaClO_2$ was 0.011 M and initial molar ratio of $NaClO_2$ and HCl was 1:1. Diameter of the reactor was 2.62 cm and length of 60.96 cm. Total volumetric flow rate entering the reactor was varied from 2.8 to 10.8 $cm^3\ s^{-1}$. Total mass of catalyst was 157.6 g, average particle size 0.12 cm.

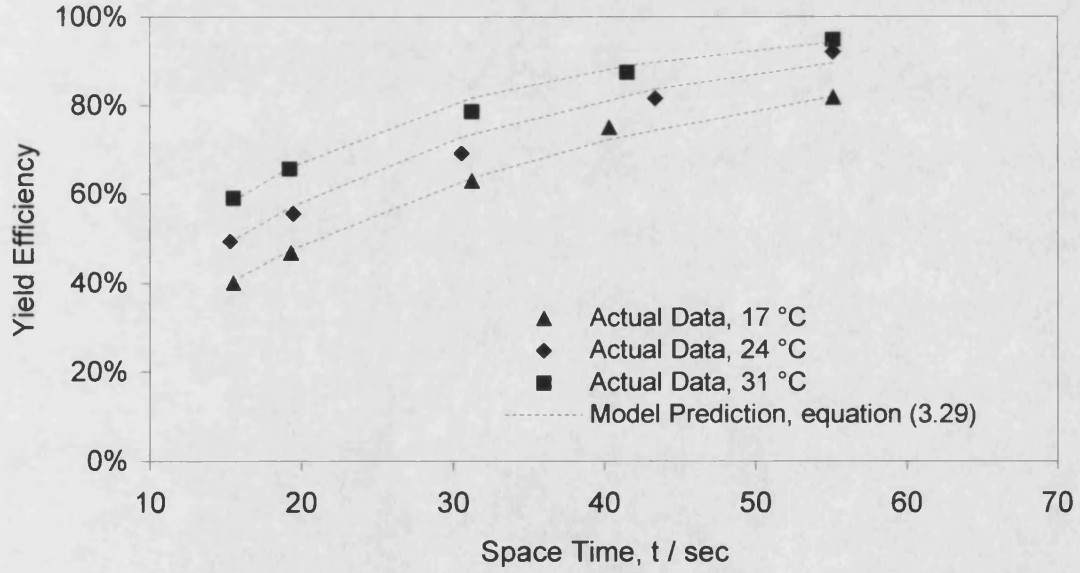

Figure 3.15 Chlorine Dioxide Yield Efficiency versus Space-Time at Various Temperatures – Reactor C: Concentration of $NaClO_2$ was 0.011 M and initial molar ratio of $NaClO_2$ and HCl was 1:1. Diameter of the reactor was 2.62 cm and length of 30.48 cm. Total volumetric flow rate entering the reactor was varied from 2.8 to 10.8 $cm^3\ s^{-1}$. Total mass of catalyst was 155.4 g, average particle size 0.055 cm.

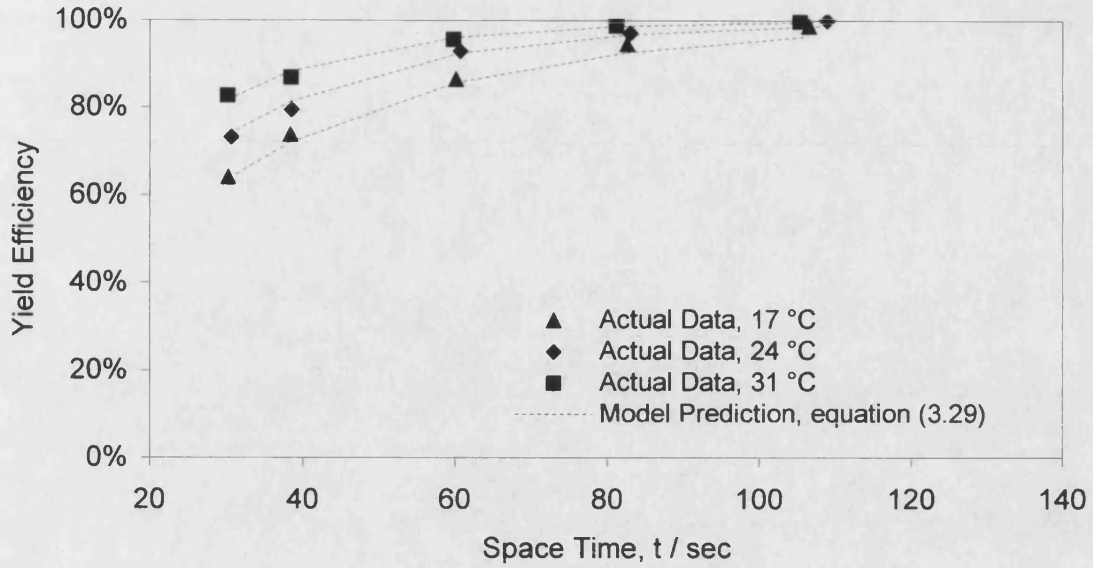

Figure 3.16. Chlorine Dioxide Yield Efficiency versus Space-Time at Various Temperatures – Reactor D: Concentration of $NaClO_2$ was 0.011 M and initial molar ratio of $NaClO_2$ and HCl was 1:1. Diameter of the reactor was 2.62 cm and length of 60.96 cm. Total volumetric flow rate entering the reactor was varied from 2.8 to 10.8 cm^3 s^{-1}. Total mass of catalyst was 310.9 g, average particle size 0.055 cm.

3.7 Conclusions

3.7.1 Fixed-Bed Catalytic Reactor

Chlorine dioxide yield efficiency was not affected by the change in velocity, giving the indication that mass transfer across the thin film surrounding the catalyst particle was not the controlling factor. At lower temperature (17 to 24 °C), the yield efficiency was the approximately the same for both particle sizes studied. At a higher temperature (31 °C), greater yield efficiencies were seen with the small particles, indicating that mass transfer through the catalyst particle began to take control in the larger particles. Chlorine dioxide yield efficiency increased as the temperature increased, showing that the intrinsic kinetic rate of the chemical reaction followed the Arrhenius Law expression.

3.7.2 Fixed-Bed Catalytic Reactor Model

A mathematical model was developed with the intent to evaluate the operation of a fixed-bed catalytic reactor. The model provided a method to systematically study the effects of differing space-time, particle size, velocity, and temperature on the operation of the reactor. An empirical approach was used to describe the rate equation in the fixed-bed

catalytic reactor; a power-law form employed for homogeneous reactions. The apparent order of the reaction, values of the exponents on concentrations, and specific reaction rate were determined by fitting the equation to the experimental data. The first-order kinetic expression correlated the experimental data well. Dilute electrolyte theory was used and the model considered an isothermal and steady state operation.

The model characterised the performance of a catalyst by use of a global rate constant, which incorporated film diffusion, particle diffusion and the intrinsic chemical reaction rate. Test simulations were made and compared to actual performance data. Under all of the conditions studied, varying velocity, space-time, and temperature with two particle sized catalyst, the model predicted results that were within 6.5 % of actual experimental data. It is best to consider that the final rate equation is a satisfactory interpretation of the kinetic data and for use in scale-up efforts.

3.8 Recommendations

3.8.1 Fixed-Bed Catalytic Reactor

The prospect of being able to use a much lower cost feedstock to produce chlorine dioxide is enticing. One example is the use of sodium chlorate instead of sodium chlorite. Attempts at small-scale chlorate-based generation have combined concentrated acid such as hydrochloric acid (HCl) with sodium chlorate ($NaCLO_3$).

The reaction between sodium chlorate and a strong acid is known to occur very slowly and inefficiently at ambient temperatures and is therefore unacceptable for commercial purposes [22]:

$$2\,NaClO_3 + 4\,HCl \rightarrow 2\,ClO_2 + Cl_2 + 2\,NaCl + 2\,H_2O \qquad (3.50)$$

and

$$2\,NaClO_3 + 6\,HCl \rightarrow 3\,Cl_2 + 2\,NaCl + 3\,H_2O \qquad (3.51)$$

Chlorine dioxide is formed by reaction (3.50), but not formed by reaction (3.51), which competes with reaction (3.50).

Common methods to elevate the reaction rate and improve efficiency include contacting the reactants at an elevated temperature or the use of excess acid. At elevated

temperatures, chorine dioxide in solution degasses and poses a serious safety risk. Generally, between 10 and 15 % is considered the maximum concentration desirable when handling gaseous chlorine dioxide. When excess acid is used, the acid sets up a competing reaction that produces chlorine. A catalyst can also be used to elevate the reaction rate and improve efficiency. Platinum in combination with other platinum group metal, such as ruthenium, rhodium, palladium, osmium, and iridium, can be effective as a catalyst for the generation of chlorine dioxide from sodium chlorate and a strong acid [23-29].

An electrochemical acidification cell can be used to provide the strong acid and a catalyst functioning to elevate the rate of reaction could alleviate the impact of low reaction rates and inefficiencies associated with the generation of chlorine dioxide from sodium chlorate and a mineral acid.

3.8.2 Fixed-Bed Catalytic Reactor Model

The mathematical model developed in this Chapter describes a general model of a fixed-bed catalytic reactor based upon classical kinetic and catalytic theories. The validity of the model was successfully tested in the few cases studied.

In the laboratory, it is difficult to achieve the same fluid dynamic behaviour in the reactor as in a commercial scaled reactor. There are two factors that cause this to be true. Firstly, reactor diameter has to be large enough to reduce flow channelling along the reactor walls. Secondly, high linear flow velocity through single-pass reactors require a significantly amount of feed and associated output of product, resulting in large storage vessels. Such feed and product quantities can pose a safety hazard in the laboratory. It is difficult to reduce the feed reservoir volume, because of the need to maintain a constant feed quality to allow for comparison of one catalyst or process condition to another. The product receiver vessel is not such a problem since it can be periodically emptied. In summary, the fluid dynamics of a laboratory fixed-bed catalytic reactor most likely will not be the same as in a commercial reactor. This mismatch must be recognised and an appropriate correlation must be developed.

References

1 Worstell, J. H. (2000), 'Succeed at Reactor Scale-Up', *Chem. Engr. Prog.*, 55.

2 Taylor, H. S. (1925), *Proc. Roy. Soc.* (London), **A108**, 105.

3 Balandin, A. A. (1958), *Advances in Catalysis*, Academic Press, New York, NY. 96.

4 Beeck, O. (1950), *Disc. Faraday Soc.*, **8**, 118.

5 Boudart, M. (1950), 'Pauling's Theory of Metals in Catalysis', *J. Am. Chem. Soc.*, **72**, 1040.

6 Dowden, D. A. (1948), *Research*, **1**, 239.

7 Dowden, D. A., P.W. Reynolds (1950), *Disc. Faraday Soc*, **8**, 187.

8 P.H. Emmett (ed.) (1954), *Catalysis*, Van Nostrand Reinhold Company, New York, NY.

9 Advances in Catalysis (1949), Academic Press Inc., New York, NY.

10 Balandin, A. A. (1968), *Scientific Selection of Catalyst*, A. Aledjem, Davy Publishing Company, Hartford, CT.

11 Sinfelt, J. H. (1973), *American Institute of Chemical Engineers*, **19**, 673.

12 Berkman, S., J. C. Morrell, and G. Egloff (1940), *Catalysis*, Van Nostrand Reinhold Company, New York, NY.

13 Innes, W. B., in P. H. Emmett (ed.) (1954), *Catalysis*, Van Nostrand Reinhold Company, New York, NY, **1**, Chpt. 7.

14 Worstell, J. H, M. L. Doll, and J. H. Worstell (2000), 'What's Causing Your Catalyst to Decay?', *Chem. Engr. Prog.*, 59.

15 Nicolis, G. and I. Prigogine (1977), *Self-Organisation in Non-Equilibrium Systems*, John Wiley & Sons, New York, NY.

16 Douglas, J. M., Process Dynamics and Control (1972), *Analysis of Dynamic Systems*, Prentice Hall, Upper Saddle River, NJ, **1**.

17 Froment, G. F. and Bischoff, K. B. (1979), *Chemical Reactor Analysis and Design*, John Wiley & Sons, New York, NY.

18 Cussler, E. L. (1997), *Diffusion: Mass Transfer in Fluid Systems* (2^{nd} ed), Cambridge University Press, 226.

19 Standards Methods for the Examination of Water and Wastewater, 1998, APHA, AWWA, and WEF, Washington (20^{th} Edition); Iodometric Method 4500-ClO_2.

20 Gordon, G., R. G. Kieffer, and D. H. Rosenblatt (1972), 'The Chemistry of Chlorine Dioxide', *Progress in Inorganic Chemistry*, **15**.

21 The Chlorite Manual (2001), Sterling Pulp Chemicals Ltd., Toronto, Ontario, Canada.

22 Isa, I., M. Shibuya, and M. Ebisawa, *Process For Manufacturing Chlorine Dioxide*, U.S. Patent 4,051,229, September 27, 1977.

23 Isa, I., M. Shibuya, and M. Ebisawa, *Manufacture Of Chlorine Dioxide By Reduction of a Specified Chlorate*, U.S. Patent 4,154,810, May 15, 1979.

24 Isa, I., M. Shibuya, and M. Ebisawa, *Manufacturing Chlorine Dioxide with Thallium and Silver or Palladium Catalysts*, U.S. Patent 4,169,134, September 25, 1979.

25 Isa, I., M. Shibuya, and M. Ebisawa, *Process For Manufacturing Chlorine Dioxide*, U.S. Patent 4,051,229, September 27, 1977.

26 Hardee, K., A. Gordon, C. Pyle, and R. K. Sen, *Preparation of Chlorine Dioxide with Platinum Group Metal Oxide Catalysts*, U.S. Patent 4,362,707, December 7, 1982.

27 Hardee, K., A. Gordon, C. Pyle, and R. K. Sen, *Method and Catalyst for Making Chlorine Dioxide*, U.S. Patent 4,381,290, April 26, 1983.

28 Hardee, K., A. Gordon, C. Pyle, and R. K. Sen, *Catalyst for Making Chlorine Dioxide*, U.S. Patent 4,501,824, February 26, 1985.

29 Hardee, K., A. Gordon, C. Pyle, and R. K. Sen, *Method and Electrocatalyst for Making Chlorine Dioxide*, U.S. Patent 4,426,263, January 17, 1984.

CHAPTER 4

CONCLUSION

Specific conclusions for the electrochemical acidification cell and fixed-bed catalytic reactor were made at the end of Chapters 2 and 3, respectively. The project is summarised in this chapter along with a design strategy, an economical analysis, a strategy for selecting a different catalyst, and a final discussion.

4.1 Project Summary

This project focused on a unique chlorine dioxide generation process, comprising of an electrochemical acidification cell and a fixed-bed catalytic reactor. Chapter 1 discussed the uses, advantages, and generation of chlorine dioxide. Chlorine dioxide shows promise of good disinfection performance, without the disadvantage of forming large quantities of undesirable halogenated by-products.

Chapters 2 and 3 described an electrochemical acidification cell and fixed-bed catalytic reactor, respectively, and some of the main principles behind their operation. Experiments were conducted to determine the time required to reach steady state. For the electrochemical acidification cell, steady state was reached after three hours of operation when an adjustment was made to one of the operating variables. The rise to steady state in the fixed-bed catalytic reactor occurred within 15 minutes of operation. Samples were taken hourly and all experimental runs were stopped when three consecutive samples gave steady readings in performance.

Screening experiments were done to assure that the variables selected for the detailed study were of importance. Feed concentration, temperature, velocity, and applied current were selected for the electrochemical acidification cell, while particle size, temperature, velocity, and space-time were selected for the fixed-bed catalytic reactor.

Mathematical models of chemical processes are used in the design, operation, and optimisation of industrial reactors. A reliable mathematical model identifies the system and quantitatively describes the rates of the processes taking place within the boundaries of the system. A mathematical model for each process was also developed in Chapters 2 and 3, primarily on chemical engineering principles of reaction engineering and reactor hydrodynamics. The experimental methods and the methodology used to process the

data for parameter estimation were described. Fitting experimental data to the predicted behaviour verified the models and their accuracy. Under all of the conditions studied, the model predicted results that were within 15.0 % of actual experimental data for the electrochemical acidification cell and within 6.5 % for the fixed-bed catalytic reactor.

All of the analysis and mathematical modelling were performed with many assumptions and by ignoring some important factors. Although there were restrictions imposed by the assumptions made, they still provided a realistic model for both the electrochemical acidification cell and fixed-bed catalytic reactor. However, it may be still worth the effort to relax one or more of the assumptions if the objective is to develop a full-scale chlorine dioxide generation system utilising these processes. Any one or all of the assumptions made could be relaxed at the expense of additionally complicating the analysis.

4.2 Design Strategy

In summary, an integrated process is described whereby an electrochemical acidification cell is integrated with a fixed-bed catalytic reactor to achieve a more efficient method of generating chlorine dioxide and to avoid some of the limitations in the existing electrochemical methods of generation chlorine dioxide.

The mathematical model of the fixed-bed catalytic reactor can be used to design and to establish optimum operating conditions for chlorine dioxide production. Once determined, this information can be used as input variables in the mathematical model for the design of the electrochemical acidification cell. Also, variations in both processes can be examined and optimised to ensure the required throughput at a minimum expense per unit of production.

There are several variables that need to be considered before detailed design and optimisation can be initiated. These variables include; temperature, chlorine dioxide concentration, chlorine dioxide yield (purity), chlorine dioxide production rate, the dimensions of the electrochemical acidification cell, and the pressure drop through the fixed-bed catalytic reactor.

Almost invariably, the single most important parameter we wish to either solve or control is the reaction yield. There is a lot of confusion on what the guideline is for chlorine dioxide yield. The USEPA's proposed Disinfectant/ Disinfectant By-Product (D/DBP) set a performance criterion of 95 % conversion of chlorite ions to chlorine dioxide for chlorine

dioxide generators (USEPA, April 1999). The chorine dioxide regulations in the Code of Federal Regulations (21 CFR 173.300, April 2001) states that chlorine dioxide generator effluent contains at least 90 wt. % chlorine dioxide with respect to all chlorine species. In any case, this means that unreacted precursor chemicals are minimised in the chlorine dioxide effluent. This sets a high standard for the chlorine dioxide purity or reaction yield. There are certain conditions that can decompose chlorine dioxide into chloride, chlorite and chlorate. Such conditions include photodecomposition by U.V. light and hydrolysis with increasing pH. Therefore, a reaction yield as close to 100 % is essential.

The chlorine dioxide dosage rate in grams per hour is usually a given condition or a requirement for a specific application. It is based on the treatment objectives, which dependents on the demand of the source water and the residual required to fulfil the treatment objective (see Appendix A). Dosage rates can range from 5 to over 500 g hr^{-1}.

With the chlorine dioxide dosage rate known, the flow rate is determined by the concentration of chlorine dioxide produced. The maximum concentration of chlorine dioxide typically produced in commercial generators is approximately 4,000 ppm. This is to minimise the concentration of chlorine dioxide gas in equilibrium with the solution. At aqueous chlorine dioxide concentrations of greater than 4,000 ppm, there is a risk of chlorine dioxide exceeding its solubility limit and creating a vapour phase that is dangerous. Gas phase chlorine dioxide concentration in excess of 10 vol. % at 40 °C can decompose explosively into chlorine (Cl_2), oxygen (O_2), and heat, liberating approximately 104.6 kJ $mole^{-1}$ [1-6]:

$$ClO_2 \rightarrow 0.5\,Cl_2 + O_2 \tag{4.1}$$

At 40 °C and 101.32 kPa, the Henry's law constant for chlorine dioxide is 2.24 x 10^{-3} kPa ppm^{-1} (see Appendix B). From the following equation:

$$x_{ClO_2} = \frac{P_{ClO_2}}{H_{ClO_2}} = \frac{y_{ClO_2} P}{H_{ClO_2}} \tag{4.2}$$

where x is the ClO_2 concentration in the liquid phase, y the chlorine dioxide concentration in the vapour phase, P the total pressure, and H_{ClO2} the Henry's law constant for chlorine dioxide in water. At the conditions described above, the chlorine dioxide concentration in the liquid equals 4,500 ppm. This justifies the value of the maximum concentration.

Once the flow rate is determined, the electrochemical cell and fixed-bed reactor dimensions can be determined. Most industrial membrane cells are constructed on the plate-and-frame principle. The membranes are typically 300 to 2,500 cm^2 in area, very thin to minimise their resistance, between 0.1 to 0.6 mm thick, and are either homogenous or heterogeneous. Inert plastic screen, typically polyethylene, placed in each space between the membranes support them. The screen also serves to maintain the membranes at a fixed distance apart to guide the electrolyte flow and to act as turbulent promoters. Increasing turbulence promotes mixing of the water, use of the membrane area, and the transfer of ions. The spacing between the membrane or compartment thickness is typically set to some minimum practical value that will permit ease of assembly, while still affording a low electrical resistance compartment. High compartment resistance is not desirable, especially when high currents are required. Large values of $I^2 R$ will result in wasted power, a need for a high voltage output power supply, and undesirable heat evolution. In practice, compartment thicknesses are in the range of 0.2 to 1.0 cm. Flow velocities range from 18 to 35 cm s^{-1}, and the maximum pressure for membrane cells is generally limited to 345 kPa.

With some minor modifications, cation exchange resin can be used in place of the plastic screen. There are a number of cells available from various manufacturers and distributors whose dimensions are optimised for a given mode of operation. ElectroCell AB (Täby, Sweden) offers a variety of plate-and-frame cell designs; Electro MP cell, ElectroSyn cell, Micro-Flow cell, and ElectroProd cell. Any one of these cells can be used as the electrochemical acidification cell.

Once the area of the electrode is known, a current density must be selected. The anode life can be somewhat controlled by varying the metal oxide loading. Unfortunately, the anode manufacturers do not quantify the metal oxide loading, but rather label them generally as light, medium, and heavy loadings. With most DSA® anodes employed in electrochemical cells, the current density usually are below 10 mA cm^{-2}, since above this value the life of the anode will diminish rapidly. The life expectancies of DSA® EC-600 in light, medium and heavy loadings are typically on the order of 1,000, 3,000, and greater than 100,000 days, respectively, at a current density of 100 A m^{-2}. However, loss of life is possible under certain operating conditions. Approximately 50 % loss of life is expected at temperatures between 60 to 80 °C at pH units of less than 2. No loss of life is predicted at temperatures between 5 to 90 °C at pH units between 2 to 12.

Fixed-bed reactors are also commonly designed on a basis of a pressure drop per unit length of packing. In most reactors filled with catalyst, the design value for pressure drop is usually is in the range of 2.3 to 22.6 kPa per meter of bed depth.

The temperature of the feed water is known, or is determined by outside conditions over which we have little control. The temperature of water sources around the world differs enormously, and to a lesser degree, those from a single source differ from season to season. The temperature range is generally between 5 and 35 °C. Since temperature affects the kinetics of a reaction, *e.g.* the lower the inlet temperature, the lower the maximum attainable reaction yield will be, it is best to design a system at the lowest temperature expected at the location of operation.

Lastly, due to the corrosive nature of chlorine dioxide, the operation of any chlorine dioxide generator will be limited by the ability of the components to perform as required. All components in contact with chlorine dioxide should be comprised of halogenated polymers because of their resistance to hydrolysis and oxidation. Such halogenated polymers include polytetrafluoroethylene (PTFE), fluorinated ethylene propylene copolymer (FEP), perfluoropropylalkoxy copolymer (PFA), and perfluopromethylalkoxy copolymer (MFA). Also, chorine dioxide is sensitive to light and readily decomposes upon exposure to ultraviolet light [7]. Therefore, chemically compatible materials that protect chlorine dioxide from ultraviolet light are recommended. The necessity for additional research and development is required to find the proper materials so that the greatest reaction yield and product purity with the least amount of maintenance can be achieved.

4.3 Economical Analysis

Costs of a system are essentially proportional to the quantity of chlorine dioxide generated per unit time. Cost figures for the various chlorine dioxide generators commercially available are difficult to estimate. There are costs associated with the usage of water, chemical, and electricity, capital charges, required ancillary equipment, required service/maintenance, and pumping.

For water treatment, commercial chlorine dioxide generators can be broadly classified as chlorite-based, chlorate-based, or electrochemical systems. The differences between each generation method are governed to a large extent by the generation chemistry, *i.e.* the kinetics and thermodynamics of the reaction. Most large-scale generators use

sodium chlorate, while most small-scale generators use sodium chlorite. Although sodium chlorate is considerably less expensive than sodium chlorite, it is much more difficult and expensive to convert to chlorine dioxide. The economic breakpoint between chlorite and chlorate is on the order of 4,000 kg h^{-1} of chlorine dioxide. Electrochemical systems are mostly used for small-scale generation and are capable of producing up to 1,000 g h^{-1} of chlorine dioxide.

Typically, generators output can be maximised under optimised conditions to produce 95 % yields based on the conversion of the starting material. Also, chemical-based generators are competitively priced such that it can be assumed that capital charges, required ancillary equipment, required service/maintenance, and pumping costs are similar. Electrochemical systems have the advantage of using only one precursor. However, due to the nature of all electrochemical systems, softened water is always required. This may increase the capital charge as well as the service/maintenance costs when compared to chemical-based systems since a water softener system is needed to pretreat the feed water.

An operating cost analysis will be performed on the described process. The electrochemical acidification cell results from experiments 3 and 4 in Table 2.12 and the fixed-bed catalytic reactor results from experiment 22b in Table 3.16 will be used for the analysis. The flow rate through the cell and reactor was 3.85 cm^3 s^{-1} at 25 °C. The sodium chloride conductivity to the cell was approximately 3,000 µS cm^{-1} at 25 °C. A controlled current of 8.0 A (521 A m^{-2}) was applied between the electrodes, yielding a current efficiency of approximately 62.2 %. The sodium chlorite concentration to the reactor was approximately 1,000 ppm, with a [HCl]:[$NaClO_2$] molar ratio of 1.0. The chlorine dioxide concentration exiting the reactor was 581 ppm, at a yield of 97.6 %. The cost for the production of one kilogram of chlorine dioxide will be the basis:

1. Sodium Chloride (NaCl)
    - NaCl Required: 1.67 kg (28.6 moles)
    - Cost per Weight: £0.53 per kg
    - NaCl Cost: (1.67 kg)(£0.53) = £0.88
2. Sodium Chlorite ($NaClO_2$)
    - $NaClO_2$ Required: 1.72 kg (19.0 moles)
    - Cost per Weight: £1.76 per kg
    - $NaClO_2$ Cost: (1.72 kg)(£1.76 kg^{-1}) = £3.03
3. Soft Water
    - Soft Water Required: 1.71 m^3

- Cost per Volume: £0.77 per m^3
- Water Cost: (0.77 m3)(£1.71 m^{-3}) = £1.32

4. Electricity
    - Electricity Required: 6.4 kW h
    - Utility Cost: £0.13 per kW h
    - Electricity Cost: (16.4 kW h)(£0.13 kW^{-1} h^{-1}) = £2.13

The total operating cost is approximately £7.36 per one kilogram of chlorine dioxide. This cost estimate excludes capital charges, required ancillary equipment, required service/maintenance, and pumping costs.

This operating cost estimate will be compared to a commercial acid:chlorite system. Generators employing acid:chlorite solutions processes are available from ProMinent Fluid Controls (Pittsburgh, PA). ProMinent's Bello Zon CDVa series generators run with a capacity of 35 to 2,000 g h^{-1} of chlorine dioxide. For this particular system, a dilute 7.5 % sodium chlorite ($NaClO_2$) solution and 9 % hydrochloric acid (HCl) solution in a 1:1 ratio are metered via dosing pumps into a reactor where they combine to form a 2 % (20,000 ppm) solution of chlorine dioxide. The chlorine dioxide concentrate from the reactor is immediately diluted and injected into water for the end use concentration. For optimum efficiency, the following conditions are necessary;

- Upper limit concentration in the system of 2 % (20,000 ppm)
- Excess of HCL of greater than 350 %
- Reaction time of greater than 10 minute at 20 °C

Research has shown HCl-activation of $NaClO_2$ to have a yield of 97 %, only which approximately 75 to 78 % of the chlorite ions are converted to chlorine dioxide. Prominent claims that chlorine dioxide is generated at a high purity level due the excess of HCl above the stoichiometric requirements according to equation (1.8).

ProMinent's Bello Zon CDVa 35 Generator

1. Hydrochloric Acid (HCl)
    - HCl Required: 2.06 kg (56.5 moles)
    - Cost per Weight: £0.74 per kg
    - HCl Cost: (2.06 kg)(£0.74 kg^{-1}) = £1.52
2. Sodium Chlorite ($NaClO_2$)
    - $NaClO_2$ Required: 1.72 kg (19.0 moles)
    - Cost per Weight: £1.76 per kg
    - $NaClO_2$ Cost: (1.72 kg)(£1.76 kg^{-1}) = £3.03

The total cost is approximately £4.55 per one kilogram of chlorine dioxide. Again, this cost estimate excludes capital charges, required ancillary equipment, required service/maintenance, and pumping costs.

It is difficult is make a fair economical comparison between the described process and a commercial acid:chlorite system due to the concentration at which they generate chlorine dioxide. The analysis favoured the acid:chlorite system, showing an operating cost difference of £2.75 per one kilogram of chlorine dioxide. However, before making a decision based on price, there are two important factors that must be considered. These factors are based on safety.

The first area of concern is the concentration at which the chlorine dioxide is generated in the acid:chlorite system. As previously discussed, the maximum chlorine dioxide concentration produced in a generator should not exceed 4,000 ppm. This is to minimise the chlorine dioxide gas in equilibrium with the solution. Gas phase chlorine dioxide concentrations in excess of 10 % can decompose explosively.

The second area of concern is associated with the safety and handling of a mineral acid, such as hydrochloric acid and sulphuric acid, in the acid:chlorite system. Both processes utilise a sodium chlorite solution. Sodium chlorite solutions are sold in a stabilised form, containing up to 5.0 % sodium hydroxide (NaOH) and sodium carbonate (Na_2CO_3). The safety and handling concerns are minimal unless allowed to evaporate to dryness. However, the use of a mineral acid in a workspace requires special attention. All mineral acids are highly corrosive and control measures must be implemented to prevent or minimise exposure to the worker. The vapours of mineral acids are highly pungent and corrosive and can further complication the risk assessment. All control measures recommended must be implemented in the risk assessment procedure; to prevent the exposure entirely or to further reduce it as far as practicability.

4.4 Catalyst Selection

The catalyst industry is a large business. In 1996, total sales in the United States were above $1 billion [8]. Furthermore, approximately one-third of the (material) gross national product (GNP) of the United States involves a catalytic process somewhere along its production chain [9]. However; catalysts are often expensive and product quality strongly depends on their performance, thus, they must be used properly. Also, the design of

catalytic equipment (e.g., reactors) is critical. For the process described, a platinum catalyst was used for the generation of chlorine dioxide. One platinum formulation was evaluated on two different size support materials.

For most chemical processes, there are several catalyst choices. There is a large range of uses for platinum metal. Today's catalytic converters and tomorrow's fuel cells are just two of the many applications that use a catalyst comprising of platinum.

Platinum catalysts and their specifications can be found on the Internet from various manufacturers. Once a type is selected, technical magazines and journals can be used to learn about their performance from an independent source. If data on a specific formulation is not available, often reports on catalysts with similar compositions can be found. The objective is to locate reports that discuss critical factors, such as durability, selectivity, resistance to poisons, temperature range, etc.

There has been several catalyst formulations developed for increasing the conversion of chlorine dioxide, comprising of oxides of at least one platinum group metal, found in Group VIII of the Periodic Table of Elements, with at least one electrically conductive valve metal oxide, such as niobium, zirconium, titanium, tantalum, aluminium, or tungsten. The majority of the formulations were developed for reducing chlorate ions in a strong acid environment [10-16], while other formulations were developed for oxidizing chlorite ions in the presence of chlorine [17-19] or for chemically reducing chloric acid [20].

After selecting promising candidates, experiments can be conducted to compare activity, selectivity and durability, using actual operating conditions when possible. As previously mentioned, space-time is an important variable but often, it may be difficult to reproduce the space-times observed in full-size reactors in a laboratory. Activity and selectivity can be compared through experimentation or by a kinetic model. Experimental data can be fitted to a kinetic model and the model parameter can be compared.

Varying space-time at a constant temperature to obtain a given degree of conversion over the catalyst can compare activity between different catalysts. Keeping all variables constant, including the degree of conversion, can compare selectivity between different catalysts. Because the deactivation mechanism is rarely known, experiments should be conducted at process conditions, and should be run as long as it takes to obtain the desired information. Accelerating deactivation by raising the temperature or changing the

feed composition should only be conducted if the deactivation mechanism is known and understood.

Due to the difficulties in keeping conversion constant, it is often not possible to directly compare the performance of different catalyst sample from the experimental results. A simple mathematical model can therefore be used to fit the experimental data. The objective is to use the model as a method to compare different catalyst types rather than to understand the governing mechanisms. The model can also be used to extrapolate the results beyond the range of variables investigated. With the chemical reactor and reaction kinetics being the two components of a model, first-order kinetics and an ideal reactor model (plug flow) may be all that is needed for this purpose.

If the intent is to use a mathematical model to interpret experimental results, experiments to obtain conversion versus time at process conditions at several temperatures and space-times should be conducted. Conversion curves will provide values for the activation energy and frequency factor. If different catalyst presents the same activation energy, then the rate-limiting step is the same for all catalyst, indicating that each catalyst is promoting the same reaction step. If the activation energies are not different, then each catalyst is promoting a different reaction path, possibly leading to different by-products. In this case, compare the selectivity between each catalyst.

Once completing the comparative analysis in the laboratory, an analysis of only the promising candidates should be continued on a larger scale. The flow pattern in a larger scale reactor may be different than that of a laboratory reactor. However, reaction mechanisms do not change with reactor geometry or flow patterns, but counterintuitive phenomena may occur [21]. Also, mechanical properties can become apparent in the larger-scale experiments, such as catalyst particles may abrade and/or crush.

The final catalysts selection should be made on the basis of process economics. Remember, catalyst performance (activity, selectivity, durability, etc.) has far more impact on overall process economics than does the cost of the catalyst.

4.5 Final Discussion

Because of its chemistry and physical properties, chlorine dioxide is probably the most powerful and environmentally safe biocide in use today. Chlorine dioxide kills spores, viruses, fungi, and algae within the first minutes of contact over a wide pH range. Its

selective reactivity makes chlorine dioxide useful in many applications for which chlorine and other biocides are unsuitable. Its efficacy has been well documented in the laboratory, in pilot-studies, and in full-scale studies using potable and wastewater [22]. Used extensively in the Pulp and Paper Industry, new applications for chlorine dioxide in other areas, such as drinking, process, industrial, and waste water, are increasingly being investigated.

Because of its instability, chlorine dioxide cannot be transported and must be generated on site at the point of use and dissolved in water. However, despite the care and safety considerations that must be taken when using chlorine dioxide, the potential advantages of using this chemical greatly outweigh the possible disadvantage of on site production. When produced and handled properly, chlorine dioxide is an extremely effective and powerful biocide, superior to all other biocides on a mass dosage basis.

Like chlorine and ozone, chlorine dioxide is an oxidising biocide that kills microorganisms by disruption of nutrients across the cell wall. When compared to chlorine and ozone, it is very selective and will not react with most organic compounds, requiring smaller doses to maintain a residual sufficient to kill microorganisms. In addition, chlorine dioxide does not form chlorinated organic compounds, such as THM's. Chlorinated organic compound formation is becoming increasingly important. Environmental concerns about chlorinated organic compounds are resulting in increasingly stringent regulations, causing the EPA to set a Maximum Concentration Level (MCL) of 0.10 ppm for total trihalomethanes (TTHMs).

Chlorine dioxide remains as a true gas in solution allowing it to be more reactive and gives it the ability to reach all points in a system. Because it is a true gas and very soluble, it can penetrate biofilm where it oxidises the polysaccharide matrix that holds the biofilm together.

Finally, chlorine dioxide and its primary by-products chlorite and chlorate ions all break down to chloride ions. This, together with non-formation of toxic or carcinogenic chlorination by-products and no build-up of toxic organic or inorganic by-products gives it the least environmental impact of any biocide in use today. These properties makes chlorine dioxide unique among all other biocides.

With regard to primary disinfection in potable water treatment, mostly all chlorine dioxide generation methods employ sodium chlorite as the precursor chemical. The conversion

of sodium chlorite to chlorine dioxide is achieved via an oxidation reaction involving either chemical or electrochemical means of generation. In the chemical-based systems, the chemistry of reacting chlorine or a mineral acid with chlorite ions implies that a number of factors must be controlled to achieve high conversion rates. Because an excess of chemical is always required, chlorine or a mineral acid will pass into the water stream. The presence of chlorine can lead to high chlorate levels whereas the presence of mineral acid can contribute to increased metal corrosion and higher levels of total dissolved solids (TDS). Also, both chlorine and mineral acids are highly corrosive and control measures must be implemented to prevent or minimise exposure to the worker.

In contrast to the chemical-based systems, the electrochemical generators are typically single chemical units, which utilise electrical current for the generation of chlorine dioxide. The majority of the systems reply on the direct electrolysis of chlorite ions. To maintain high conversion efficiency, chlorine dioxide must be extracted from the anolyte. This creates two areas of concern. Firstly, there is a possibility of extracting acid or chlorine with the chlorine dioxide, and secondly, build-up of impurities on the electrode surface will prevent efficient long-term operation.

The other types of electrochemical-based systems rely on the generation of acid via the electrolysis of water. These systems use materials that are sensitive to oxidation, which will prevent efficient long-term operation. Also, they often require salt additives to increase conversion efficiency, thereby decreasing the purity of the chorine dioxide produced.

A unique process was developed that overcomes the described negative features in both the chemical-based and electrochemical systems. This process generates chlorine dioxide by passing feed water through an electrochemical acidification cell, blending the acidified effluent with a solution of sodium chlorite, and then passing it through a fixed-bed catalytic reactor.

The process was characterised through experimentation and was mathematically modelled. The results of the model were in good agreement with the experimental data. The model can now be useful for analysing, scaling up, designing, and optimising a chlorine dioxide reaction and reactor system. It can also be used to predict upset conditions. For example, feed water characteristic typically fluctuate over time. The changing of the seasons or changes within the operation of the plant can increase or decrease feed water temperature and flow rate.

In a pilot-plant system, concentrated sodium chlorite solution will mostly likely be fed by a metering pump to a static mixer wherein the sodium chlorite is mixed with the effluent of the electrochemical acidification cell to form a sodium chlorite feed stream, which is fed to the fixed-bed catalytic reactor. If the flow rate decreases, the space-time and concentration of sodium chlorite to the reactor will increase. Also, in the acidification cell, the heat removed by the solution is directly related to flow rate. If the flow rate decrease, the temperature of the solution will increase. All of these factors will affect the kinetics of the system. The model can therefore be used to determine the performance of the system under these conditions.

References

1. Chlorine Dioxide Generators, Technical Data Sheet, Vulcan Chemical, Birmington, AL.

2. Chemical & Engineering News (1951), Aug. 6, 3196.

3. Chemical & Engineering News (1951), Oct. 22, 4459.

4. Othmer, K., (1978) Encyclopedia of Chemical Technology, Wiley-Interscience, New York, NY.

5. Gerhartz, W. (1987), Ullman's Encyclopedia of Industrial Chemistry, VCH Publishing, New York, NY.

6. Bretherick, L., P. G. Urben, and M. J. Pitt (1999), Handbook of Reactive Chemical Hazards, Butterworth-Heinemann, Burlington, MA.

7. Cosson, H. and E. R. Ernst (1994), *Ind. Eng. Chem. Res.*, **33**, 1468.

8. Fogler, H. S. (1999), 'Elements of Chemical Reaction Engineering', 3rd ed., Prentice Hall, Upper Saddle River, NJ, 582.

9. Mortbidelli, M. (2001), 'Catalyst Design', Cambridge University Press, Cambridge, U.K.

10. Isa, I., M. Shibuya, and M. Ebisawa, *Process For Manufacturing Chlorine Dioxide*, U.S. Patent 4,051,229, September 27, 1977.

11. Isa, I., M. Shibuya, and M. Ebisawa, *Manufacture Of Chlorine Dioxide By Reduction Of a Specified Chlorate*, U.S. Patent 4,154,810, May 15, 1979.

12. Isa, I., M. Shibuya, and M. Ebisawa, *Manufacturing Chlorine Dioxide with Thallium and Silver or Palladium Catalysts*, U.S. Patent 4,169,134, September 25, 1979.

13. Hardee, K., A. Gordon, C. Pyle, and R. K. Sen, *Preparation of Chlorine Dioxide with Platinum Group Metal Oxide Catalysts*, U.S. Patent 4,362,707, December 7, 1982.

14. Hardee, K., A. Gordon, C. Pyle, and R. K. Sen, *Method and Catalyst for Making Chlorine Dioxide*, U.S. Patent 4,381,290, April 26, 1983.

15. Hardee, K., A. Gordon, C. Pyle, and R. K. Sen, *Catalyst for Making Chlorine Dioxide*, U.S. Patent 4,501,824, February 26, 1985.

16. Hardee, K., A. Gordon, C. Pyle, and R. K. Sen, *Method and Electrocatalyst for Making Chlorine Dioxide*, U.S. Patent 4,426,263, January 17, 1984.

17. Ringo, J. P., *Catalyst Enhanced Generation of Chlorine Dioxide*, U.S. Patent 5,008,096, April 16, 1991.

18. Peterson, T. H., J. V. Griepenburg, and K. F. Keating, *Catalyst System for Producing Chlorine Dioxide*, U.S. Patent 5,391,533, February 21, 1995.

19. Daly, F. P., J. Deuber, and D. Ostgard, *Catalyst for the Synthesis of Chlorine Dioxide*, U.S. Patent 5,435,984, July 25, 1995.

20. Kaczur, J. J., D. W. Cawlfield, S. K. Mendiratta, and K. E. Woodard, *Catalytic Process for Chlorine Dioxide Generation from Chloric Acid*, U.S. Patent 5,599,518, February 4, 1997.

21. Loffler, D. G. (2001), "Avoid Pitfalls in Evaluating Catalyst Performance", *Chem. Eng. Prog.*, **97** (7), 74.

22. Aieta, E. M. and J. D. Berg (1986), "A Review of Chlorine Dioxide in Drinking Water Treatment", *J. Amer. Water Works Ass*, **78**, 62.

APPENDICES

APPENDIX A

Chlorine Dioxide Treatment

Depending on the treatment objectives, two different treatments methods can be used; an intermittent and a continuous treatment method. Since both methods are based on establishing a chlorine dioxide residual, the oxidant-demand of the water must be known in order to determine a chlorine dioxide treatment dose. The following relationship shows the relationship between chlorine dioxide dose, oxidant-demand, and residual concentration:

$$\text{Chlorine Dioxide Dose} = \text{Oxidant-Demand} - \text{Residual Concentration} \qquad \text{(A.1)}$$

Oxidant-Demand

The chemical characteristics of water sources around the world differ tremendously, and to a lesser degree, those from a single source differ from season to season. The amount of chlorine dioxide required to achieve a desired objective clearly reflects these differences. Therefore, for effective disinfection control necessitates adjustment in chlorine dioxide feed not only to allow for the variations in water flow, but also to compensate for variations in water quality. In general, potable surface water will have an oxidant-demand of 0.1 to 2.0 ppm and potable ground water will be approximately 0.1 to 1.0 ppm. Most food flumes and industrial process waters will be between 5.0 and 20.0 ppm. Species that react with chlorine dioxide include inorganic reducing substances, certain organic species, and carbonaceous material.

Chlorine dioxide rapidly oxidises iron (II) to iron (III), manganese (II) to manganese (III), and sulphides to sulphates. It also oxidises a variety of sulphur compounds, such as thiamine, thiothiamine, and mercaptans. However, chlorine dioxide does not react with bromide and ammonia. Chlorine dioxide rapidly oxidises aliphatic tertiary amines and phenolic compounds while reacting somewhat slower with organic disulphites. The reaction with organic compounds is primarily an oxidative process. Since chlorine dioxide is not a chlorinating agent, the reaction with organics does not lead to the formation of organochlorinated products. These materials consume the chlorine dioxide supplied, and some of the reactions may occur before disinfection is accomplished.

Materials in water that influence the oxidant-demand complicate the use of chlorine dioxide for disinfection because sufficient chlorine dioxide must be applied not only to destroy organisms, but to compensate for the chlorine dioxide consumed by these reactions. Reactions with inorganic species are generally very rapid whereas reactions with organic materials are generally slow and their extent depends upon the concentration of chlorine dioxide present. A high concentration of these materials may require removal (pre-cleaning) prior to the addition of chlorine dioxide. This will avoid unnecessary demand as well as the associated extra cost.

Oxidant-demand is defined as the difference between the amount of chlorine dioxide applied to the water and the amount remaining at the end of a specified contact period. It expresses a definite equilibrium of chemical reactions of chlorine dioxide in water under known conditions. For achieving the desired equilibrium of chemical reactions, it is necessary to allow sufficient time and to provide an unreacted residual. For a particular water source, the chlorine dioxide demand will vary with the amount of chlorine dioxide applied, the time of contact, and the temperature. Determination of its magnitude must take all of these factors into consideration.

Residual Concentration

The residual concentration of chlorine dioxide required for a particular application is related to the objective of the treatment. It will vary from place-to-place and from time-to-time. Where disinfection is the objective, temperature, oxidant-demand, and organism vulnerability to chlorine dioxide are of primary concern. With long contact periods, a low concentration of chlorine dioxide will typically fulfil the objective of disinfection, whereas short contact times require higher chlorine dioxide concentrations to accomplish equivalent disinfection. The effectiveness of chlorine dioxide increases with temperature and is not influenced by pH. The ability of chlorine dioxide to remain as an undissociated gas in solution contributes to its oxidising power over a wide pH range.

It had been proven that chlorine dioxide is an efficient and fast biocidal agent over a large pH range. It can effectively kill pathogenic bacteria at parts-per-million (ppm) concentrations. Chlorine dioxide is also a very effective viruscidal agent. Therefore, the control of disinfection using chlorine dioxide is based on the attainment of a definite residual concentration. Typically, proper disinfection effect with chlorine dioxide can be accomplished with only a small residual concentration (0.1 to 1.0 ppm) above the oxidant-demand of the water.

Effective Mixing

As with all disinfection systems, mixing is a significant parameter. Applications exhibiting good levels of disinfection all have good mixing in common. Without mixing, disinfection is not possible even with a reasonable dosage of chlorine dioxide. Various strategies can be used to influence the mixing intensity. Such methods include the use of velocity gradients, electronic mixers, recirculation pumps, and corrugated baffles in the disinfection chamber.

Methods of Analysis for Low ClO_2 Levels

A number of methods have been used or proposed for the measurement of chlorine dioxide [1,2]. The analytical chemistry of a solution of chlorine dioxide is complicated by its volatility, its sensitivity to light and instability over time, and interferences from related redox species. Also, some of the techniques are labour-intensive, use expensive equipment, and require a high degree of technical skill. Different methods are required for low and high chlorine dioxide concentrations. Residual concentrations in treated waters are low, less than 10 ppm, while chlorine dioxide concentrations from generators are much higher, greater than 500 ppm.

Most of the methods rely on the oxidising power of chlorine dioxide and are based on reactions with reducing agents. The four methods currently employed for low ClO_2 concentration measurements are volumetric starch iodide (iodometric titration), modified colorimetric titration with orthotolidine, amperometric titration, and spectrophotometrically with the standard DPD (N,N-diethyl-*p*-phenylenediamine) method.

Iodometric titration method is questionable, even for the carefully controlled chlorine dioxide standards in research laboratories. For actual samples, which may contain a large number of interferences, the method is almost certain to produce erroneous results. Methods that determine concentrations by difference are potentially inaccurate and subject to large accumulative errors with respect to both accuracy and precision. The DPD method determines concentrations by difference.

Reliable methods for measuring chlorine dioxide include the amperometric method and an ultraviolet-based method [3]. Amperometric methods have excellent utility in laboratories with highly trained personnel. Amperometric titration is the standard

comparison for determining chlorine dioxide residual concentration in natural and treated waters. Most utilities us a continuous amperometric titrator to control the disinfection process by monitoring chlorine dioxide residuals.

Ultraviolet spectophotometry utilising continuous-flow automated methods has a great potential for accurate and precise measurements. Its advantages include ease of operation and high sample throughput [4]. Flow injection analysis and continuous flow methods exhibit superior selectivity.

APPENDIX B

Properties of Sodium Chlorite

Chlorine dioxide is generated when sodium chlorite is either chlorinated or acidified, or both, under appropriate pH and temperature. Sodium chlorite solutions are normally available at concentrations greater than 25 wt. %. This concentration achieves the lowest freezing point and therefore less susceptible to handling difficulties in cold weather. Chlorine dioxide produced in external generators typically use solutions of 25 wt. % sodium chlorite or less to charge the generator. Sodium chlorite solutions are available in 55 gallon (208 liter) drums, 275 gallon (1041 liter) non-returnable totes, and tank trucks.

Sodium chlorite is available in dry form or as a 31.25 % or 50 % solution. Chemical and physical properties are given in Tables B.1 and B.2 [5].

Table B.1 Properties of Dry Sodium Chlorite

Sodium Chlorite (min.) / %	80
Sodium Chloride / %	11 - 19
Water (max.) / %	6
Appearance	White Flakes
Bulk Density / kg m^{-3}	
Loose	860
Packed	1120

Table B.2 Properties of 31.25 % and 50 % Sodium Chlorite Solution

	31.25 % Solution	50 % Solution
Sodium Chlorite (min.) / %	25	38
Sodium Chloride (max.) / %	3	3.5
Water / %	70 - 75	55 - 61
Appearance	Clear, Pale, Yellow	Slightly Cloudy, Pale Yellow
Bulk Density at 35°C / kg m^{-3}	10.1	11.4
Crystallisation Point / °C	-7	25

The solubility of pure sodium chlorite ($NaClO_2$) as a function of temperature is shown in Table B.3 [6,7]. The solubility of $NaClO_2$ ranges from approximately 436 g L^{-1} at 5 °C to

approximately 810 g L^{-1} at 45 °C. Crystallisation of $NaClO_2$ from aqueous solutions yields $NaClO_2 \cdot 3H_2O$ below 37.4 °C and anhydrous $NaClO_2$ above 37.4 °C.

Table B.3 $NaClO_2$ Solubility in Water at Various Temperatures

Temperature / °C	$NaClO_2$ / wt. %	Density / g cm^{-3}	$NaClO_2$ / g L^{-1}
5	33.9	-	-
10	-	-	-
15	38.1	1.331	507.1
20	-	-	-
25	43.6	1.391	606.5
30	46.4	-	-
35	50.4	1.465	738.4
40	-	-	-
45	54.0	1.501	810.5

The density of pure sodium chlorite solutions as a function of concentration is shown in Table B.4 [8].

Table B.4 Density of Pure $NaClO_2$ Solution at 20 °C

Conc. / %	Conc. / g L^{-1}	Density / g cm^{-3}	Conc. / %	Conc. / g L^{-1}	Density / g cm^{-3}
1	10.06	1.006	21	245.9	1.171
2	20.26	1.013	22	259.6	1.180
3	30.60	1.020	23	273.5	1.189
4	41.12	1.028	24	287.8	1.199
5	51.80	1.036	25	302.3	1.209
6	62.58	1.043	26	316.9	1.219
7	73.57	1.051	27	331.8	1.229
8	84.72	1.059	28	246.9	1.239
9	96.03	1.067	29	362.2	1.249
10	107.5	1.075	30	377.7	1.259
12	130.9	1.091	32	409.9	1.281
13	143.0	1.100	33	426.0	1.291
14	155.1	1.108	34	442.7	1.302
16	180.0	1.125	36	477.0	1.325
18	205.7	1.143	38	511.9	1.347
20	232.2	1.161	40	548.4	1.371

Table B.5 shows the density of pure sodium chlorite solutions at various concentrations as a function of temperature [8].

Table B.5 Density of Pure $NaClO_2$ Solutions at Various Temperatures

Temperature / °C	Density / g cm^{-3}				
	7.5 wt. %	15 wt. %	25 wt. %	31 wt. %	37 wt. %
0	1.059	1.122	1.217	-	-
5	1.058	1.121	1.215	1.278	1.346
10	1.057	1.120	1.213	1.276	1.343
15	1.056	1.119	1.211	1.273	1.340
20	1.055	1.117	1.209	1.270	1.336
25	1.053	1.115	1.206	1.266	1.332
30	1.052	1.113	1.203	1.263	1.328
35	1.050	1.110	1.200	1.259	1.323
40	1.047	1.107	1.196	1.255	1.318

The viscosity of pure sodium chlorite solutions at various concentrations as a function of temperature is shown in Table B.6 [8].

Table B.6 Viscosity of Pure $NaClO_2$ Solutions at Various Temperatures

Temperature / °C	Viscosity (cP)				
	7.5 wt. %	15 wt. %	25 wt. %	31 wt. %	37 wt. %
0	2.033	2.414	3.518	4.696	6.387
5	1.747	2.079	3.043	4.144	5.648
10	1.516	1.808	2.656	3.692	5.039
15	1.327	1.585	2.337	3.319	4.533
20	1.171	1.401	2.072	3.008	4.109
25	1.040	1.247	1.851	2.747	3.752
30	0.931	1.118	1.664	2.562	3.449
35	0.839	1.008	1.474	2.338	3.189
40	0.760	0.915	1.341	2.177	2.965

The vapour pressure of pure sodium chlorite solutions at various concentrations as a function of temperature is shown in Table B.7 [8].

Table B.7 Vapour Pressure of Pure $NaClO_2$ Solutions at Various Temperatures

Temperature / °C	Vapour Pressure (mm Hg)				
	7.5 wt. %	15 wt. %	25 wt. %	31 wt. %	37 wt. %
0	4.432	4.286	4.055	3.895	3.716
5	6.335	6.125	5.795	5.567	5.310
10	8.923	8.627	8.163	7.841	7.480
15	12.398	11.988	11.343	10.895	10.394
20	17.007	16.443	15.559	14.945	14.257
25	23.047	22.283	21.085	20.252	19.320
30	30.875	29.852	28.246	27.131	25.882
35	40.916	39.560	37.433	35.954	34.300
40	53.669	51.891	49.100	47.161	44.991

Properties of Chlorine Dioxide

Some of the generally recognised physical properties of chlorine dioxide are found in Table B.8 [9-11]. Pure chlorine dioxide exists almost entirely as the permanent free-radical monomer. The chlorine-oxygen bonds show predominantly double-bound character, forming an angle of about 117.5° with a chlorine-oxygen bond of 1.47 Å and a dipole moment of 1.69 debye units.

Table B.8 Chlorine Dioxide Properties

Molecular Weight	67.45
Melting Point	-59 °C
Boiling Point	11 °C
Solubility Limit, 25 °C, 34.5 mm Hg	~ 3.0 g L^{-1}
$\Delta G°$ at 25 °C	2.95 kcal mol^{-1}
$\Delta H°$ at 25 °C	25 kcal mol^{-1}
$\Delta S°$ at 25 °C	43.9 eu (aq)
Partition Coefficient, 35 °C	21.5
Molar Absorptivity, 360 nm	1,225 to 1,250 cm^{-1} M^{-1}

Chlorine dioxide as a gas is very reactive and unstable. It can decompose violently at concentrations greater than 10 % volume in the air or at temperatures above 100 °C (210 °F) according to the following equation:

$$2\,ClO_2 \rightarrow Cl_2 + 2\,O_2 \qquad (B.1)$$

Gaseous chlorine dioxide is also light sensitive and will readily decompose upon exposure to ultraviolet light [12] to produce chlorine trioxide (ClO_3), which thermally decomposes to chlorine and water. Chlorine dioxide is highly soluble in water as a true gas. It is chemically stable at temperatures less than 40 °C and at concentrations less than 4.0 g L^{-1}. This is why chlorine dioxide is used almost exclusively in the form of an aqueous solution.

At 25 °C, chlorine dioxide is about 23 times as concentrated in the aqueous solution than in the gas phase in which it is at equilibrium or about 10 times more soluble in water than chlorine [13]. Henry's Constant as a function of temperature for solutions of chlorine dioxide in water is shown in Table B.9 [15-17]. The vapour pressure of chlorine dioxide in water at various concentrations as a function of temperature is shown in Table B.10 [8].

The stability of dissolved chlorine dioxide depends on the pH of the solution. It is relatively stable in weak acidic solution and rather less stable in neutral solution. At pH's greater than 8, chlorine dioxide hydrolyses rapidly to form chlorate (ClO_3^-) and chlorite ions (ClO_2^-) [18]:

$$2\,ClO_2 + 2\,OH^- \rightarrow ClO_2^- + ClO_3^- + H_2O \qquad (B.2)$$

The rate of hydrolysis increases with increasing pH. At pH's less than 2, chlorine dioxide decomposes to chloric acid ($HClO_2$) and hydrochloric acid (HCl):

$$6\,ClO_2 + 3\,H_2O \rightarrow 5\,HClO_2 + HCl \qquad (B.3)$$

ClO_2 in aqueous solution is light sensitive. Upon exposure to ultraviolet light, it decomposed through free radicals to give chlorate (ClO_3^-) and chloride (Cl^-) ions [12,14]:

$$10\,ClO_2 + 5\,H_2O + h\nu \rightarrow 6\,ClO_3^- + 4\,Cl^- + 10\,H^+ + 3.5\,O_2 \qquad (B.4)$$

In summary, the stability of chlorine dioxide is associated to its purity and concentration, and exposure to light and heat. Chlorine dioxide should be uses soon after its preparation, but may be stored for several weeks with negligible degradation by keeping the solution at low temperature and away from light.

Table B.9 Henry's Constant for Solutions of Chlorine Dioxide in Water

Temperature / °C	Henry's Constant / kPa ppm^{-1}
0	5.07×10^{-4}
5	6.54×10^{-4}
10	7.96×10^{-4}
15	9.61×10^{-4}
25	1.15×10^{-3}
30	1.61×10^{-3}
40	2.24×10^{-3}

Table B.10 Vapour Pressure of ClO_2 in Water at Various Temperatures

ClO_2, g L^{-1}	Vapour Pressure of Chlorine Dioxide in Water							
	5 °C	10 °C	15 °C	20 °C	25 °C	30 °C	35 °C	40 °C
1	4.938	6.087	7.449	9.052	10.93	13.11	15.64	18.56
2	9.876	12.17	14.90	18.10	21.86	26.23	31.29	37.11
3	14.81	18.26	22.35	27.16	32.79	39.34	46.93	55.67
4	19.75	24.35	29.79	36.21	43.72	52.46	62.57	74.22
6	29.63	36.52	44.69	54.31	65.58	78.69	93.86	111.3
8	39.51	48.70	59.59	72.42	87.44	104.9	125.1	148.4
10	49.38	60.87	74.49	90.52	109.3	131.1	156.4	185.6
12	59.26	73.04	89.38	108.6	131.2	157.4	187.7	222.7
14	69.14	85.22	104.3	126.7	153.0	183.6	219.0	259.8
16	79.01	97.39	119.2	144.8	174.9	209.8	250.3	296.9
18	88.89	109.6	134.1	162.9	196.7	236.1	281.6	334.0
20	98.76	121.7	149.0	181.0	218.6	262.3	312.9	371.1

In addition to the data presented above, other key properties of chlorine dioxide, such as vapour pressure, heat capacity, spectra, etc., can be found on the National Institute of Standards and Technology Chemistry WebBook (http://webbook.nist.gov/chemistry/). A phase diagram for the ClO_2-H_2O system can be found in U.S. Patent 2,683,651 (1954).

APPENDIX C

Spectrophotometer Calibration

Pure chlorine dioxide solution for use in calibrating the HACH model 2010 spectophotomer was generated according to the method described in Standards Methods [19], Section 411A (see Figure C.1). The concentrations of sulphuric acid and sodium chlorite were increase by 50 %, compared to the recommendations in Standard Methods, to obtain higher chlorine dioxide concentrations in the stock solution. The concentration obtained was 750 to 1,000 ppm as ClO_2. The chlorine dioxide solution was standardised immediately prior to calibration by the iodometric method described in Standards Methods [19], Section 411A.

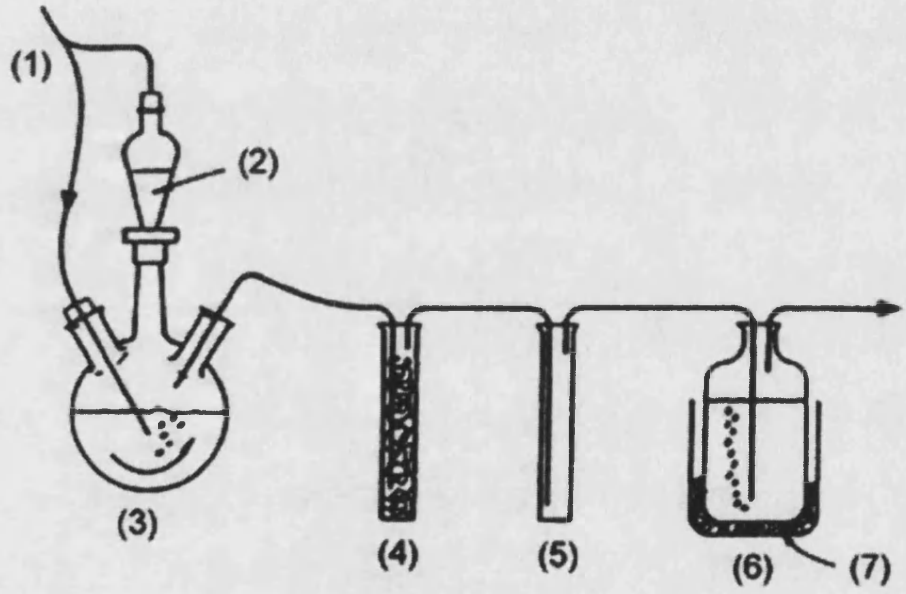

Figure C.1 Chlorine dioxide generator using acid activation of a sodium chlorite solution to prepare approximately 750 ppm ClO_2 stock solution; (1) Air Supply, (2) Sulphuric Acid, (3) Reaction Vessel, (4) Sodium Chlorite Salt Tower, (5) Dust Trap, (6) Chlorine Dioxide Stock Solution, and (7) Ice Bath.

Before the spectrophotometer was calibrated for chlorine dioxide readings, the U.V. lamp was replaced and the wavelength calibrated according to manufacturer's instruction for calibrating wavelength on 2010 series meters. Dilutions of the pure chlorine dioxide solution to yield concentrations in the range of 50 to 750 ppm range were prepared and

measured using the spectrophotometer. Actual concentrations of chlorine dioxide were plotted against measured spectrophotometer values to obtain a calibration equation (see Figure C.2). With the measured spectrophotometer value, the actual concentration of chlorine dioxide was calculated using the following calibration equation:

$$C_{ClO2}\big|_{Actual} = 1.23\, C_{ClO2}\big|_{Measured} - 23.13 \qquad \text{(C.1)}$$

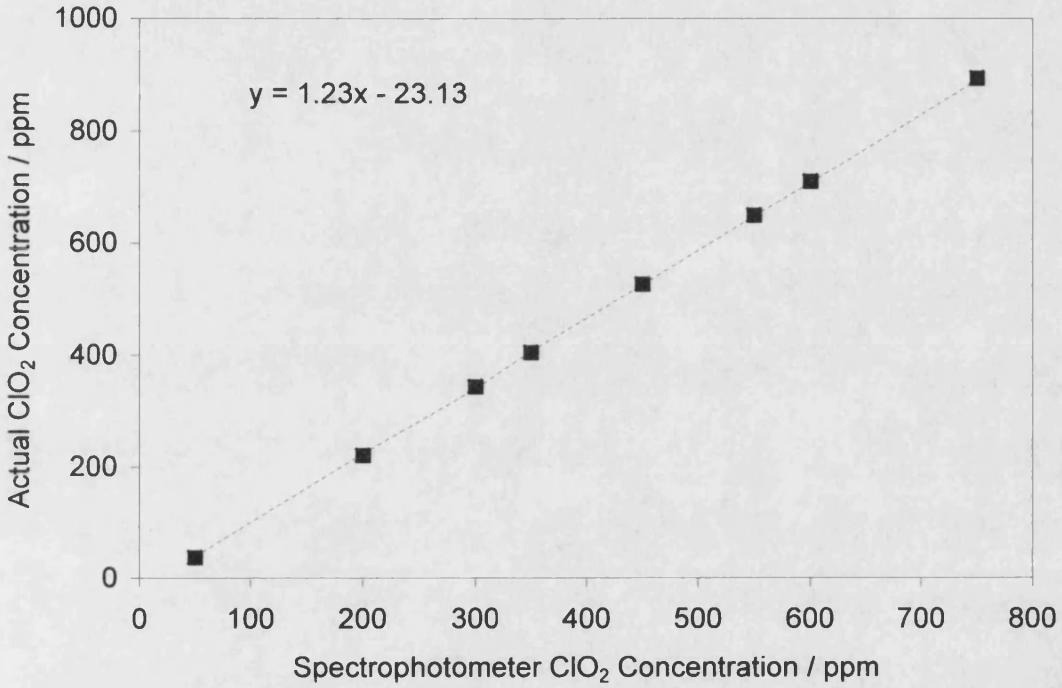

Figure C.2 Chlorine Dioxide Calibration Plot; actual chlorine dioxide concentrations versus measured spectrophotometer concentrations

APPENDIX D

The Use of Solver

In the Tools menu in Microsoft® Excel 2000, there is a tool called Solver. Solver can find an optimal value for a formula in one cell (target cell) on a worksheet. Solver works with a group of cells that are related, either directly or indirectly, to the formula in the target cell. Solver adjusts the values in the changing cells you specify (adjustable cells) to produce the result you specify from the target cell formula. Constraints can be applied to restrict the values Solver can use in the model, and the constraints can refer to other cells that affect the target cell formula.

For example, $\overline{\eta}_{in}$ in equation (2.62) was selected as the adjustable cell.

$$-a\ln(1-\overline{\eta}_A)-(a-1)\overline{\eta}_A = \frac{z_A F}{i} b C_A W \qquad (2.62)$$

Initially, a value was selected for $\overline{\eta}_{in}$ and the left-hand side of equation (2.62) was inputted in a cell [CELL 1]:

$$[\text{CELL 1}] = -a\ln(1-\overline{\eta}_A)-(a-1)\overline{\eta}_A \qquad (D.1)$$

The right-hand side of equation (2.62) was also inputted in another cell [CELL 2]:

$$[\text{CELL 2}] = \frac{z_A F}{i} b C_A W \qquad (D.2)$$

A target cell was specified by the difference in the right- and left-hand sides of equation (2.70):

$$[\text{TARGET CELL}] = [\text{CELL 1}] - [\text{CELL 2}]$$

Solver varied $\overline{\eta}_{in}$ until the target cell equalled zero, when [CELL 1] equalled [CELL 2], or when the left side of equation (2.62) equalled the right-hand side.

With $\overline{\eta}_{in}$ known, the same procedure was applied to equation (2.66), whereas $\overline{\eta}_{out}$ was the adjustable cell and the difference in the right- and left-hand sides of equation (2.66) was the target cell:

$$\frac{b}{v}Y = \ln\left(\frac{\overline{\eta}_{in}}{\overline{\eta}_{out}}\right) - a\ln\left(\frac{1-\overline{\eta}_{in}}{1-\overline{\eta}_{out}}\right) \tag{2.66}$$

The calculated current efficiency was determined by:

$$\eta_c = \frac{(\overline{\eta}_{in} + \overline{\eta}_{out})}{2} \tag{2.67}$$

APPENDIX E

General Water and Wastewater Treatment

Chlorine dioxide is uses as both an oxidant and a disinfectant in water and wastewater treatment. The required dosage will vary with process conditions and the degree of contamination present. For most municipal and other potable water systems, a chlorine dioxide residual concentration of up to 2.0 ppm is sufficient to provide adequate disinfection, whereas for most municipal and other wastewater systems, a chlorine dioxide residual concentration of up to 5.0 ppm is sufficient to provide adequate disinfection.

Chlorine dioxide has been and is currently being used for a variety of purposes in many applications. The specific applications that follow are taken from the Vulcan Chemical's Technical Data Sheets [20].

Aldehyde Destruction

Aldehydes are produced by a number of industrial processes. Their treatment is a common problem, particularly in the photographic industry. In general, chlorine dioxide can oxidise aldehydes to the corresponding carboxylic acid.

Chlorine dioxide can oxidise formaldehyde initially, to formic acid and then to carbon dioxide. Paraformaldehyde can be depolymerised and eliminated completely by oxidation with chlorine dioxide.

Pesticides Destruction

Some pesticides can be oxidise to less toxic materials by chlorine dioxide. Specifically, DMDT (methylchor) and aldrin react with chlorine dioxide. With parathion, the reaction is slow near neutral pH. However, when the pH id above 8, less biodegradable herbicides such as paraquat and diquat are eliminated within a few minutes.

Tallow Bleaching

Tallow, a fat by-product of the meat packing industry, is used by the cosmetic and soap industries. Light-coloured tallows are more useful and valuable than dark-coloured

tallows. Chlorine dioxide bleaches colour bodies present in the tallow, converting low-grade material to high-grade material.

Upgrading tallow is accomplished by *in-situ* generation of chlorine dioxide from sodium chlorite solution and sulphuric acid. After adding water and heating the tallow to 60 °F to melt the tallow, 0.1 % (by weight) of sodium chlorite is added. This is followed by 0.025% (by weight) of 66° Be sulfuric acid (H_2SO_4).

When the bleaching is complete, the mixture is neutralised with dilute caustic to prevent the re-formation of colour. This treatment can lower the colour from a *Fatty Acid Colour* of 13 or 11A to a *Fatty Acid Colour* of 7 or less.

Food Plant Process Water Treatment

Chlorine dioxide is effective for use in controlling microbiological growth in flume water and other food processing water systems, such as chill water systems and hydrocoolers. The required dosage will vary with process conditions and the degree of contamination present. Depending on the requirements of the specific water system, chlorine dioxide should be added to achieve a residual concentration between 0.3 to 5.0 ppm.

Flume water is used to transport fruits and vegetables during processing. Dirt and organic compounds leeched from the fruit and vegetables provide nutrients for microorganisms. As food processing plants recycle more water, organic loading and microbiological growth increases. To control microbiological growth in flume water, chlorine dioxide can be applied to potato flume water at a maximum concentration of 1.0 ppm. For other un-cut fruits and vegetables, such as tomatoes and citrus fruits, a maximum dosage of 5.0 ppm may be used. Chlorine dioxide is not registered for use on cut fruits and vegetables. Treatment of the fruits and vegetable with chlorine dioxide must be followed by a potable water rinse, or by blanching, cooking, or canning.

Algae and Bacterial Slime Control

Chlorine dioxide is effective for controlling the microbiological growth of bacterial slime and algae. The pyrolle ring of the chlorophyll is attacked by chlorine dioxide, cleaving the ring such that the chlorophyll becomes inactive. Since algae cannot function without chlorophyll metabolism, they are destroyed. The recommended dosage that can control bacterial slime and algae populations is between 0.1 and 5.0 ppm. Chlorine dioxide may

be applied either continuously or intermittent. The typical chlorine dioxide residual concentration range is 0.1 to 1.0 ppm for continuous doses, and 0.1 to 5.0 ppm for intermittent doses. The minimum acceptable residual concentration of chlorine dioxide is 0.1 ppm for a minimum one-minute contact time.

A one-shot dose of chlorine dioxide to the reservoir nightly is another effective treatment method. This prevents photodegradation of chlorine dioxide by sunlight during the day hours. The kill action is fast enough to be effective before sunrise. A dosage of 1.0 ppm can control bacterial slime and algae populations. This treatment should be repeated as often as necessary to maintain control.

Mollusk Control

Chlorine dioxide can be used for mollusk control in commercial and industrial recirculating and one-pass cooling water systems. The required dosages will vary with the system type, system conditions, the degree of water contamination present, and the desired level of control. Depending on the extent of the infestation, chlorine dioxide can be applied either continuously or intermittently to achieve the necessary residual concentration. The typical chlorine dioxide residual for continuous dose should be maintained at concentrations up to 2.0 ppm. For intermittent dose, chlorine dioxide should be added to obtain a chlorine dioxide residual concentration of 0.2 to 25.0 ppm. Repeat as necessary to maintain control. For the control of veliger, a larval mollusk in the stage when it has developed a velum, a continuous chlorine dioxide residual of 0.1 to 0.5 ppm should be maintained.

Poultry Chill Water Disinfection

Chlorine dioxide can be used as an antimicrobial agent in poultry chill water. The chlorine dioxide should be fed below the water level in the chill tank and the residual concentration should not exceed 3.0 ppm at the midway point in the chill tank. The purity of the chlorine dioxide must be at least 90 % by weight (21 CFR 173.69a).

Iron and Manganese Removal

The dissolved metals, iron and manganese, are objectionable in both drinking and process waters. If not removed, they can cause stains and deposits. Chlorine dioxide

can oxidise these metals to form compounds that are insoluble at pH unit's of greater than 7.

For dissolved manganese, 2.5 ppm of chlorine dioxide is required to oxidise 1.0 ppm of manganese (Mn^{2+}) to manganese dioxide (MnO_2):

$$2\ ClO_2 + 5\ Mn^{2+} + 6\ H_2O \rightarrow 5\ MnO_2 + 12\ H^+ + 2\ Cl^- \qquad \text{(E-1)}$$

For dissolved iron, 1.2 ppm of chlorine dioxide is required to oxidise 1.0 ppm of ferrous (Fe^{2+}) ion to ferric ion (Fe^{3+}), which is precipitated as iron hydroxide ($Fe(OH)_3$):

$$ClO_2 + 5\ Fe(HCO_2)_2^+ + 2\ H_2O \rightarrow 5\ Fe(OH)_3 + 10\ CO_2 + Cl^- + H^+ \qquad \text{(E-2)}$$

Chlorine dioxide can rapidly oxidise dissolved iron but is unable to oxidise dissolved iron that has been chelated by organic compounds.

Both MnO_2 and $Fe(OH)_3$ are insoluble in water and can be filtered out prior to exiting the treatment plant. In both cases, approximately 99 % of the MnO_2 and $Fe(OH)_3$ can be removed through a 0.45 micron filter after five minutes of contact time.

Amine and Mercaptans Odour Control

The major sources of odorous substances in many industries are associated with mercaptans and substituted amines. These compounds have a disagreeable odour and can cause nausea. They must therefore be removed from process water prior to discharge.

Mercaptans are the sulphur analogue of alcohols (RSH). Between pH's between 5 and 9, 4.5 ppm of chlorine dioxide can instantaneously oxidise 1.0 ppm of mercaptans (expressed as sulphur) to the respective sulphonic acid (RSO_3H)/sulphonate compound, destroying the mercaptan odour. Similarly, chlorine dioxide reacts with organic sulphides and disulphides. These organic disulfides (RSSR) are intermediate oxidation products of mercaptans, which can revert back to mercaptans. Both compounds have a disagreeable odour. Chlorine dioxide can split organic disulfides at the sulphur atoms and oxidise them to sulphonic acid, destroying the odour.

Amines are the organic analogue of ammonia (NH_3). Replacing a hydrogen (H) ion with an alkyl group (R) forms a primary amine (RNH_2); replacing two hydrogen ions forms a secondary amine (R_2NH); replacing three hydrogen ions forms a tertiary amine (R_3N). Substituting alkyl groups for hydrogen atoms increases the objectionable odour of the amine.

The reactivity of chlorine dioxide towards amines increases with the degree (amount) of substitution and pH of the reaction mixture. Chlorine dioxide does not react with ammonia and primary amines. At pH's above 7, an average of 5.0 ppm of chlorine dioxide oxidises 1 ppm of secondary aliphatic amine (expressed ad nitrogen), removing all tracing of amine odour. The higher the pH of the reaction mixture (chlorine dioxide and secondary and/or tertiary aliphatic amines), the more rapidly oxidation proceeds. At pH's between 5 and 9, an average of 10.0 ppm of chlorine dioxide oxidises 1.0 ppm of tertiary aliphatic amine (expressed ad nitrogen), removing all tracing of amine odour.

Cyanide Destruction

Cyanides (CN^-) are used to solubilise metal ions in basic solution. Consequently, they are found in wastewater from metal plating and mining industries. They are very toxic and must be removed from wastewater prior to discharge.

There are two forms of cyanide: oxidisable and non-oxidisable cyanides. Oxidisable cyanides consist of free cyanide and labile metal-cyanide complexes. Chlorine dioxide can oxidise simple cyanide to a less toxic substance cyanante and/or carbon dioxide and nitrogen. The end product depends on reaction conditions. At pH's less than 10, 2.5 ppm of chlorine dioxide can oxidises 1.0 ppm of cyanide ion to cyanate (CNO^-).

$$\text{pH} < 9: \qquad CN^- \rightarrow OCN^- \qquad \text{(E-3)}$$

At pH's greater than 10, 5.5 ppm of chlorine dioxide oxidise 1.0 ppm of cyanide ion to carbon dioxide (CO_2) and nitrogen (N_2).

$$\text{pH} > 10: \qquad 2\,CN^- \rightarrow 2\,CO_2 + N_2 \qquad \text{(E-4)}$$

Chlorine dioxide also oxidises thiocycyanate to sulphate and cyanate. In neutral solutions, an average of 3.5 ppm of chlorine dioxide can oxidise 1.0 ppm of thiocycyanate ion (SCN^-) to sulphate (SO_4^{2-}) and cyanate.

$$pH = 7: \qquad SCN^- \rightarrow SCN^- + SO_4^{2-} \qquad \text{(E-5)}$$

Non-oxidisable cyanides consists of non-labile metal-cyanides complexes, typically iron-cyanide complexes ($Fe[CN]_6^{-2}$ or $Fe[CN]_6^{-3}$). These cannot be treated with chlorine dioxide or with other oxidants.

Phenol Destruction

Phenols (C_6H_5OH) are produced by many industries including the chemical, plastics, coke, steel and petroleum industries. Chlorine dioxide can effectively destroys phenols in waste or drinking water without forming objectionable by-products. At pH's less than 10, 1.5 ppm of chlorine dioxide rapidly can oxidises 1 ppm of phenol to benzoquinone. At pH's above 10, 3.3 ppm of chlorine dioxide can slowly oxidise phenols to a mixture thought to be low molecular weight, nonaromatic, carboxylic acids, such as oxalic and maleic acids. At pH of 7, the phenol reaction is rapid and complete; all phenols are consumed.

Sulphide Odour Control

Sulphides (S^{2-}) are produced by both biological and chemical action. Anaerobic bacteria in many applications produce sulphides biologically. In addition to their disagreeable "rotten egg" odour, sulphides are corrosive and extremely toxic. Consequently, they must be removed from waste streams prior to discharge.

Chlorine dioxide is used for two purposes; to destroy sulphides without forming colloidal sulphur, which can plug the equipment and to kill the bacteria that form the sulphide. It can be used over a broad pH range to oxidise sulphide without the formation of colloidal sulphur. For continuous feeds, chlorine dioxide may be applied at dosages slightly higher than sulphide's oxidative demand as determined by a demand study. Between pH 5 to 9, an average of 5.2 ppm of chlorine dioxide can be used to instantly oxidise 1.0 ppm of sulphide ion (S^{2-}) to sulphate (SO_4^{2-}):

$$5 < pH < 9: \qquad S^{2-} \rightarrow SO_4^{2-} \qquad \text{(E-6)}$$

For intermittent treatment, chlorine dioxide should be applied at a shock dosage of 200 to 3000 ppm.

Sulphur Destruction

Reduced sulphur compounds are a broad class of oxy-sulphur compounds, such as sulphite (SO_3^-) and thiosulphate ($S_2O_3^{2-}$), which have an oxidant demand. These compounds are found in the waste streams of the petroleum, steel, paper and most chemical industries. Their high oxidant demand can cause eutrophication of natural waters and excessive chlorine demand in wastewaters treated by POTWs (Publicly Owned Treatment Works).

Chlorine dioxide effectively oxidises these species to sulphate ions (SO_4^{2-}) over a broad pH range of 5 to 9. Below a pH of 4, sodium chlorite may be used without the generation of chlorine dioxide. Since these compounds are usually found in mixtures of various ratios, the required chlorine dioxide dosage must be determined for each application.

APPENDIX F

Integration of equation (2.58)

$$\frac{1}{(C_A - C_A^*)}\partial\left(\frac{1}{1+\frac{a(C_A - C_A^*)}{C_A^*}}\right) = \frac{z_A F}{i} b\,\partial x$$

Set $x = w$

$$\frac{1}{(C_A - C_A^*)}\partial\left(\frac{1}{1+\frac{a(C_A - C_A^*)}{C_A^*}}\right) = \frac{z_A F}{i} b\,\partial w$$

Set $C_A^* = x$

$$\frac{z_A F}{i} b\,\partial w = \frac{1}{C_A - x}\partial\left(\frac{1}{1+\frac{a(C_A - x)}{x}}\right) = \left(\frac{1}{C_A - x}\right)\frac{\partial}{\partial x}\left(\frac{x}{x + a(C_A - x)}\right)\partial x$$

$$= \left(\frac{1}{C_A - x}\right)\frac{\partial}{\partial x}\left(\frac{x}{aC_A - (a-1)x}\right)\partial x$$

Set

$$u = x \qquad v = aC_A - (a-1)x$$

$$\frac{\partial u}{\partial x} = 1 \qquad \frac{\partial v}{\partial x} = -(a-1)$$

$$\frac{\partial}{\partial x}\left(\frac{x}{x + a(C_A - x)}\right)\partial x = \left(\frac{(aC_A - (a-1)x + (a-1)x)}{(aC_A - (a-1)x)^2}\right)\partial x = \left(\frac{aC_A}{(aC_A - (a-1)x)^2}\right)\partial x$$

$$\int F\frac{b}{i}\partial w = \int\left(\frac{aC_A}{(C_A - x)(aC_A - (a-1)x)^2}\right)\partial x$$

Set

$$u = aC_A - (a-1)x \qquad v = (C_A - x),$$

$$a = aC_A \qquad b = -(a-1)$$

$$c = C_A \qquad d = -1$$

$$k = ad - bc = -C_A$$

$$z_A F \frac{b}{i} w + C_1 = \frac{aC_A}{-C_A}\left(\frac{1}{aC_A - (a-1)x} + \frac{-1}{-C_A}\ln\left(\frac{(C_A - x)}{aC_A - (a-1)x}\right)\right.$$

$$z_A F \frac{b}{i} w + C_1 = \frac{a}{C_A}\ln\left(\frac{aC_A - (a-1)x}{(C_A - x)}\right) - \left(\frac{a}{aC_A - (a-1)x}\right)$$

Boundary Condition:

$$w = 0 \qquad x = 0$$

$$C_1 = \frac{a}{C_A}\ln(a) + \left(\frac{1}{C_A}\right)$$

$$z_A F \frac{b}{i} w = \frac{a}{C_A}\ln\left(\frac{aC_A - (a-1)x}{(C_A - x)}\right) - \left(\frac{a}{aC_A - (a-1)x}\right) - \frac{a}{C_A}\ln(a) - \frac{1}{C_A}$$

$$z_A F \frac{b}{i} C_A\, w = a\ln\left(\frac{aC_A - (a-1)x}{(C_A - x)}\right) - \left(\frac{aC_A}{aC_A - (a-1)x}\right)) - a\ln(a) - 1$$

$$z_A F \frac{b}{i} C_A\, w = a\ln\left(\frac{aC_A - (a-1)x}{(C_A - x)}\right) - \left(\frac{aC_A}{aC_A - (a-1)x}\right)) - a\ln(a) - 1$$

$$z_A F C_A \frac{b}{i} w = a\ln\left(\frac{aC_A - (a-1)x}{a(C_A - x)}\right) - \left(\frac{aC_A}{aC_A - (a-1)x}\right) - 1$$

$$z_A F C_A \frac{b}{i} w = a\ln\left(\frac{aC_A - (a-1)x}{a(\bar{c} - x)}\right) - \left(\frac{aC_A - aC_A + (a-1)x}{aC_A - (a-1)x}\right)$$

$$z_A F C_A \frac{b}{i} w = a\ln\left(\frac{aC_A - (a-1)x}{a(C_A - x)}\right) - \left(\frac{(a-1)x}{aC_A - (a-1)x}\right)$$

Boundary Condition:

$$w = W \qquad x = C_A^*$$

Yields:

$$a\ln\frac{aC_A - (a-1)C_A^*}{a(C_A - C_A^*)} - \frac{(a-1)C_A^*}{aC_A - (a-1)C_A^*} = \frac{z_A F}{i} b C_A W$$

REFERENCES

1 Gates, D. J. (1998), 'The Chlorine Dioxide Handbook', *Amer. Water Works Ass.*, Denver, CO.

2 Hoehn, R. C., A. A. Rosenblatt, and D. J. Gates (1996), 'Considerations for Chlorine Dioxide Treatment in Drinking Water Supplies', *Proceedings of the American Water Works Association*, Water Quality Technology Conference, Boston, MA, Nov. 17 – 21.

3 Hong, D. C. and W. H. Rapson (1968), 'Analyses of Chlorine Dioxide, Chlorous Acid, Chorite, Chlorate, and Chloride in Composite Mixtures', *Can. J. Chem.*, **46**, 2061.

4 Gordon, G. (1988), 'Methods of Measuring Disinfectant Residuals', *J. Amer. Water Works Ass*, **9**, 94.

5 Technical Sodium Chlorite for Chlorine Dioxide Generation, Technical Data Sheet, Vulcan Chemical, Birmington, AL.

6 Taylor, M.C., J. F. White, G.P Vincent, and G.L. Cunningham (1940), *Ind. Eng. Chem.*, **32**, 899.

7 Cunningham, G. L. and T. S. Oey (1955), *J. Chem. Soc.*, **77**, 799.

8 The Chlorite Manual (2001), Sterling Pulp Chemicals Ltd., Toronto, Ontario, Canada.

9 Gates, D. J. (1998), 'The Chlorine Dioxide Handbook, Water Disinfection Series', *Amer. Water Works Ass.* Denver, CO.

10 Gordon, G., R. Kieffer, and D. Rosenblatt (1972), 'The Chemistry of Chlorine Dioxide, Progress in Organic Chemistry', John Wiley and Sons, New York, NY, **15**.

11 Kaczur, J. and D. Cawlfield (1993), 'Chlorous Acid, Chlorite, and Chlorine Dioxide', Kirk-Othmer Encyclopedia of Chemical Technology – 4th Edition, John Wiley & Sons, New York, NY, **5**, 968.

12 Cosson, H. and E. R. Ernst (1994), *Ind. Eng, Chem. Res.*, **33**, 1468.

13 Taube, H. and H. Dodgen (1949), 'Application of radioactive Chlorine to the Study of the Mechanisms of Reactions Involving Changes in the Oxidation Sates of Chlorine', *J. Amer. Chem. Soc.*, **71**, 3330.

14 Bowen, E. and W. Cheung (1932), 'The Photodecomposition of Chlorine Dioxide Solutions', *J. Chem. Soc.*, **54**:1200.

15 Kepinski, J. and J. Trzeszczynski (1964), 'Roczniki Chemii Ann'. *Soc. Chim. Polonorum*, **38**, 201.

16 Haller, J. F., and N. Graves (1955), *W.W. Tappi*, **38**, 199.

17 Ishi, A. (1958), *Chem. Eng.* (Japan), **22**, 153.

18 Granstrom, M. L. and G. F. Lee (1957), *Public Works*, **88**, 90.

19 Standards Methods for the Examination of Water and Wastewater (1998), APHA, AWWA, and WEF, Washington (20th Edition).

20 Vulcan Chemicals, Birmingham, Alabama, USA, Sodium Chlorite in Water Treatment (1998) – A Compilation of Technical Data Sheets Relating to the Use of Chlorine Dioxide.